



DEVELOPMENTS IN
PETROLEUM SCIENCE

49

INTEGRATED FLOW MODELING

J.R. Fanchi

ELSEVIER





**DEVELOPMENTS IN
PETROLEUM SCIENCE**

49

INTEGRATED FLOW MODELING



DEVELOPMENTS IN PETROLEUM SCIENCE

Volumes 1-5, 7, 10, 11, 13, 14, 16, 17, 21, 22, 23-27, 29, 31 are out of print.

- 6** *Fundamentals of Numerical Reservoir Simulation*
- 8** *Fundamentals of Reservoir Engineering*
- 9** *Compaction and Fluid Migration*
- 12** *Fundamentals of Fractured Reservoir Engineering*
- 15a** *Fundamentals of Well-log Interpretation, 1. The acquisition of logging data*
- 15b** *Fundamentals of Well-log Interpretation, 2. The interpretation of logging data*
- 18a** *Production and Transport of Oil and Gas, A. Flow mechanics and production*
- 18b** *Production and Transport of Oil and Gas, B. Gathering and Transport*
- 19a** *Surface Operations in Petroleum Production, I*
- 19b** *Surface Operations in Petroleum Production, II*
- 20** *Geology in Petroleum Production*
- 28** *Well Cementing*
- 30** *Carbonate Reservoir Characterization: A Geologic-Engineering Analysis, Part I*
- 32** *Fluid Mechanics for Petroleum Engineers*
- 33** *Petroleum Related Rock Mechanics*
- 34** *A Practical Companion to Reservoir Stimulation*
- 35** *Hydrocarbon Migration Systems Analysis*
- 36** *The Practice of Reservoir Engineering*
- 37** *Thermal Properties and Temperature related Behavior of Rock/fluid Systems*
- 38** *Studies in Abnormal Pressures*
- 39** *Microbial Enhancement of Oil Recovery – Recent Advances*
 - Proceedings of the 1992 International Conference on Microbial Enhanced Oil Recovery
- 40a** *Asphaltenes and Asphalts, I*
- 41** *Subsidence due to Fluid Withdrawal*
- 42** *Casing Design – Theory and Practice*
- 43** *Tracers in the Oil Field*
- 44** *Carbonate Reservoir Characterization: A Geologic-Engineering Analysis, Part II*
- 45** *Thermal Modeling of Petroleum Generation: Theory and Applications*
- 46** *Hydrocarbon Exploration and Production*
- 47** *PVT and Phase Behaviour of Petroleum Reservoir Fluids*
- 48** *Applied Geothermics for Petroleum Engineers*
- 49** *Integrated Flow Modeling*



DEVELOPMENTS IN
PETROLEUM SCIENCE

49

INTEGRATED FLOW MODELING

JOHN R. FANCHI

*Department of Petroleum Engineering,
Colorado School of Mines,
(Golden) Colorado, USA*



2000

ELSEVIER

Amsterdam – Lausanne – New York – Oxford – Shannon – Singapore – Tokyo



ELSEVIER SCIENCE B.V.
Sara Burgerhartstraat 25
P.O. Box 211, 1000 AE Amsterdam, The Netherlands

© 2000 Elsevier Science B.V. All rights reserved.

This work is protected under copyright by Elsevier Science, and the following terms and conditions apply to its use:

Photocopying

Single photocopies of single chapters may be made for personal use as allowed by national copyright laws. Permission of the Publisher and payment of a fee is required for all other photocopying, including multiple or systematic copying, copying for advertising or promotional purposes, resale, and all forms of document delivery. Special rates are available for educational institutions that wish to make photocopies for non-profit educational classroom use.

Permissions may be sought directly from Elsevier Science Global Rights Department, PO Box 800, Oxford OX5 1DX, UK; phone: (+44) 1865 843830, fax: (+44) 1865 853333, e-mail: permissions@elsevier.co.uk. You may also contact Global Rights directly through Elsevier's home page (<http://www.elsevier.nl>), by selecting 'Obtaining Permissions'.

In the USA, users may clear permissions and make payments through the Copyright Clearance Center, Inc., 222 Rosewood Drive, Danvers, MA 01923, USA; phone: (978) 7508400, fax: (978) 7504744, and in the UK through the Copyright Licensing Agency Rapid Clearance Service (CLARCS), 90 Tottenham Court Road, London W1P 0LP, UK; phone: (+44) 171 631 5555; fax: (+44) 171 631 5500. Other countries may have a local reprographic rights agency for payments.

Derivative Works

Tables of contents may be reproduced for internal circulation, but permission of Elsevier Science is required for external resale or distribution of such material.

Permission of the Publisher is required for all other derivative works, including compilations and translations.

Electronic Storage or Usage

Permission of the Publisher is required to store or use electronically any material contained in this work, including any chapter or part of a chapter.

Except as outlined above, no part of this work may be reproduced, stored in a retrieval system or transmitted in any form or by any means, electronic, mechanical, photocopying, recording or otherwise, without prior written permission of the Publisher.

Address permissions requests to: Elsevier Science Global Rights Department, at the mail, fax and e-mail addresses noted above.

Notice

No responsibility is assumed by the Publisher for any injury and/or damage to persons or property as a matter of products liability, negligence or otherwise, or from any use or operation of any methods, products, instructions or ideas contained in the material herein. Because of rapid advances in the medical sciences, in particular, independent verification of diagnoses and drug dosages should be made.

First edition 2000

Library of Congress Cataloging in Publication Data

A catalog record from the Library of Congress has been applied for.

ISBN: 0 444 50500 8

ISSN: 0376 7361

∞ The paper used in this publication meets the requirements of ANSI/NISO Z39.48-1992 (Permanence of Paper).
Printed in The Netherlands.

"To some special teachers: Sid Hoskins, Keith Counts,
R.C. (Bob) Amme, H.E. (Hank) Bass and R.E. (Gene) Collins"

This Page Intentionally Left Blank

About the Author

John R. Fanchi is a Professor of Petroleum Engineering at the Colorado School of Mines. He has worked in the technology centers of three major oil companies (Marathon, Cities Service, and Getty), and served as an international consultant. His oil and gas industry responsibilities have revolved around reservoir modeling, both in the areas of simulator development and practical reservoir management applications. Dr. Fanchi's publications include software systems for the United States Department of Energy and numerous articles. He is the author of four books, including *Math Refresher for Scientists and Engineers, Second Edition* and *Principles of Applied Reservoir Simulation, Second Edition*. He has a Ph.D. in physics from the University of Houston.

This Page Intentionally Left Blank

Preface

Integrated flow models make it possible to work directly with seismically generated data at any time during the life of the reservoir. An integrated flow model combines a traditional flow model with a petrophysical model. Integrated flow models simplify the data transfer process between disciplines, enhance consensus building, and provide performance predictions in a format that is familiar to subsurface resource managers. They are a natural extension of the model-centric methods that are now being used in the geosciences.

Integrated Flow Modeling presents the formulation, development and application of an integrated flow simulator (IFLO). The text discusses properties of porous media within the context of multidisciplinary reservoir modeling, and presents the technical details needed to understand and apply the simulator to realistic problems. Exercises throughout the text direct the reader to software applications using IFLO input data sets and an executable version of IFLO provided with the text. The text-software combination provides the resources needed to convey both theoretical concepts and practical skills to geoscientists and engineers.

The integrated flow model IFLO combines a petrophysical model with a three-dimensional, three-phase, multicomponent extended black oil simulator. IFLO models isothermal, Darcy flow in up to three dimensions. It assumes reservoir fluids can be described by up to three fluid phases (oil, gas, and water) with physical properties that depend on pressure and composition. Natural gas

and injected solvent are allowed to dissolve in both the oil and water phases. The extended black oil simulator is capable of modeling conventional black oil and dry gas reservoir systems, as well as miscible processes, such as CO₂ flooding and enriched gas flooding. The resulting model includes calculations of important reservoir geophysical attributes.

A feature unique to IFLO is the integration of a petrophysical model with an extended flow simulator. The integrated flow model IFLO performs acoustic velocity and impedance calculations. These reservoir geophysical calculations make it possible to track changes in seismic variables as a function of time, which is the basis for 3-D time-lapse (4-D) seismic analysis.

IFLO was designed to run on personal computers with Intel Pentium or equivalent processors in a Windows environment. IFLO contains a combination of multicomponent, pseudomiscible features and reservoir geophysical options that cannot be found elsewhere. The text-software combination is well-suited for learning how to use a reservoir simulator, developing an understanding of reservoir management concepts, and for solving many types of reservoir engineering problems.

This text/software combination is suitable for geoscientists and engineers with an interest in integrated flow modeling. It can be used in multidisciplinary graduate classes, continuing education classes, short courses, or for self-study. The software is suitable for a variety of integrated flow studies, as illustrated by the accompanying input data files.

I would like to thank the students who took my graduate course in integrated flow modeling at the Colorado School of Mines for their comments and suggestions. I would also like to thank Kathy, Tony, and Chris Fanchi for helping prepare the camera-ready manuscript. Any written comments or suggestions for improving the material are welcome.

John R. Fanchi, Ph.D.
Golden, Colorado
June 2000

Contents

About the Author.....	vii
Preface.....	ix
1 Overview	1
1.1 Program Overview	2
1.2 Conventional Black Oil Simulator Equations	4
1.3 Extended Black Oil Simulator Equations	7
1.4 Program Operation	8
1.5 Input Data File - ITEMP.DAT	9
1.6 Output Data Files	9
Exercises	10
2 Reservoir Structure	12
2.1 Coordinate Orientation	12
2.2 Traditional Mapping	13
2.3 Computer Generated Maps	15
2.4 Geostatistical Mapping	18
2.5 Bulk Volume and Net Volume	24
Exercises	25
3 Porosity	27
3.1 Porosity Defined	27
3.2 Net Pore Volume and Saturation	29
3.3 Statistics of Porosity Distributions	30
3.4 Characteristic Volume	38
Exercises	39

4	Permeability	41
4.1	Darcy's Law	41
4.2	Permeability	47
4.3	Directional Dependence of Permeability	49
4.4	Permeability Averaging	52
	Exercises	55
5	Critical Sample Size	57
5.1	Critical Sample Size for Porosity	57
5.2	Permeability Distributions	60
5.3	Critical Sample Size for Permeability	64
5.4	Measures of Permeability Heterogeneity	66
	Exercises	69
6	Petrophysical Model	71
6.1	Compressional and Shear Velocities	71
6.2	Estimates of Moduli	73
6.3	Moduli from Acoustic Velocities	75
6.4	Acoustic Impedance and Reflection Coefficient	76
6.5	Geostatistical Correlations	77
	Exercises	83
7	Relative Permeability	85
7.1	Effective Permeability and Relative Permeability	85
7.2	Two-Phase Relative Permeability	87
7.3	Averaging Relative Permeability Data	91
7.4	Two-Phase Relative Permeability Correlations	93
7.5	Three-Phase Relative Permeability Correlations	97
	Exercises	100
8	Capillary Pressure	102
8.1	Basic Concepts	102
8.2	Capillary Pressure	105
8.3	Capillary Pressure Measurements	107
8.4	Capillary Pressure Correlation Methods	111
	Exercises	114
9	Extended Rock-Fluid Interactions	115
9.1	Miscible Conditions	115

9.2	Solid Precipitation	116
9.3	Water Blocking	117
9.4	Mobility Control	117
9.5	Effective Relative Permeability and Capillary Pressure	118
9.6	Transmissibility	119
	Exercises	123
10	Fluid Properties	124
10.1	Fundamental Fluid Property Concepts	124
10.2	Black Oil Model PVT Data	130
10.3	Extrapolating Saturated Curves	132
10.4	Bubble Point Tracking	133
10.5	Extended Fluid Properties Model	134
	Exercises	138
11	Fluid Displacement	140
11.1	Mobility	140
11.2	Fractional Flow	142
11.3	Recovery Efficiency	146
11.4	Production Stages	148
11.5	Miscible Displacement Models	150
	Exercises	155
12	Formulation of Flow Equations	156
12.1	Conservation of Mass	156
12.2	Flow Equations for Three-Phase Flow	158
12.3	Recasting the Flow Equations	162
12.4	Introduction of the Capillary Pressure Concept	164
12.5	Extended Black Oil Simulator Equations	166
	Exercises	167
13	Source/Sink Terms	169
13.1	Productivity Index	169
13.2	Rate Constraint Representation	172
13.3	Pressure Constraint Representation	175
13.4	Well Constraints	176
13.5	Aquifer Models	178
	Exercises	179

14	Solution of the Extended Flow Equations	181
14.1	The Finite Difference Concept	181
14.2	Derivative of Accumulation Terms	186
14.3	Volume Integration and Discretization	186
14.4	Multi-Variable Newton-Raphson IMPES Procedure	188
	Exercises	192
15	IFLO Applications	194
15.1	Monitoring Frontal Advance	194
15.2	Scheduling 4-D Seismic Surveys	197
15.3	Improved Oil Recovery Examples	198
	Exercises	203
	Appendix A: Introduction to IFLO	207
A.1	Program Review	207
A.2	Program Configuration	210
A.3	Input Data File - ITEMP.DAT	210
A.4	Example Input Data Sets	211
	Appendix B: Initialization Data	214
B.1	Model Dimensions and Geometry	215
B.2	Seismic Velocity Parameters	220
B.3	Porosity, Permeability, and Transmissibility Distributions	225
B.4	Rock Regions	231
B.5	Relative Permeability and Capillary Pressure Tables	232
B.6	Fluid PVT Tables	234
B.7	Miscible Solvent Data	236
B.8	Pressure and Saturation Initialization	242
B.9	Run Control Parameters	245
B.10	Analytic Aquifer Models	249
	Appendix C: Recurrent Data	250
C. 1	Timestep and Output Control	250
C.2	Well Information	253

Appendix D: Program Supplement	260
D.1 Initialization Options	260
D.2 Run Control Features	265
D.3 Output Options	268
REFERENCES.....	273
INDEX.....	281

This Page Intentionally Left Blank

Chapter 1

Overview

The development and implementation of 3-D, model-centric methods based upon computer-generated 3-D representations of the earth are changing the way the industry characterizes reservoirs [Lumley and Behrens, 1997; Jack, 1998; Tobias, 1998]. The integration of data from different disciplines will be further enhanced by the use of flow models that include petrophysical calculations [Fanchi, 1999]. Integrated flow models make it possible to work directly with seismically generated data at any point during the life of the reservoir. They simplify the data transfer process between disciplines, enhance consensus building, and provide performance predictions in a format that is familiar to reservoir managers. Integrated flow models are a natural extension of the model-centric methods that are now being used in the geosciences. The extension of petrophysical algorithms to include data generated by multi-component, 3-D seismic surveys should add even more data for accurate reservoir characterization and optimized reservoir management.

The formulation, development and application of an integrated reservoir flow simulator IFLO is the focus of this text. The integrated flow simulator includes traditional fluid flow equations and a petrophysical model. The program IFLO is a pseudomiscible, multicomponent, multidimensional fluid flow simulator. IFLO models isothermal, Darcy flow in up to three dimensions. It

2 Integrated Flow Modeling

assumes reservoir fluids can be described by up to three fluid phases (oil, gas, and water) with physical properties that depend on pressure and composition. Natural gas and injected solvent are allowed to dissolve in both the oil and water phases. A feature unique to IFLO is the integration of a petrophysical model with a flow simulator. The integrated flow model IFLO performs acoustic velocity and impedance calculations. These reservoir geophysical calculations make it possible to track changes in seismic variables as a function of time, which is the basis for 3-D time-lapse (4-D) seismic analysis.

All of the data requirements of the integrated flow model IFLO are discussed within the context of reservoir modeling, and the mathematics needed to understand and apply the simulator IFLO is presented. Examples illustrate the concepts involved and demonstrate the range of applicability of the simulator. The rest of this chapter provides a summary of the flow equations solved by the simulator and an introduction to the operational characteristics of IFLO.

1.1 Program Overview

IFLO was designed to run on personal computers with Intel Pentium or equivalent processors. This size simulator is well-suited for learning how to use a reservoir simulator, developing an understanding of reservoir management concepts, and for solving many types of reservoir engineering problems. It is an inexpensive tool for performing studies that call for more sophistication than is provided by analytical solutions, yet do not require the use of full-featured commercial simulators. It provides a combination of multicomponent, pseudomiscible options and reservoir geophysical options that cannot be found elsewhere.

IFLO is a modified version of MASTER, a black oil simulator with multicomponent, pseudomiscible options for modeling carbon dioxide or nitrogen flooding [Ammer, et al., 1991]. MASTER is an improved version of BOAST, an implicit pressure-explicit saturation (IMPES) simulator published by the U.S. Department of Energy in 1982 [Fanchi, et al., 1982]. IFLO includes several

enhancements to MASTER using algorithms from earlier versions of BOAST, BOAST II [Fanchi, et al., 1987], and BOAST4D [Fanchi, 2000].

A comparison of differences between MASTER and IFLO is given in the following tables. Table 1-1 shows that a variety of useful geoscience and reservoir engineering features have been added to IFLO, including the representation of horizontal or deviated wells, improvements for modeling heterogeneous reservoir characteristics, and the calculation of important reservoir geophysical information.

Table 1-1
Comparison of Reservoir Model Differences

FEATURE	MASTER	IFLO
Well completions	Vertically contiguous	Flexible
Well controls	Limited	Expanded
Horizontal/Deviated well	Not available	New
Gas production well	Not available	New
Compressional velocity	Not available	New
Shear velocity	Not available	New
Acoustic impedance	Not available	New
Reflection coefficient	Not available	New
Modify ϕ, K	Input ϕ, K	Input ϕ, K or multiply by factor
Modify transmissibility	Input transmissibility	Multiply by factor
Modify pore volume	Not available	Multiply by factor
Net thickness	Not available	New
Zero pore volume blocks	Not available	New
Analytic aquifer model	Not available	New

4 Integrated Flow Modeling

In addition, IFLO includes changes to improve computational performance. Several of the more important changes are listed in the following table.

Table 1-2
Comparison of Computational Differences

FEATURE	MASTER	IFLO
Saturation table end points	Set to -0.1 and 1.1	Set to 0.0 and 1.0
Time stepping and reports	Requires counter times time step size	User enters elapsed times only
Programming language	FORTRAN 77	FORTRAN 90
Dynamic Redimensioning	Not Available	New

IFLO has been tested under a variety of conditions, including: oil and gas reservoir depletion, waterflooding, gas injection into an undersaturated oil reservoir, aquifer influx into a gas reservoir, and carbon dioxide injection. Favorable comparisons with other simulators have been obtained. IFLO is based on a mass conserving, Newton-Raphson formulation. IFLO includes a material balance correction that reduces cumulative material balance error to the magnitude of material balance error associated with a single time step. Options have been added to extend the applicability of IFLO to more complex systems.

1.2 Conventional Black Oil Simulator Equations

The black oil simulator mass conservation equations for the oil, water and gas phases are derived in Chapter 12. They are summarized here to show an important subset of the equations that are being solved by IFLO. Reservoir fluids are described by up to three fluid phases (oil, gas, and water), whose physical properties are functions of pressure only. Solution gas may be present

in both the oil and water phases. The black oil simulator equations can be succinctly written as follows:

Oil

$$-\nabla \cdot \frac{\vec{v}_o}{B_o} - \frac{q_o}{\rho_{osc}} = \frac{\partial}{\partial t} \left(\phi \frac{S_o}{B_o} \right) \quad (1.1)$$

Water

$$-\nabla \cdot \frac{\vec{v}_{wo}}{B_w} - \frac{q_w}{\rho_{wsc}} = \frac{\partial}{\partial t} \left(\phi \frac{S_w}{B_w} \right) \quad (1.2)$$

Gas

$$\begin{aligned} & -\nabla \cdot \left[\frac{\vec{v}_g}{B_g} + \frac{R_{so}}{B_o} \vec{v}_o + \frac{R_{sw}}{B_w} \vec{v}_w \right] - \frac{q_g}{\rho_{gsc}} \\ &= \frac{\partial}{\partial t} \left\{ \phi \left[\frac{S_g}{B_g} + \frac{R_{so}}{B_o} S_o + \frac{R_{sw}}{B_w} S_w \right] \right\} \end{aligned} \quad (1.3)$$

Letting the subscript p denote o (oil), w (water), and g (gas), the symbols in Eqs. (1.1) to (1.3) are defined as follows:

- B_p = formation volume factor of phase p
- q_p = mass flow rate per unit reservoir volume of phase p
- R_{so} = solubility of gas in oil
- R_{sw} = solubility of gas in water
- S_p = saturation of phase p
- v_p = Darcy's velocity of phase p
- ρ_{psc} = density of phase p at standard conditions
- ϕ = porosity

Three additional equations – called auxiliary equations – are employed when solving the preceding fluid flow equations. They are the saturation constraint equation,

6 Integrated Flow Modeling

$$S_o + S_w + S_g = 1 \quad (1.4)$$

the oil-water capillary pressure definition,

$$P_{cow}(S_w) = P_o - P_w \quad (1.5)$$

and the gas-oil capillary pressure equation

$$P_{cgo}(S_g) = P_g - P_o \quad (1.6)$$

where P_p is the pressure of phase p , P_{cow} is the oil-water capillary pressure, and P_{cgo} is the gas-oil capillary pressure.

Darcy's velocity for phase p is

$$\bar{v}_p = -K \frac{k_p}{\mu_p} \nabla \Phi_p \quad (1.7)$$

where K is a permeability tensor that is usually assumed to be diagonalized along its principal axes, k_p and μ_p are relative permeability and viscosity of phase p respectively. The phase potentials Φ_p are given as functions of depth z by

$$\Phi_o = P_o - \frac{\rho_o z}{144}, \Phi_w = P_o - P_{cow} - \frac{\rho_w z}{144}, \Phi_g = P_o + P_{cgo} - \frac{\rho_g z}{144} \quad (1.8)$$

Phase densities are calculated from input PVT data as follows:

$$\rho_o = \frac{1}{B_o} [\rho_{osc} + R_{so} \rho_{gsc}], \rho_w = \frac{1}{B_w} [\rho_{osc} + R_{sw} \rho_{gsc}], \rho_g = \frac{\rho_{gsc}}{B_g} \quad (1.9)$$

Expressions for rock and saturated phase compressibilities are

$$c_r = \frac{1}{f} \frac{\partial f}{\partial P_o}, c_g = -\frac{1}{B_g} \frac{\partial B_g}{\partial P_o}, \\ c_o = -\left[\frac{1}{B_o} \frac{\partial B_o}{\partial P_o} - \frac{B_g}{B_o} \frac{\partial R_{so}}{\partial P_o} \right], c_w = -\left[\frac{1}{B_w} \frac{\partial B_w}{\partial P_o} - \frac{B_g}{B_w} \frac{\partial R_{sw}}{\partial P_o} \right] \quad (1.10)$$

The functional form of properties like density and compressibility change when the traditional black oil simulator formulation is extended. The extended formulation is outlined in the next section.

1.3 Extended Black Oil Simulator Equations

The flow equations for the extended black oil simulator used in IFLO allow for the dissolution of more than one soluble species. This is useful for miscible flooding using such substances as carbon dioxide, nitrogen and air. The flow equations are presented below [Ammer, et al., 1991]:

Stock Tank Oil

$$\nabla \cdot \frac{Kk_{ro}^e}{\mu_o^e B_o} \nabla \Phi_o - \frac{q_o}{\rho_{osc}} = \frac{\partial}{\partial t} \left(\phi \frac{S_o}{B_o} \right) \quad (1.11)$$

Water plus Surfactant

$$\nabla \cdot \frac{Kk_{rw}^e}{\mu_w^e B_w} \nabla \phi_w - \frac{q_w}{\rho_{wsc}} = \frac{\partial}{\partial t} \left(\phi \frac{S_w}{B_w} \right) \quad (1.12)$$

Surfactant

$$\nabla \cdot x_s \frac{Kk_{rw}^e}{\mu_w^e B_w} \nabla \phi_w - x_s \frac{q_w}{\rho_{wsc}} = \frac{\partial}{\partial t} \left(\phi x_s \frac{S_w}{B_w} \right) \quad (1.13)$$

Soluble Species

$$\begin{aligned} \nabla \cdot & \left[v_i \frac{Kk_{rg}^e}{\mu_i^e B_i} \nabla \phi_i + v_i R_{io} \frac{Kk_{ro}^e}{\mu_o^e B_o} \nabla \Phi_o + v_i R_{iw} \frac{Kk_{rw}^e}{\mu_w^e B_w} \nabla \phi_w \right] - \frac{q_i}{\rho_{isc}} \\ &= \frac{\partial}{\partial t} \left\{ \phi v_i \left[\frac{S_g}{B_i} + \frac{R_{io}}{B_o} S_o + \frac{R_{iw}}{B_w} S_w \right] \right\} \end{aligned} \quad (1.14)$$

for $i = \{g, 1, \dots, N_s\}$ where N_s is the number of soluble species, x_s is the surfactant volume fraction, and v_i is the volume fraction of component i . The superscript e in the above equations shows that an effective fluid property is

8 Integrated Flow Modeling

being calculated. Effective fluid properties are based on the extended fluid property model discussed in Chapter 10. The extended fluid property model is an extension of work first presented by Todd and Longstaff [1972], Watkins [1982], and Chase and Todd [1984]. The extended fluid property model used in IFLO is the adaptation developed by Ammer, et al. [1991].

Equations (1.11) through (1.14) are discretized and solved numerically in IFLO. They include the conventional black oil flow equations presented in Section 1.2 as a special case.

1.4 Program Operation

The program IFLO provided with the text is included as an integral component of the text-software set. It is therefore worthwhile to acquaint the reader with the software. IFLO runs in the Windows 95/98/NT operating system environment. Dynamic memory management is used to control computer memory requirements for different model sizes. The maximum number of blocks in the standard configuration provided with this text is 1000. It is enough to run many commonly encountered reservoir problems and the exercises in the text. Other memory allocation controls, such as the number of blocks in a given direction or the number of wells in the model, are entered by the user as part of the input data file.

IFLO must be copied to a folder on your hard drive before running. The following procedure is recommended for a CD drive D and hard drive C running Windows 95/98/NT:

1. Open **Windows Explorer** and select your CD drive.
2. Use a **Windows**-based Unzip program to extract all of the files from the **IFLO** file on the CD to a folder on your hard drive.
3. Run **IFLO** by double clicking on the **IFLO.EXE** file on your hard drive.

1.5 Input Data File - ITEMP.DAT

IFLO reads a file called ITEMP.DAT and outputs to files ITEMP.TSS, ITEMP.PLT, ITEMP.ARR, and ITEMP.ROF. The output files are discussed below. You should copy and rename any files you wish to save because IFLO overwrites the ITEMP.* files each time it runs.

IFLO input data is divided into two parts: initialization data, and recurrent data. Initialization data include data that is set at the beginning of the study and is not expected to change during a model run. Such data includes the reservoir description and fluid properties. Recurrent data are data that are expected to change during the course of a simulation. Recurrent data include well schedules and time step control information. IFLO technical details are discussed in more detail in later chapters.

The easiest way to prepare a new data file is to edit an old one. This will give you an example of the formats needed for most options. If you start with an old data set, make sure that you check all applicable data entries and make changes where appropriate.

1.6 Output Data Files

You are given the option at the start of an IFLO run to direct output to either the screen or to a set of files. It is often worthwhile to send output to the screen when first building and debugging a data set. IFLO will abort at the point in the data set where it encounters improperly entered data. For evaluating run results, it is preferable to send output to files. In this case, a one line time step summary is sent to the screen each time step so that you can monitor the progress of a run.

All output files are in ASCII or text format so that they may be read by a variety of commercially available spreadsheets. IFLO output may then be manipulated using spreadsheet options. This is especially useful for making plots or displaying array data. Different output files are defined so that simulator output file sizes are more manageable. The output files are designed to contain information that is logically connected, e.g. well data in one file, reservoir

10 Integrated Flow Modeling

information that is logically connected, e.g. well data in one file, reservoir property distributions in another file. The different output files are described in Appendix A.

Exercises

- 1-1. The user's manual for IFLO is presented in the Appendices. The program IFLO may be prepared for execution as follows:
 - A. Prepare a directory (or folder) called "path\IFLO" on your hard drive. Path is the drive and directory path to the new folder.
 - B. Copy all files from the disk to the new directory.
 - C. Copy file Exam7.dat to itemp.dat and run IFLO.
 - D. Select option "Y" to write the run output to files.
- 1-2. Open itemp.tss and determine how many days were in the simulation run in Exercise 1-1.
- 1-3. Open itemp.rof and determine the original oil in place for the data set run in Exercise 1-1.
- 1-4. The program 3DVIEW may be used to view the reservoir structure associated with IFLO data sets. 3DVIEW is a visualization program that reads IFLO output files with the extension "arr". To view a reservoir structure, using 3DVIEW, proceed as follows:

Use your file manager to open your folder containing the IFLO files. Unless stated otherwise, all mouse clicks use the left mouse button.

- Start 3DVIEW (double click on the application 3DVIEW.EXE)
- Click on the button "File".
- Click on the "Open Array File".
- Click on "Rim-2D.arr" in the File List.
- Click on "OK".

At this point you should see a structure in the middle of the screen. The structure is an anticlinal reservoir with a gas cap and oil rim. To view different

perspectives of the structure, hold the left mouse button down and move the mouse. With practice, you can learn to control the orientation of the structure on the screen.

The gridblock display may be smoothed by clicking on the “Project” button and selecting “Smooth Model Display”. The attribute shown on the screen is pressure “P”. To view other attributes, click on the “Model” button, set the cursor on “Select Active Attribute” and then click on another attribute. For example, select oil saturation “SO”. The oil rim should be visible on the screen. The oil rim can be viewed from different angles by holding the left mouse button down and moving the mouse. The best view of the oil rim is a plan view obtained by looking down at the structure.

To exit 3DVIEW, click on the “File” button and then click on “Exit”.

Chapter 2

Reservoir Structure

Reservoir models are quantified and prepared for use in flow simulators by preparing detailed maps of variables that define reservoir structure and fluid distribution in three-dimensional space. The mapping/contouring process is the point where geological and geophysical interpretations have their greatest impact on the final representation of the reservoir. This chapter describes different geological mapping strategies.

2.1 Coordinate Orientation

The IFLO reservoir model assumes a block-centered grid with the axes aligned using the right-handed coordinate system illustrated in Figure 2-1. The top layer ($K = 1$) is shown. The second layer ($K = 2$) is below the $K = 1$ layer, and so on. Block nodes are located at the center of an element of symmetry. In our case, the element of

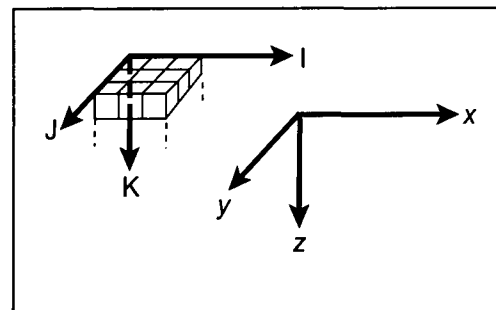


Figure 2-1. Coordinate system.

symmetry is a parallelogram. Several other gridding schemes are possible, but are not coded in IFLO.

2.2 Traditional Mapping

The different parameters that must be digitized for use in a grid include elevations or structure tops, permeability in three orthogonal directions, porosity, gross thickness, net to gross thickness and, where appropriate, descriptions of faults, fractures and aquifers. The resulting maps are digitized by overlaying a grid on the maps and reading a value for each gridblock. The digitizing process is sketched in Figures 2-2a through 2-2d [Fanchi, 2000].

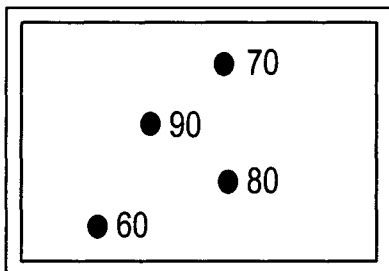


Figure 2-2a. Gather data.

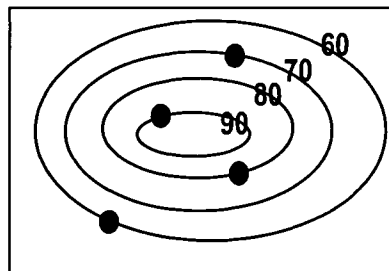


Figure 2-2b. Contour data.

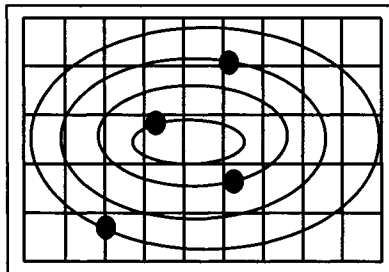


Figure 2-2c. Overlay grid.

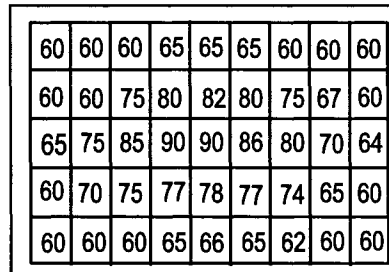


Figure 2-2d. Digitize data.

The contouring step is the point where geological interpretation is included in the flow model. The following contouring guidelines are worth noting from a technical, rather than scientific, perspective.

14 Integrated Flow Modeling

- A. Contour lines do not branch.
- B. Contour lines do not cross.
- C. Contour lines either close or run off the map.
- D. Steep slopes have close contour lines.
- E. Gentle or flat slopes have contour lines that are far apart.

The first three of these guidelines are illustrated in Figure 2-3. Figures 2-3a and 2-3b are examples of contouring that violate the guidelines. Figure 2-3c agrees with guideline C. Guidelines A through E above should be applied to any type of contour map. Discontinuities in contour lines are possible, but need to be justified by the inferred existence of geologic discontinuities such as faults.

Several geological principles should be followed in the contouring process. A few which are applicable to stratigraphy are listed in Table 2-1 for illustration.

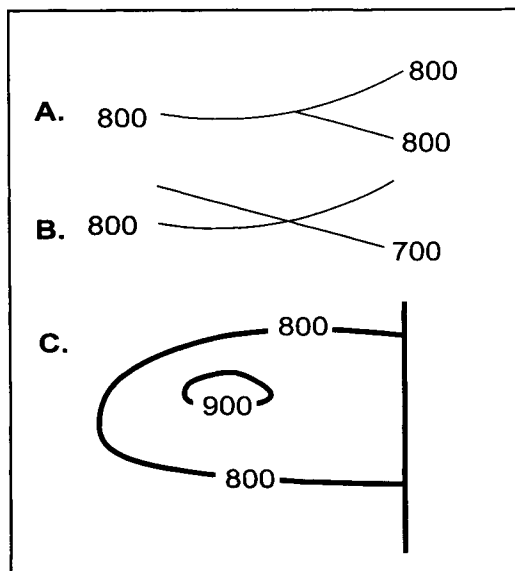


Figure 2-3. Examples of Contour Tips.

Table 2-1
Selected Geological Principles

Principle	Remarks
Uniformitarianism	The present is the key to the past. Processes at work on the earth today operated in the same way in the past, although the rates may have changed.
Original Horizontality	Sedimentary rocks are typically deposited in a horizontal plane.

Table 2-1
Selected Geological Principles

Principle	Remarks
Lateral Continuity	Sedimentary units are normally continuous across a sedimentary basin, although the facies, or type of rock, may change.
Superposition	The deepest formation in a sequence of strata is usually the oldest and shallower strata are successively younger.

2.3 Computer Generated Maps

An important function of geologic maps is to present values of a spatially distributed property at any point on a surface or within a layer. Examples of spatially distributed properties are structure top, net thickness and porosity. Maps of spatially distributed properties can be generated by computer using a variety of techniques.

One of the simplest algorithms that can be coded in a computer program to generate a map is to distribute property values over a surface or within a layer by using inverse distance weighting of all applicable control point values. The control point values correspond to property values measured at wells or determined by seismic methods that apply to the surface or layer of interest. The formula for inverse distance weighting is

$$V_x = \frac{\sum_{i=1}^N (V_i / d_i)}{\sum_{i=1}^N (1/d_i)} \quad (2.1)$$

where V_x is the value of the property at x calculated from N known values $\{V_i\}$ of the property at distances $\{d_i\}$ from x . Inverse distance weighting assigns more weight to control points close to location x and less weight to control points further away. The weighting factor is the inverse of control point distance

16 Integrated Flow Modeling

from x . For example, the value at a point x that is at the distances $\{d_A, d_B\}$ from two known values $\{V_A, V_B\}$ is

$$V_x = \frac{\frac{V_A}{d_A} + \frac{V_B}{d_B}}{\frac{1}{d_A} + \frac{1}{d_B}} \quad (2.2)$$

Figure 2-4 illustrates the example with two control points. If only one value V_C is known ($N = 1$), then $V_x = V_C$ for all values of x .

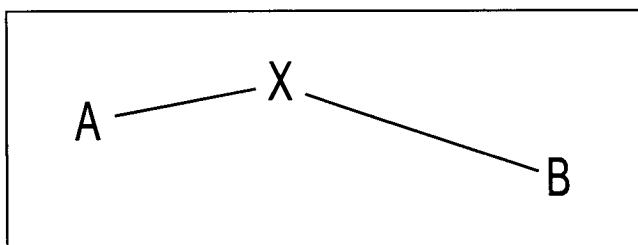


Figure 2-4. Inverse Distance Weighting with Two Control Points {A, B}.

Inverse distance weighting is an example of a technique that uses control points in the neighborhood of an unknown point to estimate the property value at the point. A more general expression for distributing an attribute using a weighted average is

$$A_{avg} = \frac{\sum_{i=1}^N W(r_i, R) \cdot A_i}{\sum_{i=1}^N W(r_i, R)} \quad (2.3)$$

where

- A_{avg} = weighted average value of attribute
- A_i = value of attribute at control point i
- W = weighting function
- r_i = distance from the interpolated point to control point i

R = user specified search radius

N = number of control points

A control point is any spatial location with a known value. It could be a well location, or a value that is imposed by the mapper using soft data such as seismic indications of structure boundaries. The search radius R constrains the number of control points N that are used to determine the weighted average value of the attribute. An example of a weighting function is the weighting function in Eq. (2.1), namely $1/d$. Another example of a weighting function with a search radius is

$$W(r, R) = \left(1 - \frac{r}{R}\right)^2 \cdot \left(\frac{R}{r}\right)^x \quad (2.4)$$

where the value of the exponent x is entered by the user.

Another technique for determining the spatial distribution of a property by computer is to fit a surface through the control points. This technique is referred to here as trend surface analysis. Two examples of trend surface analysis use linear and quadratic functions to fit a plane and a conic section through a set of control points.

Linear trend surface analysis uses regression to fit a line through all control point values in a given direction. The regression model for linear trend surface analysis is

$$V_{loc} = a_0 + a_1 x_{loc} + a_2 y_{loc} \quad (2.5)$$

where V_{obs} is the observed value at the control point, and $\{x_{loc}, y_{loc}\}$ are the {x-axis, y-axis} locations of the control point. At least three control points are needed to determine the regression coefficients $\{a_0, a_1, a_2\}$. The combination of orthogonal lines in 2-D yields a planar surface through the control points. Linear trend surface analysis is useful for modeling linear trends such as constant regional dip.

Quadratic trend surface analysis uses regression to fit a quadratic function through all control point values in a layer. The regression model for quadratic trend surface analysis is

18 Integrated Flow Modeling

$$V_{obs} = a_0 + a_1 x_{loc} + a_2 y_{loc} + a_3 x_{loc}^2 + a_4 x_{loc} y_{loc} + a_5 y_{loc}^2 \quad (2.6)$$

where V_{obs} is the observed value at the control point, and $\{x_{loc}, y_{loc}\}$ are the {x-axis, y-axis} locations of the control point. At least six control points are needed to determine the regression coefficients $\{a_0, a_1, a_2, a_3, a_4, a_5\}$. Quadratic trend surface analysis can fit a curved surface to data, and is therefore useful in representing structures such as anticlines or synclines. Quadratic trend surface analysis requires more control points than linear trend surface analysis to fit the larger set of regression coefficients.

The techniques described above are relatively simple examples of technology that can be used to generate geologic maps using computer programs. More sophisticated computer mapping packages exist and are used to prepare 2-D, 3-D and 4-D maps of spatially distributed parameters. Geostatistics is an example of a more sophisticated mapping technology that is based on the spatial distribution of statistically correlated properties.

2.4 Geostatistical Mapping

Geostatistics is a branch of "applied statistics" that attempts to describe a property which is distributed in space with some degree of continuity. For example, porosity and permeability are spatially dependent properties which are suitable for geostatistical description. Before describing the application of geostatistical modeling to flow modeling, it is worthwhile to discuss the notion of statistics as it is applied to the description of porous media and the definition of heterogeneity.

Statistical Definition of Reservoir Heterogeneity

Reservoirs are volumes of rock grains and pore space. Every measurement of any rock property is on a sample of some specific size: a core plug, for example. The description of the heterogeneous quality of a reservoir is in terms of values for the property in question, their spatial position in the reservoir and the size of the individual samples. The number of samples affects the reliability of a constructed characterization of the reservoir. With these concepts

in mind, we visualize the reservoir as an ensemble of elements each having the volume of one of our samples.

Values of rock properties have meaning only for samples of rock of some macroscopic size which contain large numbers of pores, or grains of rock matrix material. However, these values are not unique because of random elements in the depositional process and subsequent diagenetic history. Measurements of any one rock property on many neighboring samples within a given depositional structure exhibit some frequency distribution of values.

We can define statistical homogeneity of a depositional structure, or just "homogeneity", as the condition in which the same frequency distribution of each property is found throughout the structure. Heterogeneity is then the absence of homogeneity.

In comparing frequency distributions of any rock property in spatially distinct regions of a depositional unit, we note that every measured value of the rock property should be on a sample of the same size because the form of the frequency distribution is determined in large part by the sample size for each measurement. This was shown many years ago by Collins [1961].

Depositional environment determines the statistical heterogeneity of rock when viewed on any size scale. Only within a depositional unit can we expect to see "similar" frequency distributions of any rock property everywhere. A reservoir might be statistically heterogeneous only on the core plug scale but could be treated deterministically on a larger scale with all rock properties being smooth functions of spatial position in the reservoir. The larger scale defines a critical sample volume in which we do not see "statistical" fluctuations in values of a rock property among adjacent samples. We may still see regional trends, that is, deterministic variations with spatial position. In this case, the observed values of the rock property can be contoured, or expressed as a deterministic function of position coordinates $\{x, y, z\}$ in the reservoir.

The importance of sample size in characterizing rock properties has been stressed by many authors. As early as 1961, Collins [1961] showed that variance in porosity distribution depended on sample size. Bear [1972] stressed the need to identify an appropriate averaging volume for assigning a macroscopic property to a porous medium. Haldorsen and Lake [1989] have

20 Integrated Flow Modeling

schematically illustrated the role of various scales on the description of a reservoir property. They defined four conceptual scales to account for variations in the range of data applicability. The four scales are related to averaging volume in Table 2-2.

Table 2-2
Reservoir Characterization Scales

Micro Scale	the size of a few pores only
Macro Scale	the size of conventional core plugs
Mega Scale	the size of gridblocks in full field flow models
Giga Scale	the total formation or regional scale

It is instructive to see how the scale influences the analysis of a porous medium. As an example, consider a porous medium, such as a core plug, with bulk volume V . We subdivide the volume V into a number n of elements each with volume ε , thus

$$V = n\varepsilon \quad (2.7)$$

as shown in Figure 2-5. Each element is sampled to determine if it is either grain or pore space. This means the elements are defined on the micro scale.

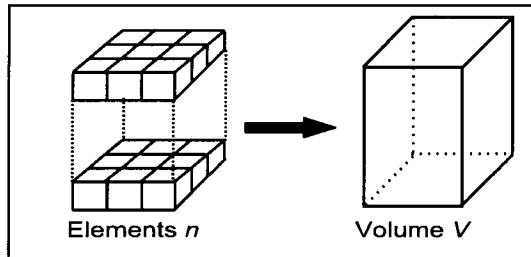


Figure 2-5. Elements of Volume.

Let x be the number of elements that are pore space. Porosity is expressed in terms of x as

$$\varphi = x/n \quad (2.8)$$

and pore volume is

$$V_p = \frac{x}{n} n\epsilon = x\epsilon \quad (2.9)$$

In this formulation, each element is either grain or pore space. This type of distribution is described by the binomial distribution.

The binomial distribution gives the probability that in n independent trials an element of pore space is encountered x times. Let p denote the probability that pore space is encountered in a single trial and $q = 1 - p$ is the probability that grain is encountered. In terms of these variables, the binomial distribution is

$$f_b(x) = \binom{n}{x} p^x q^{n-x} \quad (2.10)$$

with the binomial coefficient

$$\binom{n}{x} = \frac{n!}{x!(n-x)!} \quad (2.11)$$

If the number of elements n is large, the DeMoivre-Laplace Central Limit theorem says that the binomial distribution becomes the normal distribution

$$f_N(x) = \frac{1}{\sqrt{2\pi}\sigma} \exp\left[-\frac{1}{2}\left(\frac{x-\mu}{\sigma}\right)^2\right] \quad (2.12)$$

with mean $\mu = np$ and standard deviation $\sigma = \sqrt{npq}$. We now recognize that the average porosity $\bar{\phi} = p$ so that σ becomes

$$\sigma = \sqrt{\frac{V}{\epsilon} pq} = \sqrt{\frac{V}{\epsilon} \bar{\phi}(1-\bar{\phi})} \quad (2.13)$$

The effect of sample size on the distribution is estimated using Eq. (2.13) as follows.

Suppose we compare two distributions of elements with volumes ϵ_a , ϵ_b . The bulk volume is a constant so that

$$V = n_a \epsilon_a = n_b \epsilon_b \quad (2.14)$$

22 Integrated Flow Modeling

and the ratio of standard deviations is

$$\frac{\sigma_a}{\sigma_b} = \sqrt{\frac{\varepsilon_b}{\varepsilon_a}} \quad (2.15)$$

If $\varepsilon_a > \varepsilon_b$, then $n_a < n_b$ for a constant bulk volume and $\sigma_a > \sigma_b$ from Eq. (2.15). The distribution with larger elements ε_a has fewer elements and a smaller standard deviation. Let us recall at this point that the elements in the analysis are assumed to be small enough that they are either a pore or a grain. An analysis on a different scale would require a different treatment [for example, see Chapters 3 through 5, or Collins, 1961, Chapter 1].

Equation (2.15) shows that rock properties are functions of the averaging volume. The value of a rock property can vary within a scale and from one scale to another. An important task of reservoir characterization and associated integrated flow modeling is to find a suitable scale for developing a reservoir model that can be used to prepare reliable performance predictions.

Geostatistical Modeling

Geostatistical modeling can proceed at many different levels. One of the simplest applications is to perform a variogram analysis to help quantify reservoir anisotropy and spatial correlations of well log data such as porosity. One of the most complex applications is the preparation of multiple realizations for use in conditional simulation runs.

Although considerable work has been done to date, it is not always clear whether the geostatistical approach will generate a more accurate representation of the reservoir than would detailed analyses by experienced geologists and reservoir engineers. Unlike conventional geologic models, geostatistical models have the potential to quantify the range of error in the model.

Three principal objectives are usually associated with the development and application of geostatistical methods. They are:

- Assess the applicability of geostatistics to reservoir characterization and consequent fluid flow simulation.
- Improve the engineer's ability to make performance predictions for use in reservoir management.

- Transfer the effects of "data uncertainty" associated with reservoir modeling into uncertainties associated with performance predictions.
- Geostatistical objectives are achieved using semi-variogram models to identify spatial correlations of rock properties such as porosity and permeability.

The goal of a semi-variogram model is to model spatial correlations with the semi-variance $\gamma(h)$. Semi-variance is defined as

$$\gamma(h) = \frac{1}{2 N(h)} \sum_{i=1}^{N(h)} [Z(x_i) - Z(x_i - h)]^2 \quad (2.16)$$

where $Z(x_i)$ is the value of a spatially distributed property at the point x_i ; h is the spatial vector or "lag" distance between a data point at $x_i + h$ and the data point x_i ; and $N(h)$ is the number of data pairs that are approximately separated by the lag vector h . The lag vector h has both length and orientation, consequently the sum must account for both the length and orientation of data separation.

The semi-variogram model is usually depicted as a plot of semi-variance versus lag. An example of a semi-variogram model is shown in Figure 2-6. The

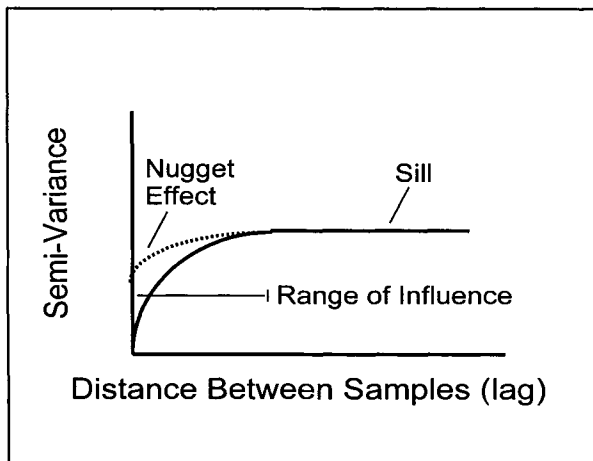


Figure 2-6. Sketch of a Semi-Variogram Model.

sill is the horizontal section of the semi-variogram. If the lag separation between data points is large enough to reach the sill of the semi-variogram, then the

24 Integrated Flow Modeling

data points have minimal influence on one another and are effectively uncorrelated. The nugget is the value of the semi-variance at zero lag.

2.5 Bulk Volume and Net Volume

The bulk volume of a block that is shaped like a parallelepiped is given by the triple scalar product

$$V_B = |\vec{U} \cdot (\vec{V} \times \vec{W})| \quad (2.17)$$

The vectors $\{\vec{U}, \vec{V}, \vec{W}\}$ are aligned along the axes of the parallelepiped and have magnitudes that are equal to the lengths of the sides of the parallelepiped

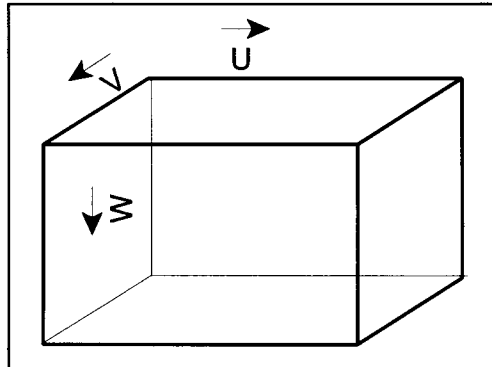


Figure 2-7 Triple Scalar Product.

(Figure 2-7). In Cartesian coordinates, we have the result

$$V_B = |L_x \hat{i} \cdot (L_y \hat{j} \times L_z \hat{k})| = L_x L_y L_z \quad (2.18)$$

in terms of the lengths $\{L_x, L_y, L_z\}$ of the sides of the Cartesian block.

Bulk volume V_B of an IFLO gridblock is the product of area A times gross thickness H :

$$V_B = AH \quad (2.19)$$

The area of a gridblock is the product of the x -direction block length Δx and the y -direction block length Δy , thus $A = \Delta x \Delta y$. Gross thickness H is the block length in the z -direction Δz .

Bulk volume is a measure of the gross volume in the system. It includes both rock volume and pore volume. To determine the volume of the system that is commercially significant, the gross volume must be adjusted by introducing the concept of net thickness.

Net thickness h is the thickness of the commercially significant formation. The net to gross ratio η is the ratio of net thickness h to gross thickness H :

$$\eta = h/H, \quad 0 \leq \eta \leq 1 \quad (2.20)$$

Net thickness is always less than or equal to gross thickness.

As an illustration, suppose gross thickness includes 4 feet of impermeable shale and 16 feet of permeable sandstone, the gross thickness is 20 feet and the net thickness is 16 feet. The net to gross ratio is 16 feet / 20 feet or 0.8. An inactive block, that is, a block that does not contribute to reservoir behavior, can be defined by setting either net to gross ratio to zero or net thickness to zero. Gross thickness should retain its nonzero value to preserve the correct physical structure in the vertical dimension.

Exercises

- 2-1. A. Sketch the grid in EXAM1.DAT (material balance).
B. Sketch the grid in EXAM2.DAT (vertical column).
C. Sketch the grid in EXAM3.DAT (Buckley-Leverett)
D. Sketch the grid in EXAM4.DAT (primary depletion)

- 2-2. A. Run EXAM3.DAT. When does water breakthrough occur (define water breakthrough as the time when WOR > 1%)? Hint: Change the maximum allowed time (TMAX in Section UM 2.9) to 730 days.
B. Change the pore volume multiplier in EXAM3.DAT from 0.5 to 1.0 and run the new data set. When does water breakthrough occur?
C. Compare the results in 2A and 2B and explain the difference in production performance. Include additional quantitative information if necessary.

26 Integrated Flow Modeling

2-3. If a gridblock does not effect the behavior of the model, it can be neglected by setting pore volume to 0. Specify which of the following two options is preferable and justify your selection: A. Set gross thickness to 0; or B. Set net thickness to 0.

2-4. Run RIM-2D.DAT (gas cap with oil rim). Plot a plan view (x-y view) of initial oil saturation. Hint: import the file into a spreadsheet and prepare a graph.

Chapter 3

Porosity

A value of porosity must be entered for every gridblock in the model. There are a variety of techniques for determining the porosity distribution. Examples of techniques include contouring and geostatistics. The approach presented here introduces important statistical concepts that help characterize the reservoir properties needed for integrated flow modeling.

3.1 Porosity Defined

Porosity is the fraction of a porous material that is pore space, that is, the space in the bulk volume that is not occupied by rock grains. Therefore, porosity is the ratio of pore volume to bulk volume:

$$\phi = \frac{V_p}{V_b} \quad (3.1)$$

where

ϕ = porosity [fraction]

V_p = pore volume within rock

V_b = bulk volume of rock

28 Integrated Flow Modeling

There are two types of porosity. Primary porosity is the original porosity in a porous medium that results from sediment deposition. Secondary porosity is the incremental increase in primary porosity due to chemical dissolution of reservoir rocks. Secondary porosity is especially significant in carbonates. Table 3-1 shows porosity values in different types of reservoir rock.

Table 3-1
Porosity and Lithology

<i>Reservoir Rock Type</i>	<i>Porosity Range, %</i>	<i>Typical Porosity, %</i>
Sandstone	15-35	25
Unconsolidated Sand	20-35	30
Carbonate		
• Intercrystalline limestone	5-20	15
• Oolitic limestone	20-35	25
• Dolomite	10-25	20

Porosity may be measured in the laboratory or *in situ*, that is, in the field. The advantages and disadvantages of the measurements are summarized in Table 3-2.

Table 3-2
Porosity Measurements

<i>Type of Measurement</i>	<i>Advantages</i>	<i>Disadvantages</i>
Lab measured ϕ (core analysis)	more accuracy	<ul style="list-style-type: none">• small fraction of reservoir sampled• <i>in situ</i> reservoir conditions may change ϕ measured under lab conditions (usually low pressure)
<i>In situ</i> measured ϕ (logs and well tests)	much larger part of reservoir is sampled	indirect measurement yields less accuracy

3.2 Net Pore Volume and Saturation

The value of porosity that is needed for modeling may be less than the actual porosity of the rock, because the model flow equations use a porosity that presumes the pore space is connected from one gridblock to another. Most porous media contain a fraction of pores that are not in communication with the flow path. This pore volume is ineffective. Effective pore space (V_P)_{eff} is the interconnected pore space that communicates with a well. Effective porosity is defined as the ratio of effective pore space to bulk volume, thus

$$\phi \equiv \frac{(V_P)_{\text{eff}}}{V_B} \quad (3.2)$$

Unless stated otherwise, any further discussion using porosity will assume that the porosity of interest is effective porosity, and the subscript "eff" will not be written.

Pore volume V_P is the product of bulk volume and porosity ϕ :

$$V_P = \phi V_B \quad (3.3)$$

where bulk volume is defined as area A times gross thickness H . The volume of net pay is the product of pore volume and net to gross ratio:

$$V_{\text{pay}} = \eta V_P = \eta H A \phi = h A \phi \quad (3.4)$$

The saturation S_ℓ of phase ℓ is the fraction of the volume of pore space occupied by phase ℓ . The volume V_ℓ of phase ℓ in the pay interval is the product of net pay volume and phase saturation:

$$V_\ell = S_\ell V_{\text{pay}} = S_\ell h A \phi \quad (3.5)$$

The sum of the saturations in the pay interval must equal one. If the system has N_ℓ phases, the saturation constraint is

$$\sum_{\ell=1}^{N_\ell} S_\ell = 1 \quad (3.6)$$

30 Integrated Flow Modeling

For an oil-water-gas system, the saturation constraint is $S_o + S_w + S_g = 1$ where the subscripts {*o*, *w*, *g*} refer to oil, water and gas respectively.

3.3 Statistics of Porosity Distributions

Many statistical concepts and mathematical relationships are applicable to the distribution of a variety of reservoir parameters. Following Collins [1985], we use porosity as an example to set forth several common statistical concepts and relationships.

Each block of volume *v* in Figure 3-1 has some value of the property in

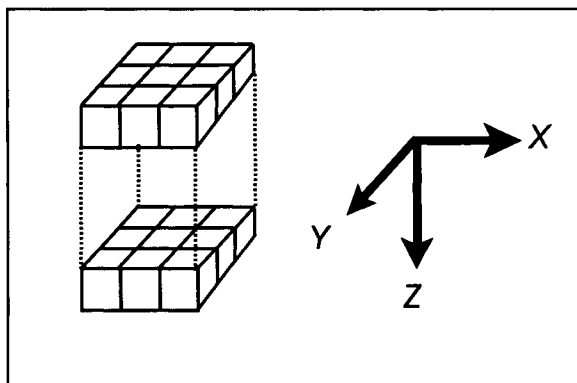


Figure 3-1. Ensemble of Elements.

question, such as porosity ϕ . The set of data that is needed to characterize the properties of each block is sometimes referred to as the “data volume.”

We define the probability for the porosity of a sample taken at the position $\{x, y, z\}$ to have a value between ϕ and $\phi + d\phi$ as

$$dP = \rho(\phi|x, y, z, v)d\phi \quad (3.7)$$

This is a conditional probability with the distribution function $\rho(\phi|x, y, z, v)$ conditioned by position in the reservoir $\{x, y, z\}$ and sample size *v*. For this distribution

$$P(\phi|x, y, z, v) = \int_0^\phi \rho(\phi'|x, y, z, v)d\phi' \quad (3.8)$$

is the probability that a sample of volume, v , taken from the reservoir at the center of the sample from location $\{x, y, z\}$, will be found to have porosity with a value between $\phi' = 0$ and $\phi' = \phi$. Since $0 \leq \phi' \leq 1$ is necessary, we have the normalization condition

$$\int_0^1 p(\phi' | x, y, z, v) d\phi' = 1; \quad (3.9)$$

with the interpretation that $0 \leq \phi' \leq 1$ is a certainty.

This statistical description does not apply to a specific reservoir because the actual spatial distribution of ϕ within a specific reservoir is fixed before we ever take a sample. What is visualized here is an ensemble of reservoirs exhibiting porosity between ϕ and $\phi + d\phi$ for the sample at $\{x, y, z\}$. Only through this abstract ensemble concept can we legitimately apply a probability formula to a particular reservoir.

Most studies assume that the probability distribution function for ϕ is the same at every point in the rock stratum. In other words, the probability distribution function $p(\phi | x, y, z, v)$ is independent of $\{x, y, z\}$ throughout the specific rock stratum in question. This assumption implies that the rock is statistically homogeneous with respect to ϕ for samples of volume v . We now examine the consequences of the assumption of statistical homogeneity.

An objective of statistical studies using core data is to determine the form of the statistically homogeneous distribution $p(\phi | v)$. The following method is based upon the Law of Large Numbers of probability theory. This law states that if an event $E = E_j$ from a set of J events has probability p_j , and out of N trials the event E_j is observed to occur N_j times, then the relationship between the observed frequency f_j of the event

$$f_j = \frac{N_j}{N} \quad (3.10)$$

and the probability P_j that the event E_j will occur is

$$\lim_{N \rightarrow \infty} |P_j - f_j| = 0 \quad (3.11)$$

32 Integrated Flow Modeling

If the number of trials is large enough, then P_j and f_j are arbitrarily close in value. The frequency of occurrence f_j of event j can then be used as the probability P_j that the event E_j will occur.

The Law of Large Numbers is applied to porosity data by dividing the interval $0 \leq \phi \leq 1$ into a countable number of class intervals, C_j for $j = 1, \dots, J$. Each observation of porosity is assigned to a class interval C_j corresponding to a porosity interval

$$\phi_j - \frac{\Delta\phi}{2} \leq \phi \leq \phi_j + \frac{\Delta\phi}{2} \quad (3.12)$$

where the $\phi_j, j = 1, 2, \dots, J$, are equally spaced values of ϕ . The probability P_j for ϕ to belong to class C_j is

$$P_j = \int_{\phi_j - \frac{\Delta\phi}{2}}^{\phi_j + \frac{\Delta\phi}{2}} \rho(\phi' | v) d\phi' \approx \rho(\phi_j | v) \Delta\phi \quad (3.13)$$

and

$$\phi_{j+1} = \phi_j + \Delta\phi \text{ for all } j \quad (3.14)$$

If we collect N_w core plug values for ϕ from the rock stratum penetrated by a well, and find N_{wj} of these plugs to have ϕ belonging to the class C_j , we have

$$f_{wj} = \frac{N_{wj}}{N_w} \approx \rho(\phi_j | v) \Delta\phi \quad (3.15)$$

by the Law of Large Numbers. Assuming Eq. (3.15) is an equality, we compute the distribution $\rho(\phi_j | v)$ for the set of porosity observations $\{\phi_j; j = 1, 2, \dots, J\}$ for a well.

Frequently, it is more convenient to retain the description of the porosity distribution in terms of the discrete class intervals C_j defined above rather than the continuous variable ϕ . For this we use Eq. (3.15) to define the frequency distribution of porosity in the samples from a well as f_{wj} . Then we can plot a histogram for porosity.

If the assumption of statistical homogeneity for this reservoir rock is correct, then applying the same procedure to the core data of another well should yield the same distribution, $\rho(\phi_j | v)$. Note, however, that in each well, the number of samples N_w must be sufficiently large that the two sides of Eq. (3.15) actually have “near the same value.” Often, this is not even close to being an equality because N_w is too small. Thus, we have what is called the sampling problem.

One solution to the sampling problem is to make N_w as large as possible within budgetary constraints. On the basis of the statistical homogeneity assumption, a simple way to increase the number of samples is to combine data from all wells into one frequency calculation. Thus, for the set of wells $\{w = 1, 2, \dots, W\}$ we have

$$N_j = \sum_{w=1}^W N_{wj} \quad (3.16)$$

for each class interval C_j , and the total number of samples is

$$N = \sum_{w=1}^W N_w \quad (3.17)$$

By summing over all of the wells, N can be many times larger than any of the N_w and we can use

$$\frac{N_i}{N} = \rho(\phi_j | v) \Delta \phi \quad (3.18)$$

to compute $\rho(\phi_j | v)$ from the core data with greater confidence.

A simple demonstration of the sampling problem and the need for data is shown by the moving average discussion in Fanchi [2000]. More elaborate demonstrations and studies are easily carried out, but the message here is clear – a lot of data is required to define the distribution function for any rock property.

How many samples must be collected to define the distribution function for some property of reservoir rock? Experience has shown that for core plugs, several hundred samples are needed to define the distribution function for

34 Integrated Flow Modeling

porosity, with one hundred plugs being a reasonable lower bound. It is often necessary to perform studies with less than this number of samples. When the sample data set is relatively small, the values of properties calculated from the data set should be viewed as approximations subject to refinement with the collection of additional information.

Studies of core data show that the probability distribution function (pdf) for porosity is the normal distribution, and the pdf for the logarithm of permeability is the normal distribution. The normal, or Gaussian, pdf for porosity ϕ with sample size v is given by the equation

$$\rho(\phi|v) = \frac{1}{\sqrt{2\pi}\sigma_\phi} e^{-\frac{(\phi-\bar{\phi})^2}{2\sigma_\phi^2}} \quad (3.19)$$

where $\bar{\phi}$ is the mean and σ_ϕ is the standard deviation of the pdf. For this pdf to apply, we require that

$$\rho(0|v) = 0 = \rho(1|v) \quad (3.20)$$

for otherwise the normalization condition

$$\int_0^1 \rho(\phi|v) d\phi = 1 \quad (3.21)$$

is not satisfied by Eq. (3.19).

Although the normal form for $\rho(\phi|v)$ is not always valid, it is reasonably satisfied. Let us assume Eq. (3.20) is satisfied and proceed to examine some properties of the normal distribution, $\rho(\phi|v)$, given in Eq. (3.19). In the process, we define some general terms that are applicable to other distributions.

The normal pdf in Eq. (3.19) is symmetric about the mean $\bar{\phi}$ such that

$$\rho(\bar{\phi} + \Delta\phi|v) = \rho(\bar{\phi} - \Delta\phi|v) \quad (3.22)$$

The number $\bar{\phi}$ is the most probable value for ϕ . It is the value of ϕ that satisfies the extremum condition

$$\frac{d\rho(\bar{\phi}|v)}{d\phi} = 0 \quad (3.23)$$

For the normal pdf, $\bar{\phi}$ is the arithmetic mean, or expectation value, defined by

$$\langle \phi \rangle = \int_0^1 \phi \rho(\phi|v) d\phi = \bar{\phi} \quad (3.24)$$

It is also the median value of the pdf, thus

$$P(\bar{\phi}|v) = \int_0^{\bar{\phi}} \rho(\phi|v) d\phi = \frac{1}{2} \quad (3.25)$$

The median is the value of ϕ for which one-half of all sample ϕ values fall below $\bar{\phi}$ and one-half above $\bar{\phi}$. The value of $\bar{\phi}$ is also the mode, or the value of ϕ that corresponds to the maximum value of the pdf. The equality of mean, median and mode is a mathematical equality that applies to any quantity described by a normal pdf.

The mean square variance of ϕ about $\bar{\phi}$, or the dispersion in ϕ about $\bar{\phi}$, is

$$\langle (\phi - \bar{\phi})^2 \rangle = \int_0^1 (\phi - \bar{\phi})^2 \rho(\phi|v) d\phi = \sigma_{\phi}^2 \quad (3.26)$$

and this is the square of the standard deviation, σ_{ϕ} , of the distribution.

The arithmetic mean value, $\langle \phi \rangle$, defined in Eq. (3.24) is one example of a class of mean values. In general, the m^{th} order mean is defined as

$$\langle \phi^m \rangle^{\frac{1}{m}} = \left[\int_0^1 \phi^m \rho(\phi|v) d\phi \right]^{\frac{1}{m}} \quad (3.27)$$

Thus, $m = 1$ is the arithmetic mean, $m = -1$ is the harmonic mean, and $m = 0$ is the geometric mean. It is important to note that the inequality

$$\langle \phi^m \rangle^{\frac{1}{m}} > \langle \phi^n \rangle^{\frac{1}{n}} \quad (3.28)$$

holds for any distribution if $m > n$. Using the letters A , G , H as subscripts to label arithmetic, geometric and harmonic mean values, we have for any type of distribution

$$\phi_A > \phi_G > \phi_H \quad (3.29)$$

36 Integrated Flow Modeling

We can understand why the distribution function for ϕ must be of the normal form for large sample size v by considering a central limit theorem from probability theory.

The Lyapunov Theorem

The Lyapunov theorem [Larsen and Marx, 1985, Section 7.4] is a central limits theorem. It shows how independent random variables behave when the number of independent random variables becomes very large. In particular, we are interested in the probability distribution $\rho(x)$ for x formed as the sum

$$x = x_1 + x_2 + \dots + x_n \quad (3.30)$$

of n independent random variables, x_i , $i = 1, 2, \dots, n$. Each random variable has the arithmetic mean $\langle x_i \rangle = 0$, and obeys a rather weak constraint on the forms of their individual distribution functions, $\rho_i(x_i)$. The independence of the x_i means that the distribution for any x_i does not depend on another of the x_j . When this weak constraint (which implies that the distributions $\rho_i(x_i)$ are not too "spread out" about $x = 0$) is satisfied, then the theorem asserts that $\rho(x)$ must have the normal form

$$\rho(x) = \frac{1}{\sqrt{2\pi}\sigma} e^{-\frac{x^2}{2\sigma^2}} \quad (3.31)$$

if n is sufficiently large. Here,

$$\sigma^2 = \sigma_1^2 + \sigma_2^2 + \dots + \sigma_n^2 \quad (3.32)$$

is the dispersion in x with the σ_i^2 , $i = 1, 2, \dots, n$ being the dispersions in the individual x_i . The Lyapunov Theorem shows that almost any random variable x which is the sum of a large number n of independent random variables will have a normal distribution.

Mathematical Basis for the Normal Distribution in Porosity

The Lyapunov theorem applies to porosity of rocks in the following way: we view any core plug of volume v as a collection of a large number n of elements, each of volume ϵ . Thus,

$$V = n\varepsilon \quad (3.33)$$

is the bulk volume and

$$V_p = \phi_1\varepsilon + \phi_2\varepsilon + \dots + \phi_n\varepsilon \quad (3.34)$$

is the pore volume of the sample. The porosities $\phi_j, j = 1, 2, \dots, n$ are porosities of the n elements and are statistically independent random variables. We assert that all of the ϕ 's have the same form of probability distribution, $\rho_1(\phi_1|\varepsilon)$. The probability distribution ρ_1 is not in general a normal form, but we assume it satisfies the conditions of the Lyapunov theorem.

$$\bar{\phi} = \frac{V_p}{V} = \frac{\phi_1 + \phi_2 + \dots + \phi_n}{n} \quad (3.35)$$

Equations (3.33) and (3.34) give the following expression for ϕ : Subtracting $\bar{\phi}$ from both sides of Eq. (3.35) lets us write

$$\phi - \bar{\phi} = \frac{\phi_1 - \bar{\phi}}{n} + \frac{\phi_2 - \bar{\phi}}{n} + \dots + \frac{\phi_n - \bar{\phi}}{n} \quad (3.36)$$

Then, substituting x for $\phi - \bar{\phi}$ and x_i for $(\phi_i - \bar{\phi})/n$, we see that $(\phi - \bar{\phi})$ is the sum of n independent random variables. Each random variable x has mean zero, in accordance with the Lyapunov theorem in Eq. (3.30), if $\bar{\phi}$ is the mean of ϕ_i under $\rho_i(\phi_i|\varepsilon)$. Therefore, we must have

$$\rho(\phi|V) = \frac{1}{\sqrt{2\pi}\sigma_\phi} e^{-\frac{-(\phi-\bar{\phi})^2}{2\sigma_\phi^2}} \quad (3.37)$$

for n large enough, and

$$\sigma_\phi^2 = \left\langle \frac{(\phi_1 - \bar{\phi})^2}{n^2} \right\rangle + \left\langle \frac{(\phi_2 - \bar{\phi})^2}{n^2} \right\rangle + \dots + \left\langle \frac{(\phi_n - \bar{\phi})^2}{n^2} \right\rangle \quad (3.38)$$

is the dispersion of the sum in Eq. (3.36).

Since the ϕ_i all have the same distribution, $\rho_i(\phi_i|\varepsilon)$, we have for all $i = 1, 2, \dots, n$,

$$\left\langle (\phi_i - \bar{\phi})^2 \right\rangle = \sigma_{\phi_i}^2 = \int_0^1 (\phi' - \bar{\phi})^2 \rho_1(\phi_1|\varepsilon) d\phi' \quad (3.39)$$

38 Integrated Flow Modeling

Substituting Eq. (3.39) into (3.38) gives

$$\sigma_{\phi}^2 = n(\sigma_{\phi_i}^2/n^2) = \sigma_{\phi_i}^2/n \quad (3.40)$$

Replacing n with Eq. (3.33) and simplifying lets us write

$$\sigma_{\phi} = \sqrt{\frac{\varepsilon}{n}} \sigma_{\phi_i} \quad (3.41)$$

The above derivation displays the conditions under which the distribution function for core plug porosities has the normal form with a standard deviation σ_{ϕ} . The standard deviation varies inversely as the square root of volume per sample v .

3.4 Characteristic Volume

Suppose we compute σ_{ϕ_1} for the distribution $\rho_1(\phi | \epsilon_0)$ for the special case of ϵ_0 so small that every sample is either solid sand grain or all pore space. We call ϵ_0 the characteristic volume element. For this case, the distribution $\rho_1(\phi | \epsilon_0)$ is expected to look essentially like Figure 3-2 with two large spikes around the porosity values 0 and 1.

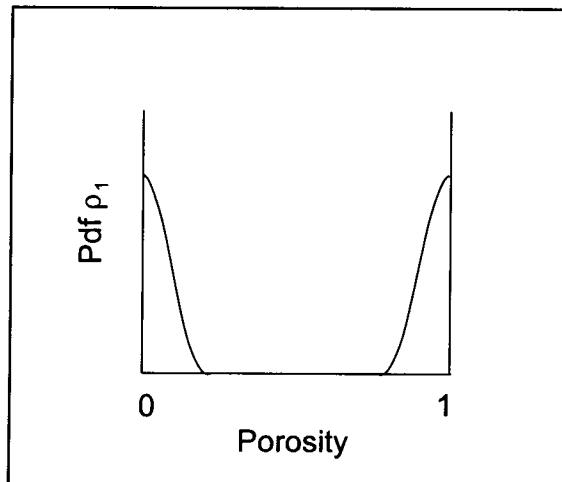


Figure 3-2. Porosity Distribution for Characteristic Sample Size.

For this distribution, we have from the definition of σ_{ϕ_1} ,

$$\sigma_{\phi_1}^2 = \int_0^1 (\phi - \bar{\phi})^2 p_1(\phi | \varepsilon_0) d\phi \approx (0 - \bar{\phi})^2(1 - \bar{\phi}) + (1 - \bar{\phi})^2 \bar{\phi} \quad (3.42)$$

or,

$$\sigma_{\phi_1} \approx \sqrt{\bar{\phi}(1 - \bar{\phi})} \quad (3.43)$$

Then we have for σ_ϕ the result

$$\sigma_\phi = \sqrt{\frac{\varepsilon_0}{n} \bar{\phi}(1 - \bar{\phi})} \quad (3.44)$$

The value of the characteristic volume ε_0 must be related to the size and uniformity of the pores of the rock. We can compute the value of ε_0 for a particular rock using observed values of σ_ϕ and $\bar{\phi}$ for samples of a given volume, v . Substituting the numbers used above, we solve for ε_0 and find

$$\varepsilon_0 = 5.1 \cdot 10^{-6} \text{ ft.}^3 \quad (3.45)$$

or in S.I. units,

$$\varepsilon_0 = 1.44 \cdot 10^{-1} \text{ cm}^3 \quad (3.46)$$

Thus, we see that for samples as small as 0.14 cc each sample should exhibit a porosity of either one or zero, approximately. In addition, if characteristic volume ε_0 and permeability are related to the uniformity and mean size of pores in the rock, we expect a correlation to exist between ε_0 and rock permeability.

Exercises

- 3-1. Run EXAM8.DAT (gas reservoir depletion).
 - A. What is OGIP?
 - B. When does the run end?
 - C. What is the average pressure at the end of the run?

- 3-2. Decrease pore volume in EXAM8.DAT by 25% and run the new data set.
 - A. What is OGIP?

40 *Integrated Flow Modeling*

- B. When does the run end?
 - C. What is the average pressure at the end of the run?
- 3-3. Explain the difference in production performance between Exercises 3-1 and 3-2. Include additional quantitative information to support your explanation if necessary. You may need to examine other output files to develop an understanding of reservoir model results.

Chapter 4

Permeability

The flow of fluids in a porous medium depends on the connectivity of pores. Permeability is a measure of pore connectivity in the equations describing fluid flow in porous media. It is discussed below in a variety of contexts ranging from its definition in terms of Darcy's law to permeability averaging techniques.

4.1 Darcy's Law

Darcy's Law is the basic equation describing fluid flow in porous media. Darcy's equation for single phase flow is

$$Q = -0.001127 \frac{KA}{\mu} \frac{\Delta P}{\Delta x} \quad (4.1)$$

where the physical variables are defined in oil field units as

- Q flow rate [bbl/day]
- K permeability [md]
- A cross-sectional area [ft^2]
- P pressure [psi]

42 Integrated Flow Modeling

μ fluid viscosity [cp]

Δx length [ft]

Darcy's Law says that rate is proportional to cross-sectional area times pressure difference ΔP across a length Δx , and is inversely proportional to the viscosity of the fluid. The minus sign shows that the direction of flow is opposite to the direction of increasing pressure; fluids flow from high pressure to low pressure in a horizontal (gravity-free) system. The proportionality constant is referred to as permeability.

Darcy's law is based on a linear relationship between flow rate and pressure difference:

$$q = -0.001127K \frac{A \Delta P}{\mu \Delta x} \text{ or } \frac{\Delta P}{\Delta x} = -\left(\frac{q}{0.001127A}\right) \frac{\mu}{K} \quad (4.2)$$

Dimensional analysis shows that permeability has dimensions of L^2 (area) where L is a unit of length:

$$\begin{aligned} K &= \frac{\text{rate} \times \text{viscosity} \times \text{length}}{\text{area} \times \text{pressure}} \\ &= \frac{\left(\frac{L^3}{\text{time}}\right)\left(\frac{\text{force} \times \text{time}}{L^2}\right)L}{L^2\left(\frac{\text{force}}{L^2}\right)} = L^2 \end{aligned} \quad (4.3)$$

The areal unit (L^2) is physically related to the cross-sectional area of pore throats in rock. Pore throat size is related to grain size. Larger grains generally create larger pore throats. In turn, larger pore throats imply a larger value of L^2 and correspondingly greater permeability.

Superficial Velocity and Interstitial Velocity

Darcy velocity is the superficial velocity u of the fluid, that is, it is the volumetric flow rate q divided by the macroscopic cross-sectional area A normal to flow [Bear, 1972; Lake, 1989], thus $u = q/A$ in appropriate units. The velocity of the fluid through the porous rock is called the interstitial, or "front", velocity.

The interstitial velocity v is the actual velocity of a fluid element as the fluid moves through the tortuous pore space in the porous medium. Interstitial velocity v is related to the superficial velocity u by the relation $v = u/\phi = uq/\phi A$ where ϕ is porosity. Thus, interstitial velocity is usually several times larger than superficial velocity.

Factors Affecting The Validity of Darcy's Law

The validity of Darcy's law depends on the flow regime. Flow regimes are classified in terms of the dimensionless Reynolds number [Fancher and Lewis, 1933]

$$N_{Re} = 1488 \frac{\rho v_D d_g}{\mu} \quad (4.4)$$

where

ρ fluid density [lbm/ft³]

v_D superficial (Darcy) velocity [ft/sec]

d_g average grain diameter [ft]

μ absolute viscosity [cp]

Reynolds number is the ratio of inertial (fluid momentum) forces to viscous forces. It can be used to distinguish between laminar and turbulent fluid flow (Table 4-1). A low Reynolds number corresponds to laminar flow, and a high Reynolds number corresponds to turbulent flow.

Table 4-1
Reynolds Number Classification of Flow Regimes

FLOW REGIME	DESCRIPTION [Govier, 1978, pg. 2-10]
Laminar	Low flow rates ($N_{Re} < 1$)
Inertial	Moderate flow rates ($1 < N_{Re} < 600$)
Turbulent	High flow rates ($N_{Re} > 600$)

44 Integrated Flow Modeling

The linearity of Darcy's law is an approximation that is made by virtually all commercial simulators. Fluid flow in a porous medium can have a nonlinear effect that is represented by the Forcheimer equation. Forcheimer noticed that turbulent flow had the quadratic pressure dependence

$$\frac{\Delta P}{\Delta x} = - \left(\frac{q}{0.001127A} \right) \frac{\mu}{K} + \beta \rho \left(\frac{q}{A} \right)^2 \quad (4.5)$$

for fluid with density ρ and turbulence factor β . A minus sign and unit is inserted in the first order rate term on the right hand side to be consistent with the rate convention used in Eq. (4.1). The nonlinear effect becomes more important in high flow rate gas wells.

Darcy's Law is valid if it is being used to describe laminar flow. Darcy's law does not account for turbulent flow caused by high flow rates. Permeability calculated from Darcy's law is less than true rock permeability at turbulent flow rates. The Forcheimer equation provides a more accurate relationship between pressure and turbulent flow rate than Darcy's law, but it also requires enough flow rate versus pressure data to determine the quadratic pressure dependence.

Radial Flow of Liquids

Darcy's law for steady-state, radial, horizontal liquid flow is

$$Q = - \frac{0.00708Kh(P_w - P_e)}{\mu B \ln(r_e / r_w)} \quad (4.6)$$

where

Q liquid flow rate [STB/D]

r_w wellbore or inner radius [ft]

r_e outer radius [ft]

K permeability [md]

h formation thickness [ft]

P_w pressure at inner radius [psi]

P_e pressure at outer radius [psi]

μ viscosity [cp]

B formation volume factor [RB/STB]

The inclusion of formation volume factor converts volumetric flow rate from reservoir to surface conditions.

Given the above expression for Darcy's law, the rate Q is positive for a production well $\{P_w < P_e\}$ and negative for an injection well $\{P_w > P_e\}$. The outer radius r_e is usually equated to the drainage radius of the well. Different procedures may be used to estimate r_e . The procedure depends on the application. For example, if a reservoir simulation is being conducted, the value of r_e depends on the gridblock size [Fanchi, 2000]. The error in rate determination associated with the estimate of r_e is less than a similar error associated with other parameters such as permeability because the radial flow calculation uses the logarithm of r_e . It is therefore possible to tolerate larger errors in r_e than other flow parameters and still obtain a reasonable value for radial flow rate.

Radial Flow of Gases

Consider Darcy's Law in radial coordinates:

$$q_r = -0.006328 \frac{2\pi rhK}{\mu} \frac{dP_r}{dr} \quad (4.7)$$

where distance is defined as positive moving away from the well, and

q_r gas rate [rcf/d]

r radial distance [ft]

h zone thickness [ft]

μ gas viscosity [cp]

K permeability [md]

P_r reservoir pressure [psia]

The subscript r denotes reservoir conditions. To convert to surface conditions, denoted by subscript s , we calculate

$$q_s = \frac{q_r}{B_g} \quad (4.8)$$

46 Integrated Flow Modeling

where

q_s gas rate [scf/d]

B_g gas formation volume factor [rcf/scf]

Gas formation volume factor B_g is given in terms of pressure P , temperature T and gas compressibility factor Z from the real gas equation of state as

$$B_g = \frac{P_s}{P_r} \frac{T_r}{T_s} \frac{Z_r}{Z_s} \quad (4.9)$$

The rate at surface conditions becomes

$$q_s = -0.03976 \frac{rhK}{\mu} \frac{P_r}{P_s} \frac{T_s}{T_r} \frac{Z_s}{Z_r} \frac{dP_r}{dr} \quad (4.10)$$

with q_s in scf/d.

If we assume a constant rate, we can rearrange Eq. (4.10) and integrate to get

$$q_s \int_{r_w}^{r_e} \frac{dr}{r} = q_s \ln \frac{r_e}{r_w} = -0.03976 \frac{KhT_s Z_s}{P_s T_r} \int_{P_w}^{P_r} \frac{P_r}{\mu Z_r} dP_r \quad (4.11)$$

Subscripts w and e denote values at the wellbore radius and external radius respectively. In terms of real gas pseudopressure $m(P)$, the radial form of Darcy's law becomes

$$q_s = -0.01988 \frac{KhT_s Z_s}{P_s T_r} \left(\ln \frac{r_e}{r_w} \right) \left[m(P_e) - m(P_w) \right] \quad (4.12)$$

Pseudopressure $m(P)$ is calculated by numerical integration of the pseudopressure equation

$$m(P) = 2 \int_{P_{ref}}^P \frac{P'}{\mu_g Z} dP' \quad (4.13)$$

and P_{ref} is a reference pressure (typically 0 psia). Specifying the standard conditions $Z_s = 1$, $P_s = 14.7$ psia and $T_s = 60^\circ\text{F} = 520^\circ\text{R}$ gives Darcy's law for the radial flow of gas:

$$q_s = -0.703 \frac{Kh}{T_r \left(\ln \frac{r_e}{r_w} \right)} [m(P_e) - m(P_w)] \quad (4.14)$$

Rearranging Eq. (4.14) gives

$$m(P_e) = m(P_w) - \frac{1.422 T_r \left(\ln \frac{r_e}{r_w} \right)}{Kh} q_s \quad (4.15)$$

which shows that $m(P_e)$ is proportional to q_s and inversely proportional to permeability.

4.2 Permeability

Permeability has meaning as a statistical representation of a large number of pores. A Micro Scale measurement of grain size distribution shows that different grain sizes and shapes affect permeability. Permeability usually decreases as grain size decreases. It may be viewed as a mathematical convenience for describing the statistical behavior of a given flow experiment. In this context, transient testing gives the best measure of permeability over a large volume. Despite its importance to the calculation of flow, permeability and its distribution will not be known accurately. Seismic data can help define the distribution of permeability between wells if a good correlation exists between seismic amplitude and a rock quality measurement that includes permeability.

Permeability depends on rock type. Clastic (sand and sandstone) reservoir permeability is usually provided by matrix pores, and is seldom influenced by secondary solution vugs. Natural or man-made fractures can contribute significant flow capacity in a clastic reservoir. Clean, unconsolidated sands may have permeabilities as high as 5 to 10 darcies. Compacted and cemented sandstone rocks tend to have lower permeabilities. Productive sandstone reservoirs usually have permeabilities in the range of 10 to 1000 md.

Carbonate reservoirs consist of limestone and dolomite. They are generally less homogeneous than clastic reservoirs and have a wider range of grain size distributions. Typically carbonates have very low matrix permeabilities, as low as 0.1 to 1.0 md in some cases, but carbonates often have extensive natural fracture systems. Significant permeability is possible from secondary porosity associated with features such as vugs and oolites.

The presence of clay can affect permeability. Clay material may swell on contact with fresh water, and the resulting swelling can reduce the rock's permeability by several orders of magnitude. This effect needs to be considered whenever an aqueous phase is being injected into a reservoir. Water compatibility tests should be designed to minimize the adverse interaction between injected water and the formation.

Porosity – Permeability Correlations

One task of the reservoir characterization process is to seek correlations between porosity and permeability. Several correlation schemes are possible, but the most common is to plot core porosity versus the log of permeability. The existence of straight line segments can be used to identify rock types and a correlation between porosity and permeability. The porosity-permeability relationship is often referred to as a phi-k crossplot.

Klinkenberg's Effect

Klinkenberg found that the permeability for gas flow in a porous medium depends on pressure according to the relationship

$$k_g = k_{abs} \left(1 + \frac{b}{P} \right) \quad (4.16)$$

where

k_g apparent permeability calculated from gas flow tests

k_{abs} true absolute permeability of rock

\overline{P} mean flowing pressure of gas in the flow system

b Klinkenberg's factor

The factor b is a constant for gas in a particular porous medium. When the factor $(1 + b/\bar{P}) \geq 1$, then $k_g \geq k_{abs}$. As pressure increases, $(1 + b/\bar{P})$ approaches 1 and k_g approaches k_{abs} .

The cause of the pressure dependence is the "slippage" of gas molecules along pore walls. At higher gas pressures, slippage along pore walls is reduced. At low pressures, the calculated permeability for gas flow k_g may be greater than true rock permeability. Measurements of k_g are often conducted with air and are not corrected for the Klinkenberg effect. This should be borne in mind when comparing k_g with permeability obtained from other sources, such as well tests.

4.3 Directional Dependence of Permeability

Up to this point in the discussion we have assumed that flow is occurring in a horizontal direction. In general, flow occurs in dipping beds. Let us define a new quantity called the potential of phase i as

$$\phi_i = P_i - \gamma_i(\Delta z) \quad (4.17)$$

here Δz is depth from a datum, P_i is the pressure of phase i , and γ_i is the pressure gradient. If we rewrite Darcy's law for single phase flow in the form

$$q = -\frac{0.001127KA}{\mu} \frac{d\phi}{dz} \quad (4.18)$$

we find that no vertical movement can occur when $d\Phi/dz = 0$. Thus, Eq. (4.18) expresses the movement of fluids in a form that accounts for gravity equilibrium. We have assumed in Eq. (4.18) that the value of permeability is the same in the horizontal and the vertical direction. Is this true? Does permeability depend on direction?

It is not unusual to find that permeability has a directional component: that is, permeability is larger in one direction than another [for example, see Fanchi, et al., 1996]. In one dimension, Darcy's law says that rate is proportional to pressure gradient. This can be expressed in vector notation for single phase flow as

$$\bar{q} = -0.001127 K \frac{A}{\mu} \nabla \Phi \quad (4.19)$$

where we are using the concept of potential to account for gravity effects. Equation (4.19) represents the following three-dimensional set of equations:

$$\begin{aligned} q_x &= -0.001127 K \frac{A}{\mu} \frac{\partial \Phi}{\partial x} \\ q_y &= -0.001127 K \frac{A}{\mu} \frac{\partial \Phi}{\partial y} \\ q_z &= -0.001127 K \frac{A}{\mu} \frac{\partial \Phi}{\partial z} \end{aligned} \quad (4.20)$$

Equation (4.20) can be written in matrix notation as

$$\begin{bmatrix} q_x \\ q_y \\ q_z \end{bmatrix} = -0.001127 K \frac{A}{\mu} \begin{bmatrix} \partial \Phi / \partial x \\ \partial \Phi / \partial y \\ \partial \Phi / \partial z \end{bmatrix} \quad (4.21)$$

where permeability K is treated as a single constant. A more general extension of Eq. (4.21) is

$$\begin{bmatrix} q_x \\ q_y \\ q_z \end{bmatrix} = -0.001127 \frac{A}{\mu} \begin{bmatrix} K_{xx} & K_{xy} & K_{xz} \\ K_{yx} & K_{yy} & K_{yz} \\ K_{zx} & K_{zy} & K_{zz} \end{bmatrix} \begin{bmatrix} \partial \Phi / \partial x \\ \partial \Phi / \partial y \\ \partial \Phi / \partial z \end{bmatrix} \quad (4.22)$$

where permeability is now treated either as a 3×3 matrix with 9 elements or a tensor of rank two (a vector is a tensor of rank one and a scalar is a tensor of rank zero). The diagonal permeability elements $\{K_{xx}, K_{yy}, K_{zz}\}$ represent the usual dependence of rate in one direction on pressure differences in the same direction. The off-diagonal permeability elements $\{K_{xy}, K_{xz}, K_{yx}, K_{yz}, K_{zx}, K_{zy}\}$ account for the dependence of rate in one direction on pressure differences in orthogonal directions. Expanding Eq. (4.22) gives the corresponding set of three equations demonstrating this dependence:

$$\begin{aligned} q_x &= -0.001127 \frac{A}{\mu} \left[K_{xx} \frac{\partial \Phi}{\partial x} + K_{xy} \frac{\partial \Phi}{\partial y} + K_{xz} \frac{\partial \Phi}{\partial z} \right] \\ q_y &= -0.001127 \frac{A}{\mu} \left[K_{yx} \frac{\partial \Phi}{\partial x} + K_{yy} \frac{\partial \Phi}{\partial y} + K_{yz} \frac{\partial \Phi}{\partial z} \right] \\ q_z &= -0.001127 \frac{A}{\mu} \left[K_{zx} \frac{\partial \Phi}{\partial x} + K_{zy} \frac{\partial \Phi}{\partial y} + K_{zz} \frac{\partial \Phi}{\partial z} \right] \end{aligned} \quad (4.23)$$

It is mathematically possible to find a coordinate system $\{x', y', z'\}$ in which the permeability tensor has the diagonal form

$$\begin{bmatrix} K_{x'x'} & 0 & 0 \\ 0 & K_{y'y'} & 0 \\ 0 & 0 & K_{z'z'} \end{bmatrix}$$

The coordinate axes $\{x', y', z'\}$ are called the principal axes of the tensor and the diagonal form of the permeability tensor is obtained by a principal axis transformation. The flow equations along the principal axes are

$$\begin{aligned} q_{x'} &= -0.001127 \frac{A}{\mu} \left[K_{x'x'} \frac{\partial \Phi}{\partial x'} \right] \\ q_{y'} &= -0.001127 \frac{A}{\mu} \left[K_{y'y'} \frac{\partial \Phi}{\partial y'} \right] \\ q_{z'} &= -0.001127 \frac{A}{\mu} \left[K_{z'z'} \frac{\partial \Phi}{\partial z'} \right] \end{aligned} \quad (4.24)$$

The principal axes in a field can vary from one point of the field to another because of permeability heterogeneity.

In principle, simulators can account for directional dependence using Eq. (4.23). In practice, however, the tensor permeability discussed in the literature by, for example, Bear [1972] and Lake [1988], is seldom reflected in a simulator. Most reservoir simulators assume the model of a reservoir is based on a coordinate system that diagonalizes the tensor as in Eq. (4.24). This is usually not the case, and can lead to numerical errors [Fanchi, 1983]. Modelers are beginning to realize that the full permeability tensor is needed to adequately

represent fluid flow in flow models that are using a coarser representation than their associated reservoir models [Fanchi, 2000].

The form of the permeability tensor depends on the physical medium, typically a reservoir formation. The medium is said to be anisotropic if two or more elements of the diagonalized permeability tensor are different. If the elements of the diagonalized permeability tensor are equal so that

$$K_{x'x'} = K_{y'y'} = K_{z'z'} = K \quad (4.25)$$

then the medium is said to be isotropic in permeability. In other words, permeability does not depend on direction. If the isotropic permeability does not change from one position in the medium to another, the medium is said to be homogeneous in permeability, otherwise it is considered heterogeneous. Most reservoirs exhibit some degree of anisotropy and heterogeneity.

Vertical Permeability

Horizontal permeability is usually the permeability for flow in the direction parallel to the plane of deposition, while vertical permeability is usually the permeability for flow in the direction transverse to the plane of deposition. These directions can be effectively interchanged if a formation has a high dip angle.

Vertical permeability can be measured in the laboratory or in pressure transient tests conducted in the field. In many cases vertical permeability is not measured and must be assumed. A rule of thumb is to assume vertical permeability is approximately one tenth of horizontal permeability. These are reasonable assumptions when there is no data to the contrary.

4.4 Permeability Averaging

Permeability averaging poses a problem in the estimation of a representative average permeability for use in Darcy's equation. Several techniques exist for estimating an average value. A few of the simplest are presented in this section, while a more rigorous analysis is presented in Chapter 5. The procedure for calculating the average permeability is presented for linear flow

in parallel beds. Similar procedures apply to the other permeability averaging techniques.

Parallel Beds — Linear Flow

Linear flow through parallel beds of differing permeability is illustrated in Figure 4-1.

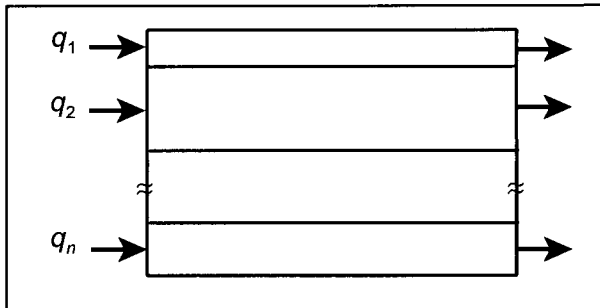


Figure 4-1. Beds in Series.

Pressure is constant at each end of the flow system, and total flow rate is the sum of the rates q_i in each layer i :

$$q = \sum_i q_i \quad (4.26)$$

Suppose layer i has length L , width w , net thickness h_i and permeability k_i . Applying Darcy's Law for linear flow of a fluid with viscosity μ gives

$$\frac{k_{ave} h_t w (p_1 - p_2)}{\mu L} = \sum_i \frac{k_i h_i w (p_1 - p_2)}{\mu L} \quad (4.27)$$

where the sum is over all layers. After canceling common terms, we obtain the expression

$$k_{ave} h_t = \sum_i k_i h_i \quad (4.28)$$

where h_t is total thickness and k_{ave} is an average permeability. Solving for k_{ave} gives

$$k_{ave} = \frac{\sum_i k_i h_i}{\sum_i h_i} \quad (4.29)$$

54 Integrated Flow Modeling

Average permeability for parallel flow through beds of differing permeabilities equals the thickness weighted average permeability. If the thickness of all beds is equal, k_{ave} is the arithmetic average.

Parallel Beds — Radial Flow

The average permeability for radial flow in parallel beds is the same relationship as linear flow, namely weighted average:

$$k_{ave} = \frac{\sum_i k_i h_i}{\sum_i h_i} \quad (4.30)$$

Beds in Series — Linear Flow

The average permeability for beds in series is the harmonic average:

$$k_{ave} = \frac{\sum_i L_i}{\sum_i L_i / k_i} \quad (4.31)$$

where bed i has length L_i and permeability k_i .

Beds in Series — Radial Flow

For a system with three beds, the average permeability for radial flow in beds in series is the harmonic average:

$$k_{ave} = \frac{\ln(r_e / r_w)}{\frac{\ln(r_e / r_2)}{k_3} + \frac{\ln(r_2 / r_1)}{k_2} + \frac{\ln(r_1 / r_w)}{k_1}} \quad (4.32)$$

where r_e is the radius to the outer ring and corresponds to the drainage radius of the system.

Random Flow

For permeability values distributed randomly, the average permeability is a geometric average:

$$k_{ave} = \left(k_1^{h_1} \cdot k_2^{h_2} \cdot k_3^{h_3} \cdots k_n^{h_n} \right)^{1/\sum_{i=1}^n h_i} \quad (4.33)$$

where h_i is the thickness of interval i with permeability k_i , and n is the number of intervals.

Permeability Averaging in a Layered Reservoir

The average permeability for a layered reservoir can be estimated using the following procedure:

Determine the geometric average for each layer.

Determine the arithmetic average of the geometric averages, weighted by the thickness of each layer.

Several other procedures exist for determining the average permeability of a layered reservoir. One method that can be applied with relative ease is to perform a flow model study using two models. One model is a cross-section model with all of the geologic layers treated as model layers. The other model is a single layer model with all of the geologic layers combined in a single layer. Flow performance from the cross-section model is compared with the flow performance of the single layer model. Permeability in the single layer model is adjusted until the performance of the single layer model is approximately equal to the performance of the cross-section model. The resulting permeability is an “upscaled”, or average permeability, for the cross-section model.

Exercises

- 4-1. A. Run EXAM7.DAT (SPE1 example) and specify time, pressure, oil rate, GOR, and cumulative oil and gas production at end of run.
 B. Double all permeability values in EXAM7.DAT and specify time, pressure, oil rate, GOR, and cumulative oil and gas production at end of run.
 C. What was the effect of doubling permeability?
 D. Set all vertical permeabilities to 0 in the original data set and specify time, pressure, oil rate and GOR at end of run.
 E. What was the effect of setting vertical permeability to 0?

56 Integrated Flow Modeling

- 4-2. A. Run EXAM8.DAT (gas reservoir) for 730 days and specify time, pressure and gas rate at the end of the run.
- B. Set vertical permeability = one tenth of horizontal permeability in EXAM8.DAT and rerun the model for 730 days. Specify time, pressure and gas rate at the end of the run.
- C. What was the effect of changing vertical permeability?

Chapter 5

Critical Sample Size

Collins [1985] developed a procedure for estimating the critical sample size needed to conduct a statistical analysis of rock properties. This procedure is presented here to demonstrate how much data should be obtained for a statistically significant analysis of rock properties. Equations for estimating critical sample size are provided for both porosity and permeability.

5.1 Critical Sample Size for Porosity

The normal form for the conditional distribution of porosity $\rho(\phi | v)$ given a sample volume v with a standard deviation σ_ϕ is given by Eq. (3.37). It shows that distributions of ϕ constructed using two different sample sizes having volumes v_a and v_b respectively should have standard deviations $\sigma_{\phi a}$ and $\sigma_{\phi b}$ in the ratio

$$\frac{\sigma_{\phi a}}{\sigma_{\phi b}} = \sqrt{\frac{V_b}{V_a}} \quad (5.1)$$

Equation (5.1) assumes that the ϕ 's have the same distribution $\rho_i(\phi_i | e)$ for both sample sizes. Sample distributions are sketched in Figure 5-1.

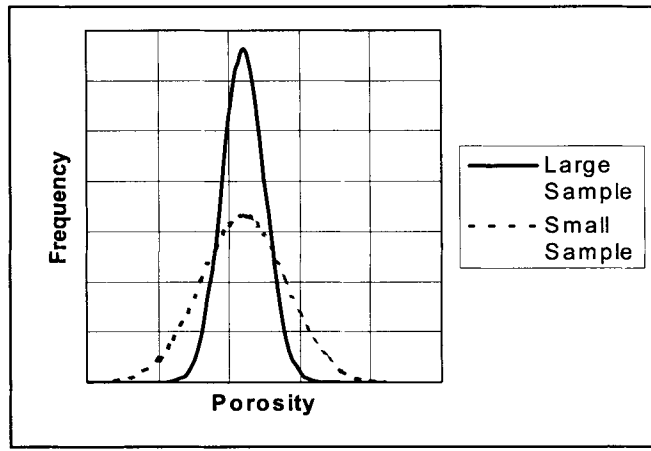


Figure 5-1. Effect of Sample Size on Porosity Distribution.

For samples of sufficiently large volume, the variance, or dispersion, in ϕ about $\bar{\phi}$ can be made so small that statistical variations in ϕ might be totally negligible. The sample volume v_c for which this is the case is the critical sample size v_c defined by the following procedure.

From the distribution $\rho(\phi|v_c)$ in ϕ for samples of volume v_c we can construct the probability P of finding a sample with porosity ϕ such that

$$|\phi - \bar{\phi}| > \delta = 0.01\bar{\phi} \quad (5.2)$$

The inequality in Eq. (5.2) corresponds to an “error” in ϕ of 1%.

Using the distribution given by Eq. (3.37) and the definition of dP in Eq. (3.7) we have

$$P = P(|\phi - \bar{\phi}| > \delta | v_c) = 1 - \int \frac{1}{\sqrt{2\pi}\sigma_{\phi c}} e^{-\frac{(\phi-\bar{\phi})^2}{2\sigma_{\phi c}^2}} d\phi \quad (5.3)$$

since probability is normalized to unity. This is rearranged to the more tractable form

$$P = 1 - \frac{2}{\sqrt{\pi}} \int_0^{\frac{\delta}{\sqrt{2\sigma_{\phi c}}}} e^{-x^2} dx \quad (5.4)$$

The integral

$$\frac{2}{\sqrt{\pi}} \int_0^{\frac{\delta}{\sqrt{2}\sigma_{\phi c}}} e^{-x^2} dx = \operatorname{erf}\left(\frac{\delta}{\sqrt{2}\sigma_{\phi c}}\right) \quad (5.5)$$

is the error function with argument $y = \delta/\sqrt{2}\sigma_{\phi c}$.

We now set $P = 0.01$ for one chance in a hundred of observing $|\phi - \bar{\phi}| > \delta$. A table for $\operatorname{erf}(y)$ is used to solve

$$0.01 = 1 - \operatorname{erf}(y) \quad (5.6)$$

for the value of y . This gives $y = 1.535$, or

$$\frac{\delta}{\sigma_{\phi c}} = 2.578 \quad (5.7)$$

Recalling the definition of δ from Eq. (5.2) gives

$$\sigma_{\phi c} = \frac{0.01\bar{\phi}}{2.578} = 3.88 \cdot 10^{-3}\bar{\phi} \quad (5.8)$$

Now this can be used with Eq. (5.1) to obtain an explicit expression for the value of v_c that yields this value of $\sigma_{\phi c}$, i.e. we use

$$\frac{\sigma_{\phi c}}{\sigma_\phi} = \sqrt{\frac{v}{v_c}} \quad (5.9)$$

for $\sigma_{\phi c}$ in Eq. (5.8) and solve for v_c . The result is

$$v_c = 6.65 \cdot 10^4 \frac{v \sigma_\phi^2}{\bar{\phi}^2} \quad (5.10)$$

where σ_ϕ is the standard deviation observed for a sample of volume v .

The above results have the following interpretation. If we examine a rock stratum using samples each of volume v_c , as defined by Eq. (5.10), there is only one chance in a hundred that a sample will be found with ϕ differing from $\bar{\phi}$ by more than one percent. As an example, suppose $\bar{\phi} = 0.279$ and $\sigma_\phi = 0.03$ for conventional core plugs which are typically one inch in diameter

60 Integrated Flow Modeling

and about 2.5 inches long. We calculate v to be about $1.136 \cdot 10^{-3}$ ft.³. Inserting these numbers into Eq. (5.10) we compute the critical sample size

$$v_c = 0.873 \text{ ft.}^3 \quad (5.11)$$

which is equivalent to the combined volume of about 769 core plugs.

In assessing the significance of v_c , we could change P from “one chance in a hundred” to “one chance in a thousand.” The only change in Eq. (5.10) for v_c is an increase in the numerical factor from 6.65 to 15.38. This changes v_c in our example from about 0.873 ft.³ to about 2.01 ft.³.

5.2 Permeability Distributions

The statistical procedure used to analyze porosity in Chapter 3 [Collins, 1985] is applied to the analysis of permeability in this section. Distribution functions for permeability in rock strata have an apparently good description using the normal form

$$dP(\ln K | v) = \frac{e^{-\frac{(\ln K - \ln K_G)^2}{2\sigma_K^2}}}{\sqrt{2\pi}\sigma_K} d(\ln K) \quad (5.12)$$

with an anticipated dependence on the standard deviation σ_K of the log normal distribution of permeability, and possibly the geometric mean of permeability sample volume v . The geometric mean of the distribution is defined by

$$\ln K_G = \langle \ln K \rangle \quad (5.13)$$

where $\langle \ln K \rangle$ is the expectation value, or average, of $\ln K$. The variance σ_K^2 is

$$\sigma_K^2 = \langle [(\ln K) - (\ln K_G)]^2 \rangle \quad (5.14)$$

A more conventional definition for the geometric mean K_G is derived from Equation (5.13) as follows.

Suppose we partition $\ln K$ into class intervals of equal width centered on $\ln K_j$ with $\{j = 1, 2, \dots, J\}$. We have from Eq. (5.13) the relation

$$\langle \ln K \rangle = \sum_{j=1}^J (\ln K_j) f_j \quad (5.15)$$

with f_j the fraction of data in the class interval $\ln K_j - (\Delta \ln K)/2$ to $\ln K_j + (\Delta \ln K)/2$. We express f_j in terms of a probability distribution function $p(\ln K | v)$ as

$$f_j = \int_{\ln K_j - \Delta \ln K/2}^{\ln K_j + \Delta \ln K/2} p(\ln K | v) d\ln K = \frac{N_j}{N} \quad (5.16)$$

where a number N_j of N samples have $\ln K$ in this class interval. With this, we can write Eq. (5.15) as

$$\ln K_G = \sum_{j=1}^J \frac{N_j}{N} (\ln K_j) \quad (5.17)$$

Let $\{K_i\}$ be the set of N sample values for the individual samples. The value $\ln K_i \approx \ln K_j$ occurs N_j times for the j^{th} class interval. Equation (5.17) becomes

$$\ln K_G = \sum_{i=1}^N \frac{\ln K_i}{N} = \frac{1}{N} \ln \prod_{i=1}^N K_i \quad (5.18)$$

This form then gives

$$K_G = [K_1 K_2 K_3 \dots K_N]^{\frac{1}{N}} \quad (5.19)$$

as the direct calculation of the geometric mean value of K from N sample values.

The m^{th} order mean is the geometric mean as $m \rightarrow 0$, thus

$$K_G = \lim_{m \rightarrow 0} \langle K^m \rangle^{\frac{1}{m}} \quad (5.20)$$

We can write Eq. (5.20) in the equivalent form

$$K_G = \lim_{m \rightarrow 0} \langle e^{m \ln K} \rangle^{\frac{1}{m}} \quad (5.21)$$

and perform a series expansion of the exponential to obtain

$$K_G = \lim_{m \rightarrow 0} \left\langle 1 + m \ln K + \frac{m^2}{2!} (\ln K)^2 + \dots \right\rangle^{\frac{1}{m}} \quad (5.22)$$

62 Integrated Flow Modeling

This is equivalent, in the limit, to

$$K_G = \lim_{m \rightarrow 0} [1 + m \langle \ln K \rangle]^{\frac{1}{m}} \quad (5.23)$$

Comparing Eq. (5.23) with the limit form of the exponential [Larsen, et al., 1990, pg. 361]

$$\lim_{n \rightarrow \infty} \left(1 + \frac{1}{n} x \right)^n = e^x \quad (5.24)$$

shows that

$$K_G = \exp \langle \ln K \rangle \quad (5.25)$$

where $m = 1/n$. Equation (5.25) is equivalent to Eq. (5.13).

The Basis for Log-Normal Permeability Distributions

The log-normal form for permeability distributions is generally accepted as the correct form for statistically homogeneous rocks. We demonstrate here that the log-normal form applies to a wide class of porous media if some reasonable assumptions are satisfied.

We begin with the postulate that, for a sufficiently large sample of any uncorrelated, statistically homogenous porous medium, the permeability of the sample is the geometric mean of the elements making up the sample. Furthermore, we view a core plug as made up of n elements, each of volume ϵ , having permeabilities K_1, K_2, \dots, K_n drawn at random without correlation from a parent population having some probability distribution $p_1(K|\epsilon)$. Like porosity, the permeabilities $\{K_j\}$ are permeabilities of the n elements and are statistically independent random variables with mean zero. We assume n to be large enough that with negligible error the permeability of the core plug is, by the above postulate,

$$K = (K_1 K_2 K_3 \cdots K_n)^{\frac{1}{n}} \quad (5.26)$$

Taking the natural logarithm of Eq. (5.25) gives

$$\ln K = \frac{\ln K_1}{n} + \frac{\ln K_2}{n} + \cdots + \frac{\ln K_n}{n} \quad (5.27)$$

and $\ln K$ is a random variable with some distribution function.

The geometric mean, K_G , of the distribution $\rho(K|\epsilon)$ is

$$\ln K_G = \langle \ln K_1 \rangle_1 = \int_0^\infty (\ln K) \rho_1(k|\epsilon) dK \quad (5.28)$$

where we assume $\rho_1(K|\epsilon)$ applies to each K_i , and the limits of the integral over K range from 0 to ∞ . Subtracting $\ln K_G$ from both sides of Eq. (5.26) gives

$$\ln \frac{K}{K_G} = \frac{\ln(K_1 / K_G)}{n} + \frac{\ln(K_2 / K_G)}{n} + \dots + \frac{\ln(K_n / K_G)}{n} \quad (5.29)$$

Given the assumption preceding Eq. (5.29), we see that $\ln K/K_G$ is a random variable with mean zero formed as the sum of n statistically independent random variables each with mean zero. Therefore, if the $\rho_i(K_i|\epsilon)$ satisfy reasonable constraints and n is sufficiently large, we have, from the Central Limits theorem, the result that $\ln K/K_G$ is normally distributed with mean zero. Thus, the distribution is

$$\rho(\ln K | v) = \frac{e^{-\frac{(\ln K - \ln K_G)^2}{2\sigma_K^2}}}{\sqrt{2\pi}\sigma_K} \quad (5.30)$$

with variance

$$\sigma_K^2 = \frac{1}{n^2} \left\langle \left(\ln \frac{K_1}{K_G} \right)^2 \right\rangle + \frac{1}{n^2} \left\langle \left(\ln \frac{K_2}{K_G} \right)^2 \right\rangle + \dots + \frac{1}{n^2} \left\langle \left(\ln \frac{K_n}{K_G} \right)^2 \right\rangle \quad (5.31)$$

There are n terms in Eq. (5.30). Each of the expectation values on the right has the same value σ_{K1}^2 , so

$$\sigma_K^2 = \frac{1}{n} \sigma_{K1}^2 \quad (5.32)$$

Also n is just v/ϵ , so we have

$$\sigma_K = \sqrt{\frac{\epsilon}{v}} \sigma_{K1} \quad (5.33)$$

64 Integrated Flow Modeling

Thus, the dispersion in $\ln K$ about $\ln K_G$ varies inversely as the sample volume v .

The preceding analysis shows that the log normal form for permeability distributions has a similar basis to the normal form for porosity distribution if Eq. (5.25) is valid. Both porosity and the logarithm of permeability exhibit a "spread," or standard deviation, that varies inversely as the square root of sample volume v .

5.3 Critical Sample Size for Permeability

In view of the results of the previous section all of the arguments used to define and calculate a critical sample size for porosity can be applied to the logarithm of permeability. Thus, we begin by noting from Eq. (5.32) that for sample volumes v_a and v_b we have

$$\frac{\sigma_{K_a}}{\sigma_{K_b}} = \sqrt{\frac{v_b}{v_a}} \quad (5.34)$$

in analogy with the standard deviation for porosity σ_ϕ .

We define the critical sample size v_c as that sample volume which yields only one chance in a hundred for an error in $\ln K$ to exceed a difference δ_K , thus

$$|\ln K - \ln K_G| > \delta_K \quad (5.35)$$

This definition differs slightly from the definition of critical sample size for porosity because we are working here with $\ln K$ rather than K itself. Note that for $|K - K_G|$ small we have

$$|\ln K - \ln K_G| \approx \frac{|K - K_G|}{K_G} \quad (5.36)$$

In this case, Eq. (5.34) appears as

$$|K - K_G| > \delta_K K_G \quad (5.37)$$

This is the same form as our discussion of porosity in which we replaced δ_K with the factor 0.01.

We use Eq. (5.33) to find an expression for critical volume v_{CK} associated with the standard deviation σ_{KC} in the form

$$\frac{\sigma_{CK}}{\sigma_K} = \sqrt{\frac{v}{v_{CK}}} \quad (5.38)$$

The standard deviation σ_{CK} is the standard deviation of the normally distributed variable $\ln K$ which satisfies

$$P(|\ln K - \ln K_G| > \delta_K) = 1 - \text{erf}\left(\frac{\delta_K}{\sqrt{2}\sigma_{KC}}\right) \quad (5.39)$$

with $P = 0.01$. This yields

$$\frac{\delta_K}{\sigma_{KC}} = 2.578 \quad (5.40)$$

Note that δ_K refers to error in $\ln K$, and σ_{KC} to the standard deviation in $\ln K$.

Combining equations (5.37) and (5.39) gives

$$v_{CK} = \frac{6.65v}{\delta_K^2} \sigma_K^2 \quad (5.41)$$

as the general equation to be used to compute v_{CK} . From the example in Chapter 5.1, $v = 1.136 \times 10^{-3} \text{ ft.}^3$ and a reasonable value of σ_K is 0.87. If we require $\delta_K = 0.01$, we find

$$v_{CK} = \frac{(6.65)(1.136 \cdot 10^{-3})(0.87)^2}{10^{-4}} \quad (5.42)$$

or

$$v_{CK} = 57.2 \text{ ft.}^3 \quad (5.43)$$

Therefore, in this example we would need a sample with a volume of about 57 ft.^3 to have only one chance in a hundred for the permeability to differ from the "true" permeability, K_G , by more than one percent, i.e. $\delta_K = 0.01$ in Eq.

(5.36). By contrast, the critical sample size for porosity is 0.873 ft^3 . The sample size needed to obtain a negligible dispersion in ϕ about $\bar{\phi}$ is much smaller than the sample size needed to obtain a negligible dispersion in $\ln K$ about $\ln \bar{K}$. If we recall here that permeability from pressure transient testing is an effective permeability for a large volume, the above analysis shows that the well test permeability has a better chance of being a more reliable average permeability for the drainage area of the well than permeability from core plugs.

5.4 Measures of Permeability Heterogeneity

It is often useful to represent permeability heterogeneity with a single number. This number is referred to here as a measure of permeability heterogeneity. Several such measures exist [Lake and Jensen, 1989]. The Dykstra-Parsons coefficient and the Lorenz coefficient are described in this section as illustrations. The procedure outlined below makes some simplifying assumptions that are not too restrictive in practice, but make it possible to calculate permeability heterogeneity measures with relative ease. These measures may be used to verify that the permeability distribution used in a model has comparable heterogeneity to the permeability distribution observed in an analysis of field data.

Dykstra-Parsons Coefficient

The Dykstra-Parsons coefficient can be estimated for a log normal permeability distribution as

$$V_{DP} = 1 - \exp \left[-\sqrt{\ln(k_A/k_H)} \right] \quad (5.44)$$

where k_A is the arithmetic average

$$k_A = \frac{1}{n} \sum_{i=1}^n k_i \quad (5.45)$$

and k_H is the harmonic average

$$\frac{1}{k_H} = \frac{1}{n} \sum_{i=1}^n \frac{1}{k_i} \quad (5.46)$$

The Dykstra-Parsons coefficient should be in the range $0 \leq V_{DP} \leq 1$. For a homogeneous reservoir, $V_{DP} = 0$ because $k_A = k_H$. An increase in heterogeneity increases V_{DP} . Typical values of the Dykstra-Parsons coefficient are in the range $0.4 \leq V_{DP} \leq 0.9$.

As an example of a Dykstra-Parsons coefficient calculation, suppose we have a 3-layer case with the following permeabilities:

Layer 1: $k = 35$ md

Layer 2: $k = 48$ md

Layer 3: $k = 126$ md

The arithmetic average is

$$k_A = \frac{1}{n} \sum_{i=1}^n k_i = \frac{1}{3}(126 + 48 + 35) = 69.7$$

and the harmonic average is

$$\frac{1}{k_H} = \frac{1}{n} \sum_{i=1}^n \frac{1}{k_i} = \frac{1}{3} \left(\frac{1}{126} + \frac{1}{48} + \frac{1}{35} \right)$$

or $k_H = 52.3$ md. Using these average values, we estimate the Dykstra-Parsons coefficient for a log normal permeability distribution to be

$$V_{DP} = 1 - \exp[-\sqrt{\ln(69.7/52.3)}] = 1 - \exp[-0.536] = 0.415$$

Lorenz Coefficient

The Lorenz coefficient requires a bit more work than the Dykstra-Parsons coefficient. We begin by calculating the following quantities:

$$F_m = \text{cum flow capacity} = \sum_{i=1}^m k_i h_i / \sum_{i=1}^n k_i h_i; \quad m = 1, \dots, n \quad (5.47)$$

and

$$H_m = \text{cum thickness} = \sum_{i=1}^m h_i / \sum_{i=1}^n h_i; \quad m = 1, \dots, n \quad (5.48)$$

for n = number of reservoir layers. Layers should be arranged in order of decreasing permeability, thus $i = 1$ has thickness h_1 and the largest perm k_1 while $i = n$ has thickness h_n and the smallest perm k_n . By definition, the

cumulative flow capacity should be in the range $0 \leq F_m \leq 1$ and cumulative thickness should be in the range $0 \leq H_m \leq 1$ for $0 \leq m \leq n$.

The Lorenz coefficient is defined in terms of a plot of F_m versus H_m (Figure 5-2). The Lorenz coefficient L_C is two times the area enclosed between the

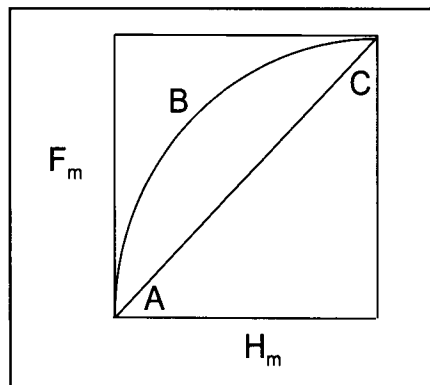


Figure 5-2. Lorenz Coefficient Plot.

Lorenz curve ABC in the figure and the diagonal AC . The Lorenz coefficient has the range $0 \leq L_C \leq 1$. For a homogeneous reservoir, the Lorenz coefficient satisfies the equality $L_C = 0$. An increase in heterogeneity increases the value of the Lorenz coefficient L_C . Typical values of the Lorenz coefficient are in the range $0.2 \leq L_C \leq 0.6$.

An estimate of the Lorenz coefficient is obtained by assuming all permeabilities have equal probability so that the trapezoidal rule can be used to estimate area. The result is

$$L_C = \frac{1}{2n} \left[\left(\sum_{i=1}^n \sum_{j=1}^n |k_i - k_j| \right) / \sum_{i=1}^n k_i \right] \quad (5.49)$$

It is not necessary to order permeabilities using this estimate. Notice that in the homogeneous case, all of the permeabilities are equal so that we have the relationship $k_i = k_j$. Substituting this equality into Eq. (5.49) gives the Lorenz coefficient $L_C = 0$. In the ideal homogeneous case, the Lorenz coefficient is zero, as indicated above.

We illustrate the application of Eq. (5-49) by again considering a 3-layer case with the following permeabilities:

Layer 1: $k = 35 \text{ md}$

Layer 2: $k = 48 \text{ md}$

Layer 3: $k = 126 \text{ md}$

We estimate L_c by first performing the double summation

$$\begin{aligned} \sum_{i=1}^n \sum_{j=1}^n |k_i - k_j| &= |126 - 48| + |126 - 35| + |48 - 126| \\ &\quad + |48 - 35| + |35 - 126| + |35 - 48| = 364 \end{aligned}$$

and the single sum

$$\sum_{i=1}^n k_i = 126 + 48 + 35 = 209$$

The result is

$$L_c = \frac{1}{2n} \left[\left(\sum_{i=1}^n \sum_{j=1}^n |k_i - k_j| \right) \Big/ \sum_{i=1}^n k_i \right] = \frac{1}{6} \left[\frac{364}{209} \right] = 0.29$$

Exercises

- 5-1. A. The number of core plug samples with volume v that are needed to match the critical sample size v_c is $N = v_c/v$. Rearrange Eq. (5.10) to express N in terms of variance and average porosity.
B. Calculate N for a cylindrical core plug with $\phi = 0.279$ and $\sigma_\phi = 0.03$.

- 5-2. A. Derive Eq. (5.40).
B. Calculate the number of core plug samples $N_K = v_{CK}/v$ that are needed to match the critical sample size for a permeability distribution characterized by the parameters $\sigma_K = 0.87$ and $\delta_K = 0.01$. Hint: Rearrange Eq. (5.40).

70 *Integrated Flow Modeling*

- 5-3. A. Estimate the Dykstra-Parsons coefficient for vertical permeability in file EXAM2.DAT (vertical column).
- B. Estimate the Lorenz coefficient for vertical permeability in file EXAM2.DAT.

Chapter 6

Petrophysical Model

Monitoring changes in the seismic characteristics of a reservoir as the reservoir is produced is the basis of 4-D seismic monitoring [Anderson, 1995; He, et al., 1996; Lumley and Behrens, 1997; Jack, 1998; Fanchi, et al., 1999]. This is done in IFLO by calculating seismic attributes and associated petrophysical data requirements [Fanchi and Batzle, 2000] as a function of time. The seismic attributes are defined below. A discussion of geostatistical correlations between rock properties is then presented.

6 .1 Compressional and Shear Velocities

Two of the most important seismic parameters are compressional velocity (V_P) and shear velocity (V_S). Compressional velocity and shear velocity for an isotropic, homogeneous medium are calculated from the expressions [Schön, 1996; McQuillin, et al., 1984]:

$$V_P = \sqrt{\frac{S}{\rho_B}}, S = K^* + \frac{4}{3}\mu^* \quad (6.1)$$

and

72 Integrated Flow Modeling

$$V_s = \sqrt{\frac{\mu^*}{\rho_B}} \quad (6.2)$$

where

S stiffness

K^* effective bulk modulus

μ^* effective shear modulus

ρ_B effective bulk density = $(1-\phi)\rho_{ma} + \phi\rho_f$

Stiffness S in Eq. (6.1) is a measure of the rock frame stiffness and pore fluid stiffness. Inspection of Eq. (6.1) shows that compressional velocity increases as stiffness increases. On the other hand, shear velocity depends only on μ^* and ρ_B . Consequently, measurements of both compressional and shear velocities can provide information about different lithologies and fluid types that would not be available with a measurement of only compressional velocity or shear velocity.

Bulk density for a porous rock is given by $\rho_B = (1-\phi)\rho_{ma} + \phi\rho_f$ where

ρ_{ma} density of grains (solid matrix material)

ρ_f fluid density = $\rho_o S_o + \rho_w S_w + \rho_g S_g$

ϕ porosity

Bulk and fluid densities and porosities are usually derived from a combination of the neutron porosity and density logs. Oil, water and gas densities (ρ_o , ρ_w , ρ_g) and saturations (S_o , S_w , S_g) can be obtained from a variety of sources.

Measurements of compressional and shear velocities are often reported using the ratio V_p/V_s . The advantage of working with the ratio is the elimination of bulk density, which may be a poorly known quantity. This can be seen by taking the ratio of Eqs. (6.1) and (6.2) to find

$$\frac{V_p}{V_s} = \sqrt{\frac{K^* + \frac{4\mu^*}{3}}{\mu^*}} = \sqrt{\frac{4}{3} + \frac{k^*}{\mu^*}} \quad (6.3)$$

Noting that the moduli K^* and μ^* are greater than zero, we see from Eq. (6.3) that the ratio $V_p/V_s \geq \sqrt{4/3}$.

6.2 Estimates of Moduli

A widely used expression for K^* was derived by Gassmann [1951] from the theory of elasticity of porous media [also see Schön, 1996; McQuillin, et al., 1984]:

$$K^* = K_B + \frac{\left[1 - \frac{K_B}{K_G}\right]^2}{\frac{\phi}{K_F} + \frac{1-\phi}{K_G} - \frac{K_B}{K_G^2}} \quad (6.4)$$

where

K_B bulk modulus of porous matrix ("dry frame")

K_G bulk modulus of grains

K_F bulk modulus of fluid

In addition to rock properties such as porosity and moduli, Gassmann's model depends on phase properties, and fluid saturations. The bulk modulus of the fluid in Eq. (5.4) is the inverse of fluid compressibility: $K_F = 1/c_r$. For a mixture, fluid compressibility is estimated from a volume average of the phase compressibilities (c_o , c_w , c_g), as $c_r = c_o S_o + c_w S_w + c_g S_g$ for an immiscible oil, water and gas mixture. IFLO includes solvent that can substantially modify fluid compressibility. The appropriate fluid compressibility for the extended black oil formulation in IFLO is

$$c_r = c_T - c_r \quad (6.5)$$

where c_T is total compressibility and c_r is rock compressibility.

Gassmann's equation represents perfect coupling between the pore fluid and the solid skeleton of the porous medium [Schön, 1996]. This relation is strictly valid only for isotropic, homogeneous, monomineralic media. Other petrophysical models could be used in the integrated flow model, such as a frequency dependent theory presented by Biot [1956], and Geertsma and Smit [1961]. Gassmann's equation is sometimes referred to in the literature as the Biot-Geertsma-Gassmann equation, or BGG equation. It is widely used in

74 Integrated Flow Modeling

petrophysics because of its relative simplicity and limited data requirement. All of the required input can either be directly derived or at least estimated from well logs.

Once K^* is known, it is possible to estimate compressional and shear velocities for an isotropic, homogeneous medium using Eqs. (6.1) and (6.2). Fluid movement can change the effective bulk modulus in a region of the reservoir according to Eq. (6.4). The change in K^* leads to a change in stiffness and compressional velocity, as illustrated in Eq. (6.1). By contrast, Eq. (6.2) shows that shear velocity does not depend on bulk modulus. Therefore, shear velocity is relatively insensitive to pore fluid content. Measurements of compressional and shear velocity can be used to distinguish structure from fluid content. The technology for monitoring both compressional and shear velocities is referred to as full vector wavefield, or multicomponent, imaging.

Four petrophysical parameters must be included in IFLO to allow the use of Gassmann's equation: the bulk modulus of the porous matrix K_B , the bulk modulus of the grains K_G , the effective shear modulus μ^* , and the matrix density ρ_{ma} . The IFLO user must enter K_B , K_G , μ^* , and ρ_{ma} since these parameters cannot be calculated from traditional black oil simulator input data.

The references give values that may be used if the data are not available from well logs such as shear wave logging tools, or laboratory measurements of parameters such as acoustic velocities or the dry frame Poisson's ratio. For example, Figure 6-1 shows that bulk modulus and shear

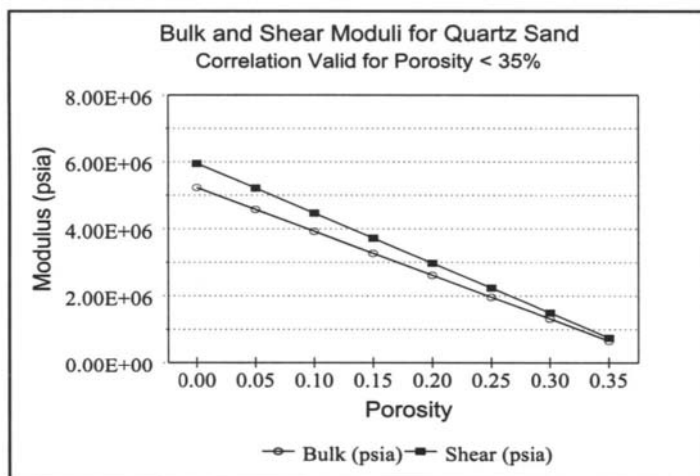


Figure 6-1. Illustration of the relationship between bulk and shear moduli.

modulus are linear functions of porosity for quartz sandstone [Murphy, et al., 1993] for porosity less than 35%. The grain modulus K_G equals the bulk modulus K_B when porosity equals zero.

Each of the petrophysical parameters $\{K_B, K_G, \mu^*, \rho_{ma}\}$ can vary throughout the reservoir. Therefore, the IFLO user is allowed to specify $\{K_B, K_G, \mu^*, \rho_{ma}\}$ as spatially dependent variables.

6.3 Moduli from Acoustic Velocities

Measurements of shear and compressional velocities provide a direct means of determining bulk moduli. Equations (6.1) and (6.2) can be rearranged to express moduli in terms of measured acoustic velocities, thus

$$K' = \rho_B \left[V_P^2 - \frac{4}{3} V_S^2 \right] \quad (6.6)$$

Similarly, measurements of shear velocity can be combined with measurements of bulk density to yield the effective shear modulus:

$$\mu' = \rho_B V_S^2 \quad (6.7)$$

Recall that bulk density requires both matrix density and fluid density. Often velocities, particularly shear velocities, are not available and estimates must be made from general correlations. An example of a correlation between acoustic velocities in sandstone, porosity, and clay content C is given by Castagna, et al. (1985):

$$V_P = 5.81 - 9.42 \phi - 2.21C \quad (6.8)$$

and

$$V_S = 3.89 - 7.07 \phi - 2.04C \quad (6.9)$$

The units are km/s for acoustic velocities, while clay volume and porosity are in fractional content. Notice the linear dependence of acoustic velocity on porosity. Similar correlations are available from such sources as Han, et al. [1986] and Vernik [1998].

76 Integrated Flow Modeling

The grain modulus K_G is often estimated from lithology. For example, K_G for quartz is 38 MPa (5.5×10^6 psia). Alternatively, measurement of shear velocity and compressional velocity at zero porosity yields an effective bulk modulus that equals grain modulus, thus

$$K_G = K_B = K^* \text{ at } \phi = 0 \quad (6.10)$$

This result can be derived using Gassmann's equation and recognizing that bulk modulus equals grain modulus as porosity goes to zero. Bulk modulus can be calculated from measured acoustic velocities, fluid properties, matrix density and the value of grain modulus estimated above from

$$K_B = \frac{K^* \left(\frac{\phi}{K_F} + \frac{1-\phi}{K_G} \right) - 1}{\frac{\phi}{K_F} + \frac{1-\phi}{K_G} - \frac{2}{K_G} + \frac{K^*}{K_G^2}} \quad (6.11)$$

This equation was derived by solving Gassmann's equation for bulk modulus, and calculating effective bulk modulus using Eq. (6.6).

6.4 Acoustic Impedance and Reflection Coefficient

Acoustic impedance Z is defined as the product of bulk density and acoustic velocity. The acoustic impedance for compressional velocity is

$$Z = \rho_B V_P \quad (6.12)$$

Acoustic impedance is used to calculate the reflection coefficient of an interface between two geologic beds. Suppose a seismic wave is incident through upper layer 1 and is reflected at the interface between layer 1 and lower layer 2. The reflection coefficient is the ratio of the amplitude of the reflected wave divided by the amplitude of the incident wave. The reflection coefficient RC at the interface between two layers with acoustic impedances Z_1 and Z_2 is given by

$$RC = \frac{Z_2 - Z_1}{Z_2 + Z_1} \quad (6.13)$$

The numerator in Eq. (6.13) is the change in acoustic impedance, while the denominator is two times the mean acoustic impedance. The transmission coefficient at the interface between the same two layers is

$$TC = \frac{2Z_1}{Z_2 + Z_1} \quad (6.14)$$

Notice that the sum of reflection and transmission coefficients is unity, thus $RC + TC = 1$.

6.5 Geostatistical Correlations

Every measurement of any rock property is on a sample of some specific size. The description of the heterogeneous quality of a reservoir is in terms of property values, the spatial position of the property in the reservoir, and the size of the individual samples. The spatial distribution of a property is the focus of this section, which parallels Collins' [1985] presentation.

Joint Distributions and Conditional Distributions

The statistical description of K and ϕ variations within depositional units can be expressed in terms of a joint distribution of K and ϕ . This description requires a few more basic concepts from probability theory: marginal probability distribution, conditional probability, and statistical correlation.

Consider two continuous random variables x and y , and let $dP(x', y')$ denote the probability for $x < x' < x + dx$ and $y < y' < y + dy$. Also, suppose a joint probability distribution $\rho(x, y)$ exists such that

$$dP(x, y) = \rho(x, y) dx dy \quad (6.15)$$

Then the marginal probability for x , without regard for y , is

$$dP_x(x) = \left[\int_0^{\infty} \rho(x, y) dy \right] dx = \rho_x(x) dx \quad (6.16)$$

where, for simplicity, we assume both x and y range from 0 to ∞ . The bracketed term is the marginal probability distribution $\rho_x(x)$, thus

$$\rho_x(x) = \int_0^{\infty} \rho(x,y) dy \quad (6.17)$$

Similarly, a marginal probability distribution $\rho_y(y)$ is defined by interchanging x and y . The result is

$$\rho_y(y) = \int_0^{\infty} \rho(x,y) dx \quad (6.18)$$

and

$$dP_y(y) = \rho_y(y) dy \quad (6.19)$$

The conditional probability for $x < x' < x + dx$ given that a particular y has been observed is

$$dP_{cx}(x|y) = \frac{dP(x,y)}{dP_y(y)} \quad (6.20)$$

or

$$dP_{cx}(x|y) = \frac{\rho(x,y)}{\rho_y(y)} dx \quad (6.21)$$

The conditional distribution function for x is

$$\rho_{cx}(x|y) = \frac{\rho(x,y)}{\rho_y(y)} \quad (6.22)$$

which is the ratio of the joint distribution in x and y to the marginal distribution in y .

Actually, we have already treated conditional distributions for both ϕ and $\ln K$. When we partition data into classes on $\ln K$ and then construct the distribution of ϕ within one $\ln K$ class we have, in fact, constructed a conditional distribution for ϕ . This should be denoted as the conditional probability density for ϕ given $\ln K$, thus $\rho(\phi|\ln K)$.

Conditional Probability Example

The meaning of conditional probabilities is easily understood in terms of a simple example. Consider a “dart board” with area elements numbered and cross-hatched as shown in Figure 6-2. There are 16 elements, all equally likely to be hit in a toss of the dart. The probability of the joint event of a number j and a color c is

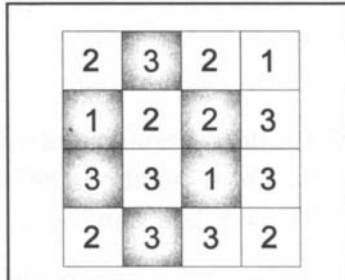


Figure 6-2. Dart Board.

$$P(j,c) = \frac{N(j,c)}{N} \quad (6.23)$$

where $N(j, c)$ is the number of squares showing the number j and the color c while N is the total number of squares.

The unconditional, or marginal probability for a color c is

$$P'(c) = \sum_j \frac{N(j,c)}{N} = \frac{N(c)}{N} \quad (6.24)$$

where $N(c)$ is the total number of squares showing the color c without regard for the number contained in the square. Then the conditional probability for j to occur, given that the color c has been observed, is

$$P_c(j|c) = \frac{P(j,c)}{P'(c)} = \frac{N(j,c)}{N(c)} \quad (6.25)$$

from the definitions given above.

What we have in the conditional probability is a reduction of the range of possible events. For example, if c is “dark,” D , then Eq. (6.25) refers to a reduced dart board as in Figure 6-3. Specific numerical results, for this example are

$$P(2,D) = \frac{1}{16}$$

and

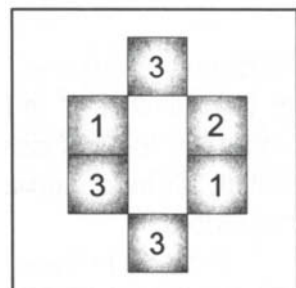


Figure 6-3. Reduced Dart Board.

$$P_c(2|D) = \frac{1}{6}$$

Statistical Dependence and the Correlation Function

From the above definitions, we see that the joint distribution of ϕ and $\ln K$ for core data can be expressed in two forms,

$$\rho(\phi, \ln K | v) = \rho_1(\phi | v) \rho_{12}(\ln K | \phi, v) \quad (6.26)$$

and

$$\rho(\phi, \ln K | v) = \rho_2(\ln K | v) \rho_{21}(\phi | \ln K, v) \quad (6.27)$$

Equating the right hand sides of the above equations and rearranging gives the correlation function $C(\phi, \ln K | v)$ as

$$C(\phi, \ln K | v) = \frac{\rho_{12}(\ln K | \phi, v)}{\rho_2(\ln K | v)} = \frac{\rho_{21}(\phi | \ln K, v)}{\rho_1(\phi | v)} \quad (6.28)$$

We obtain a third form for the joint distribution:

$$\rho(\phi, \ln K | v) = \rho_1(\phi | v) \rho_2(\ln K | v) C(\phi, \ln K | v) \quad (6.29)$$

The correlation function is always positive. If $C = 1$, we find from Eq. (6.28) that

$$\rho_{12}(\ln K | \phi, v) = \rho_2(\ln K | v) \quad (6.30)$$

and similarly

$$\rho_{21}(\phi | \ln K, v) = \rho_1(\phi | v) \quad (6.31)$$

Equations (6.30) and (6.31) state that the conditional probability, $\rho_{12}d(\ln K)$, for $\ln K$, given that ϕ has occurred, is equal to $\rho_2d(\ln K)$. In this case, the probability for $\ln K$ does not depend on ϕ , and we say that ϕ and $\ln K$ are statistically independent. Conversely, if $C \neq 1$, then ϕ and $\ln K$ are statistically dependent.

If ϕ and $\ln K$ are statistically independent, then a “scattergram,” or plot of ϕ versus $\ln K$ for all core plugs, would show no trend at all. In fact, of course, such scattergrams often show a trend.

The Semi-Variogram and Statistical Correlation

A mathematical tool for studying correlations of rock properties is the semi-variogram. The semi-variogram V is closely related to the statistical correlation R . We first introduced the semi-variogram in Section 2.4. We now define the variogram and show its relationship to R before discussing the value of variograms to the understanding of reservoir heterogeneities.

A semi-variogram can be calculated from a traverse of measured values of a parameter such as permeability at equally spaced points along a line in much the same way that the correlation in this data is calculated. Thus we compute from measured values K_1, K_2, \dots, K_N at equally spaced points the sum

$$\bar{V}(m) = \sum_{i=1}^{N-m} \frac{(K_{i+m} - K_i)^2}{2(N-m)} \quad (6.32)$$

This is evaluated for various values of the separation between points m . The product $m\Delta h$ is the actual distance ξ between pairs of points used in Eq.(6.32) if Δh is the spacing between adjacent pairs of points. The actual mathematical definition for $V(\xi)$ corresponding to the above calculational procedure is

$$\bar{V}_{12} = \frac{1}{2} \langle (K'_2 - K'_1)^2 \rangle \quad (6.33)$$

where K' is measured at a point \vec{r}_2 in the depositional unit while K is measured at \vec{r}_1 . Expanding Eq. (6.33) gives

$$\bar{V}_{12} = \frac{1}{2} [\langle K'^2 \rangle_2 - 2\langle K' K \rangle_{12} + \langle K^2 \rangle_1] \quad (6.34)$$

The correlation \bar{R}_{12} between K' and K is

$$\bar{R}_{12} = \langle (K - \bar{K}_1)(K' - \bar{K}_2) \rangle \quad (6.35)$$

where

$$\bar{R}_{12} = \iint (K - \bar{K}_1)(K' - \bar{K}_2) p_1(K|v) p_2(K'|v) C_{12}(K, K', v) dK dK' \quad (6.36)$$

and $C_{12}(K, K', v)$ is the correlation function between K and K' . The value $C_{12} = 1$ means there is no correlation between the observations K and K' . The averages \bar{K}_1 and \bar{K}_2 for a continuous distribution are given by the integrals

$$\bar{K}_1 = \langle K \rangle_1 = \int K p_1(K|v) dK \quad (6.37)$$

and

$$\bar{K}_2 = \langle K' \rangle_2 = \int K' p_2(K'|v) dK' \quad (6.38)$$

Expanding the integrand in \bar{R}_{12} gives

$$\bar{R}_{12} = \langle KK' - \bar{K}_1 K' - \bar{K}_2 K + \bar{K}_1 \bar{K}_2 \rangle \quad (6.39)$$

The average values \bar{K}_1 and \bar{K}_2 can be factored out of the expectation value calculation to give

$$\bar{R}_{12} = \langle KK' \rangle - \bar{K}_1 \langle K' \rangle_2 - \bar{K}_2 \langle K \rangle_1 + \bar{K}_1 \bar{K}_2 \quad (6.40)$$

Applying the definitions of \bar{K}_1 and \bar{K}_2 lets us write

$$\bar{R}_{12} = \langle KK' \rangle - \bar{K}_1 \bar{K}_2 - \bar{K}_2 \bar{K}_1 + \bar{K}_1 \bar{K}_2 \quad (6.41)$$

which simplifies to the form

$$\bar{R}_{12} = \langle KK' \rangle - \bar{K}_1 \bar{K}_2 \quad (6.42)$$

Substituting Eq. (6.42) into (6.34) gives

$$\bar{V}_{12} = \left[\frac{1}{2} (\langle K'^2 \rangle_2 + \langle K^2 \rangle_1) - \langle K \rangle_1 \langle K' \rangle_2 - \bar{R}_{12} \right] \quad (6.43)$$

If the depositional unit is statistically homogenous, meaning without change in the statistical distribution, then

$$\langle K \rangle_1 = \langle K' \rangle_2 \quad (6.44)$$

and

$$\langle K^2 \rangle_1 = \langle K'^2 \rangle_2 \quad (6.45)$$

so we then have

$$\bar{V}(\xi) = [\langle K^2 \rangle - \langle K \rangle^2 - \bar{R}(\xi)] \quad (6.46)$$

and both V and R are functions only of the separation vector $\vec{\xi}$ between points of observation.

Finally we note that

$$\bar{\sigma}_K^2 = [\langle K^2 \rangle - \langle K \rangle^2] \quad (6.47)$$

where $\bar{\sigma}_K^2$ and σ_K^2 are variances in K and $\ln K$ respectively. For small σ_K , $\bar{\sigma}_K \approx K_G \sigma_K$.

The general relationship between $\bar{V}(\vec{\xi})$ and $\bar{R}(\vec{\xi})$ in a statistically homogenous unit becomes

$$\bar{V}(\vec{\xi}) = \bar{\sigma}_K^2 - \bar{R}(\vec{\xi}) \quad (6.48)$$

In fact, since $\bar{R} \rightarrow \sigma_K^2$ as $\vec{\xi} \rightarrow 0$ we see that

$$\frac{\bar{V}(\vec{\xi})}{\bar{\sigma}_K^2} = 1 - \frac{\bar{R}(\vec{\xi})}{\bar{\sigma}_K^2} \quad (6.49)$$

In most rocks this has the form

$$\frac{\bar{V}}{\bar{\sigma}_K^2} = 1 - e^{-\xi/\lambda} \quad (6.50)$$

for a particular direction of traverse in the rock, with λ being the correlation length, or integral scale, in the direction of the traverse. The form obtained in Eqs. (6.48) through (6.50) for $V(\vec{\xi})$ apply only to depositional units free of trends, otherwise we must go back to the general form in Eq. (6.43).

Exercises

6-1. Run file RIM-2D.DAT. What are the initial and final acoustic velocity ratios across the oil rim? Hint: Open the output file and make a table showing index I , oil saturation, gas saturation, and V_p/V_s for blocks $I = 1$ to 10 and $J = 6$.

6-2. Set grain modulus = bulk modulus in RIM-2D.DAT file. Run the revised model. What is the effect on calculated acoustic velocity ratio V_p/V_s ?

84 *Integrated Flow Modeling*

6-3. Change porosity in the original RIM-2D.DAT file from 0.25 to 0.2. Use Figure 6-1 to obtain new values of bulk and shear moduli. Run the revised model. What are the initial and final acoustic velocity ratios V_p/V_s across the oil rim? Hint: see Exercise 6-1.

Chapter 7

Relative Permeability

Reservoir flow models calculate saturation as a function of time. The change in saturation effects the movement of different fluid phases through the interconnected pore space. The measure of interconnectedness of pore space is permeability. When more than one phase is moving, the permeability needs to be modified to account for the relative movement of the two or more phases in the pore space. Multiphase flow is modeled by including relative permeability curves in the simulator. Saturation end points for the relative permeability curves are used to establish initial fluids-in-place in addition to modeling flow behavior.

This chapter briefly reviews the concept of effective permeability and defines relative permeability. It introduces the concept of mobility and shows how relative permeability affects Darcy's law. Relative permeability averaging techniques and correlations are then presented.

7.1 Effective Permeability and Relative Permeability

Absolute permeability is a measure of the capacity of the rock to transmit a single fluid. Permeability to each phase in the interconnected pore space is

called effective permeability. Interfacial tension associated with the mixing of immiscible fluids tends to increase resistance to flow of fluids through the interconnected pore space. Consequently, the sum of the effective permeabilities for each phase ℓ is less than the absolute permeability, thus

$$\sum_{\ell=1}^N (k_{\ell})_{\text{eff}} \leq k_{\text{abs}} \quad (7.1)$$

where N is the number of phases present. The effective permeability of multiphase flow is represented by defining relative permeability.

Suppose we make the following assignments:

- k_o effective permeability to oil
- k_w effective permeability to water
- k_g effective permeability to gas

Given the value of effective permeability, we define relative permeability as the ratio of effective permeability to a reference permeability, thus:

$$k_r = \frac{k_{\text{eff}}}{k_{\text{ref}}} \quad (7.2)$$

where

- k_{eff} effective permeability of fluid [md]
- k_{ref} reference permeability, [md]

The reference permeability is typically the absolute permeability of air. If we designate the reference or base permeability as k , we obtain the following often used effective permeabilities:

$$\begin{aligned} \text{oil: } k_{ro} &= \frac{k_o}{k}, \\ \text{water: } k_{rw} &= \frac{k_w}{k}, \\ \text{gas: } k_{rg} &= \frac{k_g}{k}. \end{aligned} \quad (7.3)$$

It can be seen from these definitions that relative permeability varies between 0 and 1 because $k_{\text{eff}} \leq k$. The sum of the relative permeabilities over all phases ℓ at the same time and place satisfies the inequality

$$\sum_{\ell=1}^N k_{r\ell} \leq 1 \quad (7.4)$$

7.2 Two-Phase Relative Permeability

The most common multiphase flow phenomena involve the movement of two phases through the same interconnected pore space at the same time. The most frequently occurring two-phase relative permeability systems are discussed below.

Oil-Water Two-Phase Relative Permeability

Consider a two-phase, water-wet system containing oil and water phases. The relative permeability k_r curves are a function of water saturation S_w . Typically, the shape of the k_r curve is concave upward. The relative permeability of phase ℓ ($k_{r\ell}$) goes to 0 before the corresponding phase saturation S_ℓ reaches 0. The last observation shows that one fluid phase cannot be completely displaced from a porous medium by injecting another phase.

The point where k_r goes to 0 is the end point of the relative permeability curve. For water, the end point is called the irreducible water saturation, $S_{w\text{irr}}$ or the connate water saturation. For oil, the end point is called residual oil saturation, $S_{o\text{r}}$.

Wettability can be inferred by examining relative permeability curves. Several indicators are described below. The wettability indicators are not a substitute for laboratory measurements, but can aid in the characterization of the fluid flow environment.

One of the most often used wettability indicators is the point of intersection on the saturation axis of two relative permeability curves. The point of intersection implies the following wettability:

- Water-wet system if the curves cross at $S_w > 0.5$
- Oil-wet system if the curves cross at $S_w < 0.5$

Another wettability indicator is the relative permeability to water at S_{or} , thus

- Typically ≤ 0.3 for water-wet system
- Typically ≥ 0.5 for oil-wet system

The value of relative permeabilities at end point saturations also indicate wettability as follows:

- For water-wet system, k_{rw} at $S_{or} \ll k_{ro}$ at S_{wirr}
- For oil-wet system, k_{rw} at $S_{or} \approx k_{ro}$ at S_{wirr} .

Finally, an oil-wet system usually satisfies the inequality $S_{wirr} \lesssim 0.1$.

Hysteresis: Imbibition Versus Drainage

The shape of a relative permeability curve depends on its history. A drainage curve results from a history in which the non-wetting phase displaced the wetting phase. An example of a drainage system is the displacement of oil by water during oil migration and accumulation. An imbibition system, on the other hand, has a history in which the wetting phase displaced the non-wetting phase. It is exemplified by a waterflood in a water-wet reservoir.

Figure 7-1 shows characteristics of drainage and imbibition k_r curves in a water-wet, oil-water system. Notice that there is very little difference in k_{rw} between imbibition and drainage, whereas the k_{ro} imbibition curve deviates noticeably from the drainage curve. In this case, hysteresis is more significant in the oil (non-wetting phase) curve. In general, relative permeability hysteresis is most pronounced in the non-wetting phase. One model for including relative permeability hysteresis effects in reservoir simulation is dis-

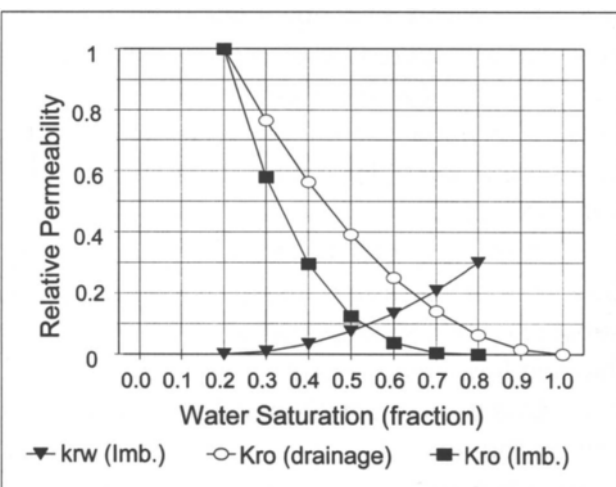


Figure 7-1. Typical water-oil relative permeability curves.

is discussed by Killough [1976]. Killough's model also applies to capillary pressure hysteresis.

End Points

End points define the amount of mobile oil saturation S_o . The initial water saturation S_{wi} defines oil in place at the start of waterflood and can be adjusted as needed if gas saturation S_g is greater than 0. Residual oil saturation S_{or} defines the fraction of oil remaining in the pore space after a waterflood.

Laboratory experiments may not accurately duplicate actual values of the end points S_{wi} and S_{or} . Laboratory measurements of k_r end points may need adjusting.

Independent estimates of S_{wi} can be made from logs, oil-cut core data, or P_c measurements. One goal of an integrated study is to construct a data base with a consistent set of data. To achieve consistency using data from a variety of sources, values of S_{wi} from k_r experiments may need to be adjusted. Independent estimates of S_{or} are difficult and often require corrections.

Gas-liquid Two-phase Relative Permeability

Gas is the nonwetting phase during two-phase flow of gas and oil, and two-phase flow of gas and water. Critical gas saturation, S_{gc} , is the gas saturation at which gas first begins to flow in a reservoir. The value of S_{gc} usually varies from 0 and 10%, and a reasonable value in the absence of measurements is a value between 2 and 5%.

Hysteresis occurs in gas relative permeability in a manner similar to that in oil-water systems. Residual or trapped gas saturation (S_{gr} or S_{gt}) is the maximum value of S_g where the relative permeability to gas $k_{rg} = 0$. Typical values of S_{gr} or S_{gt} range from 15 to 40%.

Effects of Relative Permeability on Flow Rates

Darcy's equation for linear, multiphase flow is

$$q = \frac{0.001127 k k_r A \Delta p}{\mu B L} \quad (7.5)$$

90 Integrated Flow Modeling

where

- q flow rate [STB/D]
- k absolute or base permeability [md]
- k_r relative permeability [fraction]
- A cross-sectional area [sq ft]
- Δp pressure drop [psi]
- μ fluid viscosity [cp]
- B formation volume factor [RB/STB]
- L length between two measured pressures [ft]

Oil and water flow rates using Darcy's law for two-phase flow are

$$q_o = \frac{0.001127 k k_o A \Delta p}{\mu_o B_o L} = \frac{0.001127 k_o A \Delta p}{\mu_o B_o L} \quad (7.6)$$

and

$$q_w = \frac{0.001127 k k_w A \Delta p}{\mu_w B_w L} = \frac{0.001127 k_w A \Delta p}{\mu_w B_w L} \quad (7.7)$$

where k_o and k_w are the effective permeabilities to oil and water, respectively.

The total flow rate for the two-phase system is found by summing individual phase flow rates. At reservoir conditions, the formation volume factors are $B_o = B_w = 1$ reservoir volume/standard volume so that the total flow rate is

$$\begin{aligned} q_t (\text{reservoir conditions}) &= q_o + q_w \\ &= \frac{0.001127 A \Delta p}{L} \left[\frac{k_o}{\mu_o} + \frac{k_w}{\mu_w} \right] \end{aligned} \quad (7.8)$$

The ratio of effective permeability to viscosity is called mobility. The ratio of relative permeability to viscosity is called relative mobility. Oil and water mobilities are defined as

$$\text{oil mobility} = \lambda_o = \frac{k_o}{\mu_o} \text{ and} \\ \text{water mobility} = \lambda_w = \frac{k_w}{\mu_w}. \quad (7.9)$$

Total mobility is the sum of the individual phase mobilities:

$$\lambda_T = \sum_{\ell=1}^N \lambda_\ell \quad (7.10)$$

Total mobility, and hence total flow rate for a given pressure drop, varies over the mobile saturation range. Total mobility is a minimum at the intersection of the relative permeability curves. Thus, identifying the saturation corresponding to the minimum of the total mobility curve gives information about the wettability of the system.

7.3 Averaging Relative Permeability Data

Relative permeability data are generally measured and reported for laboratory analysis of several core samples from a particular well. The group of k_r curves should be sorted by lithology or pore type and averaged to determine a representative set of relative permeability curves. Two of the more common and generally applicable averaging methods are discussed here.

Normalization of Curves

One way to average a set of relative permeability curves is to normalize them. The normalization procedure requires that saturation end points are known for each set of relative permeability curves. This method works best if a reliable determination of S_{or} can be made.

The first step in the normalization process is to redefine saturation in the range between 0 and 1. Normalized saturations for an oil-water system are

$$S_w' = \frac{S_w - S_{wirr}}{1 - S_{or} - S_{wirr}} \quad (7.11)$$

92 Integrated Flow Modeling

where

S_{wirr} irreducible water saturation

S_{or} residual oil saturation

S_w^* normalized water saturation

The normalized water saturation has the following values:

$$S_w^* = 0 \text{ for } S_w = S_{wirr}$$

$$S_w^* = 1 \text{ for } S_w = 1 - S_{or}$$

Normalized saturations for a gas-oil system are defined in an analogous manner. In particular, the normalized oil saturation for a gas-oil system is defined as

$$S_o^* = \frac{S_o - S_{or}}{S_{oirr} - S_{or}} = \frac{S_{oirr} - S_g - S_{or}}{S_{oirr} - S_{or}} \quad (7.12)$$

where $S_g^* = 1 - S_o^*$. The normalized oil saturation has the following values:

$$S_o^* = 1 \text{ for } S_g = 0$$

$$S_o^* = 0 \text{ for } S_o = S_{or}$$

A set of relative permeability curves is obtained by averaging k_r measurements at several values of S_w or S_g . The average, normalized curve has end point saturations of 0 and 1. End point saturations must be "de-normalized" to obtain reservoir values. The de-normalized water saturation for a water-oil system is

$$S_{w(\text{new})} = S_w^* (1 - S_{or} - S_{wi}) + S_{wi} \quad (7.13)$$

where: $S_{w(\text{new})}$ is S_w on the new, shifted curve and

S_{wi} initial water saturation

S_{or} residual oil saturation

For a gas-oil system, the de-normalized oil saturation is

$$S_{o(\text{new})} = S_o^* (S_{oi} - S_{or}) + S_{or} \quad (7.14)$$

where $S_{o(\text{new})}$ is S_o on the shifted curve, and

S_{oi} initial oil saturation
 S_{or} residual oil saturation

Simple Average

Another method is to fit an average curve through all of the representative data. The most representative end points should be selected since they will probably be different for all curves.

7.4 Two-Phase Relative Permeability Correlations

Many correlations exist for two-phase relative permeabilities. The correlations have been developed from a variety of sources, such as capillary tube models, statistical models of capillary bundles, microscopic network models, and empirical correlations. Correlations are typically used in the absence of laboratory measurements or multiphase production data. Correlations are not a substitute for laboratory measurements. They should be used in conjunction with laboratory data, or when laboratory data are not available. The following commonly used models are reasonable for many purposes.

Honarpour, et Al., Correlations

One of the most widely used sets of correlations are those of Honarpour, et al. (1982). The Honarpour, et al. equations depend on rock type and wettability. Intermediate wetting yields significantly higher values of k_{rw} over the mobile saturation range, while k_{ro} is unchanged. Carbonate equations predict lower k_{rw} for the water-wet system, and higher k_{rw} for the intermediate wet system than the sandstone/conglomerate equations. The correlations are presented as a function of wettability and lithology below.

Terms used in the correlations are defined below:

S_{wi} irreducible water saturation
 S_{gc} critical gas saturation
 S_{orw} residual oil saturation in water-oil system

S_{org} residual oil saturation in gas-oil system

k_a absolute air permeability [md]

$k_{rg(S_{org})}$ relative permeability to gas at residual oil saturation

k_{rw} for water-wet sandstone/conglomerate:

$$k_{rw} = 0.035388 \left(\frac{S_w - S_{wi}}{1 - S_{wi} - S_{orw}} \right) - 0.010874 \left(\frac{S_w - S_{orw}}{1 - S_{wi} - S_{orw}} \right)^{2.9} + 0.56556 (S_w)^{3.6} (S_w - S_{wi}) \quad (7.15)$$

k_{rw} for oil and intermediate-wet sandstone/conglomerate:

$$k_{rw} = 1.5814 \left(\frac{S_w - S_{wi}}{1 - S_{wi}} \right)^{1.91} - 0.58617 \left(\frac{S_w - S_{orw}}{1 - S_{wi} - S_{orw}} \right) (S_w - S_{wi}) - 1.2484\phi(1 - S_{wi})(S_w - S_{wi}) \quad (7.16)$$

k_{row} for sandstone/conglomerate with any wettability:

$$k_{row} = 0.76067 \left(\left(\frac{\frac{S_o}{1 - S_{wi}} - S_{orw}}{1 - S_{orw}} \right)^{1.8} \left(\frac{S_o - S_{orw}}{1 - S_{wi} - S_{orw}} \right)^{2.0} + 2.6318\phi(1 - S_{orw})(S_o - S_{orw}) \right) \quad (7.17)$$

k_{rog} for sandstone/conglomerate with any wettability:

$$k_{rog} = 0.98372 \left(\frac{S_o}{1 - S_{wi}} \right)^4 \left(\frac{S_o - S_{org}}{1 - S_{wi} - S_{org}} \right)^2 \quad (7.18)$$

k_{rg} for sandstone/conglomerate with any wettability:

$$k_{rg} = 1.1072 \left(\frac{S_g - S_{gc}}{1 - S_{wi}} \right)^2 k_{rg(S_{org})} + 2.7794 \left(\frac{S_{org}(S_g - S_{gc})}{1 - S_{wi}} \right) k_{rg(S_{org})} \quad (7.19)$$

k_{rw} for water-wet limestone/dolomite:

$$k_{rw} = 0.0020525 \left(\frac{S_w - S_{wi}}{\phi^{2.15}} \right) - 0.051371 (S_w - S_{wi}) \left(\frac{1}{k_a} \right)^{0.43} \quad (7.20)$$

k_{rw} for oil and intermediate-wet limestone/dolomite:

$$\begin{aligned} k_{rw} = & 0.29986 \left(\frac{S_w - S_{wi}}{1 - S_{wi}} \right) - 0.32797 \left(\frac{S_w - S_{orw}}{1 - S_{wi} - S_{orw}} \right)^2 (S_w - S_{wi}) \\ & + 0.413259 \left(\frac{S_w - S_{wi}}{1 - S_{wi} - S_{orw}} \right)^4 \end{aligned} \quad (7.21)$$

k_{row} for oil and intermediate-wet limestone/dolomite:

$$k_{row} = 1.2624 \left(\frac{S_o - S_{orw}}{1 - S_{orw}} \right) \left(\frac{S_o - S_{orw}}{1 - S_{wi} - S_{orw}} \right)^2 \quad (7.22)$$

k_{rog} for oil and intermediate-wet limestone/dolomite:

$$k_{rog} = 0.93752 \left(\frac{S_o}{1 - S_{wi}} \right)^4 \left(\frac{S_o - S_{org}}{1 - S_{wi} - S_{org}} \right)^2 \quad (7.23)$$

k_g for oil and intermediate-wet limestone/dolomite:

$$\begin{aligned} k_g = & 1.8655 \frac{(S_g - S_{gc})S_g}{(1 - S_{wi})} k_{rg(S_{org})} + 8.0053 \frac{(S_g - S_{gc})S_{org}^2}{(1 - S_{wi})} \\ & - 0.02589 (S_g - S_{gc}) \left(\frac{1 - S_{wi} - S_{org} - S_{gc}}{(1 - S_{wi})} \right)^2 \\ & \times \left(1 - \frac{1 - S_{wi} - S_{org} - S_{gc}}{(1 - S_{wi})} \right)^2 \left(\frac{k_a}{\phi} \right)^{0.5} \end{aligned} \quad (7.24)$$

Observations

The end point k_{ro} at S_{wirr} in both the water-oil and gas-oil systems, is one. The Honarpour, et al. equations assume that $k_{abs} = k_{ro}(S_{wc})$. If a different base permeability is used, the data must be adjusted.

In the vicinity of S_{wirr} , the Honarpour, et al. equations fail to predict k_{rw} and the generated curve must be extrapolated over this saturation range.

Gas-oil equations predict smooth and consistent values in the range between $S_g = 0$ and residual liquid saturation. Extrapolation beyond this mobile saturation range can lead to unrealistic results. For example, a plot of k_{ro} shows that the calculated k_{ro} can become negative. The user may have to truncate calculated relative permeability values to fit in the physically meaningful range from 0 to 1.

Saturation Exponent Method

Another representation of relative permeability curves for multiphase flow is the saturation exponent method. The saturation exponent method is based on an empirical functional relationship between saturation and relative permeability. The following equations are used to fit smooth curves over any desired saturation range.

Water:

$$k_{rw} = k_{rw}^* \left(\frac{S_w - S_{wc}}{1 - S_{orw} - S_{wc}} \right)^{n_w} \quad (7.25)$$

Oil in an oil-water system:

$$k_{row} = k_{row}^* \left(\frac{1 - S_{orw} - S_w}{1 - S_{orw} - S_{wc}} \right)^{n_{ow}} \quad (7.26)$$

Gas:

$$k_{rg} = k_{rg}^* \left(\frac{S_g - S_{gc}}{1 - S_{lrg} - S_{gc}} \right)^{n_g} \quad (7.27)$$

Oil in a gas-oil system:

$$k_{rog} = k_{rog}^* \left(\frac{1 - S_{lrg} - S_g}{1 - S_{lrg}} \right)^{n_{og}} \quad (7.28)$$

The multiplier (k_i^*) is the end point relative permeability of phase (i) at the corresponding end point saturation (S_{wc} , S_{orw} , or S_{lrg}). The saturation S_{lrg} is the

total residual liquid saturation in the gas-oil system (including S_{wc}). The equations must satisfy $k_{rog} = k_{row}$ at S_{wirr} and $S_g = 0$ for both water-oil and gas-oil systems to be physically consistent. To simplify data adjustments, these equations are often fit to either laboratory data or data obtained from Honarpour's equations.

The exponent (n_i) for phase i controls the curvature of the k_r curve. The geometric curves associated with different values of the exponent are summarized below.

Exponent n_i	Function of Saturation
1	straight line
> 1	concave upward
< 1	concave downward

7.5 Three-Phase Relative Permeability Correlations

Three-phase relative permeabilities can be measured in the laboratory using techniques such as steady-state displacement and dynamic displacement. Laboratory measurements can be costly, time-consuming, and inaccurate. Consequently, three-phase k_{ro} are usually estimated from models of three-phase behavior using two-phase k_r curves.

Some methods available in many commercial simulators are described below. The effective relative permeability model in IFLO is described in more detail in Chapter 9.

STONES1 Method

Stone [1973] has provided two of the most commonly used three-phase relative permeability methods [Dietrich and Bondor, 1976]. These methods were originally based on two sets of two-phase k_r data: water displacing oil; and gas displacing oil at S_{wc} . Both sets of two-phase k_r data are referenced to the effective oil permeability at S_{wirr} , thus $k_{row} = k_{rog} = 1$ at $S_g = 0$ and $S_w = S_{wc}$. One implementation of the STONES1 method is described below.

98 Integrated Flow Modeling

End point values must satisfy $k_{row} = k_{rog}$ at $S_g = 0$ and $S_w = S_{wc}$, but end point values need not equal one. The curve k_{ro} is a function of both S_w and S_g . The STONES1 equation can be written

$$k_{ro} = \left(\frac{S_o^*}{k_{rocw}} \right) \beta_w \beta_g \quad (7.29)$$

where k_{rocw} = relative permeability to oil at S_{wc} ,

$$\beta_w = \frac{k_{row}}{1 - S_w^*} \quad (7.30)$$

and

$$\beta_g = \frac{k_{rog}}{1 - S_g^*} \quad (7.31)$$

In these equations, the relative permeability to oil in the presence of water k_{row} is set equal to k_{ro} from oil-water data, and the relative permeability to oil in the presence of gas k_{rog} is set equal to k_{ro} from gas-oil data.

Normalized phase saturations S^* are defined as

$$\begin{aligned} S_o^* &= \frac{S_o - S_{om}}{1 - S_{wc} - S_{om}} \\ S_w^* &= \frac{S_w - S_{wc}}{1 - S_{wc} - S_{om}} \\ S_g^* &= \frac{S_g}{1 - S_{wc} - S_{om}} \end{aligned} \quad (7.32)$$

where S_{om} = minimum S_{or} from the two two-phase data sets. Water relative permeability k_{rw} is obtained from oil-water data as a function of S_w only, and gas relative permeability k_{rg} is obtained from gas-oil data measured at S_{wc} , as a function of S_g only. Gas-water data are *not* used. This assumes that

- k_{rw} in a gas-water system = k_{rw} in a water-oil system
- k_{rg} in a gas-water system = k_{rg} in a water-oil system

This assumption is not always valid.

STONES2 Method

The second Stone correlation used the same assumptions as the first Stone correlation, namely $k_{row} = k_{rog} = 1.0$ at $S_w = S_{wc}$ and $S_g = 0$. The end point values satisfy $k_{row} = k_{rog}$ at $S_g = 0$ and $S_w = S_{wc}$, but end point values need not equal one.

The water and gas relative permeability curves k_{rw} and k_{rg} are treated as in the STONES1 method. Oil relative permeability k_{ro} is a function of both S_w and S_g . It is calculated from

$$k_{ro} = k_{rocw} \left(\frac{k_{row}}{k_{rocw}} + k_{rw} \right) \left(\frac{k_{rog}}{k_{rocw}} + k_{rg} \right) - k_{rw} - k_{rg} \quad (7.33)$$

Eclipse Method

An alternative method that assumes that three-phase saturations will vertically segregate in each grid node due to gravitational forces is included in the commercial simulator ECLIPSE. Total height of each node is separated into a water zone and a gas zone. The thickness of the different zones is calculated from average phase saturations in the node.

The fractional thickness of the gas zone is

$$y_{\text{gas}} = \frac{S_g}{S_g + S_w - S_{wco}} \quad (7.34)$$

where S_{wco} is S_{wc} in the gas-oil system. The fractional thickness of the water zone is

$$y_{\text{water}} = \frac{S_w - S_{wco}}{S_g + S_w - S_{wco}} \quad (7.35)$$

Oil flow is weighted by the gas and water zone thicknesses:

$$k_{ro} = y_{\text{gas}} k_{rog} + y_{\text{water}} k_{row} = \frac{S_g k_{rog} + (S_w - S_{wco}) k_{row}}{S_g + S_w - S_{wco}} \quad (7.36)$$

The ECLIPSE default method is not intended to model three-phase k_{ro} in a well mixed system. It is intended to model oil flow from a partially gravity segregated reservoir.

Discussion

All three of the methods described above significantly reduce the three-phase value of k_{ro} relative to its two-phase value. The STONES2 method has the greatest reduction of the methods described above.

A comparison of three-phase k_{ro} correlations with laboratory data shows that a reliable three-phase relative permeability algorithm that can be applied with confidence to any reservoir does not exist. If three-phase flow is expected to have a major impact on project performance, it is wise to perform a sensitivity study to determine the impact of several different three-phase k_{ro} correlations on model results.

Exercises

- 7-1. A. Run EXAM10.DAT (gas reservoir cross-section with aquifer). Report the time, pressure, gas rate at the end of the run. What is the seismic velocity ratio in block (1,1,2) at the start and end of the run?
B. Set critical gas saturation to zero and rerun the model. Report the time, pressure, gas rate at the end of the run. What is the seismic velocity ratio in block (1,1,2) at the start and end of the run?
C. Explain the differences between A and B.

- 7-2. A. Run EXAM6.DAT (5-spot waterflood) and report the OOIP, time, pressure, oil rate and water rate at the end of the run.
B. Change the grid so all blocks are 160 ft long by 160 ft wide. Leave all wells in their original blocks. Rerun the model and report the OOIP, time, pressure, oil rate and water rate at the end of the run.
C. Fit a saturation exponent curve to k_{rw} and k_{row} . (Hint: use a spreadsheet.) Enter the new curves in the data set and rerun the model used in 7-2B. Report the OOIP, time, pressure, oil rate and water rate at the end of the run.
D. Explain the differences between A, B and C.

- 7-3. A. Run EXAM3.DAT (Buckley-Leverett) for up to 730 days or until the run stops under its original run controls. Report the time, pressure, oil rate and water rate at the end of the run.
- B. Multiply the permeability in EXAM3.DAT by 2 and rerun the model. Report the time, pressure, oil rate and water rate at the end of the run.
- C. Multiply all values of k_w by 0.5 in the original version of EXAM3.DAT and rerun the model. Report the time, pressure, oil rate and water rate at the end of the run.
- D. Explain the differences between A, B and C. Hint: compare the pressure gradient between the injection well block and the production well block for each run at the end of the first year.

Chapter 8

Capillary Pressure

Two quantities are essential to the understanding of the distribution and behavior of multiple fluid phases occupying the same pore space: relative permeability and capillary pressure. Relative permeability was discussed in the previous chapter. This chapter focuses on capillary pressure. Chapter 9 discusses refinements to the ideas presented here and in Chapter 7.

8.1 Basic Concepts

Some basic concepts must be introduced as prerequisites for understanding capillary pressure. The concepts are interfacial tension, wettability and contact angle. They are defined here.

Interfacial Tension

On all interfaces between solids and fluids, and between immiscible fluids, there is a surface free energy resulting from electrical forces. These forces cause the surface of a liquid to occupy the smallest possible area and act like a membrane. Interfacial tension (IFT) refers to the tension at a liquid-/liquid interface. Surface tension refers to the tension at a gas/liquid interface.

Interfacial tension is energy per unit of surface area, or force per unit length. IFT is usually expressed in milli-Newtons/meter or the equivalent dynes/cm. The value of IFT depends on the composition of the two fluids at the interface between phases. Table 8-1 lists a few examples:

Table 8-1
Examples of Interfacial Tension

Fluid Pair	IFT Range (mN/m or dyne/cm)
Air-Brine	72-100
Oil-Brine	15-40
Gas-Oil	35-65

IFT can be estimated using the Macleod-Sugden correlation and Fanchi's procedure for estimating parachors (Fanchi, JPT, 1990). The Weinaug-Katz variation of the Macleod-Sugden correlation is

$$\sigma^{1/4} = \sum_{i=1}^{N_c} P_{ch,i} \left(x_i \frac{\rho_L}{M_L} - y_i \frac{\rho_V}{M_V} \right) \quad (8.1)$$

where

σ interfacial tension [dyne/cm]

P_{ch} parachor [(dynes/cm)^{1/4}/(g/cm³)]

M_L molecular weight of liquid phase

M_V molecular weight of vapor phase

ρ_L liquid phase density [g/cm³]

ρ_V vapor phase density [g/cm³]

x_i mole fraction of component i in liquid phase

y_i mole fraction of component i in vapor phase

Parachors are empirical parameters. The parachor of component i can be estimated using the molecular weight M_i of component i and the empirical regression equation

$$P_{ch,i} = 10.0 + 2.92 M_i \quad (8.2)$$

This procedure works reasonably well for molecular weights ranging from 100 to 500. A more accurate procedure for a wider range of molecular weights is given by Fanchi [1990].

Wettability

Wettability is the ability of a fluid phase to preferentially wet a solid surface in the presence of a second immiscible phase. We saw in Chapter 7 that relative permeability depends on wettability. The wetting, or wettability, condition in a rock/fluid system depends on IFT.

Changing the type of rock or fluid can change IFT and, hence, wettability of the system. Adding a chemical such as surfactant, polymer, corrosion inhibitor, or scale inhibitor can alter wettability.

Contact Angle

Wettability is measured by contact angle. Contact angle is always measured through the more dense phase. Contact angle is related to interfacial energies by

$$\sigma_{os} - \sigma_{ws} = \sigma_{ow} \cos\theta \quad (8.3)$$

where:

σ_{os} interfacial energy between oil and solid [dyne/cm]

σ_{ws} interfacial energy between water and solid [dyne/cm]

σ_{ow} interfacial energy, or IFT, between oil and water [dyne/cm]

θ contact angle at oil-water-solid interface measured through the water phase [degrees]

Examples of contact angle are presented in Table 8-2 for different wetting conditions.

Table 8-2
Examples of Contact Angle

Wetting Condition	Contact Angle, degrees
Strongly Water-wet	0-30

Table 8-2
Examples of Contact Angle

Wetting Condition	Contact Angle, degrees
Moderately Water-wet	30-75
Neutrally Wet	75-105
Moderately Oil-wet	105-150
Strongly Oil-wet	150-180

Robust methods for measuring wettability in the reservoir have not yet been developed. Consequently, wettability is usually measured in the laboratory. Several factors can affect laboratory measurements of wettability. Wettability can be changed by contact of the core during coring with drilling fluids or fluids on the rig floor, and contact of the core during core handling with oxygen and/or water from the atmosphere. Laboratory fluids should also be at reservoir conditions to obtain the most reliable measurements of wettability. Based on laboratory tests, most known reservoirs have intermediate wettability and are preferentially water wet.

8.2 Capillary Pressure

Capillary pressure is the pressure difference across the curved interface formed by two immiscible fluids in a small capillary tube:

$$P_c = P_{nw} - P_w \quad (8.4)$$

where

P_c capillary pressure [psi]

P_{nw} pressure in nonwetting phase [psi]

P_w pressure in wetting phase [psi]

Capillary Pressure Theory

Equilibrium between fluid phases in a cylindrical capillary tube with radius r and cross-sectional area πr^2 is satisfied by the relationship *force up* = *force*

106 Integrated Flow Modeling

down. The forces acting on the fluids are

$$\begin{aligned} \text{force up} &= \text{IFT acting around perimeter of capillary tube} \\ &= \sigma \cos \theta \times 2\pi r \end{aligned}$$

and

$$\begin{aligned} \text{force down} &= \text{density difference} \times \text{cross-sectional area} \times \\ &\quad \text{height of capillary rise in tube} \\ &= (\rho_w - \rho_{air})\pi r^2 h \end{aligned}$$

Capillary pressure P_c is defined as the force/unit area. Dividing the forces by the cross-sectional area of the capillary tube gives

$$P_c = \text{force up} / \pi r^2 = \text{force down} / \pi r^2.$$

Capillary Pressure and Pore Radius

Expressing capillary pressure in terms of force up per unit area gives:

$$P_c = \frac{2\pi r \sigma \cos \theta}{\pi r^2} = \frac{2\sigma \cos \theta}{r} \quad (8.5)$$

where

r pore radius [cm]

σ interfacial (or surface) tension [mN/m or dynes/cm]

θ contact angle [degrees]

Equation (8.5) shows that an increase in pore radius will cause a reduction in capillary pressure while a decrease in IFT will cause a decrease in capillary pressure.

Equivalent Height

Expressing P_c in terms of force down leads to the expression

$$P_c = \frac{\pi r^2 h (\rho_w - \rho_{air})}{\pi r^2} = h (\rho_w - \rho_{air}) \quad (8.6)$$

where

h height of capillary rise [ft]

P_c capillary pressure [psi]

ρ_w water, or wetting phase, density gradient [psi/ft]

ρ_{air} air, or nonwetting phase, density gradient [psi/ft]

Solving for h yields the defining relationship between capillary pressure and equivalent height, namely

$$h = \frac{P_c}{(\rho_w - \rho_{air})} \quad (8.7)$$

The equivalent height provides an estimate of the height of the transition zone between immiscible phases. A more precise definition of transition zone is given in the following section. Equivalent height is inversely proportional to the difference in densities between two immiscible phases. The relatively large density difference between gas and liquid results in a smaller transition zone height than the relatively small difference between two liquid phase densities.

Equilibrium Initialization

Capillary pressure can be used to establish the initial saturation distribution in the reservoir. The procedure used in IFLO is described in detail in the User's Manual Program Supplement.

8.3 Capillary Pressure Measurements

Capillary pressure cannot be measured directly in a reservoir. It can be inferred from information that indicates the height of a transition zone, such as well log information. Capillary pressure is usually determined in the laboratory by centrifuge experiments that provide a relationship between capillary pressure P_c and water saturation S_w . A typical P_c versus S_w curve has the following features (see Figure 8-1):

- The drainage P_c curve starts at $S_w = 100\%$.
- Water saturation S_w decreases as oil is forced into the rock. The pressure required to force the first droplet of oil into the rock is called entry pressure (or threshold pressure).

- As pressure increases above entry pressure, more oil enters the rock. Eventually no further reduction in S_w occurs. The minimum S_w is called irreducible water saturation, S_{wirr} .
- P_c can be converted to an equivalent height. This height is referenced to the free water level — the level at which the oil-water contact (OWC) would occur in the absence of a porous medium, i.e. at porosity $\phi = 100\%$. At the free water level, $P_c = 0$.

- The zone of rapidly-changing S_w above the entry pressure and below S_{wirr} defines the transition zone between the oil reservoir and the water column.
- The OWC is the elevation at which S_o first appears. In practice, other definitions of OWC might be used, such as the deepest occurrence of water-free oil production.

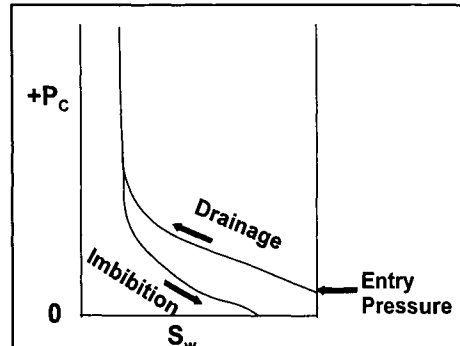


Figure 8-1. Capillary Pressure and Hysteresis.

Capillary Pressure Hysteresis

Capillary pressure is a function of saturation and depends on the direction of saturation change. The dependence of capillary pressure on the direction of saturation change implies that capillary pressure depends on the history of fluid movement in the region of interest. The drainage curve is the capillary pressure curve that results when the wetting phase saturation is decreasing. The imbibition curve is obtained when the wetting phase saturation is increasing.

The difference in paths between the drainage and imbibition curves is called hysteresis. For an oil-water system, oil trapped in an immobile state at the end of imbibition is called residual oil saturation, S_{or} . Hysteresis is illustrated in Figure 8-1.

Capillary Pressure in Reservoirs

Capillary pressure in reservoirs depends on the interfacial tension (IFT) between two immiscible fluids; the contact angle between rock and fluid; and the pore radius of the rock. The contact angle is a function of wettability, and pore radius is a microscopic rock property.

Equation (8.5) shows that P_c decreases as pore radius increases. Rock with large pore radii usually have a larger permeability than rock with smaller pore radii. Thus, high permeability rocks have lower P_c than lower permeability rocks containing the same fluids.

Capillary Pressure and Irreducible Water Saturation

Capillary forces explain why water is retained in oil and gas zones. In water-wet reservoirs, water coats rock surfaces and is preferentially held in smaller pores. Nonwetting hydrocarbon phases occupy the central parts of larger pores.

Rocks with large pores are associated with low P_c and low S_{wirr} . Examples of rocks with large pores are coarse-grained sand, coarse-grained oolitic carbonates, and vuggy carbonates. High P_c and high S_{wirr} are associated with fine grained reservoir rocks.

Correcting Capillary Pressure Measurements

Laboratory measurements of P_c should be conducted with reservoir oil and water at reservoir temperature. In practice P_c measurements are sometimes made using more convenient laboratory fluids, and are almost always made at laboratory conditions. It is therefore necessary to have a method of converting laboratory measurements to reservoir conditions.

Laboratory measurements of P_c are converted to reservoir conditions using the relationship

$$P_{c(res)} = P_{c(lab)} \frac{\sigma_{res} |\cos\theta|_{res}}{\sigma_{lab} |\cos\theta|_{lab}} \quad (8.8)$$

where

$P_{c(res)}$	capillary pressure corrected to reservoir conditions and reservoir fluids [psig]
$P_{c(lab)}$	capillary pressure measured in laboratory [psig]
σ_{res}	IFT between reservoir fluids at reservoir conditions [mN/m or dyne/cm]
σ_{lab}	IFT between laboratory fluids at laboratory conditions [mN/m or dyne/cm]
θ_{res}	contact angle for reservoir conditions and fluids [degrees]
θ_{lab}	contact angle for laboratory conditions and fluids [degrees]

Data that are valid for the temperature of interest should be used because both IFT and contact angle vary with temperature. Some typical values are shown in Table 8-3.

Table 8-3
Laboratory Value of IFT and Contact Angle at 72° F.

Fluid Pair	Typical Interfacial Tension, (mN/m)	Contact Angle, degrees
Air and water	72	0
Air and mercury	480	140
Mineral oil and water	40	20

In the absence of laboratory data, estimates of IFT and contact angle must be used. IFT is discussed in Section 8-1. Contact angle estimates based on wettability can be made from data contained in Table 8-4.

Table 8-4
Reservoir Values of IFT and Contact Angle

Fluid Pair	Typical Interfacial Tension (mN/m)	Contact Angle (degrees)
Gas/water	40-70	0
Crude/water	10-35	30-150

8.4 Capillary Pressure Correlation Methods

Rock samples with different pore-size distribution, permeability, and porosity will yield different P_c curves. Several techniques correlate P_c and S_w from lab data. Some of the most common are outlined below. The quality of each correlation should be checked whenever possible against known results.

Leverett's *J*-function

Leverett's *J*-function is defined as:

$$J(S_w) = \frac{P_{c(lab)}}{\sigma_{lab} |(\cos\theta)_{lab}|} \left(\sqrt{\frac{K}{\phi}} \right)_{lab} \quad (8.9)$$

where

$P_{c(lab)}$ Laboratory-measured capillary pressure [psi]

$J(S_w)$ Leverett's *J*-function

K core sample permeability [md]

ϕ core sample porosity [fraction]

σ_{lab} lab value of IFT [dyne/cm]

θ_{lab} lab value of contact angle

Given the function $J(S_w)$, we can obtain capillary pressure as

$$P_{c(res)} = \frac{J(S_w) \sigma_{res} |(\cos\theta)_{res}|}{\left(\sqrt{\frac{K}{\phi}} \right)_{res}} \quad (8.10)$$

The corresponding height of any water saturation S_w above the free water level is the equivalent height

$$h = \frac{J(S_w) \sigma_{res} |(\cos\theta)_{res}|}{(\rho_w - \rho_o) \left(\sqrt{\frac{K}{\phi}} \right)_{res}} \quad (8.11)$$

where

$P_{c(res)}$	reservoir P_c [psi]
h	height above free water level [ft]
K	permeability [md]
ϕ	porosity [fraction]
σ_{res}	reservoir value of IFT [dyne/cm]
θ_{res}	reservoir value of contact angle
$(\rho_w - \rho_o)$	density difference between oil and water [psi/ft]

The Leverett J -function is calculated using the following procedure:

- 1) calculate $J(S_w)$ for each P_c point
- 2) plot $J(S_w)$ versus S_w for all points
- 3) draw a smooth curve through the points
- 4) calculate P_c or h for each S_w for any set of desired K and ϕ
- 5) plot P_c or h versus S_w

Alternative Correlations

Capillary pressure can occasionally be correlated with other rock properties. A few of these correlations are outlined below.

P_c vs. $\log K$

The following procedure can be used to seek a correlation between capillary pressure and the logarithm of permeability. We begin by plotting water saturation S_w against $\log K$ for constant values of P_c :

- (1) At a given value of P_c , obtain the value of S_w for each core sample and plot $\log K$ versus S_w .
- (2) Repeat Step (1) for enough values of P_c to cover the expected P_c range. Plot $\log K$ versus S_w for all values of P_c .
- (3) Enter the plot obtained in (2) at any permeability and read S_w for each P_c value.

This method is reliable if approximately straight lines are obtained in a plot of P_c versus $\log K$. If the data are scattered, it may be possible to improve the correlation by introducing another correlating parameter, namely porosity ϕ .

P_c vs. $\log k$ and ϕ

The following procedure evaluates ϕ and $\log K$ as correlating parameters:

- (1) For a given value of P_c , plot $\log K$ vs S_w .
- (2) On the plot created in (1), find two samples with similar ϕ and draw a straight line of constant ϕ . This line honors core data.
- (3) Draw additional constant- ϕ lines parallel to the line picked in (2).
- (4) Enter the plot at a desired K , read to the intersection with the constant- ϕ line, then down to the S_w corresponding to P_c for the given ϕ, K .
- (5) Repeat steps (1) - (4) to find S_w for the P_c range expected in the reservoir. A plot of P_c vs S_w gives the P_c curve at the desired ϕ, K .

Estimating Wettability

Wettability is difficult to measure, but is needed for a variety of reasons, such as selecting contact angle and correcting capillary pressure P_c , interpreting reservoir performance, and evaluating improved recovery methods. Wettability may be estimated from a relationship between P_c and S_w using the following U.S. Bureau of Mines (USBM) method [Tiab and Donaldson, 1996, Chapter 6].

We begin by establishing a relationship between P_c and S_w . The relationship is usually obtained by measuring P_c versus S_w with a centrifuge. Once we have a plot of P_c versus S_w , we calculate the areas (A , B) in Figure 8-2.

The wettability index is defined as $\log_{10}(\text{Area } A)/(\text{Area } B)$ and has the following interpretation:

- Positive values of wettability index indicate a water-wet system.
- Negative values of wettability index indicate an oil-wet system.

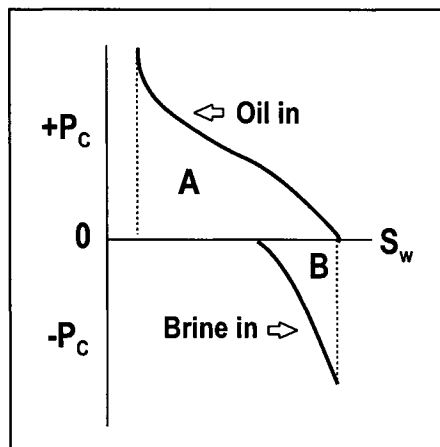


Figure 8-2. USBM Wettability Index Areas.

114 Integrated Flow Modeling

- Values more positive than +1 or more negative than -1 are rare.

In a strongly water-wet system, Area A is often ten times Area B, resulting in a wettability index of +1. The wettability index for a strongly oil-wet system will be approximately -1. Most wettability indices vary between +0.5 and -0.5.

Exercises

- 8-1. A. Run ARCO1.DAT (enriched gas injection) and record original volumes in place, time, pressure, oil rate, water rate, and gas rate at the end of the run.
B. Set $P_{cow} = 0$ in the data set and rerun the model. Record original volumes in place, time, pressure, oil rate, water rate, and gas rate at the end of the run.
C. Set $P_{cgo} = 0$ and $P_{cow} = 0$ in the original ARCO1.DAT file and rerun the model. Record original volumes in place, time, pressure, oil rate, water rate, and gas rate at the end of the run.
D. Explain the differences between A, B and C.
- 8-2. Permeability is considered a measure of the cross-sectional area of a pore. Use this observation and the concept of pore radius to answer the following questions.
 - A. Is capillary pressure greater in a high permeability reservoir or a low permeability reservoir? Justify your answer.
 - B. Is the transition zone thicker in a high permeability reservoir or a low permeability reservoir? Justify your answer.

Chapter 9

Extended Rock-Fluid Interactions

Some of the most critical data in terms of their effect on simulator performance are the relative permeability and capillary pressure curves. They model the interaction between reservoir rock and fluids. Relative permeability and capillary pressure functions for traditional flow simulators are discussed in Chapters 7 and 8. Algorithms that include additional effects associated with miscible flow are discussed in this chapter, followed by a discussion of the transmissibility between gridblocks.

9.1 Miscible Conditions

The formulation of IFLO includes a weighting factor α to control the transition from immiscible to miscible conditions. The weighting factor is defined in terms of two pressures P_1 and P_2 . If the gridblock pressure $P \leq P_1$, then fluids in the gridblock exist in immiscible conditions. If the gridblock pressure $P \geq P_2$, then fluids in the gridblock exist in miscible conditions. The transition between immiscible and miscible conditions occurs in the pressure range from P_1 to P_2 . The weighting factor α is used to interpolate properties between immiscible and miscible conditions. By definition,

$$\alpha = \begin{cases} 0 & \text{when } P \leq P_1 \\ \frac{P - P_1}{P_2 - P_1} & \text{when } P_1 < P < P_2 \\ 1 & \text{when } P \geq P_2 \end{cases} \quad (9.1)$$

Physically, P_1 may be interpreted as the first contact miscible pressure PMISC and P_2 as the multicontact miscible pressure PMCM in Record 8 of the IFLO User's Manual, Appendix B.8.

Miscible conditions are achieved in a gridblock when $P >$ PMISC and solvent in place in the gridblock exceeds VSMISC (Record 8, Appendix B.8). In this case, all oil, natural gas and solvents in the gridblock are treated as fully miscible. All oil in excess of the saturation SORM or SOMIN (Record 8, Appendix B.8) is recoverable under miscible conditions.

If $P <$ PMCM, then oil is treated as immiscible with the natural gas-solvent mixture. All natural gas and solvents in the gridblock are treated as fully miscible.

A more detailed treatment of fluid property behavior in a miscible system is presented in Chapter 10.

9.2 Solid Precipitation

Displacement of oil by carbon dioxide is often accompanied by the precipitation of a semisolid or asphaltene substance [Shelton and Yarborough, 1977]. This phenomenon cannot be rigorously modeled in a three-phase simulator, but its influence on a carbon dioxide displacement process is approximated in IFLO using the following algorithm.

Solid precipitation of oil is allowed to occur when oil saturation in a gridblock drops below the user-specified minimum oil saturation SOMIN (Record 8, Appendix B.7). In this case, the stock tank volume of precipitated oil is set equal to the volume of oil in the block divided by the oil formation volume factor in the block. Relative permeability to oil is set to 0 in the gridblock. Water and gas relative permeabilities in the gridblock are multiplied by a user-specified reduction factor REDK (Record 8, Appendix B.7).

9.3 Water Blocking

The efficiency of solvent injection can be adversely affected if the solvent is unable to contact oil. One barrier to solvent contacting oil is the presence of water. The effect is called water blocking. Water blocking is modeled in IFLO as follows.

Residual oil saturation in the presence of water (S_{ow}) is determined from the oil-water relative permeability table. The water-blocked oil saturation (S_{twb}) is estimated from the relationship

$$S_{twb} = \frac{S_{ow}}{1 + \beta \cdot \left(\frac{k_m}{k_{rw}} \right)} \quad (9.2)$$

where k_m and k_{rw} denote the non-aqueous and aqueous phase relative permeabilities respectively.

Equation (9.2) was proposed by Chase and Todd [1984]. They recommended that $\beta = 1$ for highly water-wet sandstones and $\beta = 5$ for mixed-wettability systems. The case in which no oil is contacted by solvent is represented by $\beta = 0$. A very large value of β will make S_{twb} approach 0 and corresponds to the case in which all of the oil is contacted by solvent.

9.4 Mobility Control

The presence of 0.1 to 1.0 percent surfactant in injected water can lead to a reduction in carbon dioxide mobility [Bernard, et al., 1980]. This effect is modeled in IFLO as follows.

Reservoir water and surfactant-bearing water are assumed to be completely miscible. If the mobility control option is on, the gas phase mobility is reduced based on the saturation of surfactant-bearing S_c water in the gridblock and a user-specified mobility reduction table. If we define x_s as the ratio of the volume of water containing surfactant to the total water volume, then $S_c = x_s S_w$ where S_w is the water saturation in the gridblock. The surfactant-bearing water saturation S_c corresponds to the normalized surfactant concen-

tration specified by the user in the mobility reduction table (Record 28, Appendix B.7). The gas phase mobility reduction is achieved by multiplying gas phase mobility by the factor $\text{FRCO}_2 \cdot \text{SCI}$ where FRCO_2 is the mobility reduction at S_c , and SCI is a user-specified saturation concentration index (Record 26, Appendix B.7).

9.5 Effective Relative Permeability and Capillary Pressure

Effective relative permeability curves for the oleic and gaseous phases are given by the following relations:

$$k_{ro}^e = (1 - \alpha_m) k_{ro} + \alpha_m \left(\frac{S_o}{1 - S_w} \right) k_m \quad (9.3)$$

and

$$k_{rg}^e = (1 - \alpha_m) k_{rg} + \alpha_m \left(\frac{S_g}{1 - S_w} \right) k_m \quad (9.4)$$

where the weighting factor α_m is given by

$$\alpha_m = \alpha \cdot \min \left\{ \frac{(1 - v_g)}{v_{s, \text{misc}}}, 1 \right\} \quad (9.5)$$

The quantity v_g is the volume fraction of gas and $v_{s, \text{misc}}$ is the total solvent volume fraction required to obtain full miscibility. The parameter $v_{s, \text{misc}}$ is specified by the user. The effective gas-oil capillary pressure is

$$P_{cgo}^e = (1 - \alpha_m) P_{cgo} \quad (9.6)$$

When miscible conditions are achieved in IFLO, the non-aqueous phase relative permeability is set equal to the relative permeability to oil k_{row} entered for the oil-water system. The three-phase oil relative permeability calculation is still used, if originally activated using code KR3P in Appendix B.4, for gridblocks with pressures below the miscibility pressure.

Single-point, upstream relative permeability weighting is used for all phases.

9.6 Transmissibility

Flow between neighboring blocks is treated as a series application of Darcy's law. We are concerned with the movement of fluids between two blocks such as those in Figure 9-1.

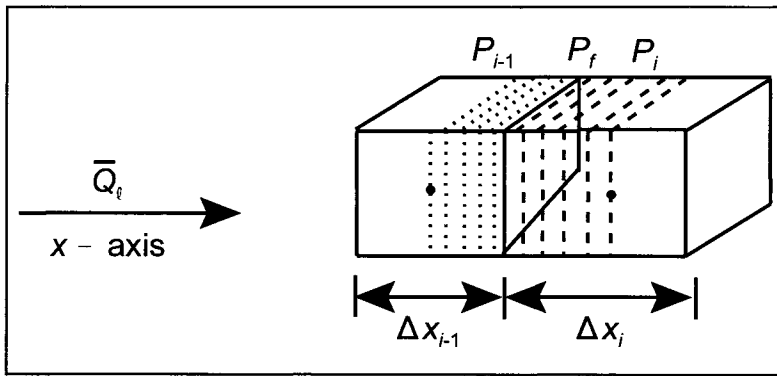


Figure 9-1. Notation for Transmissibility Calculation.

If we assume that the conditions needed for Darcy flow are satisfied, and ignoring for the moment changes in phase mobility λ_ℓ and phase formation volume factor B_ℓ , we have

$$\overline{Q}_\ell = \overline{K} \overline{A}_c \frac{k_r}{\mu_\ell B_\ell} \frac{P_{i-1} - P_i}{\Delta x_{i-1} + \Delta x_i} \quad (9.7)$$

2

where \overline{Q} is the average volumetric flow rate of phase ℓ , \overline{K} is the absolute permeability associated with a pressure drop from x_{i-1} to x_i , and \overline{A} is the cross-sectional area between x_{i-1} and x_i . To make use of the above equation, it is necessary to express the product $\overline{K} \overline{A}_c$ in terms of known variables, namely x_j , K_j , A_{cj} , where j refers to blocks $i - 1$ and i .

We begin by using Darcy's law to write the flow rates through each shaded volume element. The flow rate of phase ℓ is

$$\bar{Q}_\ell = K_{i-1} A_{c,i-1} \frac{k_{re}}{\mu_\ell B_\ell} \frac{P_{i-1} - P_f}{\frac{\Delta x_{i-1}}{2}} \quad (9.8)$$

for block $i - 1$ and

$$\bar{Q}_\ell = K_i A_{c,i} \frac{k_{re}}{\mu_\ell B_\ell} \frac{P_f - P_i}{\frac{\Delta x_i}{2}} \quad (9.9)$$

for block i . The pressure P_f refers to the pressure at the interface between block $i - 1$ and block i . Solving for $(P_{i-1} - P_f)$ and $(P_f - P_i)$ in Eqs. (9.8) and (9.9), respectively, and then adding the results yields

$$P_{i-1} - P_i = \bar{Q}_\ell \left[\frac{\frac{\Delta x_{i-1}}{2} \frac{k_{re}}{\mu_\ell B_\ell}}{K_{i-1} A_{c,i-1}} + \frac{\frac{\Delta x_i}{2} \frac{k_{re}}{\mu_\ell B_\ell}}{K_i A_{c,i}} \right] \quad (9.10)$$

Inserting this expression into Eq. (9.7) and solving for \bar{KA}_c gives

$$\bar{KA}_c = \frac{\Delta x_{i-1} + \Delta x_i}{\left(\frac{\Delta x_{i-1}}{K_{i-1} A_{c,i-1}} \right) + \left(\frac{\Delta x_i}{K_i A_{c,i}} \right)} \quad (9.11)$$

Substituting this expression back into Eq. (9.7) gives, after some simplification, the flow rate equation

$$\bar{Q}_\ell = \frac{k_{re}}{\mu_\ell B_\ell} \left[\frac{2(KA_c)_{i-1} \cdot (KA_c)_i}{\Delta x_{i-1}(KA_c)_i + \Delta x_i(KA_c)_{i-1}} \right] (P_{i-1} - P_i) \quad (9.12)$$

We still have the task of determining a suitable average for the product $k_{re}/\mu_\ell B_\ell$. Industry experience has shown that use of a phase mobility in the block which has the larger phase potential of the two neighboring blocks yields more reliable results. The calculation in IFLO uses the value of the phase saturation of the upstream block at time level n to determine an upstream phase relative

permeability. This is then combined with the arithmetic mean values of the phase viscosities and phase formation volume factors, giving

$$\frac{k_{re}}{\mu_\ell B_\ell} = \frac{k_{re(\text{upstream})}}{\left(\frac{\mu_{\ell,i-1} + \mu_{\ell,i}}{2}\right)\left(\frac{B_{\ell,i-1} + B_{\ell,i}}{2}\right)} \quad (9.13)$$

The final form of Eq. (9.12) thus becomes

$$\begin{aligned} \bar{Q}_\ell &= A'_{\ell,i-1/2} \cdot (P_{i-1} - P_i) \\ &\equiv \frac{4k_{re(\text{upstream})}}{(\mu_{\ell,i-1} + \mu_{\ell,i})(B_{\ell,i-1} + B_{\ell,i})} \left[\frac{2(KA_c)_{i-1}(KA_c)_i(P_{i-1} - P_i)}{\Delta x_{i-1}(KA_c)_i + \Delta x_i(KA_c)_{i-1}} \right] \end{aligned} \quad (9.14)$$

where $A'_{\ell,i-1/2}$ is the Darcy phase transmissibility between blocks $i-1$ and i .

If we now consider the convection term in the pressure equation, we find

$$\nabla \cdot \tilde{K} \cdot \frac{\lambda_\ell}{B_\ell} \nabla P_\ell = \frac{\partial}{\partial x} \left(K_x \frac{\lambda_\ell}{B_\ell} \frac{\partial P_\ell}{\partial x} \right) + \frac{\partial}{\partial y} \left(K_y \frac{\lambda_\ell}{B_\ell} \frac{\partial P_\ell}{\partial x} \right) + \frac{\partial}{\partial z} \left(K_z \frac{\lambda_\ell}{B_\ell} \frac{\partial P_\ell}{\partial x} \right) \quad (9.15)$$

in the principal coordinate system of the permeability tensor. Expanding the first term in Eq. (9.15) in finite difference form and using the definition of phase transmissibility, we have

$$\begin{aligned} \frac{\partial}{\partial x} \left(K_x \frac{\lambda_\ell}{B_\ell} \frac{\partial P_\ell}{\partial x} \right)_i &\approx \frac{\frac{A'_{\ell,i+1/2}}{\Delta y_i \Delta z_i} (P_{i+1} - P_i) - \frac{A'_{\ell,i-1/2}}{\Delta y_i \Delta z_i} (P_i - P_{i-1})}{\frac{\Delta x' + \Delta x''}{2}} \\ &\equiv \frac{\left(K_x \frac{\lambda_\ell}{B_\ell} \right)_{i+1/2} \left(\frac{P_{i+1} - P_i}{\Delta x''} \right) - \left(K_x \frac{\lambda_\ell}{B_\ell} \right)_{i-1/2} \left(\frac{P_i - P_{i-1}}{\Delta x_i} \right)}{\frac{\Delta x' + \Delta x''}{2}} \end{aligned} \quad (9.16)$$

where

$$\Delta x' = x_i - x_{i-1}, \quad \Delta x'' = x_{i+1} - x_i$$

Here we have assumed that the cross-sectional area remains constant from block to block, as would be the case for any rectangular grid system. If the

cross-sectional area changes from block to block, the assumption would only hold approximately. The option to include varying cross-sectional areas is a practical feature of IFLO that yields satisfactory results for many realistic situations.

Equation (9.16) is now multiplied by the bulk volume $V_B = \Delta x_i \Delta y_i \Delta z_i$ to give the result

$$V_B \frac{\partial}{\partial x} \left(K_x \frac{\lambda_\ell}{B_\ell} \frac{\partial P_\ell}{\partial x} \right)_i \approx \frac{\Delta x_i}{\left(\frac{\Delta x' + \Delta x''}{2} \right)} [A'_{\ell,i+1/2}(P_{i+1} - P_i) - A'_{\ell,i-1/2}(P_i - P_{i-1})] \\ \equiv A'_{\ell,i+1/2}(P_{i+1} - P_i) - A'_{\ell,i-1/2}(P_i - P_{i-1}) \quad (9.17)$$

where $A'_{\ell,i-1/2}$ is the finite difference phase transmissibility between block $i-1$ and block i , and the j, k indices are suppressed. IFLO uses this value of transmissibility in its calculations. Notice that the Darcy phase transmissibility A'_ℓ equals the finite difference phase transmissibility A_ℓ when the grid spacing is uniform. A similar procedure is used to obtain transmissibility values for the y and z directions.

The Transmissibility Modifications section in Appendix B.3.3 describes the directional conventions for transmissibility in the model. Transmissibility modifications are especially useful for modifying flow performance during history matching. Transmissibilities may be used to define sealing or partially sealing faults, and to define high permeability channels.

Boundary Conditions

The choice of grid and the choice of boundary conditions are intimately related, as has been discussed extensively in the literature. Selection of a grid is important in deciding how to treat differences at boundaries. The usual approach is to assume the boundary of a finite difference grid is a no-flow boundary. A block-centered grid with the no flow boundary condition has been coded in IFLO. Implementation is achieved by setting transmissibilities at boundary interfaces to zero. The transmissibilities of blocks with no net pay are set to zero to prohibit flow into or out of the block.

Exercises

- 9-1. A. Run EXAM6.DAT (5-spot waterflood) and record time, pressure, oil rate, water rate, and gas rate at the end of the run.
B. Deactivate three-phase oil relative permeability option and rerun EXAM6.DAT. Record time, pressure, oil rate, water rate, and gas rate at the end of the run.
C. Compare A and B and explain the differences.

- 9-2. A. Run XS-SPE2.DAT (gas injected into oil cross-section) and record time, pressure, oil rate, gas rate, cumulative oil production and cumulative gas production at the end of the run.
B. Set the z-direction transmissibility to zero between layers K=11 and K=12 to simulate a shale streak. Rerun XS-SPE2.DAT and record time, pressure, oil rate, gas rate, cumulative oil production and cumulative gas production at the end of the run.
C. Compare A and B and explain the differences.

Chapter 10

Fluid Properties

The extended black oil simulator requires a more complex set of fluid property algorithms than those ordinarily included in a black oil simulator. The set of fluid property algorithms in the extended black oil simulator IFLO includes the fluid property algorithms of a traditional black oil simulator as a subset. A description of the fluid property algorithms implemented in the multicomponent, pseudomiscible simulator IFLO is presented in this chapter.

10.1 Fundamental Fluid Property Concepts

Several concepts are needed to understand the fluid properties used in IFLO. These concepts are defined below for ease of reference. More detailed information about fluid properties is available in the literature, such as Amyx, et al. [1960], Pederson, et al. [1989], and McCain [1990, 1991].

Density

Density is defined as the mass of a substance divided by the volume it occupies. The density of a fluid depends on the pressure, temperature and composition of the fluid.

Composition

The composition of a fluid depends on whether the fluid consists of a pure component, such as water or methane, or is a mixture. For example, petroleum and *in situ* water are mixtures. Petroleum is a mixture of hydrocarbon compounds, and *in situ* water usually contains dissolved solids, such as salt, and may contain dissolved gases such as methane and carbon dioxide. The composition of a fluid is a list of the components contained in the fluid.

The relative amount of each component in a mixture is defined as the concentration of the component. Concentration may be expressed in a variety of units, such as volume fraction, weight fraction, or molar fraction. It is important to know the units associated with the composition. If the concentration units are not clearly expressed in a fluid report, they should be determined before use in calculations. It is common to find composition expressed in mole fractions.

The symbols $\{x_i, y_i, z_i\}$ are often used to denote the mole fraction of component i in the oil phase, gas phase, and wellstream respectively. The equilibrium K value is a measure of the amount of component i in the gas phase relative to the oil phase. It is defined as the ratio of gas phase composition to oil phase composition, thus

$$K_i = y_i / x_i \quad (10.1)$$

If component i exists entirely in the oil phase, then y_i is 0 and K_i is 0. Conversely, if component i exists entirely in the gas phase, then x_i is 0 and K_i approaches infinity. Based on these special cases, we see that the equilibrium K value for component i may range from 0 to infinity. It should be further noted that these concepts apply to hydrocarbon components as well as any other distinct molecular species, such as carbon dioxide and nitrogen. Equilibrium K values are used extensively in compositional simulators based on an equation of state.

A pseudocomponent is a set of true components. For example, a pseudocomponent can be composed of components with carbon numbers 2 and 3. The carbon number defines the number of carbon atoms in an organic component. Thus, a carbon number of 2 refers to an organic molecule with 2

carbon atoms, such as ethane. The properties of pseudocomponents are weighted averages of the properties of their true components. The weighting factor is usually a function of molecular weight.

Pressure

The average pressure on a surface is the total normal force applied to the surface divided by the area of the surface. The normal force is the component of the force that is acting perpendicularly to the surface.

Consider a fluid in the pore space of a rock. The pressure at any point in the fluid is equal in all directions. If the fluid is at rest in the pore space, the pressure is equal at all points in the fluid at the same depth. Pascal's law says that pressure applied to an enclosed fluid will be transmitted without a change in magnitude to every point of the fluid and to the walls of the container. The rate of transmission of the applied pressure through the enclosed system can be used to provide information about the system. This is the essence of pressure transient testing, which is discussed in more detail below.

Temperature

Temperature is a measure of the average kinetic energy of a system. Several temperature scales are in use. The most commonly used temperature scales are the Fahrenheit and Celsius scales. The relationship between these scales is

$$T_c = \frac{5}{9}(T_f - 32) \quad (10.2)$$

where T_c and T_f are temperatures in degrees Celsius and degrees Fahrenheit respectively.

Applications of equations of state described below require the use of absolute temperature scales. Absolute temperature may be expressed in terms of degrees Kelvin or degrees Rankine. The Kelvin scale is related to the Celsius scale by

$$T_k = T_c + 273 \quad (10.3)$$

where T_K is temperature in degrees Kelvin. The Rankine scale is related to the Fahrenheit scale by

$$T_R = T_F + 460 \quad (10.4)$$

where T_R is temperature in degrees Rankine.

Intensive and Extensive Properties

Pressure, temperature and density are examples of intensive properties. An intensive property is a fluid property which is independent of the amount of material. For example, if a cubic cell of gas in an equilibrium state is divided into two halves by a vertical partition, the gas in each half of the cell should have the same pressure and temperature. By contrast, the mass and volume in each half will be one half of the original mass and volume. Mass and volume are examples of extensive properties. An extensive property is a property that depends on the amount of material.

Compressibility

If the surface of an object is subjected to an external force, the resulting pressure applied to the object can change the volume of the object. Compressibility is a measure of the volume change resulting from the applied pressure. The fractional volume change $\Delta V/V$ of an object may be estimated from

$$\frac{\Delta V}{V} \approx -c\Delta P \quad (10.5)$$

where c is the compressibility of the object, ΔP is the pressure applied, and the minus sign implies that an increase (decrease) in applied pressure results in a decrease (increase) in the volume of the object.

Formation Volume Factor

Formation volume factor is defined as the volume occupied by a fluid phase at reservoir conditions divided by the volume occupied by the fluid phase at standard conditions. The fluid phase volume may change substantially as pressure and temperature change.

Ordinarily the volume of a fluid with constant composition will increase as the applied pressure and temperature decrease. The behavior of petroleum is made more complex because it is a mixture and can experience a change in composition as temperature and pressure change. For example, a barrel of oil at reservoir conditions (relatively high pressure and temperature) will shrink as the barrel is brought to the surface (relatively low pressure and temperature). The shrinkage is associated with the release of solution gas as the pressure and temperature of the oil decline from reservoir to surface conditions. Consequently, measurements of the change in volume as a function of pressure are desirable, especially for the oil phase.

The determination of gas formation volume factor provides an interesting contrast to the determination of oil formation volume factor. Gas formation volume factor is often determined with reasonable accuracy using the real gas equation of state

$$PV = ZnRT \quad (10.6)$$

where n is the number of moles of gas in volume V at pressure P and temperature T . The gas compressibility factor Z equals one if the gas is an ideal gas. For real gases, $Z \neq 1$ for most pressures and temperatures.

Specific Gravity

Specific gravity is defined as the density of a fluid divided by a reference density. Gas specific gravity is calculated at standard conditions using air density as the reference density. The specific gravity of gas is defined by

$$\gamma_g = \frac{M_a(\text{gas})}{M_a(\text{air})} \approx \frac{M_a(\text{gas})}{29} \quad (10.7)$$

where M_a is apparent molecular weight. Apparent molecular weight is calculated as

$$M_a = \sum_{i=1}^{N_c} y_i M_i \quad (10.8)$$

where N_c is the number of components, y_i is the mole fraction of component i , and M_i is the molecular weight of component i .

Oil specific gravity is calculated at standard conditions using fresh water density as the reference density. Oils are often characterized by specifying their API gravity, which is related to oil specific gravity γ_o at standard temperature and pressure by the equation

$$\text{API} = \frac{141.5}{\gamma_o} - 131.5 \quad (10.9)$$

Heavy oils are oils with a relatively large γ_o and a relatively low API gravity. Heavy oils typically do not contain much gas in solution. By contrast, light oils have a relatively small γ_o and a correspondingly large API gravity. Light oils typically contain a large amount of gas in solution. The presence of gas in solution, which is often called associated gas, significantly affects the average molecular weight of the oil because associated gas is composed of lower molecular weight organic components such as methane, ethane and propane.

Gas-Liquid Ratio

The gas-liquid ratio is defined as the volume of gas divided by the volume of liquid, usually oil or water. The gas volume and liquid volume should be expressed at the same temperature and pressure.

Viscosity

The coefficient of viscosity is a measure of resistance to flow of the fluid. In general, gases have a lower viscosity than liquids. The inverse of viscosity is called fluidity [McCain, 1990]. Thus, a fluid with a large viscosity has a low fluidity.

The relationship between viscosity and shear rate defines the rheology of the fluid. If fluid viscosity is independent of flow rate, the fluid is referred to as a Newtonian fluid. If fluid viscosity depends on flow rate, the fluid is considered a non-Newtonian fluid.

Two types of viscosity may be specified: dynamic viscosity μ and kinematic viscosity ν . They are related by the expression $\mu = \rho \nu$ where ρ is the density of the fluid. Dynamic viscosity μ is used in Darcy's law to calculate the rate of fluid movement fluid flow in porous media. Typically, the unit of

dynamic viscosity μ is centipoise. If fluid density ρ has the unit of g/cc, then kinematic viscosity ν has the unit of centistoke. Thus, 1 centistoke equals 1 centipoise divided by 1 g/cc.

10.2 Black Oil Model PVT Data

Typical gas and oil properties for a black oil model are sketched in Figures 10-1 and 10-2. Gas phase properties are gas formation volume factor (B_g), gas viscosity (μ_g), and liquid yield (r_s). Oil phase properties are oil formation volume factor (B_o), oil viscosity (μ_o), and solution GOR (R_{so}). These terms were described previously. Both saturated and undersaturated curves are included as functions of pressure only. Phase changes occur at the saturation pressures. Single-phase oil becomes two-phase gas-oil when pressure drops below the bubble point pressure (P_b), and single-phase gas becomes two-phase gas condensate when pressure drops below the dew point pressure (P_d).

Simulators run most efficiently when fluid property data are smooth curves. Any discontinuity in a curve can cause numerical difficulties. Ordinarily, realistic fluid properties are smooth functions of pressure except at points where phase transitions occur. As a practical matter, it is usually wise to plot input PVT data to verify the smoothness of the data. Most simulators reduce the nonlinearity of the gas formation volume factor B_g by using the inverse $b_g = 1/B_g$ to interpolate gas properties.

Reservoir fluid properties (PVT data) include fluid viscosities, densities, formation volume factors, gas solubilities, etc. These data are usually obtained by laboratory analyses applied to fluid samples taken from the reservoir. They are sketched in Figures 10-1 and 10-2. Often the PVT

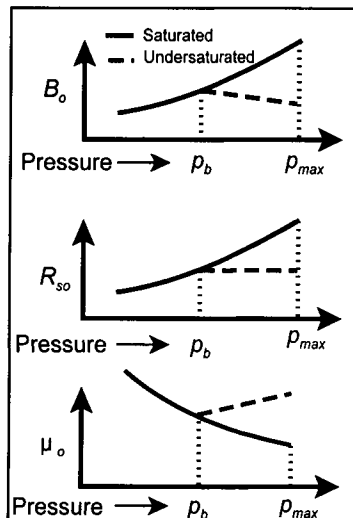


Figure 10-1. Example of oil PVT data [Fanchi, 2000].

data are not known over as wide a range of pressures as would be desirable for a reservoir simulation study. When this occurs, the fluid data base can be broadened by complementing the laboratory data with correlations and by extrapolating the laboratory-measured data. The extrapolated values should be checked to verify that they do not lead to unphysical properties, such as negative compressibility. Extrapolation of fluid property curves is discussed in more detail in Section 10.3.

Laboratory reservoir fluid analyses generally provide data from both a differential liberation experiment and a flash experiment approximating field separator conditions. The differential and flash liberation data can be significantly different for some oils. The actual behavior of the production process is some combination of the differential and flash processes. The assumption normally made in preparing PVT data for use in a black oil simulator is that the differential liberation data represent the process occurring in the reservoir and the flash data represent production to stock tank conditions. Thus, for use in the simulator, the differential liberation data should be corrected to flash values at field separation conditions. This procedure is described in the literature [Amyx, et al., 1960; Moses, 1986] and is summarized below. It is considered more reliable at higher pressures.

Physical property data obtained from a testing laboratory for a black oil system will generally be a differential liberation study coupled with a separator study. Most reservoir simulators require that these data be converted to flash conditions so that effects of surface separation are included. The conversion from differential to flash conditions requires corrections to oil formation volume factor B_o and solution gas-oil ratio R_{so} . If the separator B_o and R_{so} are known, the conversion equations are

$$B_o(P) = B_{od}(P) \frac{B_{ofbp}}{B_{odbp}} \quad (10.10)$$

and

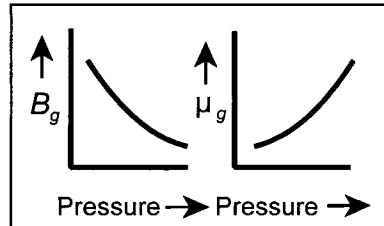


Figure 10-2. Example of gas PVT data [Fanchi, 2000].

$$R_{so}(P) = R_{sofbp} - (R_{sodbp} - R_{sod}(P)) \frac{B_{ofbp}}{B_{odbp}} \quad (10.11)$$

where the subscripts are defined as follows: *d* refers to differential liberation data; *f* refers to flash data; and *bp* refers to the bubble point.

10.3 Extrapolating Saturated Curves

Guidelines for extrapolating PVT data to pressures above the measured saturation pressure are presented below [Fanchi, 2000].

1. The B_g versus pressure curve is strongly non-linear and an extrapolation of this curve to small B_g values at high pressures can result in errors. For most natural gases, the relationship $1/B_g$ versus pressure will be very nearly linear, especially at moderate to high pressures. Plotting $1/B_g$ versus pressure and extrapolating to PMAX should provide more realistic values of B_g at higher pressures. Interpolating B_g using $1/B_g$ versus pressure substantially improves material balance.
2. Once the B_g versus P curve is fixed, R_{so} versus P and B_o versus P curves must be extrapolated so as to avoid a negative oil compressibility being calculated over any pressure increment. To ensure that negative oil compressibilities will not be calculated by the program, the following test should be used. For any pressure increment P_1 to P_2 , where $P_2 > P_1$, the following relationship should hold:

$$0 \leq -(B_{o2} - B_{o1}) + \frac{B_{g2}(R_{so2} - R_{so1})}{5.615} \quad (10.12)$$

where the units of B_o , B_g , and R_{so} are RB/STB, RCF/SCF, and SCF/ STB, respectively. Note that this test applies only to the saturated oil PVT data.

3. The above concepts also apply to the water PVT data. However, for most simulations, it can be assumed that $R_{sw} = 0.0$, thus water compressibility is approximated by $c_w \approx -(\Delta B_w / \Delta P) / B_w$.

10.4 Bubble Point Tracking

The movement of free gas into or out of a gridblock containing oil can change the total gas-oil ratio in the block and the corresponding bubble point pressure. This situation can happen in a variety of scenarios. For example, when the pressure in an undersaturated reservoir drops below the bubble point pressure, a free gas saturation will form. If the free gas saturation exceeds the critical gas saturation, the free gas becomes mobile and can be produced. In another scenario, gas injected into an oil reservoir can change the bubble point pressure as gas goes into solution. The bubble point pressure P_b in these and other scenarios depends on the reservoir oil phase pressure P and the volume of gas available. A new bubble point pressure must be calculated to obtain the correct fluid properties.

The technique of variable switching [Thomas, et al., 1976] is used to track bubble point pressure in IFLO [Ammer, et al. 1991]. The primary variables that specify the state of a gridblock depend on the condition of the gridblock, as shown in Table 10-1.

Table 10-1
Primary Variables for Bubble Point Tracking

Block with Saturated Oil $P \leq P_b$	Block with Undersaturated Oil $P > P_b$
Oil Phase Pressure Water Saturation Gas Saturation	Oil Phase Pressure Water Saturation Bubble Point Pressure

The saturated condition of the gridblock is determined at the beginning of each iteration by comparing oil phase pressure and bubble point pressure. At the end of each iteration, saturated blocks are tested for a change of state.

If gas saturation is positive in the saturated block, P_b is set equal to P . If gas saturation is negative, the gas saturation is set to zero and P_b is set slightly below the oil phase pressure, thus $P_b = P - 0.01$ psia. This makes the block slightly undersaturated as it enters the next iteration. Undersaturated blocks do not require any special switching logic. The next iteration is then performed.

10.5 Extended Fluid Properties Model

The multicomponent, pseudomiscible simulator IFLO uses the extended fluid properties model coded in the simulator MASTER [Ammer, et al., 1991]. It is an adaptation of Chase and Todd's [1984] mixing parameter method. The following presentation closely follows the discussion presented in the Technical Manual of MASTER by Ammer, et al. [1991].

The volumetric behavior of the oleic and aqueous phases is designed to account for the observed behavior of a fluid experiencing mass transfer and pressure changes. The formation volume factors of the liquid phases are

$$B_o = \left[B_o^o \left(v_g R_{so}(P_b) \right) + \Delta B_o \left(\sum_{i=1}^{N_s} v_i R_{io}(P_b) \right) \right] e^{-c_o^u(P-P_{sc})} \quad (10.13)$$

and

$$B_w = \left[B_w^o \left(v_g R_{sw}(P_b) \right) + \Delta B_w \left(v_i R_{iw}(P_b) \right) \right] e^{-c_w^u(P-P_{sc})} \quad (10.14)$$

where P_b is bubble point pressure, P_{sc} is the pressure at stock tank conditions, v_i is the volume fraction of component i for $i = \{g, 1, \dots, N_s\}$, and $\{c_o^u, c_w^u\}$ denote undersaturated oil and water compressibilities. The composition and pressure dependencies are expressed by the square bracketed term and the exponential term, respectively, in Equations (10.13) and (10.14).

The factors B_o^o and B_w^o are computed from the conventional saturated black-oil data set so that the following relationships apply:

$$B_o(P)_{\text{black oil}} = B_o^o(R_{so}(P)) e^{-c_o^u(P-P_{sc})} \quad (10.15)$$

and

$$B_w(P)_{\text{black oil}} = B_w^o(R_{sw}(P)) e^{-c_w^u(P-P_{sc})} \quad (10.16)$$

Solvent 1 (base solvent) data is used to compute the terms ΔB_o and ΔB_w so that the following relationships apply:

$$B_o(P)_1 = [B_o(P_{sc})_1 + \Delta B_o(R_{1o}(P))] e^{-c_o''(P-P_{sc})} \quad (10.17)$$

and

$$B_w(P)_1 = [B_w(P_{sc})_1 + \Delta B_w(R_{1w}(P))] e^{-c_w''(P-P_{sc})} \quad (10.18)$$

Data consistency requires that

$$B_o(P_{sc})_{\text{black oil}} = B_o(P_{sc})_1 \quad (10.19)$$

and

$$B_w(P_{sc})_{\text{black oil}} = B_w(P_{sc})_1 \quad (10.20)$$

Equations (10.19) and (10.20) are needed to assure that the extended fluid property model simplifies to the conventional black-oil fluid property model when no solvent is present.

Oleic and aqueous phase densities are related to formation volume factors by

$$\rho_o = \frac{1}{B_o} \left[\rho_{osc} + v_g R_{so} \rho_{gsc} + \left(\sum_{j=1}^{N_s} v_j R_{jo} \rho_{isc} \right) \right] \quad (10.21)$$

and

$$\rho_w = \frac{1}{B_w} \left[\rho_{wsc} + v_g R_{sw} \rho_{gsc} + v_1 R_{1w} \rho_{isc} \right] \quad (10.22)$$

Natural gas and solvent densities have the relatively simple form

$$\rho_i = \frac{\rho_{isc}}{B_i} \quad (10.23)$$

where the subscript $i = \{g, 1, \dots, N_s\}$.

Oleic phase viscosity in the presence of solvents depends on the same mechanisms as those that affect formation volume factor. Oleic phase viscosity

must account for swelling associated with mass transfer and pressure-dependent compressibility effects. The oleic phase viscosity model is

$$\begin{aligned}\mu_o &= F_s \left[\sum_{i=1}^{N_s} v_i R_{io}(P_b) \right] \\ &\times \mu_o^o [v_g R_{so}(P_b)(1 + c_{ov}(P_b - P_{sc})) + \mu_o'(P - P_b)]\end{aligned}\quad (10.24)$$

The term μ_o^o is computed from the saturated black-oil data so that the following relations apply:

$$\mu_o(P)_{\text{black oil}} = \mu_o^o(R_{so}(P))(1 + c_{ov}(P - P_{sc})) \quad (10.25)$$

and

$$c_{ov} = \frac{\mu_o'}{\mu_o^o(P_b^o)} \quad (10.26)$$

The term P_b^o is the initial bubble point pressure and μ_o' is the slope of the oil viscosity versus pressure curve above the bubble point pressure. The factor F_s is computed from the solvent 1 (base solvent) data so that the following relation applies:

$$\mu_o(P)_1 = F_s [R_{1o}(P)] \mu_o^o(P_{sc})(1 + c_{ov}(P - P_{sc})) \quad (10.27)$$

The consistency of the data requires

$$\mu_o(P_{sc})_{\text{black oil}} = \mu_o(P_{sc})_1 \quad (10.28)$$

The algorithm for aqueous phase viscosity is a function of dissolved natural gas only.

The calculation of effective gas and oleic phase viscosities and densities under miscible conditions depends on the weighting factor α defined in Chapter 8. In particular, effective viscosity is

$$\mu_i^o = (1 - \alpha)\mu_i^1 + \alpha\mu_i^2 \quad (10.29)$$

and effective density is

$$\rho_i^o = (1 - \alpha)\rho_i^1 + \alpha\rho_i^2 \quad (10.30)$$

where the subscript $i = \{o, g, 1, \dots, N_s\}$, and N_s is the number of solvents. Superscript 1 denotes effective properties for $P \leq \text{PMCM}$ and superscript 2

denotes effective properties for $P \geq PMISC$ where pressures PMCM and PMISC are multicontact miscible pressure and first contact miscible pressures, respectively.

The densities and viscosities for $P < PMCM$ are given by

$$\mu_i^1 = \mu_i^{(1-\omega_1)} \cdot \mu_{mgs}^{\omega_1} \quad (10.31)$$

and

$$\rho_i^1 = (1 - \omega_1) \rho_i + \omega_1 \rho_{mgs} \quad (10.32)$$

where the subscript $i = \{g, 1, \dots, N_s\}$. The mixing parameter ω_1 allows for incomplete mixing. Complete mixing occurs when $\omega_1 = 1$ and complete segregation occurs when $\omega_1 = 0$. The properties $\{\mu_i, \rho_i\}$ are pure component properties, while $\{\mu_{mgs}, \rho_{mgs}\}$ are the properties of a completely mixed gas phase. They are calculated from the mixing rules

$$\mu_{mgs}^{-1/4} = V_g \mu_g^{-1/4} + \sum_{j=1}^{N_s} V_j \mu_j^{-1/4} \quad (10.33)$$

and

$$\rho_{mgs} = V_g \rho_g + \sum_{j=1}^{N_s} V_j \rho_j \quad (10.34)$$

A second mixing parameter ω_2 is introduced to compute the densities and viscosities for $P > PMISC$. In this case, the soluble species are miscible with each another and with the oil phase. Effective viscosities are

$$\begin{aligned} \mu_o^2 &= \mu_o^{(1-\omega_2)} \mu_{mos}^{\omega_2} \\ \mu_g^2 &= \mu_g^{(1-\omega_2)} \mu_{mgs}^{\omega_2} \\ \mu_i^2 &= \mu_i^{(1-\omega_2)} \mu_m^{\omega_2} \quad \text{for } i = 1, \dots, N_s \end{aligned} \quad (10.35)$$

where the following mixing rules apply:

$$\mu_{mos}^{-1/4} = \frac{1}{S_o + (1 - V_g) S_g} \left(S_o \mu_o^{-1/4} + S_g \sum_{j=1}^{N_s} V_j \mu_j^{-1/4} \right) \quad (10.36)$$

and

$$\mu_m^{-\frac{1}{4}} = \frac{1}{1 - S_w} \left(S_o \mu_o^{-\frac{1}{4}} + S_g \mu_{mgs}^{-\frac{1}{4}} \right) \quad (10.37)$$

Similarly, effective densities are

$$\begin{aligned} \rho_o^2 &= (1 - \omega_2) \rho_o + \omega_2 \rho_{mos} \\ \rho_g^2 &= (1 - \omega_2) \rho_g + \omega_2 \rho_{mgs} \\ \rho_i^2 &= (1 - \omega_2) \rho_i + \omega_2 \rho_m \text{ for } i = 1, \dots, N_s \end{aligned} \quad (10.38)$$

with the mixing rules

$$\rho_{mos} = \frac{1}{S_o + (1 - v_g) S_g} \left(S_o \rho_o + S_g \sum_{j=1}^{N_s} v_j \rho_j \right) \quad (10.39)$$

and

$$\rho_m = \frac{1}{1 - S_w} \left(S_o \rho_o + S_g \rho_{mgs} \right) \quad (10.40)$$

Exercises

- 10-1. A. Run EXAM4.DAT (single well primary depletion) and record time, pressure, oil rate, water rate, gas rate and GOR at the end of the run.
- B. Double the slope BOSLP of the oil formation volume factor versus pressure curve for undersaturated oil. Rerun EXAM4.DAT and record time, pressure, oil rate, water rate, gas rate and GOR at the end of the run.
- C. Lower the bubble point pressure to 2014.7 psia in the original version of EXAM4.DAT and rerun EXAM4.DAT. Record time, pressure, oil rate, water rate, gas rate and GOR at the end of the run.
- D. Set the solution natural gas-oil ratio RSO to zero in the original version of EXAM4.DAT and rerun EXAM4.DAT. Record time, pressure, oil rate, water rate, gas rate and GOR at the end of the run.
- E. Compare the above cases and explain the differences.

- 10-2. A. Run EXAM9.DAT (gas reservoir with aquifer influx) and record time, pressure, gas rate, water rate, cumulative gas production and cumulative water production at the end of the run.
- B. Multiply water viscosity by 1.4 and rerun EXAM9.DAT. Record time, pressure, gas rate, water rate, cumulative gas production and cumulative water production at the end of the run.
- C. Compare A and B and explain the differences.

Chapter 11

Fluid Displacement

This chapter summarizes basic concepts of fluid displacement in reservoirs. More discussion can be found in several sources, such as Collins [1961], Craig [1971], Dake [1978], and Mian [1992]. A review of concepts from fractional flow theory is followed by definitions of recovery efficiency. Fluid displacement at various stages in the life of the reservoir is briefly discussed.

11.1 Mobility

Interfacial tension causes a pressure differential across the fluid boundary that is expressed by the relationship

$$P_c = P_{nw} - P_w \quad (11.1)$$

where

P_c capillary pressure between two immiscible fluids [psi]

P_{nw} pressure in the nonwetting phase [psi]

P_w pressure in the wetting phase [psi]

Capillary pressure has already been discussed in previous chapters. For ease of reference, a few terms are defined in this section that have direct application to fluid displacement.

Oil-Water Capillary Pressure

Oil is the nonwetting phase in a water-wet reservoir. Capillary pressure for an oil-water system is

$$P_{cow} = P_o - P_w \quad (11.2)$$

where

P_o pressure in the oil phase [psi]

P_w pressure in the water phase [psi]

Capillary pressure increases with height above the oil-water contact (OWC) as water saturation decreases.

Gas-Oil Capillary Pressure

In gas-oil systems, gas usually behaves as the nonwetting phase and oil is the wetting phase. Capillary pressure between oil and gas in such a system is

$$P_{coo} = P_g - P_o \quad (11.3)$$

where

P_o pressure in the oil phase [psi]

P_g pressure in the gas phase [psi]

Relative Permeability

The general definition of relative permeability is

$$k_r = \frac{k_{eff}}{k_{abs}} \quad (11.4)$$

where

k_r relative permeability between 0 and 1

k_{eff} effective permeability [md]

k_{abs} absolute permeability [md]

Fluid phase relative permeabilities for oil, water and gas phases respectively are defined by the ratios

$$k_{ro} = k_o / k, k_{rw} = k_w / k, k_{rg} = k_g / k. \quad (11.5)$$

Mobility

Fluid phase mobility is defined as the ratio of effective phase permeability to phase viscosity, thus

$$\begin{aligned}\lambda_o &= \frac{k_o}{\mu_o} \text{ for oil,} \\ \lambda_w &= \frac{k_w}{\mu_w} \text{ for water,} \\ \lambda_g &= \frac{k_g}{\mu_g} \text{ for gas.}\end{aligned}\tag{11.6}$$

where μ_ℓ is the viscosity of phase ℓ . The relative mobility of a phase is the relative permeability of the phase divided by the phase viscosity.

Mobility Ratio

Mobility ratio is defined as the mobility of the displacing fluid λ_d behind the flood front divided by the mobility of the displaced fluid λ_d ahead of the flood front, thus

$$M = \frac{\lambda_d}{\lambda_d} \tag{11.7}$$

An example of mobility ratio is the mobility ratio of a waterflood. It is the ratio of water mobility at residual oil saturation to oil mobility at connate water saturation:

$$M_{w,o} = \frac{(\lambda_w)_{S_{or}}}{(\lambda_o)_{S_{wc}}} = \frac{k_{rw}(S_{or}) / \mu_w}{k_{ro}(S_{wc}) / \mu_o} \tag{11.8}$$

11.2 Fractional Flow

The fractional flow of water is the ratio of water production to total production, thus

$$f_w = \frac{q_w}{q_t} = \frac{q_w}{q_w + q_o} \quad (11.9)$$

where

- f_w fractional flow of water
- f_o fractional flow of oil
- q_w water volumetric flow rate [RB]
- q_o oil volumetric flow rate [RB]
- q_t total volumetric flow rate [RB]

Notice that the flow rates are expressed in terms of reservoir volumes. The fractional flow of oil and the fractional flow of water are related by $f_w = 1 - f_o$. Based on the definition of fractional flow, we see that fractional flow should be a value between 0 and 1.

Simplified Fractional Flow Equation

A simplified fractional flow equation is obtained by replacing flow rates with Darcy's Law in the definition of fractional flow. If we neglect capillary pressure and gravity for simplicity, we obtain

$$f_w = \frac{\frac{k k_{nw} A \frac{\partial P_w}{\partial x}}{\mu_w}}{\frac{k k_{nw} A \frac{\partial P_w}{\partial x}}{\mu_w} + \frac{k k_{no} A \frac{\partial P_o}{\partial x}}{\mu_o}} \quad (11.10)$$

Since capillary pressure is neglected, we have the equality of phase pressures $P_w = P_o$ so that

$$f_w = \frac{\frac{k_{nw}}{\mu_w}}{\frac{k_{nw}}{\mu_w} + \frac{k_{no}}{\mu_o}} \quad (11.11)$$

Equation (11.11) can be expressed in terms of mobilities as

$$f_w = \frac{1}{1 + \frac{k_{ro} \mu_w}{k_{rw} \mu_o}} = \frac{1}{1 + \frac{\lambda_o}{\lambda_w}} \quad (11.12)$$

The construction of Equation (11.12) is based on some simplifying assumptions. We assumed that Darcy's Law adequately describes flow rate and that capillary pressure and gravity are negligible. With these assumptions, we obtained f_w at reservoir conditions.

Fractional Flow Equation with Gravity

Gravity can be included in the fractional flow equation as follows. First, let us consider the two-phase flow of oil and water in a tilted linear system. Darcy's Law including capillary pressure and gravity effects for linear flow is

$$q_w = \frac{-kk_{rw}A}{\mu_w} \left(\frac{\partial P_w}{\partial x} + \rho_w g \sin \alpha \right) \quad (11.13)$$

where

- α angle of dip of formation
- g gravitational constant

If we differentiate capillary pressure for a water-wet system with respect to position x along the dipping bed, we find

$$\frac{\partial P_c}{\partial x} = \frac{\partial P_o}{\partial x} - \frac{\partial P_w}{\partial x} \quad (11.14)$$

Combining Equations (11.13) and (11.14) gives

$$\frac{\partial P_c}{\partial x} = \frac{-(q_t - q_w)\mu_o}{Ak k_{ro}} - \rho_o g \sin \alpha + \frac{q_w \mu_w}{Ak k_w} + \rho_w g \sin \alpha \quad (11.15)$$

If we write the density difference as

$$\Delta \rho = \rho_w - \rho_o \quad (11.16)$$

collect terms, and simplify we obtain

$$\frac{q_w}{Ak} \left(\frac{\mu_o}{k_{ro}} + \frac{\mu_w}{k_{rw}} \right) = \frac{q_t \mu_o}{Ak k_{ro}} + \frac{\partial P_c}{\partial x} - g \Delta \rho \sin \alpha \quad (11.17)$$

Rearranging and collecting terms gives the fractional flow to water f_w in conventional oilfield units:

$$f_w = \frac{1 + 0.001127 \frac{Akk_{ro}}{\mu_o q_t} \left(\frac{\partial P_c}{\partial x} - 0.433(\gamma_w - \gamma_o) \sin \alpha \right)}{1 + \frac{k_{ro}}{k_{rw}} \frac{\mu_w}{\mu_o}} \quad (11.18)$$

where

- A cross-sectional area of flow system [ft^2]
- k absolute permeability [md]
- k_{ro} relative permeability to oil
- k_{rw} relative permeability to water
- μ_o oil viscosity [cp]
- μ_w water viscosity [cp]
- P_c capillary pressure [psi] = $P_o - P_w$
- x direction of linear flow [ft]
- α dip of flow system [degrees]
- γ_o oil specific gravity (water = 1)
- γ_w water specific gravity (water = 1)

The general expression for f_w includes all three terms governing immiscible displacement, namely the viscous term $(k_{ro}/k_{rw})(\mu_w/\mu_o)$, the capillary pressure term $\partial P_c / \partial x$, and the gravity term $(\gamma_w - \gamma_o) \sin \alpha$.

It is interesting to note that the capillary pressure and gravity terms are multiplied by $1/q_t$ in Equation (11.18). Most waterfloods have sufficiently high injection rates that capillary pressure and gravity effects can be neglected, leaving the simplified expression:

$$f_w \approx \frac{1}{1 + \frac{k_{ro}}{k_{rw}} \frac{\mu_w}{\mu_o}} \quad (11.19)$$

Equation (11.19) is in agreement with Equation (11.12), as it should be.

Gas Fractional Flow

A similar analysis can be performed to determine the fractional flow of gas f_g . The result for a gas-oil system is

$$f_g = \frac{1 + 0.001127 \frac{Akk_{ro}}{\mu_o q_t} \left(\frac{\partial P_c}{\partial x} - 0.433(\gamma_g - \gamma_o) \sin\alpha \right)}{1 + \frac{k_{ro}}{k_{rg}} \frac{\mu_g}{\mu_o}} = 1.0 - f_o \quad (11.20)$$

where

k_{rg} relative permeability to gas

μ_g gas viscosity [cp]

P_c gas-oil capillary pressure = $P_g - P_o$ [psi]

γ_g gas specific gravity [water = 1]

q_g gas flow rate [RB/D]

Immiscible displacement of oil by gas is analogous to water displacing oil with the water terms replaced by gas terms. In general, the gravity term in f_g should not be neglected unless q_t is very high because of the density difference between gas and oil.

11.3 Recovery Efficiency

Recovery efficiency is quantified by comparing initial and final volumes of fluid in place. It takes into account volumetric and displacement efficiencies. The different aspects of recovery efficiency are defined and then combined to form overall recovery efficiency.

Displacement efficiency is a measure of how effectively mobile hydrocarbons can be recovered. Although the following definitions of displacement efficiency are given for oil, similar definitions can be provided for gas.

Displacement efficiency for oil is defined as the ratio of mobile oil to original oil in place at reservoir conditions:

$$E_D = \frac{V_p S_{oi} - V_p S_{or}}{V_p S_{oi}} = \frac{S_{oi} - S_{or}}{S_{oi}} \quad (11.21)$$

where

V_p initial pore volume

S_{oi} initial oil saturation

S_{or} residual oil saturation

Displacement efficiency can approach 100% if residual oil saturation can be driven to zero. One of the goals of enhanced oil recovery processes such as miscible flooding is to reduce residual oil saturation and increase displacement efficiency.

The definition of displacement efficiency can be modified to include the effects of swelling. Swelling is represented by using surface volume rather than reservoir volume in the definition of displacement efficiency. The volume conversion is achieved by dividing reservoir volume by formation volume factor. For example, the displacement efficiency of a waterflood is

$$E_D = \frac{\frac{V_p S_{oi}}{B_{oi}} - \frac{V_p S_{or}}{B_{oa}}}{\frac{V_p S_{oi}}{B_{oi}}} = \frac{\frac{S_{oi}}{B_{oi}} - \frac{S_{or}}{B_{oa}}}{\frac{S_{oi}}{B_{oi}}} \quad (11.22)$$

where

B_{oi} oil FVF at the beginning of waterflood

B_{oa} oil FVF at the waterflood pressure

Notice that oil formation volume factor is a maximum at the bubble point pressure of the oil. If the waterflood is conducted at or just above bubble point pressure, the value of B_{oa} will be maximized and the residual oil term will be minimized. The resulting displacement efficiency for a waterflood is then maximized.

In addition to displacement efficiency, volumetric factors are needed to determine overall recovery efficiency. Areal and vertical sweep efficiencies are defined by

$$E_A = \frac{\text{swept area}}{\text{total area}} \quad (11.23)$$

and

$$E_V = \frac{\text{swept thickness}}{\text{total thickness}} \quad (11.24)$$

Reservoir flow models are useful tools for quantifying both swept area and swept thickness. The product of areal and vertical sweep efficiency is the volumetric sweep efficiency E_{vol} :

$$E_{vol} = E_A \times E_V \quad (11.25)$$

where E_A is areal sweep efficiency, and E_V is vertical sweep efficiency.

Overall recovery efficiency RE accounts for both volumetric and displacement effects. It is the product of volumetric sweep efficiency and displacement efficiency, thus

$$RE = E_D \times E_{vol} = E_D \times E_A \times E_V \quad (11.26)$$

Equation (11.25) has been used in Eq. (11.26) to express recovery efficiency in terms of displacement and sweep efficiencies.

11.4 Production Stages

The stages in the life of a hydrocarbon reservoir are depicted in Figure 11-1. The stages are identified as follows:

- | | |
|----------------------|----------------------|
| A Exploration | E Field Development |
| B Discovery | F Production Plateau |
| C Extended Well Test | G Decline |
| D Appraisal | H Abandonment |

The production life of a reservoir can begin immediately after the discovery well is drilled, or several years later after several delineation wells have been drilled. Delineation wells are used to define the reservoir boundaries, while development wells are used to optimize resource recovery. Optimization criteria may change during the life of the reservoir for a variety of reasons,

including changes in technology, economic factors, and new information obtained during various stages of reservoir production.

Primary production is ordinarily the first stage of production. It relies entirely on natural energy sources. The natural forces involved in the displacement of oil during primary production are called reservoir drives. The most common reservoir drives for oil reservoirs are water drive, solution or dissolved gas drive, and gas cap drive.

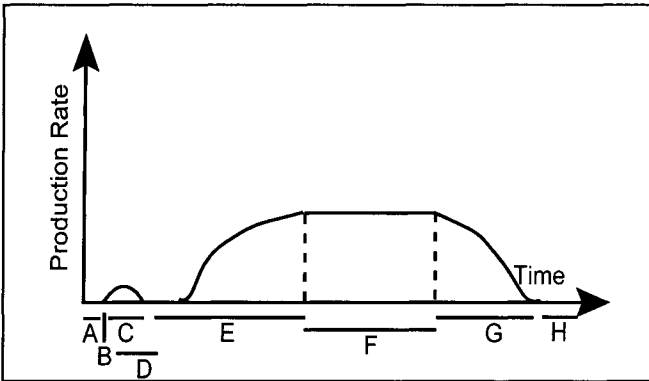


Figure 11-1. Hydrocarbon reservoir life.

The most efficient drive mechanism is water drive. In this case, water displaces oil as oil flows to production wells. In a solution gas drive, gas dissolved in the oil phase at reservoir temperature and pressure is liberated as pressure declines. Some oil moves with the gas to the production wells as the gas expands and moves to the lower pressure zones in the reservoir.

A gas cap is a large volume of gas at the top of a reservoir. Oil in a zone below the gas cap can be produced by gas cap expansion. When production wells are completed in the oil zone below the gas cap, the drop in pressure associated with pressure decline causes gas to move from the higher pressure gas cap down toward the producing wells. Gas cap movement drives oil to the wells during pressure depletion. Eventually, large volumes of gas will be produced with the oil.

Gravity drainage is the least common of the primary production mechanisms. In this case oil flows downstructure to a producing well as the result of a pressure gradient. Gravity drainage is most likely to occur in shallow, highly permeable, steeply dipping reservoirs.

Although the above discussion referred to oil reservoirs, similar comments apply to gas reservoirs. Water drive and gas expansion with reservoir pressure

depletion are the most common drives for gas reservoirs. Recovery from gas condensate reservoirs is typically less than the recovery from dry gas reservoirs because of reduced mobility near the reservoir. Mobility reduction in a gas condensate reservoir can occur when liquid condensation occurs in regions where reservoir pressure is less than dew point pressure. The condensate causes relative permeability interference and a reduction of the productive capacity of a well.

Primary depletion is usually not sufficient to optimize recovery from an oil reservoir. Oil recovery can be substantially increased by supplementing natural reservoir energy. The supplemental energy is provided using an external energy source, such as water injection or gas injection. The injection of fluid into a reservoir is referred to as pressure maintenance or secondary production. The latter term arose because injection usually followed a period of primary pressure depletion, and was therefore the second production method used in a field. Many modern reservoirs incorporate pressure maintenance early in the life of the field, sometimes from the beginning of production.

Both primary and secondary recovery processes are designed to produce oil using immiscible methods. Additional methods may be used to improve oil recovery efficiency by reducing residual oil saturation to water or gasflooding. Improved recovery technology includes traditional secondary recovery processes such as waterflooding and immiscible gas injection, as well as enhanced oil recovery (EOR) processes. EOR processes are usually classified as one of the following processes: chemical, miscible, thermal, and microbial. For a more detailed discussion of EOR processes and associated screening criteria, see such references as Taber, et al. [1996], and Green and Willhite [1998]. The simulator IFLO is applicable to primary and secondary processes, and can be applied to both immiscible and miscible gas injection processes. Some examples of miscible displacement models are described below.

11.5 Miscible Displacement Models

Miscible flooding methods include carbon dioxide injection, natural gas injection, and nitrogen injection. Miscible gas injection must be performed at

a high enough pressure to ensure miscibility between the injected gas and *in situ* oil. Miscibility is achieved when interfacial tension (IFT) between the aqueous and oleic phases is significantly reduced. The desired IFT reduction is typically from around 1 dyne/cm to 0.001 dyne/cm or less. Any reduction in IFT can improve displacement efficiency, and a near miscible process can yield much of the incremental oil that might be obtained from a miscible process. If reservoir pressure is not maintained above the minimum miscibility pressure (MMP) of the system, the gasflood will be an immiscible gas injection process.

Many miscible displacement models have been devised in an effort to match laboratory and field data. A few of these models are reviewed here to illustrate the nonlinear character of the miscible displacement process and to provide justification for the use of mixing parameter algorithms in IFLO. To show the similarities and differences between the miscible displacement models, each model is cast in the form of the nonlinear Convection-Dispersion (C-D) equation

$$\frac{\partial A(C)}{\partial t} = -\frac{\partial F(C)}{\partial x} + D \frac{\partial^2 C}{\partial x^2} \quad (11.27)$$

where C refers to concentration or saturation, $A(C)$ is the accumulation term, $F(C)$ represents flux, and D is dispersion for a Fick's law dispersion term [Collins, 1961]. The nonlinearity of the models presented below makes most of them intractable to analytical solution. The one exception is Burger's equation, which is discussed as a simplification of the model proposed by Christie and Bond [1987].

Christie and Bond's Model

Christie and Bond [1987] described the miscible displacement of a solute by a solvent using a C-D equation for solvent concentration C_s that had the accumulation and flux terms

$$A(C_s) = C_s, \quad F(C_s) = vC_s \quad (11.28)$$

with a velocity

$$v = -\lambda(C_s) \frac{\partial P}{\partial x} \quad (11.29)$$

152 Integrated Flow Modeling

The velocity v is related to the product of pressure gradient and a mobility λ that depends on solvent concentration. If the pressure gradient is constant, which is a reasonable assumption for many laboratory core floods and injector-producer pairs, Christie and Bond wrote the velocity in the form

$$v = a(1 + bC_s)^4 \quad (11.30)$$

The parameter a is related to pressure gradient in this model, and parameter b is related to the ratio of *in situ* oil and solvent viscosities by the expression

$$b = \left(\frac{\mu_o}{\mu_s} \right)^{1/4} - 1 \quad (11.31)$$

Notice the quarter power relationship in the expression for b . This relationship appears repeatedly in miscible displacement models, as shown below.

A simplification of Christie and Bond's model that has an analytical solution is Burger's equation [1948]. Burger's equation has the same accumulation and flux terms as Christie and Bond's model, but the velocity is a linear function of solvent concentration with the form

$$v = c + \frac{d}{2}C_s \quad (11.32)$$

The parameters c and d are constants. Burger's equation is a nonlinear partial differential equation with an analytical solution. It describes the propagation of a shock front. The linear C-D equation is obtained if $d = 0$. Burger's equation has the solution

$$C_s(x,t) = \frac{1}{2} \left[1 - \tanh \frac{c}{4D} \left(x - \left(c + \frac{d}{2} \right) t \right) \right] \quad (11.33)$$

for the boundary conditions

$$C(x \rightarrow -\infty, t) = 1, \quad C(x \rightarrow +\infty, t) = 0 \quad (11.34)$$

Figure 11-2 displays the solutions of Burger's equation at three different times for the parameters $c = 1.0$ ft/day, $d = 0.1$ ft/day and $D = 0.4$ ft²/day.

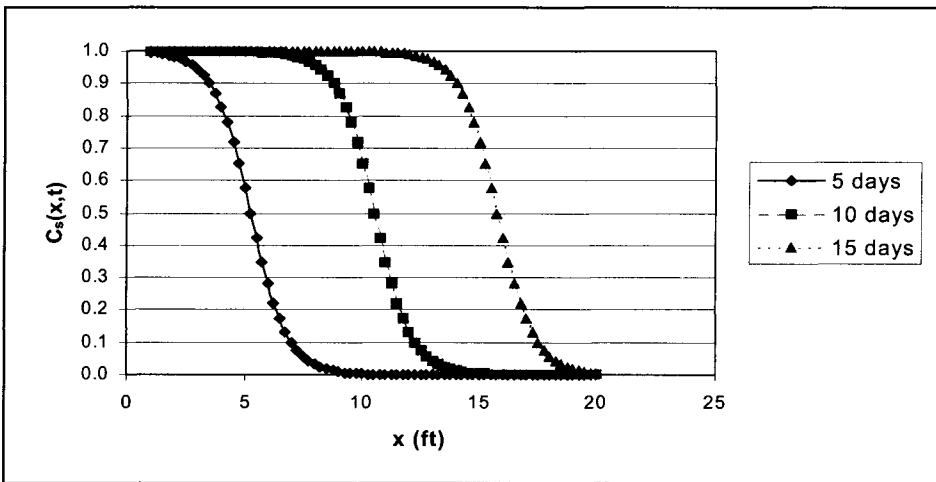


Figure 11-2. Solutions to Burger's Equation.

Fayers' Model

The accumulation and flux terms in Fayers' model [1988] are functions of solvent concentration, thus

$$A(C_s) = \phi S_f(C_s) C_s, \quad F(C_s) = q f_f(C_s) C_s \quad (11.35)$$

where ϕ is porosity, q is injection rate, and

$$S_f(C_s) = a + bC_s^\gamma, \quad f_f(C_s) = \frac{S_f/\mu_f}{S_o/\mu_o + S_f/\mu_f} \quad (11.36)$$

The subscripts s and o represent injected solvent and *in situ* oil respectively. There are three empirical parameters a , b , and γ . The effective viscosity is given in terms of constant oil and solvent viscosities as

$$\mu_f(C_s) = \left[C_s \mu_s^{-1/4} + (1 - C_s) \mu_o^{-1/4} \right]^{-4} \quad (11.37)$$

with a quarter power mixing rule.

Koval's Model

The accumulation and flux terms in Koval's model [1963] are functions of solvent saturation instead of solvent concentration, thus

$$A(S_s) = \phi S_s, \quad F(S_s) = q f_s(S_s) \quad (11.38)$$

154 Integrated Flow Modeling

where solvent fractional flow is

$$f_s(S_s) = \left[1 + \frac{\mu_{se}}{\mu_o} \left(\frac{1 - S_s}{S_s} \right) \right]^{-1} \quad (11.39)$$

The effective viscosity is given in terms of two empirical parameters α and β , and constant oil and solvent viscosities as

$$\mu_{se} = [\alpha \mu_s^{-1/4} + \beta \mu_o^{-1/4}]^{-4} \quad (11.40)$$

with a quarter power mixing rule. It is instructive to compare Eq. (11.40) with Eq. (11.37). Fayers' model treats the two empirical parameters α and β as linear functions of solvent concentration.

Todd and Longstaff's Model

The accumulation and flux terms in Todd and Longstaff's model [1972] are functions of solvent saturation instead of solvent concentration, thus

$$A(S_s) = \phi S_s, \quad F(S_s) = q f_s(S_s) \quad (11.41)$$

in agreement with Koval's model. Solvent fractional flow differs from Koval's model by adding an effective oleic phase viscosity such that

$$f_s(S_s) = \left[1 + \frac{\mu_{se}}{\mu_{oe}} \left(\frac{1 - S_s}{S_s} \right) \right]^{-1} \quad (11.42)$$

The effective viscosities are given in terms of an empirical mixing parameter ω and constant oil and solvent viscosities. The effective viscosities are

$$\mu_{se} = \mu_s^{1-\omega} \mu_m^\omega, \quad \mu_{oe} = \mu_o^{1-\omega} \mu_m^\omega \quad (11.43)$$

where the quarter power mixing rule appears in the term

$$\mu_m = [S_s \mu_s^{-1/4} + (1 - S_s) \mu_o^{-1/4}]^{-4} \quad (11.44)$$

If the mixing parameter $\omega = 0$, the effective velocities revert to the constant immiscible velocities of the solvent and oil. A variation of the Todd-Longstaff model is used in IFLO, and is described in Chapter 10.

Exercises

- 11-1. A. Run EXAM3.DAT (Buckley-Leverett waterflood) and record time, pressure, oil rate, water rate, cumulative oil production and cumulative water production at the end of the run.
B. Change the elevation of each gridblock so that the top of the reservoir ranges from a depth of 8325 ft in block I=1 to a depth of 8135 ft in block I=20. Rerun EXAM3.DAT and record time, pressure, oil rate, water rate, cumulative oil production and cumulative water production at the end of the run.
C. Calculate dip angles for both reservoirs (A and B). Compare A and B and explain the differences.
- 11-2. A. Run EXAM6.DAT (5-spot waterflood) and record time, pressure, oil rate, water rate, gas rate, and cumulative oil production at the end of the run.
B. Shut in the injection wells and rerun EXAM6.DAT as a depletion case. Record time, pressure, oil rate, water rate, gas rate, and cumulative oil production at the end of the run.
C. Compare A and B and explain the differences.

Chapter 12

Formulation of Flow Equations

Many derivations of the oil, water, and gas fluid flow equations for a black oil simulator exist in the literature [for example, see Crichlow, 1977; Peaceman, 1977]. It is instructive to provide a derivation of the traditional black oil simulator flow equations. The derivation adds physical content to the terms, and parallels the presentation originally published in Fanchi, et al. [1982]. The extension of the flow equations to a multicomponent, pseudomiscible formulation is then discussed.

12.1 Conservation of Mass

We begin by considering the flow of fluid into and out of a single reservoir block (Figure 12-1). Assume fluid flows into the block at x (J_x) and out of the block at $x + \Delta x$ ($J_{x + \Delta x}$). J denotes the fluid flux and is defined as the rate of flow of mass

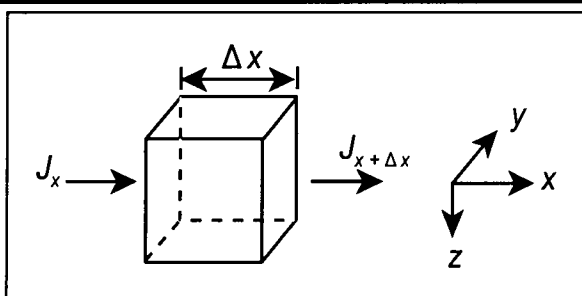


Figure 12-1. Reservoir block and coordinate convention.

per unit cross-sectional area normal to the direction of flow, which is the x direction in the present case. By conservation of mass, we have the equality:

$$\begin{aligned} & \text{mass entering the block} - \text{mass leaving the block} \\ & = \text{accumulation of mass in the block.} \end{aligned}$$

If the block has length Δx , width Δy , and depth Δz , then we can write the mass entering the block in a time interval Δt as

$$[(J_x)_x \Delta y \Delta z + (J_y)_y \Delta x \Delta z + (J_z)_z \Delta x \Delta y] \Delta t = \text{Mass in} \quad (12.1)$$

where we have generalized to allow flux in the y and z directions as well. The notation $(J_x)_x$ denotes the x direction flux at location x , with analogous meanings for the remaining terms.

Corresponding to mass entering is a term for mass exiting which has the form

$$\begin{aligned} & [(J_x)_{x+\Delta x} \Delta y \Delta z + (J_y)_{y+\Delta y} \Delta x \Delta z + (J_z)_{z+\Delta z} \Delta x \Delta y] \Delta t \\ & + q \Delta x \Delta y \Delta z \Delta t = \text{Mass out} \end{aligned} \quad (12.2)$$

We have added a source/sink term q which represents mass flow into (source) or out of (sink) a well. A producer is represented by $q > 0$, and an injector by $q < 0$.

Accumulation of mass in the block is the change in concentration of phase p (C_p) in the block over the time interval Δt . If the concentration C_p is defined as the total mass of phase p (oil, water, or gas) in the entire reservoir block divided by the block volume, then the accumulation term becomes

$$[(C_p)_{t+\Delta t} - (C_p)_t] \Delta x \Delta y \Delta z = \text{Mass accumulation} \quad (12.3)$$

Using Eqs. (12.1) through (12.2) in the mass conservation equality
 $\text{Mass in} - \text{Mass out} = \text{Mass accumulation}$

gives

$$\begin{aligned} & [(J_x)_x \Delta y \Delta z + (J_y)_y \Delta x \Delta z + (J_z)_z \Delta x \Delta y] \Delta t \\ & - [(J_x)_{x+\Delta x} \Delta y \Delta z + (J_y)_{y+\Delta y} \Delta x \Delta z + (J_z)_{z+\Delta z} \Delta x \Delta y] \Delta t \\ & - q \Delta x \Delta y \Delta z \Delta t = [(C_p)_{t+\Delta t} - (C_p)_t] \Delta x \Delta y \Delta z \end{aligned} \quad (12.4)$$

Dividing Eq. (12.4) by $\Delta x \Delta y \Delta z \Delta t$ and rearranging gives

$$\begin{aligned} -\frac{(J_x)_{x+\Delta x} - (J_x)_x}{\Delta x} - \frac{(J_y)_{y+\Delta y} - (J_y)_y}{\Delta y} \\ -\frac{(J_z)_{z+\Delta z} - (J_z)_z}{\Delta z} - q = \frac{(C_p)_{t+\Delta t} - (C_p)_t}{\Delta t} \end{aligned} \quad (12.5)$$

In the limit as Δx , Δy , Δz , and Δt go to zero, Eq. (12.5) becomes the continuity equation

$$-\frac{\partial J_x}{\partial x} - \frac{\partial J_y}{\partial y} - \frac{\partial J_z}{\partial z} - q = \frac{\partial C_p}{\partial t} \quad (12.6)$$

The oil, water, and gas phases each satisfy a mass conservation equation having the form of Eq. (12.6).

12.2 Flow Equations for Three-Phase Flow

The flow equations for an oil, water, and gas system are determined by specifying the fluxes and concentrations of the conservation equations for each of the three phases. A flux in a given direction can be written as the density of the fluid times its velocity in the given direction. Letting the subscripts o , w , and g denote oil, water, and gas, respectively, the fluxes become [Fanchi, 1986]:

$$(\vec{J})_o = \frac{\rho_{osc}}{B_o} \vec{V}_o + \frac{r_s \rho_{gsc}}{B_g} \vec{V}_g \quad (12.7)$$

$$(\vec{J})_w = \frac{\rho_{wsc}}{B_w} \vec{V}_w \quad (12.8)$$

$$(\vec{J})_g = \frac{\rho_{gsc}}{B_g} \vec{V}_g + \frac{R_{so} \rho_{gsc}}{B_o} \vec{V}_o + \frac{R_{sw} \rho_{gsc}}{B_w} \vec{V}_w \quad (12.9)$$

where r_s is the liquid content of condensate, R_{so} and R_{sw} are gas solubilities, $\{B_o, B_w, B_g\}$ are {oil, water, gas} formation volume factors in units of reservoir volume/standard volume, the subscript sc denotes standard conditions (usually

60°F and 14.7 psia in oilfield units), and ρ denotes fluid densities. The velocities \vec{v} are assumed to be Darcy velocities and their x -direction components are

$$v_{xo} = -K_x \lambda_o \frac{\partial}{\partial x} \left[P_o - \frac{\rho_o g z}{144 g_c} \right] \quad (12.10)$$

$$v_{xw} = -K_x \lambda_w \frac{\partial}{\partial x} \left[P_w \frac{\rho_w g z}{144 g_c} \right] \quad (12.11)$$

$$v_{xg} = -K_x \lambda_g \frac{\partial}{\partial x} \left[P_g - \frac{\rho_g g z}{144 g_c} \right] \quad (12.12)$$

where g is the acceleration of gravity in ft/sec², and g_c is 32.174 ft/sec² (IFLO assumes $g = g_c$). These equations should be valid for describing fluid flow in porous media even if g and g_c change, such as on the Moon, Mars, or the space shuttle. Similar expressions can be written for the y and z components.

The relative mobility λ_p of phase p is defined as the ratio of the relative permeability to flow of the phase divided by its viscosity, thus

$$\lambda_p = k_{rp} / \mu_p \quad (12.13)$$

Phase densities are related to formation volume factors and gas solubilities by

$$\rho_o = \frac{1}{B_o} [\rho_{osc} + R_{so} \rho_{gsc}] \quad (12.14)$$

$$\rho_w = \frac{1}{B_w} [\rho_{wsc} + R_{sw} \rho_{gsc}] \quad (12.15)$$

$$\rho_g = \frac{1}{B_g} [\rho_{gsc} + r_s \rho_{osc}] \quad (12.16)$$

Besides fluxes, we also need concentrations. These are given by

$$C_o = \phi \rho_{osc} \left[\frac{S_o}{B_o} + r_s \frac{S_g}{B_g} \right] \quad (12.17)$$

$$C_w = \phi \rho_{wsc} \frac{S_w}{B_w} \quad (12.18)$$

and

$$C_g = \phi \rho_{gsc} \left[\frac{S_g}{B_g} + R_{so} \frac{S_o}{B_o} + R_{sw} \frac{S_w}{B_w} \right] \quad (12.19)$$

where ϕ is the porosity and S_p is the saturation of phase p . The saturations satisfy the constraint

$$S_o + S_w + S_g = 1 \quad (12.20)$$

Combining Eqs. (12.6), (12.7) through (12.9), and (12.17) through (12.19) gives a mass conservation equation for each phase:

Oil

$$\begin{aligned} & - \left[\frac{\partial}{\partial x} \left(\frac{\rho_{osc}}{B_o} V_{xo} \right) + \frac{\partial}{\partial y} \left(\frac{\rho_{osc}}{B_o} V_{yo} \right) + \frac{\partial}{\partial z} \left(\frac{\rho_{osc}}{B_o} V_{zo} \right) \right] \\ & - q_{ot} = \frac{\partial}{\partial t} \left[\phi \rho_{osc} \left(\frac{S_o}{B_o} + r_s \frac{S_g}{B_g} \right) \right] \end{aligned} \quad (12.21)$$

Water

$$\begin{aligned} & - \left[\frac{\partial}{\partial x} \left(\frac{\rho_{wsc}}{B_w} V_{xw} \right) + \frac{\partial}{\partial y} \left(\frac{\rho_{wsc}}{B_w} V_{yw} \right) + \frac{\partial}{\partial z} \left(\frac{\rho_{wsc}}{B_w} V_{zw} \right) \right] \\ & - q_w = \frac{\partial}{\partial t} \left(\phi \rho_{wsc} \frac{S_w}{B_o} \right) \end{aligned} \quad (12.22)$$

Gas

$$\begin{aligned}
 & -\frac{\partial}{\partial x} \left(\frac{\rho_{gsc}}{B_g} V_{xg} + \frac{R_{so}\rho_{gsc}}{B_o} V_{xo} + \frac{R_{sw}\rho_{gsc}}{B_w} V_{xw} \right) \\
 & -\frac{\partial}{\partial y} \left(\frac{\rho_{gsc}}{B_g} V_{yg} + \frac{R_{so}\rho_{gsc}}{B_o} V_{yo} + \frac{R_{sw}\rho_{gsc}}{B_w} V_{yw} \right) \\
 & -\frac{\partial}{\partial z} \left(\frac{\rho_{gsc}}{B_g} V_{zg} + \frac{R_{so}\rho_{gsc}}{B_o} V_{zo} + \frac{R_{sw}\rho_{gsc}}{B_w} V_{zw} \right) - q_{gT} \\
 & = \frac{\partial}{\partial t} \left[\phi \rho_{gsc} \left(\frac{S_g}{B_g} + \frac{R_{so} S_o}{B_o} + \frac{R_{sw} S_w}{B_w} \right) \right]
 \end{aligned} \tag{12.23}$$

The rates q_{oT} and q_{gT} are total oil and gas rates, and q_w is water production rate. The densities at standard conditions are constants and can be divided out of the above equations. This reduces the equations to the following form:

Oil

$$- \left[\frac{\partial}{\partial x} \left(\frac{V_{xo}}{B_o} \right) + \frac{\partial}{\partial y} \left(\frac{V_{yo}}{B_o} \right) + \frac{\partial}{\partial z} \left(\frac{V_{zo}}{B_o} \right) \right] - \frac{q_{oT}}{\rho_{osc}} = \frac{\partial}{\partial t} \left[\phi \left(\frac{S_o}{B_o} + r_s \frac{S_g}{B_g} \right) \right] \tag{12.24}$$

Water

$$- \left[\frac{\partial}{\partial x} \left(\frac{V_{xw}}{B_w} \right) + \frac{\partial}{\partial y} \left(\frac{V_{yw}}{B_w} \right) + \frac{\partial}{\partial z} \left(\frac{V_{zw}}{B_w} \right) \right] - \frac{q_w}{\rho_{wsc}} = \frac{\partial}{\partial t} \left(\phi \frac{S_w}{B_w} \right) \tag{12.25}$$

Gas

$$\begin{aligned}
 & -\frac{\partial}{\partial x} \left(\frac{V_{xg}}{B_g} + \frac{R_{so}}{B_o} V_{xo} + \frac{R_{sw}}{B_w} V_{xw} \right) - \frac{\partial}{\partial y} \left(\frac{V_{yg}}{B_g} + \frac{R_{so}}{B_o} V_{yo} + \frac{R_{sw}}{B_w} V_{yw} \right) \\
 & -\frac{\partial}{\partial z} \left(\frac{V_{zg}}{B_g} + \frac{R_{so}}{B_o} V_{zo} + \frac{R_{sw}}{B_w} V_{zw} \right) - \frac{q_{gT}}{\rho_{gsc}} = \frac{\partial}{\partial t} \left[\phi \left(\frac{S_g}{B_g} + R_{so} \frac{S_o}{B_o} + R_{sw} \frac{S_w}{B_w} \right) \right]
 \end{aligned} \tag{12.26}$$

Equations (12.10) through (12.16), (12.20), and (12.24) through (12.26) are the basic fluid flow equations which are solved in a black oil simulator.

12.3 Recasting the Flow Equations

A glance at Eqs. (12.24) through (12.26) illustrates the computational complexity of the basic three-dimensional, three-phase black oil simulator equations. Equivalent but much simpler appearing forms for the equations are

$$-\nabla \cdot \frac{\vec{v}_o}{B_o} - \frac{q_{ot}}{\rho_{osc}} = \frac{\partial}{\partial t} \left[\phi \left(\frac{S_o}{B_o} + r_s \frac{S_g}{B_g} \right) \right] \quad (12.27)$$

$$-\nabla \cdot \frac{\vec{v}_w}{B_w} - \frac{q_w}{\rho_{wsc}} = \frac{\partial}{\partial t} \left(\phi \frac{S_w}{B_w} \right) \quad (12.28)$$

and

$$-\nabla \cdot \left(\frac{\vec{v}_g}{B_g} + \frac{R_{so}}{B_o} \vec{v}_o + \frac{R_{sw}}{B_w} \vec{v}_w \right) - \frac{q_{gt}}{\rho_{gsc}} = \frac{\partial}{\partial t} \left[\phi \left(\frac{S_g}{B_g} + R_{so} \frac{S_o}{B_o} + R_{sw} \frac{S_w}{B_w} \right) \right] \quad (12.29)$$

where the symbol $\nabla \cdot \vec{v}$ is shorthand for

$$\nabla \cdot \vec{v} = \frac{\partial}{\partial x} v_x + \frac{\partial}{\partial y} v_y + \frac{\partial}{\partial z} v_z \quad (12.30)$$

For a review of vector analysis, see a reference such as Fanchi [2000] or Kreyszig [1999].

The form of the Darcy velocities (Eqs. (12.10) through (12.12)) may be simplified by defining the potential Φ_p of phase p as

$$\phi_p = P_p - \frac{\rho_p Z}{144} \quad (12.31)$$

and we have used the assumption that $g = g_c$. In this notation, including x , y , and z directional permeabilities and unit vectors \hat{i} , \hat{j} , \hat{k} , the Darcy velocities may be written as

$$\vec{v}_o = -\tilde{K} \cdot \lambda_o \nabla \phi_o = -\lambda_o \left[\hat{i} K_x \frac{\partial \phi_o}{\partial x} + \hat{j} K_y \frac{\partial \phi_o}{\partial y} + \hat{k} K_z \frac{\partial \phi_o}{\partial z} \right] \quad (12.32)$$

$$\vec{v}_w = -\tilde{K} \cdot \lambda_w \nabla \phi_w = -\lambda_w \left[\hat{i} K_x \frac{\partial \phi_w}{\partial x} + \hat{j} K_y \frac{\partial \phi_w}{\partial y} + \hat{k} K_z \frac{\partial \phi_w}{\partial z} \right] \quad (12.33)$$

and

$$\vec{v}_g = -\tilde{K} \cdot \lambda_g \nabla \phi_g = -\lambda_g \left[\hat{i} K_x \frac{\partial \phi_g}{\partial x} + \hat{j} K_y \frac{\partial \phi_g}{\partial y} + \hat{k} K_z \frac{\partial \phi_g}{\partial z} \right] \quad (12.34)$$

We have used the dyadic notation \tilde{K} to signify that permeability is a tensor of rank two. The expanded form of Eqs. (12.32) through (12.34) employs the common assumption that the coordinate axes of our reference system are aligned along the principal axes of \tilde{K} . As discussed in Chapter 4 and associated references, this assumption impacts the ability of the simulator to accurately model fluid flow.

Combining Eqs. (12.27) through (12.29) with Eqs. (12.32) through (12.34) gives

$$\nabla \cdot \frac{\tilde{K} \lambda_o}{B_o} \cdot \nabla \phi_o - \frac{q_{oT}}{\rho_{osc}} = \frac{\partial}{\partial t} \left[\phi \left(\frac{S_o}{B_o} + r_s \frac{S_g}{B_g} \right) \right] \quad (12.35)$$

$$\nabla \cdot \frac{\tilde{K} \lambda_w}{B_w} \cdot \nabla \phi_w - \frac{q_w}{\rho_{wsc}} = \frac{\partial}{\partial t} \left(\frac{\phi S_w}{B_w} \right) \quad (12.36)$$

and

$$\begin{aligned} & \nabla \cdot \tilde{K} \cdot \left[\frac{\lambda_g}{B_g} \nabla \phi_g + \frac{R_{so} \lambda_o}{B_o} \nabla \phi_o + \frac{\lambda_w R_{sw}}{B_w} \nabla \phi_w \right] - \frac{q_{gT}}{\rho_{gsc}} \\ &= \frac{\partial}{\partial t} \left[\phi \left(\frac{S_g}{B_g} + R_{so} \frac{S_o}{B_o} + R_{sw} \frac{S_w}{B_w} \right) \right] \end{aligned} \quad (12.37)$$

Equations (12.35) through (12.37) are equivalent to Peaceman's [1977] Eqs. (1-105) through (1-107) for a three-dimensional system, except we have also allowed gas to dissolve in the water phase. Our rate and coordinate system sign conventions also differ. If these differences are taken into consideration, the formulations are seen to be equivalent.

12.4 Introduction of the Capillary Pressure Concept

The presence of oil, water, and gas phase pressures in Eqs. (12.35) through (12.37) complicates the problem. We simplify the handling of the phase pressures and potentials in the flow equations by using the capillary pressure concept. Let us define the difference in phase pressures as

$$P_{cow} = P_o - P_w \quad (12.38)$$

and

$$P_{cgo} = P_g - P_o \quad (12.39)$$

The differences P_{cow} and P_{cgo} are the capillary pressures for oil-water and gas-water systems, respectively. Experimentally P_{cow} and P_{cgo} have been observed to be principally functions of water and gas saturations, respectively. Using Eqs. (12.38) and (12.39) lets us write the water and gas phase potentials as

$$\phi_w = P_o - P_{cow} - \frac{\rho_w Z}{144} \quad (12.40)$$

and

$$\phi_g = P_o + P_{cgo} - \frac{\rho_g Z}{144} \quad (12.41)$$

Combining Eqs. (12.35) through (12.37) with Eqs. (12.40) and (12.41) and rearranging yields

Oil

$$\nabla \cdot \bar{K} \cdot \left(\frac{\lambda_o}{B_o} \right) \nabla P_o + CG_o - \frac{q_{oT}}{\rho_{osc}} = \frac{\partial}{\partial t} \left[\phi \left(\frac{S_o}{B_o} + r_s \frac{S_g}{B_g} \right) \right] \quad (12.42)$$

Water

$$\nabla \cdot \bar{K} \cdot \left(\frac{\lambda_w}{B_w} \right) \nabla P_w + CG_w - \frac{q_w}{\rho_{wsc}} = \frac{\partial}{\partial t} \left(\phi \frac{S_w}{B_w} \right) \quad (12.43)$$

Gas

$$\begin{aligned} & \nabla \cdot \left[\tilde{K} \cdot \left(\frac{\lambda_g}{B_g} + \frac{R_{so}\lambda_o}{B_o} + \frac{R_{sw}\lambda_w}{B_w} \right) \right] \nabla P_o + CG_g - \frac{q_{gT}}{\rho_{gsW}} \\ &= \frac{\partial}{\partial t} \left[\phi \left(\frac{S_g}{B_g} + \frac{R_{so}S_o}{B_o} + \frac{R_{sw}S_w}{B_w} \right) \right] \end{aligned} \quad (12.44)$$

The gravity and capillary contributions to the phase pressures have been collected in the terms CG_o , CG_w , and CG_g :

$$CG_o = -\nabla \cdot \tilde{K} \cdot \left(\frac{\lambda_o}{B_o} \right) \nabla \left(\frac{\rho_o Z}{144} \right) \quad (12.45)$$

$$CG_w = -\nabla \cdot \tilde{K} \cdot \left(\frac{\lambda_w}{B_w} \right) \nabla \left(\frac{\rho_w Z}{144} + P_{cow} \right) \quad (12.46)$$

and

$$\begin{aligned} CG_g &= \nabla \cdot \tilde{K} \cdot \frac{\lambda_g}{B_g} \nabla \left(P_{cgo} - \frac{\rho_g Z}{144} \right) \\ &\quad - \nabla \cdot \tilde{K} \cdot \left[\frac{R_{so}\lambda_o}{B_o} \nabla \left(\frac{\rho_o Z}{144} \right) + \frac{R_{sw}\lambda_w}{B_w} \nabla \left(P_{cow} + \frac{\rho_w Z}{144} \right) \right] \end{aligned} \quad (12.47)$$

Total oil and gas rates q_{oT} and q_{gT} are given in terms of phase production rates q_ℓ as

$$q_{oT} = q_o + r_s q_g \quad (12.48)$$

and

$$q_{gT} = q_g + R_{so} q_o + R_{sw} q_w \quad (12.49)$$

Formulation and fluid compressibilities in this formulation are

$$c_r = \frac{1}{\phi} \frac{\partial \phi}{\partial P_o} \quad (12.50)$$

for rock,

$$c_g = \left[\frac{1}{B_g} \frac{\partial B_g}{\partial P_o} - \frac{B_o}{B_g} \frac{\partial r_s}{\partial P_o} \right] \quad (12.51)$$

for gas,

$$c_o = - \left[\frac{1}{B_o} \frac{\partial B_o}{\partial P_o} - \frac{B_g}{B_o} \frac{\partial R_{so}}{\partial P_o} \right] \quad (12.52)$$

for oil, and

$$c_w = - \left[\frac{1}{B_w} \frac{\partial B_w}{\partial P_o} - \frac{B_g}{B_w} \frac{\partial R_{sw}}{\partial P_o} \right] \quad (12.53)$$

for water. Essentially a black oil simulator must solve Eqs. (12.42) through (12.44) and saturation constraint Eq. (12.20) for the four unknowns P_o , S_o , S_w , and S_g . All other physical properties in the equations are known, in principle, as functions of the four unknowns, or from field and laboratory data.

12.5 Extended Black Oil Simulator Equations

The flow equations for the multiphase, multidimensional pseudocomponent simulator IFLO are obtained by including terms that account for miscible effects, and by neglecting vaporized oil ($r_s = 0$). The assumption $r_s = 0$ simplifies the model formulation, but makes the simulator inappropriate for detailed studies of condensate reservoirs. The simulator can still be used to study dry gas and lean gas reservoirs with negligible condensate. The performance of reservoirs with significant condensate may be estimated using a black oil simulator with $r_s > 0$, but the most accurate predictions are obtained from compositional simulators [Kenyon and Behie, 1987]. The extended flow equations follow:

Stock Tank Oil

$$\nabla \cdot \frac{Kk_o^e}{\mu_o^e B_o} \nabla \Phi_o - \frac{q_o}{\rho_{osc}} = \frac{\partial}{\partial t} \left(\phi \frac{S_o}{B_o} \right) \quad (12.54)$$

Water plus Surfactant

$$\nabla \cdot \frac{Kk_{rw}}{\mu_w B_w} \nabla \Phi_w - \frac{q_w}{\rho_{wsc}} = \frac{\partial}{\partial t} \left(\phi \frac{S_w}{B_w} \right) \quad (12.55)$$

Surfactant

$$\nabla \cdot x_s \frac{Kk_{rw}}{\mu_w B_w} \nabla \Phi_w - x_s \frac{q_w}{\rho_{wsc}} = \frac{\partial}{\partial t} \left(\phi x_s \frac{S_w}{B_w} \right) \quad (12.56)$$

Soluble Species

$$\begin{aligned} & \nabla \cdot \left[v_i \frac{Kk_{rg}^e}{\mu_i^e B_i} \nabla \Phi_i + v_i R_{io} \frac{Kk_{ro}^e}{\mu_o^e B_o} \nabla \Phi_o + v_i R_{iw} \frac{Kk_{rw}^e}{\mu_w B_w} \nabla \Phi_w \right] \\ & - \frac{q_i}{\rho_{isc}} = \frac{\partial}{\partial t} \left\{ \phi v_i \left[\frac{S_g}{B_i} + R_{io} \frac{S_o}{B_o} + R_{iw} \frac{S_w}{B_w} \right] \right\} \end{aligned} \quad (12.57)$$

for $i = \{g, 1, \dots, N_s\}$ where N_s is the number of soluble species, x_s is the surfactant volume fraction, and v_i is the volume fraction of component i . The superscript e indicates that an effective fluid property is being calculated. Phase properties such as relative permeability and viscosity are also made dependent on the composition of injected fluids. The surfactant equation is similar to the water equation except for the inclusion of the surfactant volume fraction x_s in all terms. The soluble species equation is analogous to the gas equation with the inclusion of the volume fraction v_i of component i in all terms.

Exercises

-
- 12-1. A. Run EXAM3.DAT (Buckley-Leverett waterflood) and record time, pressure, oil rate, water rate, cumulative oil production and cumulative water production at the end of the run.
 B. Increase the number of gridblocks from 20 to 40 without changing the length of the reservoir. Rerun EXAM3.DAT and record time, pressure, oil rate, water rate, cumulative oil production and cumulative water production at the end of the run.

C. Decrease the number of gridblcoks from 20 to 5 without changing the length of the reservoir. Rerun EXAM3.DAT and record time, pressure, oil rate, water rate, cumulative oil production and cumulative water production at the end of the run.

D. Compare the results of A through C and explain the differences. Hint: plot water saturation array at the end of each run.

12-2. Repeat Exercise 12-1 using a timestep size of 1 day.

12-3. Set $x_s = 0$ and $v_i = 1$ for $i = g$ ($v_i = 0$ otherwise) in Eqs. (12.54) through (12.57). Write the resulting simplified equations for the case where there is no surfactant and the only gas component is associated gas with subscript g .

Chapter 13

Source/Sink Terms

The flow equations for the extended black oil simulator include source and sink terms. These terms are useful for modeling fluid injection or production directly from a gridblock. The source/sink terms in IFLO represent injection and production wells and analytic aquifer models. Well models and analytic aquifer models in IFLO are described in this chapter. User specified parameters for controlling these well models are defined in the User's Manual presented in the Appendices.

13.1 Productivity Index

Productivity index (PI) is defined as the ratio of rate Q to pressure drop ΔP , or $PI = Q/\Delta P$, where $\Delta P = P_e - P_w$, P_e = average reservoir pressure, and P_w = wellbore bottomhole pressure BHP. From Darcy's Law for radial oil flow we can write PI as

$$PI = \frac{Q_o}{\Delta P} = \frac{0.00708 K_e h_{net}}{\mu_o B_o [\ln(r_e / r_w) + S]} \quad (13.1)$$

The meaning and units of terms in Eq. (13.1) are the following:

μ_o	oil viscosity [cp]
B_o	oil FVF [RB/STB]
r_e	drainage radius [ft]
r_w	wellbore radius [ft]
S	skin
K_e	effective permeability to oil [md] = $k_{ro} K_{abs}$
k_{ro}	relative permeability to oil
K_{abs}	absolute permeability [md]
h_{net}	net thickness [ft]
Q_o	oil rate [STB/D]

Some of the terms in Eq. (13.1) depend on time-varying pressure and saturation, while other factors change relatively slowly or are constant with respect to time. We separate these terms to obtain

$$PI = \frac{k_{ro}}{\mu_o B_o} PID \quad (13.2)$$

where the quasi-stationary factors are collected in the PID term, that is,

$$PID = \frac{0.00708 K_{abs} h_{net}}{\ln(r_e / r_w) + S} \quad (13.3)$$

The IFLO user is expected to provide a PID for each well connection. A connection is a gridblock with a well perforation.

Vertical Wells

A value of the connection flow index PID for a vertical well can be estimated from a formula derived by Peaceman [1978]:

$$PID_k = \left[\frac{0.00708 Kh}{\ln\left(\frac{r_e}{r_w}\right) + S} \right]_k \quad (13.4)$$

where

$$r_e \approx r_o = 0.14(\Delta x^2 + \Delta y^2)^{1/2} \quad (13.5)$$

for an isotropic system. With respect to permeability, an isotropic system is a system in which x direction and y direction permeabilities are equal, ($K_x = K_y$). For a square well block in an isotropic system, $\Delta x = \Delta y$ and $r_o \approx 0.2 \Delta x$. The subscript k in Eq. (13.4) denotes the k th connection. For a well in a rectangular gridblock and an anisotropic system (that is, $K_x \neq K_y$), well PID is estimated using an effective permeability

$$K = \sqrt{K_x K_y} \quad (13.6)$$

and an equivalent well block radius

$$r_e \approx r_o = 0.28 \frac{\left[(K_y / K_x)^{1/2} \Delta x^2 + (K_x / K_y)^{1/2} \Delta y^2 \right]^{1/2}}{(K_y / K_x)^{1/4} + (K_x / K_y)^{1/4}} \quad (13.7)$$

The remaining parameters are defined as:

- K horizontal permeability of connection k [md]
- h thickness of connection k [ft]
- r_w wellbore radius [ft]
- S dimensionless skin factor

In principle, the well flow index can be related to measured values. In practice, however, the terms r_e , S , and $k_{ro}/\mu_o B_o$ are seldom well known, especially for a multiphase flowing well. As a matter of expediency, therefore, Eq. (13.4) is often used to compute an initial estimate of PID. This value can then be improved by adjusting it until the simulator computed well rates match the initial observed well rates.

Horizontal Wells

There are many ways to estimate connection flow index PID for a horizontal well [Joshi, 1991]. A PID value can be estimated for horizontal wells in a manner similar to that for vertical wells by using the Joshi formula

$$\text{PID}_k = \frac{[0.0078Kh]_k}{\left[\ln\left(\frac{a + \sqrt{a^2 - \left(\frac{L}{2}\right)^2}}{\frac{L}{2}} \right) + \frac{h}{L} \ln\left(\frac{h}{2r_w} \right) + S \right]_k} \quad (13.8)$$

where

$$a = \frac{L}{2} \left[0.5 + \sqrt{0.25 + \left(\frac{2r_{eh}}{L} \right)^4} \right]^{1/2} \quad (13.9)$$

The subscript k in Eq. (13.8) denotes the k^{th} connection. The remaining parameters are defined as:

- K horizontal permeability of connection k [md]
- h thickness of connection k [ft]
- L horizontal well length [ft]
- r_w wellbore radius [ft]
- r_{eh} drainage radius of horizontal well [ft]
- S dimensionless skin factor

The drainage radius r_{eh} of the horizontal well needs to account for elliptical flow. An estimate of r_{eh} can be obtained using the Babu-Odeh [1989] procedure.

13.2 Rate Constraint Representation

In the rate constraint representation, rates may be specified for injectors or producers. We assume the well may be completed in a total of K connections, and fluid allocation between connections is based on effective mobility λ^e and pressure differential $\Delta P_{wk} = P - P_{wb}$ between the pressure P in the block containing the well connection and the user specified wellbore flowing pressure P_{wb} .

Case 1: Pressure Differential for Specified Oil Production Rate Q_o

The pressure differential for each connection k is

$$\Delta P_{wk} = \frac{Q_o}{\sum_{k=1}^K \text{PID}_k [\lambda_o^e / B_o]_k^n} \quad (13.10)$$

where λ_l is the fluid mobility of phase l and PID is the well productivity index. Notice that a PID may be specified for each connection k . This capability lets the IFLO user take into account permeability contrast.

Case 2: Pressure Differential for Specified Water Production Rate Q_w

The pressure differential for each connection k is

$$\Delta P_{wk} = \frac{Q_w}{\sum_{k=1}^K \text{PID}_k [\lambda_w^e / B_w]_k^n} \quad (13.11)$$

Case 3: Pressure Differential for Specified Natural Gas Production Rate Q_g

The pressure differential for each connection k is

$$\Delta P_{wk} = \frac{Q_g}{\sum_{k=1}^K \text{PID}_k [\lambda_g^e / B_g]_k^n} \quad (13.12)$$

Solution gas in both oil and water is neglected when a natural gas production rate is specified. This is a reasonable assumption for wells producing primarily free natural gas. It allows IFLO to model natural gas rate specified production from natural gas-water systems.

Production rates from each connection are calculated from the pressure differentials as follows:

Oil

$$Q_{ok} = \text{PID}_k (\lambda_o^e / B_o)_k^n \Delta P_{wk} \quad (13.13)$$

Water

$$Q_{wk} = \text{PID}_k (\lambda_w^e / B_w)_k^n \Delta P_{wk} \quad (13.14)$$

Natural Gas and Solvent

$$Q_{ik} = \text{PID}_k \left(\lambda_g^e / B_g \right)_k^n \Delta P_{wk} + \left(v_i^n R_{io}^n \right)_k Q_{ok} + \left(v_i^n R_{iw}^n \right)_k Q_{wk} \quad (13.15)$$

where $\{i = g, 1, \dots, N_s\}$, v_i is the volume fraction of component i , and $R_{i\ell}$ is the solubility of component i in phase $\{\ell = o, w\}$.

Case 4: Total Production Rate Specified

When the total reservoir voidage rate Q_T is specified, the procedure is similar to the calculation for a specified rate. The expression for pressure differential is

$$\Delta P_{wk} = \frac{Q_T}{\sum_{k=1}^K \text{PID}_k \left\{ \left(\lambda_o^e \right)_k^n + \left(\lambda_w^e \right)_k^n + \left(\lambda_g^e \right)_k^n + \sum_{i=1}^{N_s} \left(\lambda_i^e \right)_k^n \right\}} \quad (13.16)$$

The pressure differential is then used in the rate Eqs. (13.13) through (13.15) to calculate rates.

Case 5: Injection Rate Specified

If the well is an injector, the user must specify the surface injection rate Q_i of component i and a well injectivity index WI_k for each connection. The components which may be injected are water, natural gas, and solvent. The injection rate for each connection is then allocated using the following formulas.

Component $\{i = w, g, 1, \dots, N_s\}$ Injection Pressure Differential

$$\Delta P_{wk} = \frac{Q_i}{\sum_{k=1}^K \frac{WI_k}{B_{ik}^n} \left\{ \left(\lambda_o^e \right)_k^n + \left(\lambda_w^e \right)_k^n + \left(\lambda_g^e \right)_k^n + \sum_{i=1}^{N_s} \left(\lambda_i^e \right)_k^n \right\}} \quad (13.17)$$

Component $\{i = w, g, 1, \dots, N_s\}$ Injection Rate

$$Q_{ik} = \frac{WI_k \Delta P_{wk}}{B_{ik}^n} \left[\left(\lambda_o^e \right)_k^n + \left(\lambda_w^e \right)_k^n + \left(\lambda_g^e \right)_k^n + \sum_{i=1}^{N_s} \left(\lambda_i^e \right)_k^n \right] \quad (13.18)$$

It is important to note that allocation of injection fluids is based on total mobilities, and not just injected fluid mobility. This is necessary for the following reason: if an injector is placed in a block where the relative permeability to the injection fluid is zero, then the simulator using injection fluid mobility only would prohibit fluid injection even though a real well would allow fluid injection. A common example would be water injection into a block containing oil and irreducible water. To avoid the unrealistic result of no fluid injection, we assume the total mobility of the block should be used. For most cases, the error of this method will only persist for a few timesteps because, in time, the mobile fluid saturation in the block will be dominated by the injected fluid.

13.3 Pressure Constraint Representation

Pressure may also be used to control the production from or injection into a well. Two types of pressure constraints are possible: explicit and implicit. Both constraints are available in IFLO and are discussed in this section.

Explicit Pressure Constraint

The pressure differential for explicit pressure specified wells is

$$\Delta P_{wk} = [P^n - P_{wb}]_k \quad (13.19)$$

where $\Delta P_{wk} > 0$ for producers and $\Delta P_{wk} < 0$ for injectors. Rates for production wells are calculated using Eqs. (13.13) through (13.15). Rates for injection wells are calculated using Eq. (13.18).

Implicit Pressure Constraint

The pressure differential for implicit pressure specified wells is

$$\Delta P_{wk} = [P^{n+1} - P_{wb}]_k \quad (13.20)$$

where $\Delta P_{wk} > 0$ for producers and $\Delta P_{wk} < 0$ for injectors. The difference between Eqs. (13.19) and (13.20) is the time level associated with the block pressure. The implicit pressure calculation requires the block pressure at the future time level $n + 1$. The recursive relations and residuals associated with

the solution of the flow equations must be modified to account for this implicit calculation of rate. Chapter 14 describes the appropriate changes to the residuals of the flow equation.

Rates for production wells are calculated using Eqs. (13.13) through (13.15). Rates for injection wells are calculated using Eq. (13.18). In all cases, the rates are calculated using a pressure differential that includes the implicit pressure.

13.4 Well Constraints

Wells are usually controlled by specifying pressure or the rate of the dominant phase, but they can be further constrained using a variety of other options. The constraints that are available in IFLO are described below as a supplement to the User's Manual.

WOR and GOR Constraints

Maximum gas-oil and water-oil ratios (GOR_{max} , WOR_{max} respectively) can be entered by the user for each oil production well. GOR for a well is defined as total gas production divided by total oil production for all active well completion intervals. If GOR for the well exceeds GOR_{max} , then the completion interval (connection) with the highest GOR will be shut in. If more than one connection has the same maximum GOR, the connection with the smallest value of KONECT (Appendix C.2) will be shut in first. If the user has entered KONECT so that it increases with depth, this procedure will shut in the shallowest connection first. The procedure is repeated until GOR is less than GOR_{max} or until the well is shut in.

The ratio WOR is defined as total water production divided by total oil production for all active well completion intervals. If WOR for the well exceeds WOR_{max} , then the completion interval (connection) with the highest WOR will be shut in. If more than one connection has the same maximum WOR, the connection with the largest value of KONECT will be shut in first. If the user has entered KONECT so that it increases with depth, this procedure will shut

in the deepest connection first. The procedure is repeated until WOR is less than WOR_{max} or until the well is shut in.

Fluid Withdrawal Constraints

Fluid withdrawal from explicit pressure controlled production wells can be constrained as follows:

- A. A minimum production rate QWMIN can be specified for a primary phase.
- B. A maximum production rate QWMAX can be specified for a primary phase.

Primary phases subject to fluid production constraints are listed in Table C-1 in Appendix C. They are oil, water, natural gas, and total fluid.

A positive value of QWMIN for a pressure controlled production well is used as the minimum allowed production rate. If the calculated primary phase production rate drops below the minimum allowed value, the well is shut in.

A positive value of QWMAX for a pressure controlled production well is used as the maximum allowed primary phase production rate. If the calculated primary phase production rate exceeds the maximum allowed value, calculated production will be reduced to the allowed value. Production from each connection is proportionally reduced by the ratio of allowed to calculated primary phase production rates.

Fluid Injection Constraints

Fluid injection using explicit pressure controlled injection wells can be constrained as follows:

- A. A minimum injection rate QWMIN can be specified for a primary phase.
- B. A maximum injection rate QWMAX can be specified for a primary phase.

Primary phases subject to fluid injection constraints are listed in Table C-2 in Appendix C. They are water and natural gas.

A negative value of QWMIN for a pressure controlled injection well is used as the minimum allowed injection rate. If the absolute value of the calculated primary phase injection rate drops below the absolute value of the minimum allowed injection rate, the well is shut in.

A negative value of QWMAX for a pressure controlled injection well is used as the maximum allowed primary phase injection rate. If the absolute value of the calculated primary phase injection rate exceeds the absolute value of the maximum allowed injection rate, calculated injection will be reduced to the allowed value. Injection from each connection is proportionally reduced by the ratio of the absolute values of allowed to calculated injection rates.

13.5 Aquifer Models

A reservoir-aquifer system can be modeled using a variety of techniques. Two of the most important classes of aquifer models are the numerical aquifer model and the analytic aquifer model. The aquifer models available in IFLO are described below.

Numerical Aquifer Model

The numerical aquifer is a representation of aquifer influx by extending the finite difference grid to cover the aquifer with gridblocks . Although this representation of the aquifer is more computationally intensive than an analytic aquifer model such as the steady-state model described below, the numerical model provides a representation of the transient aquifer behavior that is as accurate as the representation of flow in the reservoir.

Figure 13-1 illustrates a grid with the grid boundary extended to include the aquifer. Rock and fluid properties for the aquifer gridblocks must be defined. Notice that the size of the gridblocks increases as the distance of the gridblock from the reservoir boundary increases. It is reasonable to expect that saturation and pressure changes will be smaller in the more distant aquifer blocks, and therefore gridblock refinement is not as important as it is in aquifer blocks adjacent to the reservoir.

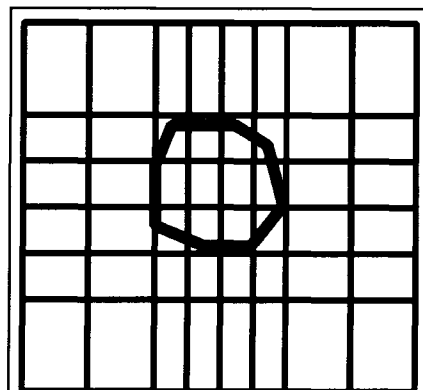


Figure 13-1. Grid with reservoir bounded by aquifer.

Analytic Aquifer Model

Analytic aquifer models represent aquifer influx as a source/sink term in the fluid flow equations. Several types of analytic aquifer models are in use, such as the Carter-Tracy [1960] aquifer model, van Everdingen-Hurst [1949] aquifer model and the Fetkovitch [1971] aquifer model. To illustrate the concept of analytic aquifer model, the steady-state aquifer model is included in IFLO. It is based on Schilthuis's assumption that the water influx rate q_{wss} is proportional to the pressure difference between the aquifer and the hydrocarbon reservoir. It is further assumed that the aquifer is sufficiently large that it experiences no net pressure change throughout the producing life of the reservoir. With these assumptions, IFLO computes an explicit pressure, steady-state aquifer influx into a specified gridblock as

$$q_{wss} = -[\text{SSAQ}(P^0 - P^n)]; \text{SSAQ} \geq 0 \quad (13.21)$$

where P^n is the gridblock pressure at the present time level n ; P^0 is the initial gridblock pressure; and SSAQ is the proportionality constant. The minus sign preceding the bracketed term indicates water is entering the block when $P^0 > P^n$.

Exercises

-
- 13-1. A. Run CS-SW.DAT (slanted well) and record time, pressure, oil rate, gas rate, cumulative oil production, cumulative gas production and cumulative material balance error for oil at the end of the run. Verify the productivity indices (PID) assuming a skin $S = -0.5$ and a wellbore radius of 0.5 ft. Sketch the wellbore trajectory relative to a grid x-z cross-section.
 B. Change the well from slanted to vertical and rerun CS-SW.DAT. Record time, pressure, oil rate, gas rate, cumulative oil production, cumulative gas production and cumulative material balance error for oil at the end of the run. Show your calculation of productivity indices (PID) for the vertical well.
 C. Compare the results of A and B and explain the differences.

180 Integrated Flow Modeling

- 13-2. A. Run EXAM5.DAT (waterflood cross-section) and record time, pressure, oil rate, water rate, cumulative oil production and cumulative water production at the end of the run.
- B. Set the minimum allowed oil rate to 100 STB/D and rerun EXAM2.-DAT. Record time, pressure, oil rate, water rate, cumulative oil production and cumulative water production at the end of the run.
- C. Compare A and B and explain the differences.
- 13-3. A. Run EXAM9.DAT (gas reservoir with aquifer influx) and record time, pressure, gas rate, water rate, cumulative gas production and cumulative water production at the end of the run.
- B. Double the aquifer influx rate and rerun EXAM9.DAT. Record time, pressure, gas rate, water rate, cumulative gas production and cumulative water production at the end of the run.
- C. Eliminate the aquifer and rerun EXAM9.DAT. Record time, pressure, gas rate, water rate, cumulative gas production and cumulative water production at the end of the run.
- D. Compare A through C and explain the differences.
- 13-4. A. Run EXAM2.DAT (vertical column model) and record time, pressure, oil rate, water rate, cumulative oil production and cumulative water production at the end of the run.
- B. Add an analytic aquifer to the base of layer 4 with a steady-state aquifer strength (SSAQ) of 20 SCF/day/psia. Rerun EXAM2.DAT and record time, pressure, oil rate, water rate, cumulative oil production and cumulative water production at the end of the run.
- C. Compare A and B and explain the differences.

Chapter 14

Solution of the Extended Flow Equations

The black oil flow equations presented in Chapter 12 can be extended to include terms and equations that allow the model to be applied to many miscible systems. The extended black oil simulator equations are recast here in a form that is suitable for solution by a numerical technique. The numerical technique is based on an iterative, Newton-Raphson formulation presented by Ammer, et al. [1991].

14.1 The Finite Difference Concept

Simulation of multiphase, multidimensional flow in a reservoir requires solving a system of coupled, nonlinear partial differential equations. For most situations, the flow equations cannot be solved analytically. Instead, the partial differential equations are approximated by algebraic equations known as finite difference equations. The finite difference equations are obtained by replacing derivatives in the partial differential equations with approximations derived from truncated Taylor series expansions. It is worthwhile to review how this is done before converting our partial differential equations to finite difference form.

Our objective is to replace unknown derivatives such as $\partial P/\partial x$ with more manageable mathematical quantities. We do this by manipulating the Taylor series:

$$\begin{aligned} P(x + \Delta x) &= P(x) + \Delta x \frac{\partial P(x)}{\partial x} \Big|_x \\ &\quad + \frac{(\Delta x)^2}{2} \frac{\partial^2 P(x)}{\partial x^2} \Big|_x + \frac{(\Delta x)^3}{6} \frac{\partial^3 P(x)}{\partial x^3} \Big|_x + \dots \end{aligned} \quad (14.1)$$

where " $|_x$ " means the derivative is evaluated at x . If we know the value of P and its derivatives at x , then by Eq. (14.1) we can compute the value of P at $x + \Delta x$. Alternately, if we know the values of $P(x)$ and $P(x + \Delta x)$, we can approximate the derivative $\partial P(x)/\partial x$ as follows.

Subtracting $P(x)$ from both sides of Eq. (14.1), dividing by Δx , and suppressing the notation " $|_x$ " gives

$$\frac{P(x + \Delta x) - P(x)}{\Delta x} = \frac{\partial P(x)}{\partial x} + \varepsilon(\Delta x) \quad (14.2)$$

where higher order derivatives are collected in the term

$$\varepsilon(x) \equiv \frac{\Delta x}{2} \frac{\partial^2 P(x)}{\partial x^2} + \frac{(\Delta x)^2}{6} \frac{\partial^3 P(x)}{\partial x^3} + \dots \quad (14.3)$$

Subtracting $\varepsilon(\Delta x)$ from both sides of Eq. (14.2) yields

$$\frac{\partial P(x)}{\partial x} = \frac{P(x + \Delta x) - P(x)}{\Delta x} - \varepsilon(\Delta x) \quad (14.4)$$

The term $\varepsilon(\Delta x)$ is known as the truncation error. If it is small compared to the difference $[P(x + \Delta x) - P(x)]/\Delta x$, then we have the approximation

$$\frac{\partial P(x)}{\partial x} \approx \frac{P(x + \Delta x) - P(x)}{\Delta x} \quad (14.5)$$

Equation (14.5) becomes an equality when $\varepsilon(\Delta x)$ vanishes. For sufficiently small values of Δx , we can use Eq. (14.5) to replace our first order derivatives of a quantity P with respect to x by a difference between two neighboring values of P separated by a finite interval Δx . Hence the right hand side of Eq. (14.5) is said to be a finite difference approximation of $\partial P(x)/\partial x$ which is correct to

first order in Δx , where the order of correctness is equal to the power of Δx in the leading term of Eq. (14.3). Expressions similar to Eq. (14.5) can be written for derivatives with respect to y , z , or t . The increment in time Δt is called the timestep size. Increments (or differences) along a spatial axis – such as Δx , Δy , or Δz – are called gridblock lengths along that axis. For example, Δz is the gridblock length along the z -axis.

Using finite difference approximations we can convert the partial differential equations to algebraic equations. Figure 14.1 illustrates the coordinate and node locations used in our three dimensional formulation. The finite difference representation in Figure 14.1 is called a seven-point stencil because seven blocks are used in the centered-difference calculation.

A forward difference approximation is used for representing time derivatives. The superscripts n and $n+1$ denote the present and next future time level respectively. Quantities with superscript n can be computed using existing data, whereas quantities with superscript $n+1$ are the unknown variables we are trying to find.

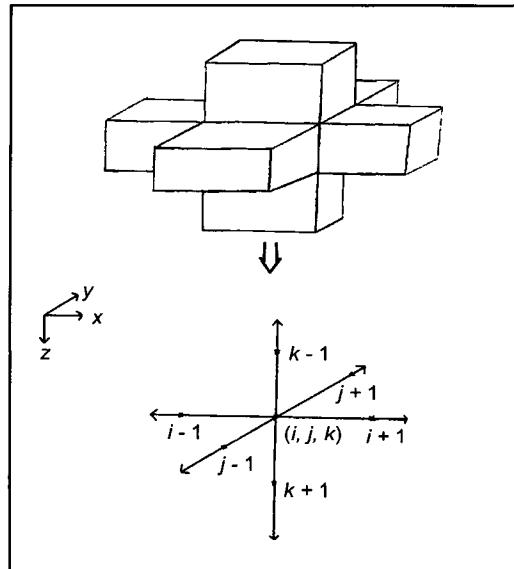


Figure 14-1. Seven-Point Stencil.

Finite Difference Approximations

We can extend the above concepts to find a number of useful approximations. Suppose we have a continuous function P of x (such as the pressure drop across a core) and we want to estimate the value of $\partial P / \partial x$. If we have

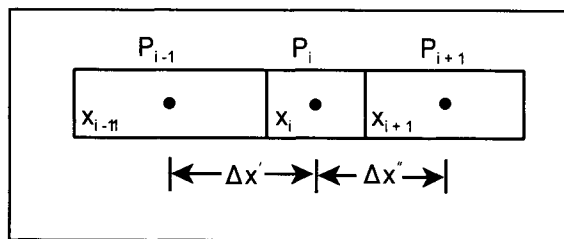


Figure 14-2. Block-Centered Notation.

values of P at locations x_i (Figure 14.2), we can estimate $\partial P / \partial x$ using Eq. (14.5) in the following form

$$\frac{\partial P(x)}{\partial x} \approx \frac{P_{i+1} - P_i}{\Delta x}, \quad \Delta x = x_{i+1} - x_i \quad (14.6)$$

where the notation P_i means the value of P at x_i , and x_i is the i^{th} node location.

An alternative approximation can be obtained by starting with the Taylor series:

$$\begin{aligned} P(x - \Delta x) &= P(x) - \Delta x \frac{\partial P(x)}{\partial x} \Big|_x + \frac{(\Delta x)^2}{2} \frac{\partial^2 P(x)}{\partial x^2} \Big|_x \\ &\quad - \frac{(\Delta x)^3}{6} \frac{\partial^3 P(x)}{\partial x^3} \Big|_x + \dots \end{aligned} \quad (14.7)$$

Manipulating Eq. (14.7) like we did Eq. (14.1) and dropping the truncation error term gives

$$\frac{\partial P(x)}{\partial x} \approx \frac{P(x) - P(x - \Delta x)}{\Delta x} \quad (14.8)$$

or, in the notation of Eq. (14.6), Eq. (14.7) becomes

$$\frac{\partial P(x)}{\partial x} \approx \frac{P_i - P_{i-1}}{\Delta x}, \quad \Delta x = x_i - x_{i-1} \quad (14.9)$$

Equation (14.6) is called the forward difference or downstream approximation of $\partial P / \partial x$, while Eq. (14.9) is termed the backward difference or upstream approximation of $\partial P / \partial x$.

Adding Eq. (14.6) and (14.9) and rearranging gives in our discrete notation

$$\frac{\partial P}{\partial x} = \frac{P_{i+1} - P_{i-1}}{2(\Delta x)} - \varepsilon(\Delta x^2) \quad (14.10)$$

where the truncation error is now second in order in Δx . Equation (14.10) is called the centered difference approximation of $\partial P / \partial x$ and is more accurate than either Eq. (14.6) or (14.9). Even though this method reduces numerical error, there are situations when it should not be used. For example, use of a time-centered difference approximation will lead to an unconditionally unstable

finite difference equation when solving the parabolic differential equation $\partial^2 P / \partial x^2 = \partial P / \partial t$.

If we add Eqs. (14.1) and (14.7) we obtain

$$P_{i+1} + P_{i-1} = 2P_i + (\Delta x)^2 \frac{\partial^2 P}{\partial x^2} \Big|_{x_i} + 2 \frac{\partial^4 P}{\partial x^4} \Big|_{x_i} \left[\frac{(\Delta x)^4}{24} \right] + \dots \quad (14.11)$$

Solving for the second derivative gives

$$\frac{\partial^2 P}{\partial x^2} = \frac{P_{i+1} + P_{i-1} - 2P_i}{(\Delta x)^2} - \varepsilon_2 (\Delta x^2) \quad (14.12)$$

where the second-order truncation error term is

$$\varepsilon_2 (\Delta x)^2 = \frac{\partial^4 P}{\partial x^4} \frac{(\Delta x)^2}{12} + \dots \quad (14.13)$$

Equation (14.12) is an approximation for second-order derivatives.

Many other finite difference approximations can be constructed using manipulations of the Taylor series. They are described extensively in the literature. For our purposes, the other approximation used in IFLO is

$$\frac{\partial}{\partial x} \left(\Gamma \frac{\partial P}{\partial x} \right) \approx \frac{\Gamma_{i+\frac{1}{2}} \left(\frac{P_{i+1} - P_i}{\Delta x''} \right) - \Gamma_{i-\frac{1}{2}} \left(\frac{P_i - P_{i-1}}{\Delta x'} \right)}{\frac{\Delta x' + \Delta x''}{2}} \quad (14.14)$$

where Γ denotes transmissibility in flow equations, and

$$\Delta x' = x_i - x_{i-1}, \quad \Delta x'' = x_{i+1} - x_i \quad (14.15)$$

The notation $\Gamma_{i-\frac{1}{2}}$ and $\Gamma_{i+\frac{1}{2}}$ means the coefficient should be evaluated at locations $x_{i-\frac{1}{2}}$ and $x_{i+\frac{1}{2}}$ respectively where $x_{i+\frac{1}{2}}$ denotes a location somewhere between x_i and $x_{i+\frac{1}{2}}$ (similarly for $x_{i-\frac{1}{2}}$). However, since the values for transmissibility Γ are usually known at the nodes x_i , some sort of averaging procedure must be used to arrive at an acceptable approximation for the physical properties that are used to determine the values of Γ at locations between nodes. The procedure for calculating IFLO transmissibilities is discussed in Chapter 9.

14.2 Derivative of Accumulation Terms

Accumulation terms have the form of the derivative of a product of factors, thus

$$\frac{d(ab)}{dt} \approx \Delta_t(ab) \quad (14.16)$$

where a and b are the factors, and Δ_t denotes the finite difference approximation to the time derivative. A straightforward chain rule expansion gives

$$\Delta_t(ab) = a^n \left[\frac{b^{n+1} - b^n}{\Delta t} \right] + b^n \left[\frac{a^{n+1} - a^n}{\Delta t} \right] \quad (14.17)$$

where the index n denotes the present time level, and Δt is the timestep size. Equation (14.7) introduces a numerical error that manifests itself as a material balance error. A consistent, mass conserving, finite difference expansion of the time derivative is

$$\Delta_t(ab) = a^{n+1} \left[\frac{b^{n+1} - b^n}{\Delta t} \right] + b^n \left[\frac{a^{n+1} - a^n}{\Delta t} \right] \quad (14.18)$$

Equation (14.18) can be rearranged to give the simplified mass conserving expansion

$$\Delta_t(ab) = \frac{a^{n+1}b^{n+1} - a^n b^n}{\Delta t} \quad (14.19)$$

In general, Eqs. (14.17) and (14.18) are not equal. If either a^n or b^n are slowly varying functions of time, or the timestep size Δt is small, then the equations are nearly equivalent.

14.3 Volume Integration and Discretization

The fluid flow equations presented in Chapter 12 are discretized using volume integration and finite difference techniques. We begin to discretize the fluid flow equations by dividing the reservoir into a set of rectangular parallelepipeds that are referred to as cells, gridblocks, or just blocks.

The volume integration procedure is illustrated by integrating the oil flow equation over block m , thus

$$\int_{V_m} \left[\nabla \cdot \frac{Kk_o^e}{\mu_o^e B_o} \nabla \Phi_o - \frac{q_o}{\rho_{osc}} \right] dV = \int_{V_m} \frac{\partial}{\partial t} \left(\phi \frac{S_o}{B_o} \right) dV \quad (14.20)$$

The volume integrals can be replaced with surface integrals using the divergence theorem. If \vec{F} is a vector field whose component functions have continuous partial derivatives in a volume V bounded by a closed surface S with a unit vector \hat{n} directed outward from V , then the divergence theorem states that [Larson, et al., 1990]

$$\int_S \vec{F} \cdot \hat{n} dS = \int_V \nabla \cdot \vec{F} dV \quad (14.21)$$

The divergence theorem is applied to Eq. (14.20) by defining the vector field

$$\vec{F} = \frac{Kk_o^e}{\mu_o^e B_o} \nabla \Phi_o \quad (14.22)$$

The block volume V_m corresponds to the volume V , and the surface S is the external surface S_{em} of the gridblock m . Applying the divergence theorem to Eq. (14.20) gives

$$\int_{S_{em}} \frac{Kk_o^e}{\mu_o^e B_o} \nabla \Phi_o \cdot \hat{n} dS - \int_{V_m} \left[\frac{q_o}{\rho_{osc}} \right] dV = \frac{\partial}{\partial t} \int_{V_m} \left(\phi \frac{S_o}{B_o} \right) dV \quad (14.23)$$

where we have switched the order of differentiation and integration on the right hand side.

Discretization is achieved by first making the following definitions. The volume integral over rate is written as

$$Q_o = \int_{V_m} \frac{q_o}{\rho_{osc}} dV = \frac{q_o}{\rho_{osc}} V_m \quad (14.24)$$

The volume integral over the accumulation term is written as

$$M_o = \int_{V_m} \left(\phi \frac{S_o}{B_o} \right) dV = \phi \frac{S_o}{B_o} V_m \quad (14.25)$$

The surface integral is written as

$$\Delta A_o \Delta \Phi_o = \int_{S_{\text{em}}} \frac{K k_o}{\mu_o B_o} \nabla \Phi_o \cdot \hat{n} dS \quad (14.26)$$

where A_o is oil phase transmissibility. Given these definitions, the spatially discretized material balance equation for oil becomes

$$\frac{dM_o}{dt} + Q_o = \Delta A_o \Delta \Phi_o \quad (14.27)$$

The time derivative in Eq. (14.27) is replaced with a backward finite difference to obtain

$$\frac{1}{\Delta t} [M_o^{n+1} - M_o^n] + Q_o^{n+1} = \Delta A_o^{n+1} \Delta \Phi_o^{n+1} \quad (14.28)$$

The superscript n denotes the present time level t^n and the superscript $n + 1$ denotes the future time level t^{n+1} . The timestep size is $\Delta t = t^{n+1} - t^n$.

The assessment of all variables at the future time level in Eq. (14.28) makes this formulation a fully implicit formulation. The IMPES technique simplifies the formulation. IMPES is invoked by approximating transmissibilities, capillary pressures and densities at time level $n + 1$ with their values at time level n . The resulting flow equation is

$$\frac{1}{\Delta t} [M_o^{n+1} - M_o^n] + Q_o^{n+1} = \Delta A_o^n \Delta \Phi_o^{n+1} \quad (14.29)$$

and

$$\Delta \Phi_o^{n+1} = \Delta P^{n+1} - \Delta \gamma_o^n D \quad (14.30)$$

The variable P is oil phase pressure, D is depth to the center of the gridblock, and γ_o is the specific weight ($\rho_o g$) of the oil phase. Similar equations apply to the other flow equations.

14.4 Multi-Variable Newton-Raphson IMPES Procedure

The IMPES equations developed above are solved using an iterative Newton-Raphson technique that solves for several variables. The iterative technique is illustrated by continuing our analysis using the oil flow equation. The residual form of Eq. (14.29) is

$$R_o^\ell = \frac{1}{\Delta t} [M_o^{\ell+1} - M_o^\ell] + Q_o^\ell - \Delta A_o^n \Delta \Phi_o^\ell \quad (14.31)$$

where the superscript ℓ denotes the iteration level for the variables that are desired at time level $n + 1$. The desired variables at time level $n + 1$ are called primary variables.

The primary variables for a saturated block are δP , δS_w , δS_g and $\{\delta v_i; i = 1, \dots, N_s\}$ where P is oil phase pressure, S_w is water saturation, S_g is gas saturation, v_i is the volume fraction of component i , and N_s is the number of solvents. The set of primary variables for an undersaturated block is the same as the set of primary variables for a saturated block except gas saturation is replaced by bubble point pressure P_b . The resulting primary variables for an undersaturated block are δP , δS_w , δP_b and $\{\delta v_i; i = 1, \dots, N_s\}$. If there is no oil in the system, as in a gas-water reservoir, the oil phase pressure is equivalent to water phase pressure since oil-water capillary pressure is zero. The variable switching logic used to treat blocks undergoing phase transitions is described in Chapter 10.

The solution process is designed to find the values of the primary variables which drive the residuals to zero in all gridblocks for all components. Mathematically this requirement is expressed as

$$R_i^\ell = 0 \text{ for } i = \{o, w, g, 1, \dots, N_s\} \quad (14.32)$$

The procedure for deriving recursive expressions for the residuals is illustrated using the oil residual.

We begin by writing the oil residual Eq. (14.31) at iteration $\ell + 1$ as

$$\begin{aligned} R_o^{\ell+1} &= \frac{1}{\Delta t} [M_o^{\ell+1} - M_o^\ell + M_o^\ell - M_o^n] + Q_o^{\ell+1} - Q_o^\ell + Q_o^\ell \\ &\quad - \Delta A_o^n \Delta \Phi_o^{\ell+1} + \Delta A_o^n \Delta \Phi_o^\ell - \Delta A_o^n \Delta \Phi_o^\ell \end{aligned} \quad (14.33)$$

We have added several terms in Eq. (14.33) that sum to zero. These terms will be used to create a recursive relation between residuals $R_o^{\ell+1}$ and R_o^ℓ . In particular, Eq. (14.33) can be written as

$$R_o^{\ell+1} = \frac{1}{\Delta t} [M_o^{\ell+1} - M_o^\ell] + J_o^n \delta P^{\ell+1} - \Delta A_o^n \Delta P^{\ell+1} + R_o^\ell \quad (14.34)$$

190 Integrated Flow Modeling

where

$$\delta P^{\ell+1} = P^{\ell+1} - P^\ell \quad (14.35)$$

and source/sink terms are represented by the quantity

$$J_o^n = \begin{cases} \text{PID} \left(\frac{k_o}{\mu_o B_o} \right)^n & \text{for implicit wells,} \\ 0 & \text{otherwise} \end{cases} \quad (14.36)$$

Values of the index PID are discussed more fully in Chapter 13. The starting value of the residual is given in terms of variables calculated at time level n , thus

$$R_o^0 = Q_o^n - \Delta A_o^n \Delta \Phi_o^n \quad (14.37)$$

Similar recursion relations are written for all components.

The iterative solution procedure is outlined in Table 14-1. It presumes that the amount M_i of component i in the gridblock at time level n is known, a tolerance ϵ (RTOL in Appendix B.9) has been specified by the user, and a maximum number of iterations (ITMAX) has been specified by the user. The procedure in Table 14-1 is referred to as the multi-variable Newton-Raphson IMPES method [Ammer, et al., 1991]. The linear solvers are discussed by Young [1971], Price and Coats [1973], Nolen and Berry [1973], Vinsome [1976], and Spillette, et al. [1986].

Table 14-1
Summary of Iterative Solution Procedure

1. Identify primary variables $\{\delta U\} = \{\delta P, \delta S_w, \delta S_g \text{ or } \delta P_b, \{\delta v_i; i = 1, \dots, N_s\}\}$
2. Calculate R_i^ℓ for $\ell = 0$ and $i = \{o, w, g, 1, \dots, N_s\}$
3. Collect and rearrange recursive residuals
$\underline{\alpha}' \delta \underline{U}^{\ell+1} = -\underline{R}^\ell$
$\underline{\alpha}'$ is acceleration matrix (Jacobian with respect to primary variables) $\delta \underline{U}^{\ell+1}$ is vector of primary variables \underline{R}^ℓ is vector of residuals

Table 14-1
Summary of Iterative Solution Procedure

4. Perform forward (Gaussian) elimination to form pressure equation

$$\left(\frac{V_p^\ell}{\Delta t} C_T^\ell + J_T^\ell \right) \delta P^{\ell+1} - \Delta A_T^\ell \Delta \delta P^{\ell+1} = -R_T^\ell$$

C_T^ℓ is total compressibility

J_T^ℓ is linear combination of source/sink terms

A_T^ℓ is linear combination of transmissibility

R_T^ℓ is linear combination of residuals

5. Solve pressure equation for δP

Linear solvers: SSOR, LSOR, D4, ORTHOMIN

6. Perform back substitution to find δS_w , δS_g or δP_b , $\{\delta v_i; i = 1, \dots, N_s\}$

7. Update local material balance error $R_i^{\ell+1} \Delta t$

8. Is $|R_i^{\ell+1} \Delta t| / M_i < \epsilon$?

If no and $\ell + 1 < \text{ITMAX}$, go to step 2.

If yes or $\ell + 1 = \text{ITMAX}$, go to next timestep.

It is important when making cross-section or 3-D runs that the pressure distribution in the model is correctly initialized. If not, phase potential differences due to gravity terms could cause fluid migration even though no wells are active. Consequently, an equilibrium initialization algorithm and a gravity segregation algorithm are available as options in IFLO. Options for defining nonequilibrium initialization are also available. Nonequilibrium initialization gives the IFLO user considerable flexibility in initializing a model, but the user needs to be careful to define appropriate pressure, saturation, or solvent distributions. Details of the initialization options are described in Appendix D.

The size of the local material balance error depends on the tolerance ϵ and the number of iterations allowed. Global material balance error is obtained by summing local material balance error over all gridblocks. A good material balance solution is achieved when both local and global material balance errors are small.

Exercises

- 14-1. A. Run EXAM7.DAT (Odeh gas injection) and record time, pressure, oil rate, gas rate, cumulative oil production, cumulative gas production and cumulative material balance error for oil at the end of the run.
- B. Reduce the maximum number of Newton-Raphson iterations (ITMAX) to 1. Rerun EXAM7.DAT and record time, pressure, oil rate, gas rate, cumulative oil production, cumulative gas production and cumulative material balance error for oil at the end of the run.
- C. Set ITMAX = 10 and reduce the residual tolerance (RTOL) to 0.0001. Rerun EXAM7.DAT and record time, pressure, oil rate, water rate, cumulative oil production, cumulative gas production and cumulative material balance error for oil at the end of the run.
- D. Compare the results of A through C and explain the differences.
- 14-2. A. Run EXAM6.DAT (5-spot waterflood) and record time, pressure, oil rate, water rate, gas rate, cumulative oil production and cumulative material balance error for oil at the end of the run.
- B. Set the code for controlling material balance error (NERR) to 0 and rerun EXAM6.DAT. Record time, pressure, oil rate, water rate, gas rate, cumulative oil production and cumulative material balance error for oil at the end of the run.
- C. Compare A and B and explain the differences.
- 14-3. A. Run EXAM7.DAT (Odeh gas injection) and record time, pressure, oil rate, gas rate, cumulative oil production, cumulative gas production and cumulative material balance error for oil at the end of the run.
- B. Select the LSOR matrix solver and rerun EXAM7.DAT. Record time, pressure, oil rate, gas rate, cumulative oil production, cumulative gas production and cumulative material balance error for oil at the end of the run.
- C. Allow the timestep size to vary from 0.5 to 5 days, beginning with a 1 day timestep size, from the end of year 5 through year 10. Rerun

EXAM7.DAT and record time, pressure, oil rate, gas rate, cumulative oil production, cumulative gas production and cumulative material balance error for oil at the end of the run.

D. Compare the results of A through C and explain the differences. Which solvers are iterative and which are direct?

- 14-4. A. Run EXAM10.DAT (gas reservoir with aquifer cross-section) and record time, pressure, gas rate, water rate, cumulative gas production, cumulative water production, cumulative error for gas and number of timesteps at the end of the run.
- B. Select the ORTHOMIN matrix solver and rerun EXAM10.DAT. Record time, pressure, gas rate, water rate, cumulative gas production, cumulative water production, cumulative error for gas and number of timesteps at the end of the run.
- C. Compare A and B and explain the differences.

Chapter 15

IFLO Applications

Previous chapters have provided insight into the utility of integrated flow models. Our focus here is on particular applications of the three-dimensional, three-phase, pseudomiscible simulator IFLO. The applications presented below illustrate important principles that can aid in the management of subsurface resources.

15.1 Monitoring Frontal Advance

Time-lapse (4-D) seismic monitoring can achieve several important results. Among them is the imaging of changes in frontal locations. The effort here is not to accurately resolve the frontal positions, but to detect qualitative changes in frontal positions that are on the order of magnitude of a gridblock. This is an important distinction because it is well known that seismic resolution is limited to approximately one quarter of the wavelength of a wavelet. Typically, this implies that the vertical resolution limit will be on the order of 10 m or more, and the limits of areal resolution are typically larger than the vertical resolution limit. Detection of changes in seismic response, however, can yield useful qualitative information for history matching purposes, especially when we note that gridblocks are typically 50 m to 100 m on a side. In this case, the

resolution of the frontal position for the formation of interest only needs to be within the areal boundaries of a gridblock. If it is, the reservoir modeler has information that can help refine the history matching process. Consequently, our interest in the following examples is in the detectability of changes. If resolution is also obtained, it is a desirable by-product.

Waterflood of an Undersaturated Oil Reservoir

The first example determines the acoustic response of a system in which undersaturated oil is subjected to displacement by injected water. Fluid properties in this example are from the case study in Fanchi [2000]. For simplicity, a horizontal, single layer model with 20 cells is used. Water is injected in one end of the linear model and produced from the other end. Acoustic impedance is monitored as a function of time at a central location, which serves as an observation point. The ratio of matrix modulus to grain modulus K_M/K_G is set to 2/3 so that some variation in the V_p/V_s ratio can appear.

The difference between oil and water phase densities and compressibilities in this example is small relative to a liquid-gas system. Consequently, the velocity ratio V_p/V_s increases slightly (approximately 0.66%) as the observation cell fills with injected water. A change of 0.5% in V_p/V_s is considered detectable.

Gas Injection into a Saturated, Light Oil Reservoir

The second example is based on the first SPE comparative solution project [Odeh, 1981]. A saturated, light (59° API) oil is produced from a corner block in the lowermost layer of a three-layer square grid. Lean gas is injected into the upper layer at the opposite corner. The injected gas is expected to propagate most rapidly through the upper layer. Therefore, an observation point was selected in the upper layer midway between the injector and producer. This point lets us observe the gas front pass as the injected gas flows toward the pressure sink at the production well. We assume $K_M/K_G = 2/3$. In this case, the velocity ratio V_p/V_s decreases (approximately 1.64%) as the gas front passes the observation cell.

Aquifer Influx into a Gas Reservoir

The previous examples did not show much response by the velocity ratio V_p/V_s to flood front passage. A third example was designed that would exhibit larger changes in V_p/V_s as a function of field performance over time. In particular, a dipping gas reservoir with aquifer influx was studied. The reservoir is represented as a dipping, 2-layer cross-section. Initial gas saturation is 70% and initial irreducible water saturation is 30%. A downdip aquifer provides pressure support and water invasion as the reservoir is produced.

The lowermost cell adjacent to the aquifer was selected as the observation cell. This cell responds most quickly to water invasion and exhibits the acoustical response associated with water front advance. The velocity ratio V_p/V_s increases by approximately 4.47% for an irreducible gas saturation of 0% as water displaces gas in the observation cell.

The petrophysical model and, by inference, petrophysical properties, have a sensitive dependence on certain input parameters. For example, the velocity ratio V_p/V_s in this application is sensitive to a change in irreducible gas saturation (S_{gr}). An irreducible gas saturation of 0% results in complete displacement of gas from the water invaded zones. The resulting elimination of gas from the calculation of reservoir geophysical attributes in the water invaded part of the reservoir causes a significant change in the ratio V_p/V_s . If the example is run with an irreducible gas saturation of 3%, the relatively large change in V_p/V_s is no longer observed because the presence of a small amount of gas significantly changed the compressibility of the system. The velocity ratio V_p/V_s increases by approximately 1.60% for an irreducible gas saturation of 3%.

Discussion

The velocity ratio V_p/V_s changed most when free gas saturation either developed in a cell that contained only liquid or completely disappeared from a cell that had a nonzero gas saturation. Kelamis, et al. [1997] observed similar gas saturation behavior in their seismic monitoring study of a clastic oil reservoir with a large gas cap in the Arabian Gulf. They referred to it as a "key

saturation signature". They concluded that the key saturation signature was needed to successfully implement a 4-D seismic monitoring program.

15.2 Scheduling 4-D Seismic Surveys

We discussed in the previous section the importance of detectability to time-lapse (4-D) seismic monitoring. Detectable changes in frontal locations yields information that can be used for a variety of purposes, such as identifying by-passed reserves. The IFLO application in this section shows that integrated studies using 4-D seismic surveys have another important task: scheduling the seismic surveys to optimize the acquisition of reservoir management information.

The fluid properties in the first SPE comparative solution project [Odeh, 1981] were used with the reservoir characterization described in the second SPE comparative solution project [Weinstein, et al., 1986]. A cross-section of an undersaturated oil reservoir with 15 layers was modeled. Permeability is isotropic and vertical permeability was assumed to be one tenth of horizontal permeability.

Layer 9 of the 15 layer cross-section is the best oil target. The lowermost layer (layer 15) is a thick, water-bearing aquifer layer. Gas was injected into the upper layers (layers 1 through 3) of the undersaturated oil reservoir cross-section while oil was being produced from the lower layers (layers 9 through 12). All layers are in vertical communication. The velocity ratio V_p/V_s in layer 3 of the injection well decreased by approximately 0.46% and decreased by 0.60% in layer 9 of the production well. Although the per cent difference in acoustic response is relatively small, the acoustic response for this particular example illustrates the following important features of 4-D seismic monitoring.

The advance of the injected gas into the cross-section is considered at 180 days and 270 days. The gas front is highlighted by displaying the change in gas saturation from the beginning of the flood to the current time. The corresponding change in the ratio of compressional to shear velocities is also considered. The presence of injected gas shows up clearly at both 180 days and 270 days. In addition, the presence of a cone of gas appears at 270 days

198 Integrated Flow Modeling

in the layers above the perforated interval of the oil production well. The appearance of the cone is explained by looking at the pressure distribution in the reservoir relative to the bubble point pressure.

The difference in reservoir pressure relative to bubble point pressure shows the appearance of a cone of free gas that is coming out of solution as reservoir pressure in the vicinity of the production well drops below the bubble point pressure of the oil. A seismic survey at 180 days would see the gas front advance but not the gas cone, while a seismic survey at 270 days would see both the gas front advance and the gas cone. The later survey would provide more information for use in a history match.

15.3 Improved Oil Recovery Examples

IFLO is an extended black oil simulator with pseudomiscible features. The examples presented below illustrate the pseudomiscible features for two types of miscible processes: enriched gasflooding (Case A), and carbon dioxide flooding (Case B). Immiscible processes are also shown for comparison. The immiscible waterflood is the base case. Immiscible natural gas injection provides a gas injection case for comparison with miscible enriched gas or carbon dioxide flooding.

A simple linear grid was used in all cases. The injection well is on the left hand side of the linear grid and the production well is on the right hand side. The linear grid is fine enough to monitor front movement and illustrate the calculation of reservoir geophysical attributes under a variety of reservoir conditions. The following parameter profiles (versus gridblock number) were considered for both cases at time 730 and 1460 days [Fanchi, 2000]: Reservoir Pressure, Oil Saturation, Water Saturation, Gas Saturation, Compressional Velocity, Shear Velocity, Compressional to Shear Velocity Ratio, and Acoustic Impedance.

The correlations published by Murphy, et al. [1993] for sandstone were used to compute shear and compressional velocities for the integrated flow model examples. The linear correlation between modulus and porosity is

approximately correct for porosity values less than 35%. The correlation shows that sandstone moduli decrease as porosity increases.

Case A. Enriched Gasflooding

Fluid and rock-fluid interaction data for the fifth SPE comparative solution project [Killough and Kossack, 1987] were used to illustrate the reservoir geophysical behavior of a miscible, enriched gasflood of a light oil (oil specific gravity = 0.62). Results for this case are referred to as SPE5 because the fluid description is based on the four-component, pseudomiscible representation used by Arco in the fifth SPE comparative solution project and included in the documentation of MASTER [Ammer, et al. 1991]. Three injection fluids were considered in Case A: water, associated natural gas, and an enriched methane solvent (77% methane, 20% propane, and 3% hexane). The following scenarios were simulated for Case A: A-1. Immiscible Waterflood (SPE5 WF); A-2. Immiscible Natural Gas Flood (SPE5 GAS); and A-3. Miscible Enriched Gas Flood (SPE5 SOL).

Several parameters in the injection well block ($I = 1$) were considered at different times to show the magnitude of the change in parameter over the life of the process (Table 15-1). The parameters are pressure (P), oil saturation (S_o), water saturation (S_w), gas saturation (S_g), compressional velocity (V_p), shear velocity (V_s), and compressional to shear velocity ratio (V_p/V_s). Minimum miscibility pressure (P_{misc}) is 3000 psia and the miscibility mixing parameters ($OM1$ and $OM2$) equal 1 unless stated otherwise. The initial parameter values at time 0 days in case SPE5 WF apply to all cases.

**Table 15-1. Parameters in Injection Well Cell ($I = 1$)
for Case A (SPE5)**

Case	Time days	P psia	S_o	S_w	S_g	V_p ft/sec	V_s ft/sec	V_p/V_s
WF	0	4.000	0.840	0.160	0.000	13,133	8,737	1.5030
	730	4.470	0.255	0.745	0.000	13,093	8,612	1.5203
	1460	4.506	0.250	0.750	0.000	13,094	8,611	1.5206
GAS	730	5,292	0.309	0.159	0.532	13,180	8,839	1.4910
	1460	5,900	0.267	0.159	0.574	13,188	8,845	1.4909
$P_{misc} = 4000$ psia	730	5,292	0.309	0.159	0.532	13,180	8,839	1.4910
	1460	5,900	0.267	0.159	0.574	13,188	8,845	1.4909

**Table 15-1. Parameters in Injection Well Cell ($I = 1$)
for Case A (SPE5)**

Case	Time days	P psia	So	Sw	Sg	V _p ft/sec	V _s ft/sec	V _p /V _s
GAS $OM1 = OM2 = 0$	730	5,291	0.309	0.159	0.532	13,180	8,839	1.4910
	1460	5,896	0.267	0.159	0.574	13,188	8,845	1.4909
SOL	730	4,133	0.024	0.160	0.816	13,205	8,865	1.4896
	1460	4,038	0.000	0.160	0.840	13,206	8,866	1.4895
SOL $P_{misc} = 4000$ psia	730	4,133	0.024	0.160	0.816	13,205	8,865	1.4896
	1460	4,114	0.000	0.160	0.840	13,205	8,865	1.4895
SOL $OM1 = OM2 = 0$	730	4,108	0.224	0.160	0.616	13,168	8,838	1.4900
	1460	4,023	0.115	0.160	0.725	13,194	8,856	1.4898

Pressure is greater than minimum miscibility pressure (MMP = 3000 psia) throughout the linear system in both gas injection cases at 1460 days. Pressure in the waterflood case is greater than bubble point pressure (2302 psia) except near the producer. The largest seismic response to the immiscible waterflood in Case A-1 occurs at the point in the reservoir where gas saturation appears. The oil in Case A is a light oil with a high API gravity. As a consequence of density differences between injected water and light oil, the seismic parameters clearly indicate the water – oil interface.

The magnitude of the change in compressional velocity for the enriched gas and natural gas injection cases is about 0.5%. Shear velocity, compressional to shear velocity ratio, and acoustic impedance change by a magnitude of approximately 1.5%, 1.2% and 2.2% respectively. The reservoir geophysical attributes show the interface between the displacing and displaced fluids, as illustrated in Figure 15-1. Acoustic impedance is normalized to a dimensionless ratio by dividing each value at 1460 days by its initial value.

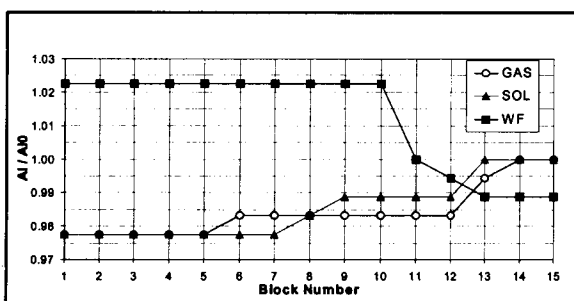


Figure 15-1. Case A (SPE5) Acoustic Impedance at 1460 Days.

Case B. Carbon Dioxide Flooding

Fluid and rock-fluid interaction data from the East Vacuum Grayburg-San Andres Unit (EVU) flood [Grigg and Schechter, 1998] were used to illustrate the reservoir geophysical behavior of a miscible, carbon dioxide flood of an oil with a specific gravity of 0.82. Three injection fluids were considered; water, associated natural gas, and carbon dioxide. The following scenarios were simulated for Case B: B-1. Immiscible Waterflood (EVU WF); B-2. Immiscible Natural Gas Flood (EVU GAS); and B-3. Miscible Carbon Dioxide Flood (EVU CO₂).

Several parameters in the injection well block ($I = 1$) were considered at different times to show the magnitude of the change in parameter over the life of the process (Table 15-2). The parameters are pressure (P), oil saturation (S_o), water saturation (S_w), gas saturation (S_g), compressional velocity (V_p), shear velocity (V_s), and compressional to shear velocity ratio (V_p/V_s). Minimum miscibility pressure (P_{misc}) is 1190 psia and the miscibility mixing parameters ($OM1$ and $OM2$) equal 1 unless stated otherwise. The initial parameter values at time 0 days in case EVU WF apply to all cases.

Table 15-2. Parameters in Injection Well Cell ($I = 1$) for Case B (EVU)

Case	Time days	P psia	S _o	S _w	S _g	V _p ft/sec	V _s ft/sec	V _p /V _s
WF	0	4,000	0.840	0.160	0.000	13,080	8,666	1.5094
	730	5,622	0.415	0.585	0.000	13,173	8,607	1.5304
	1460	4,267	0.338	0.662	0.000	13,234	8,596	1.5395
GAS	730	4,778	0.467	0.160	0.373	13,042	8,756	1.4896
	1460	3,500	0.384	0.160	0.455	13,083	8,788	1.4887
GAS <i>P_{misc} = 4000 psia</i>	730	4,778	0.467	0.160	0.373	13,042	8,756	1.4896
	1460	3,500	0.384	0.160	0.455	13,083	8,788	1.4887
GAS <i>OM1 = OM2 = 0</i>	730	4,778	0.467	0.160	0.373	13,042	8,756	1.4896
	1460	3,500	0.384	0.160	0.455	13,083	8,788	1.4887
CO ₂	730	2,765	0.329	0.161	0.511	12,686	8,523	1.4884
	1460	2,602	0.112	0.160	0.728	12,694	8,530	1.4881
CO ₂ <i>P_{misc} = 4000 psia</i>	730	2,979	0.521	0.160	0.319	12,770	8,577	1.4889
	1460	2,792	0.441	0.160	0.399	12,752	8,566	1.4887
CO ₂ <i>OM1 = OM2 = 0</i>	730	2,834	0.576	0.161	0.263	12,972	8,710	1.4894
	1460	2,548	0.480	0.160	0.359	13,020	8,744	1.4890

Pressure is greater than minimum miscibility pressure (MMP = 1190 psia) throughout the linear system in both gas injection cases at 1460 days. Pressure in the waterflood case is greater than bubble point pressure (1272 psia) everywhere so that no free gas saturation appears in the EVU WF case.

The magnitude of the change in compressional velocity for the gas injection cases is about 0.5%. Compressional velocity changes by a magnitude of up to 3.0% for the carbon dioxide injection case, and generally less than 0.5% for the waterflood and natural gas injection cases. Compressional to shear velocity ratio changes by a magnitude of up to 2.0% for the waterflood case, and about 1.4% for the carbon dioxide and natural gas injection cases. Acoustic impedance changes by a magnitude of up to 3.0% for the carbon dioxide injection and waterflood cases, and about 1.7% for the natural gas injection case. The carbon dioxide front is apparent on the "V_p" plot in Figure 15-2. Compressional velocity is normalized to a dimensionless ratio by dividing each value at 1460 days by its initial value.

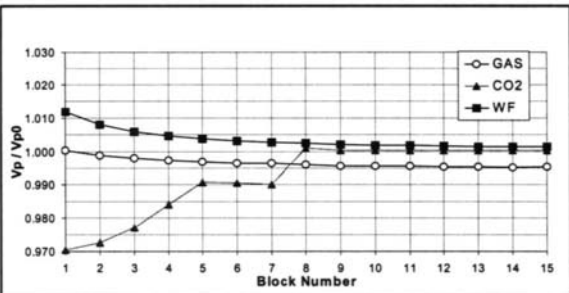


Figure 15-2. Case B (EVU) Compressional Velocity at 1460 days.

C. Parameter Sensitivity

The sensitivity of the model to variations in miscibility pressure and mixing parameter are shown for gas injection cases in Tables 15-1 and 15-2. Miscibility does not significantly affect reservoir geophysical parameters in the enriched gas injection Case A. It has a more pronounced effect in the carbon dioxide injection Case B, but the effect of varying miscibility pressure and mixing parameter on reservoir geophysical attributes in these examples is relatively small compared to factors such as the presence of gas and reservoir pressure. The main difference between immiscible and miscible floods is the mobilization of residual oil by the miscible flood.

Exercises

- 15-1. A. Run XS-SPE2.DAT (gas injected into oil cross-section) and record time, pressure, oil rate, gas rate, cumulative oil production and cumulative gas production at the end of the run.
B. Prepare a plot of the compressional to shear velocity ratio array at 180 days and 270 days.
C. Compare A and B and explain how the differences can be used to schedule 4-D seismic surveys.
- 15-2. A. Run RIM-2D.DAT (anticlinal gas reservoir) and prepare a plot of the compressional to shear velocity ratio array at the end of the run. Record time, pressure, oil rate, water rate, and gas rate at the end of the run.
B. Multiply the y -direction transmissibility by 0.1 between rows $J = 15$ and $J = 16$ to simulate a partially sealing fault. Rerun RIM-2D.DAT and prepare a plot of the compressional to shear velocity ratio array at the end of the run. Record time, pressure, oil rate, water rate, and gas rate at the end of the run.
C. Set the y -direction transmissibility to zero between rows $J = 15$ and $J = 16$ to simulate a sealing fault. Rerun RIM-2D.DAT and prepare a plot of the compressional to shear velocity ratio array at the end of the run. Record time, pressure, oil rate, water rate, and gas rate at the end of the run.
D. Compare A through C and explain how the differences can be used to study fault seals.

This Page Intentionally Left Blank

Appendices

This Page Intentionally Left Blank

Appendix A

Introduction to IFLO

The program IFLO is a pseudomiscible, multicomponent, multidimensional fluid flow simulator. IFLO models isothermal, Darcy flow in up to three dimensions. It assumes reservoir fluids can be described by up to three fluid phases (oil, gas, and water) with physical properties that depend on pressure and composition. Natural gas and injected solvent are allowed to dissolve in both the oil and water phases. A feature unique to IFLO is the integration of a petrophysical model with a flow simulator. The integrated flow model IFLO performs acoustic velocity and impedance calculations. These reservoir geophysical calculations make it possible to track changes in seismic variables as a function of time, which is the basis for 3D time-lapse (4D) seismic analysis. The features of IFLO are outlined below, and discussed in more detail in later appendices.

A.1 Program Overview

IFLO was designed to run on personal computers with Intel Pentium or equivalent processors. This size simulator is well-suited for learning how to use a reservoir simulator, developing an understanding of reservoir management

concepts, and for solving many types of reservoir engineering problems. It is an inexpensive tool for performing studies that call for more sophistication than is provided by analytical solutions, yet do not require the use of full-featured commercial simulators. It provides a combination of multicomponent, pseudomiscible options and reservoir geophysical options that cannot be found elsewhere.

IFLO is a modified version of MASTER, a black oil simulator with multicomponent, pseudomiscible options for modeling carbon dioxide or nitrogen flooding [Ammer, et al., 1991]. MASTER is an improved version of BOAST, an implicit pressure-explicit saturation (IMPES) simulator published by the U.S. Department of Energy in 1982 [Fanchi, et al., 1982]. IFLO includes several enhancements to MASTER using algorithms from earlier versions of BOAST, such as BOAST II [Fanchi, et al., 1987].

A comparison of differences between MASTER and IFLO is given in the following tables. Table A-1 shows that a variety of useful geoscience and reservoir engineering features have been added to IFLO, including the representation of horizontal or deviated wells, improvements for modeling heterogeneous reservoir characteristics, and the calculation of important reservoir geophysical information.

Table A-1
Comparison of Reservoir Model Differences

FEATURE	MASTER	IFLO
Well completions	Vertically contiguous	Flexible
Well controls	Limited	Expanded
Horizontal/Deviated well	Not available	New
Gas production well	Not available	New
Compressional velocity	Not available	New
Shear velocity	Not available	New
Acoustic impedance	Not available	New
Reflection coefficient	Not available	New

Table A-1
Comparison of Reservoir Model Differences

FEATURE	MASTER	IFLO
Modify ϕ, K	Input ϕ, K	Input ϕ, K or multiply by factor
Modify transmissibility	Input transmissibility	Multiply by factor
Modify pore volume	Not available	Multiply by factor
Net thickness	Not available	New
Zero pore volume blocks	Not available	New
Analytic aquifer model	Not available	New

In addition, IFLO includes changes to improve computational performance. Several of the more important changes are listed in the following table.

Table A-2
Comparison of Computational Differences

FEATURE	MASTER	IFLO
Saturation table end points	Set to -0.1 and 1.1	Set to 0.0 and 1.0
Timestepping and reports	Requires counter times timestep size	User enters elapsed times only
Programming language	FORTRAN 77	FORTRAN 90
Dynamic Redimensioning	Not Available	New

IFLO has been tested under a variety of conditions, including: oil and gas reservoir depletion, waterflooding, gas injection into an undersaturated oil reservoir, aquifer influx into a gas reservoir, and carbon dioxide injection. Favorable comparisons with other simulators have been obtained. IFLO is based on a mass conserving, Newton-Raphson technique. IFLO includes a material balance correction that reduces cumulative material balance error to

the magnitude of material balance error associated with a single timestep. Options from earlier versions of BOAST have been added to extend the applicability of IFLO to more complex systems.

IFLO retains the robustness of earlier versions of BOAST while substantially increasing program accuracy. Coding and algorithm enhancements increase program robustness.

A.2 Program Configuration

IFLO is designed to run under Windows 95/98/NT. Dynamic memory management is used to control the size of grids. Memory allocation controls, such as the number of blocks in a given direction or the number of wells in the model, are entered by the user as part of the input data file described in Appendix B.

IFLO must be copied to a folder on your hard drive before running. The following procedure is recommended for a CD drive D and hard drive C running Windows 95/98/NT:

1. Open **Windows Explorer** and select your CD drive.
2. Use a **Windows**-based Unzip program to extract all of the files from the **IFLO** file on the CD to a folder on your hard drive.
3. Run **IFLO** by double clicking on the **IFLO.EXE** file on your hard drive.

A.3 Input Data File - ITEMP.DAT

IFLO reads a file called ITEMP.DAT and outputs to files ITEMP.TSS, ITEMP.MBE, and ITEMP.ROF. The output files are described in Appendix D. You should copy and rename any files you wish to save because IFLO overwrites the ITEMP.* files each time it runs.

The easiest way to prepare a new data file is to edit an old one. This will give you an example of the formats needed for most options. If you start with an old data set, make sure that you check all applicable data entries and make changes where appropriate.

IFLO input data is divided into two parts: initialization data, and recurrent data. Initialization data is described in Appendix B. It includes data that is set at the beginning of the study and is not expected to change during a model run. Such data includes the reservoir description and fluid properties. Recurrent data are described in Appendix C and refers to data that is expected to change during the course of a simulation. It includes well schedules and time step control information.

A.4 Example Input Data Sets

FILE	GRID $II \times JJ \times KK$	MODEL TYPE	REMARKS
EXAM1.DAT	$1 \times 1 \times 1$	Material Balance	Primary depletion of an undersaturated oil reservoir (high GOR)
EXAM2.DAT	$1 \times 1 \times 4$	1D Vertical	Primary depletion of an undersaturated oil reservoir (moderate GOR)
EXAM3.DAT	$20 \times 1 \times 1$	1D Horizontal	Buckley-Leverett waterflood
EXAM4.DAT	$9 \times 9 \times 1$	2D Areal	Primary depletion of an undersaturated oil reservoir (moderate GOR)
EXAM5.DAT	$10 \times 1 \times 4$	2D Cross-section	Multi-layer waterflood of an undersaturated oil reservoir (high GOR)
EXAM6.DAT	$9 \times 9 \times 2$	3D	5-spot waterflood of an undersaturated oil reservoir (high GOR)
EXAM7.DAT	$10 \times 10 \times 3$	3D	Gas injection into undersaturated oil reservoir (high GOR) - Odeh example
EXAM8.DAT	$9 \times 9 \times 2$	3D	Depletion of gas reservoir

FILE	GRID II × JJ × KK	MODEL TYPE	REMARKS
EXAM9.DAT	9 × 9 × 2	3D	Depletion of gas reservoir with aquifer support
EXAM10.DAT	10 × 1 × 2	2D Cross-section	Depletion of gas reservoir with aquifer support

A.4.1 Timestep Summary File – ITEMP.TSS

A one line timestep summary is automatically printed out as a record of the progress of the run. This summary provides you with necessary information for evaluating the stability of the solution as a function of time.

A.4.2 Run Summary And Plot File – ITEMP.PLT

The run summary file contains a concise summary of total field production and injection, and fieldwide aquifer influx. The water-oil ratio WOR and gas-oil ratio GOR are ratios of total producing fluid rates. Consequently these ratios are comparable to observed fieldwide ratios. The output quantities are output as functions of time and timestep number.

A.4.3 Run Output File – ITEMP.ROF

Input data, output summaries, and well information are provided in the run output file. Rates and cumulative production/injection data for each layer of each well are summarized in the well report at times you specify. Field totals are also included.

You may output a variety of arrays whenever desired. These arrays include pressure, saturations, bubble point pressure, cumulative aquifer influx, compressional velocity, acoustic impedance and seismic reflection coefficient. Output arrays may be used as input pressure and saturation distributions for restarting a run.

It is usually unnecessary to print all of the arrays. To avoid excessive output and correspondingly large output files, you should be judicious in deciding which arrays are printed.

A.4.4 Distribution Arrays File – ITEMP.ARR

Columnar array information is provided in the distribution arrays file for a select group of arrays, such as pressure and saturation. The arrays are provided as a function of spatial position relative to a Cartesian coordinate system.

Appendix B

Initialization Data

Initialization data records are read once at the beginning of the simulation. They must be read in the order presented below. Title or heading records are read before each major and many minor sections. These records are designed to make the input data file easier to read and edit.

In many cases, codes are read that will specify the type of input to follow and the number of values that will be read. These codes increase the efficiency and flexibility of entering input data. All input data, with the exception of well names, is entered by free format. Data entered on the same line must be separated by a comma or a space.

Tabular data entered by the user should cover the entire range of values expected to occur during a simulation. The table interpolation algorithms in IFLO will return table endpoint values if the independent variable goes outside the range of the input tabular values. No message will be printed if this occurs.

If an array of input values must be read, the following input order must be followed. Layer 1 ($K = 1$) is read first. The data in each layer are read by rows, starting with row 1 ($J = 1$). Values of the array element are read for the first row starting with column 1 ($I = 1$) and proceeding to the end of the row (column $I = II$). After II values are read, the next row ($J = 2$) of values are

entered. These values must begin on a new line. This data entry procedure is repeated for all rows and, subsequently, for all layers until the complete set of array elements has been entered.

1. **Title** Up to 80 characters; this record will appear as run title.

B.1 Model Dimensions and Geometry

B.1.1 Model Dimensions

1. **Heading** Up to 80 characters.

2. **II, JJ, KK, NWELL, NWCON**

Code	Meaning
II	number of gridblocks in the x direction
JJ	number of gridblocks in the y direction
KK	number of gridblocks in the z direction
NWELL	number of wells
NWELCON	number of connections per well

3. **Heading** Up to 80 characters.

4. **KDX, KDY, KDZ, KDZNET**

KDX Control code for input of x direction grid size.

KDY Control code for input of y direction grid size.

KDZ Control code for input of z direction gross thickness.

KDZNET Control code for input of z direction net thickness.

Code	Value	Meaning
KDX	-1	The x direction grid dimensions are the same for all blocks. Read only one value.
	0	The x direction dimensions are read for each block in the first row ($J = 1$) of layer one ($K = 1$). These values are assigned to all other rows and layers. Read II values.
	1	The x direction dimensions are read for each block in layer one ($K = 1$). These values are assigned to all other layers. Read $II \times JJ$ values.
KDY	-1	The y direction grid dimensions are the same for all blocks. Read only one value.
	0	The y direction dimensions are read for each block in the first column ($I = 1$) of layer one ($K = 1$). These values are assigned to all other columns and layers. Read JJ values.
	1	The y direction dimensions are read for each block in layer one ($K = 1$). These values are assigned to all other layers. Read $II \times JJ$ values.
KDZ	-1	The z direction gross thickness is the same for all blocks. Read only one value.
	0	A constant gross thickness is read for each layer; each layer may have a different value. Read KK values.
	1	The z direction gross thickness is read for each block in the grid. Read $II \times JJ \times KK$ values.
KDZNET	-1	The z direction net thickness is the same for all blocks. Read only one value.
	0	A constant net thickness is read for each layer; each layer may have a different value. Read KK values.
	1	The z direction net thickness is read for each block in the grid. Read $II \times JJ \times KK$ values.

5. DX

DX Gridblock size in x direction (ft).
If KDX = -1, read one constant value.
If KDX = 0, read II values (one for each row).
If KDX = +1, read II × JJ values (one for each K = 1 block).

6. DY

DY Gridblock size in y direction (ft).
If KDY = -1, read one constant value.
If KDY = 0, read JJ values (one for each column).
If KDY = +1, read II × JJ values (one for each K = 1 block).

7. DZ

DZ Gross gridblock thickness in z direction (ft).
If KDZ = -1, read one constant value.
If KDZ = 0, read KK values (one for each layer).
If KDZ = +1, read II × JJ × KK values (one for each block).

8. DZNET

DZNET Net gridblock thickness in z direction (ft).
If KDZ = -1, read one constant value.
If KDZ = 0, read KK values (one for each layer).
If KDZ = +1, read II × JJ × KK values (one for each block).

NOTE: Gridblocks with zero pore volume should be defined by setting DZNET = 0 or porosity = 0. Bulk volume (DX × DY × DZ) should be a nonzero, positive value for every gridblock. The IFLO calculation assumes that all gridblocks have a nonzero pore volume. A block with zero pore volume is treated as a water filled block with a (porosity) × (net to gross ratio) = 0.0001. Transmissibilities for these blocks are set to zero to prevent flow into or out of the block.

B.1.2 Modifications to Grid Dimensions

1. **Heading** Up to 80 characters.
2. **NUMDX, NUMDY, NUMDZ, NUMDZN, IDCODE**
NUMDX Number of regions where x direction length (DX) is changed.
NUMDY Number of regions where y direction length (DY) is changed.
NUMDZ Number of regions where z direction gross thickness (DZ) is changed.
NUMDZN Number of regions where z direction net thickness (DZN) is changed.
IDCODE = 0 means do not print the modified distributions;
= 1 means print the modified distributions.
3. **I1, I2, J1, J2, K1, K2, DX**
Omit this record if NUMDX = 0.
I1 Coordinate of first region block in I direction.
I2 Coordinate of last region block in I direction.
J1 Coordinate of first region block in J direction.
J2 Coordinate of last region block in J direction.
K1 Coordinate of first region block in K direction.
K2 Coordinate of last region block in K direction.
DX New value of x direction grid size for region (ft).
4. **I1, I2, J1, J2, K1, K2, DY**
Omit this record if NUMDY = 0.
I1 Coordinate of first region block in I direction.
I2 Coordinate of last region block in I direction.
J1 Coordinate of first region block in J direction.
J2 Coordinate of last region block in J direction.
K1 Coordinate of first region block in K direction.

K2 Coordinate of last region block in K direction.
DY New value of y direction grid size for region (ft).

NOTE: NUMDY records must be read.

5. **I1, I2, J1, J2, K1, K2, DZ**

Omit this record if NUMDZ = 0.

I1 Coordinate of first region block in I direction.
I2 Coordinate of last region block in I direction.
J1 Coordinate of first region block in J direction.
J2 Coordinate of last region block in J direction.
K1 Coordinate of first region block in K direction.
K2 Coordinate of last region block in K direction.
DZ New value of z direction gross thickness for region (ft).

NOTE: NUMDZ records must be read.

6. **I1, I2, J1, J2, K1, K2, DZNET**

Omit this record if NUMDZN = 0.

I1 Coordinate of first region block in I direction.
I2 Coordinate of last region block in I direction.
J1 Coordinate of first region block in J direction.
J2 Coordinate of last region block in J direction.
K1 Coordinate of first region block in K direction.
K2 Coordinate of last region block in K direction.
DZNET New value of z direction net thickness for region (ft).

NOTE: NUMDZN records must be read.

B.1.3 Depths to Top of Gridblocks

The coordinate system used in IFLO is defined so that values in the z (vertical) direction increase as the layer gets deeper. Negative values will be read as heights above the datum.

220 Integrated Flow Modeling

1. **Heading** Up to 80 characters.

2. **KEL**

KEL Control code for input of depth values.

KEL	Meaning
0	A single constant value is read for the depth to the top of all grid-blocks in layer 1 (horizontal plane). Each layer is contiguous in this option. Depths to the top of gridblocks in layers below layer 1 are calculated by adding the layer thickness to the preceding layer top; thus $\text{Top}(I, J, K + 1) = \text{Top}(I, J, K) + DZ(I, J, K)$
1	A separate depth value must be read for each gridblock in layer 1. Read $II \times JJ$ values. Each layer is contiguous in this option. Depths to the top of gridblocks in layers below layer 1 are calculated by adding the layer thickness to the preceding layer top; thus $\text{Top}(I, J, K + 1) = \text{Top}(I, J, K) + DZ(I, J, K)$
2	A separate depth value is read for each layer. Read KK values. Each layer is horizontal (layer cake) in this option.
3	A separate depth value is read for each gridblock. Read $II \times JJ \times KK$ values.

3. **ELEV**

ELEV Depth to top of gridblock (ft).

If KEL = 0, read one constant value.

If KEL = 1, read $II \times JJ$ values (one for each block in layer 1).

If KEL = 2, read KK values (one for each layer).

If KEL = 3, read $II \times JJ \times KK$ values (one for each block).

B.2 Seismic Velocity Parameters

B.2.1 Moduli and Grain Densities

1. **Heading** Up to 80 characters.

2. KKB, KKG, KMU, KRHO

- KKB Control code for input of the frame bulk modulus (evacuated porous rock).
- KKG Control code for input of the grain bulk modulus (solid matrix material).
- KMU Control code for input of the shear modulus (evacuated porous rock).
- KRHO Control code for input of the grain density (solid matrix material).

Code	Value	Meaning
KKB	-1	Frame bulk moduli are the same for all blocks. Read only one value.
	0	A constant value of frame bulk modulus is read for each layer; each layer may have a different value. Read KK values.
	1	Frame bulk moduli are read for each block. Read II × JJ × KK values.
KKG	-1	Grain bulk moduli are the same for all blocks. Read only one value.
	0	A constant value of grain bulk modulus is read for each layer; each layer may have a different value. Read KK values.
	1	Grain bulk moduli are read for each block. Read II × JJ × KK values.
KMU	-1	Shear moduli are the same for all blocks. Read only one value.
	0	A constant value of shear modulus is read for each layer; each layer may have a different value. Read KK values.
	1	Shear moduli are read for each block. Read II × JJ × KK values.

222 Integrated Flow Modeling

Code	Value	Meaning
KRHO	-1	Grain densities are the same for all blocks. Read only one value.
	0	A constant value of grain density is read for each layer; each layer may have a different value. Read KK values.
	1	Grain densities are read for each block. Read $II \times JJ \times KK$ values.

3. KB

KB Frame bulk modulus (psia).

If KKB = -1, read one constant value.

If KKB = 0, read KK values (one for each layer).

If KKB = +1, read $II \times JJ \times KK$ values (one for each block).

NOTE: In the absence of data, a value of 3×10^6 psia is reasonable.

4. KG

KG Grain bulk modulus (psia).

If KKG = -1, read one constant value.

If KKG = 0, read JJ values (one for each layer).

If KKG = +1, read $II \times JJ$ values (one for each block).

NOTE: In the absence of data, a value of 3×10^6 psia is reasonable.

5. MU

MU Shear modulus (psia).

If KMU = -1, read one constant value.

If KMU = 0, read KK values (one for each layer).

If KMU = +1, read $II \times JJ \times KK$ values (one for each block).

NOTE: In the absence of data, a value of 3×10^6 psia is reasonable.

6. **RHOMA**

RHOMA Grain density (lbf/ft³).

If KRHO = -1, read one constant value.

If KRHO = 0, read KK values (one for each layer).

If KRHO = +1, read II × JJ × KK values (one for each block).

NOTE: In the absence of data, a value of 168 lbf/ft³ (corresponding to 2.7 g/cm³) is reasonable.

B.2.2 Modifications to Moduli and Grain Densities

1. **Heading** Up to 80 characters.

2. **NUMKB, NUMKG, NUMMU, NUMRHO, IDCODE**

NUMKB Number of regions where frame bulk modulus (KB) is changed.

NUMKG Number of regions where grain bulk modulus (KG) is changed.

NUMMU Number of regions where shear modulus (MU) is changed.

NUMRHO Number of regions where grain density (RHO) is changed.

IDCODE = 0 means do not print the modified distributions;
= 1 means print the modified distributions.

3. **I1, I2, J1, J2, K1, K2, KB**

Omit this record if NUMKB = 0.

I1 Coordinate of first region block in I direction.

I2 Coordinate of last region block in I direction.

J1 Coordinate of first region block in J direction.

J2 Coordinate of last region block in J direction.

K1 Coordinate of first region block in K direction.

K2 Coordinate of last region block in K direction.

KB New value of frame bulk modulus (psia).

NOTE: NUMKB records must be read.

4. I1, I2, J1, J2, K1, K2, KG

Omit this record if NUMKG = 0.

I1 Coordinate of first region block in I direction.
I2 Coordinate of last region block in I direction.
J1 Coordinate of first region block in J direction.
J2 Coordinate of last region block in J direction.
K1 Coordinate of first region block in K direction.
K2 Coordinate of last region block in K direction.
KG New value of grain bulk modulus (psia).

NOTE: NUMKG records must be read.

5. I1, I2, J1, J2, K1, K2, MU

Omit this record if NUMMU = 0.

I1 Coordinate of first region block in I direction.
I2 Coordinate of last region block in I direction.
J1 Coordinate of first region block in J direction.
J2 Coordinate of last region block in J direction.
K1 Coordinate of first region block in K direction.
K2 Coordinate of last region block in K direction.
MU New value of shear modulus.

NOTE: NUMMU records must be read.

6. I1, I2, J1, J2, K1, K2, RHO

Omit this record if NUMRHO = 0.

I1 Coordinate of first region block in I direction.
I2 Coordinate of last region block in I direction.
J1 Coordinate of first region block in J direction.

J2	Coordinate of last region block in J direction.
K1	Coordinate of first region block in K direction.
K2	Coordinate of last region block in K direction.
RHO	New value of grain density (lbf/ft ³).

NOTE: NUMRHO records must be read.

B.3 Porosity, Permeability, and Transmissibility Distributions

B.3.1 Porosity and Permeability

1. **Heading** Up to 80 characters.

2. **KPH, KKX, KKY, KKZ**

KPH	Control code for input of porosity.
KKX	Control code for input of x direction permeability.
KKY	Control code for input of y direction permeability.
KKZ	Control code for input of z direction permeability.

Code	Value	Meaning
KPH	-1	The porosity is constant for all gridblocks. Read only one value.
	0	A constant value is read for each layer. Read KK values.
	1	A value is read for each block. Read II × JJ × KK values.
KKX	-1	The x direction permeability is constant for all gridblocks. Read only one value.
	0	A constant value is read for each layer. Read KK values.
	1	A value is read for each block. Read II × JJ × KK values.
KKY	-1	The y direction permeability is constant for all gridblocks. Read only one value.
	0	A constant value is read for each layer. Read KK values.

Code	Value	Meaning
	1	A value is read for each block. Read $II \times JJ \times KK$ values.
KKZ	-1	The z direction permeability is constant for all gridblocks. Read only one value.
	0	A constant value is read for each layer. Read KK values.
	1	A value is read for each block. Read $II \times JJ \times KK$ values.

3. **PHI**

PHI Porosity (fraction).

If KPH = -1, read one constant value.

If KPH = 0, read KK values (one for each layer).

If KPH = +1, read $II \times JJ \times KK$ values (one for each block).

4. **PERMX**

PERMX Permeability in x direction (md).

If KKX = -1, read one constant value.

If KKX = 0, read KK values (one for each layer).

If KKX = +1, read $II \times JJ \times KK$ values (one for each block).

5. **PERMY**

PERMY Permeability in y direction (md).

If KKY = -1, read one constant value.

If KKY = 0, read KK values (one for each layer).

If KKY = +1, read $II \times JJ \times KK$ values (one for each block).

6. **PERMZ**

PERMZ Permeability in z direction (md).

If KKZ = -1, read one constant value.

If KKZ = 0, read KK values (one for each layer).

If KKZ = +1, read $II \times JJ \times KK$ values (one for each block).

B.3.2 Modifications to Porosities and Permeabilities

1. **Heading** Up to 80 characters.
2. **NUMP, NUMKX, NUMKY, NUMKZ, IPCODE**
 - NUMP Number of regions where porosity (PHI) is changed.
 - NUMKX Number of regions where x direction permeability (PERMX) is changed.
 - NUMKY Number of regions where y direction permeability (PERMY) is changed.
 - NUMKZ Number of regions where z direction permeability (PERMZ) is changed.
 - IPCODE = 0 means do not print the modified distributions;
= 1 means print the modified distributions.

3. **I1, I2, J1, J2, K1, K2, VALPHI**

Omit this record if NUMP = 0.

- I1 Coordinate of first region block in I direction.
- I2 Coordinate of last region block in I direction.
- J1 Coordinate of first region block in J direction.
- J2 Coordinate of last region block in J direction.
- K1 Coordinate of first region block in K direction.
- K2 Coordinate of last region block in K direction.

Code	Value	Meaning
NUMP	> 0	New value of porosity (fr).
	< 0	Multiply porosity by VALPHI.

NOTE: |NUMP| records must be read.

4. **I1, I2, J1, J2, K1, K2, VALKX**

Omit this record if NUMKX = 0.

I1	Coordinate of first region block in I direction.
I2	Coordinate of last region block in I direction.
J1	Coordinate of first region block in J direction.
J2	Coordinate of last region block in J direction.
K1	Coordinate of first region block in K direction.
K2	Coordinate of last region block in K direction.

Code	Value	Meaning
NUMKX	> 0	New value of x direction permeability (md).
NUMKX	< 0	Multiply x direction permeability by VALKX.

NOTE: |NUMKX| records must be read.

5. I1, I2, J1, J2, K1, K2, VALKY

Omit this record if NUMKY = 0.

I1	Coordinate of first region block in I direction.
I2	Coordinate of last region block in I direction.
J1	Coordinate of first region block in J direction.
J2	Coordinate of last region block in J direction.
K1	Coordinate of first region block in K direction.
K2	Coordinate of last region block in K direction.

Code	Value	Meaning
NUMKY	> 0	New value of y direction permeability (md).
NUMKY	< 0	Multiply y direction permeability by VALKY.

NOTE: |NUMKY| records must be read.

6. I1, I2, J1, J2, K1, K2, VALKZ

Omit this record if NUMKZ = 0.

I1	Coordinate of first region block in I direction.
I2	Coordinate of last region block in I direction.
J1	Coordinate of first region block in J direction.
J2	Coordinate of last region block in J direction.
K1	Coordinate of first region block in K direction.
K2	Coordinate of last region block in K direction.

Code	Value	Meaning
NUMKZ	> 0	New value of z direction permeability (md).
	< 0	Multiply z direction permeability by VALKZ.

NOTE: |NUMKZ| records must be read.

B.3.3 Modifications to Pore Volume and Transmissibilities

1. **Heading** Up to 80 characters.
2. **NUMPV, NUMTX, NUMTY, NUMTZ, ITCODE**
 - NUMPV Number of regions where pore volume is changed.
 - NUMTX Number of regions where x direction transmissibility (TX) is changed.
 - NUMTY Number of regions where y direction transmissibility (TY) is changed.
 - NUMTZ Number of regions where z direction transmissibility (TZ) is changed.
 - ITCODE = 0 means do not print the modified distributions;
= 1 means print the modified distributions.

NOTE: The conventions for gridblock (I, J, K) transmissibility follow:

TX(I, J, K) refers to flow between blocks I-1 and I,

TY(I, J, K) refers to flow between blocks J-1 and J, and

TZ(I, J, K) refers to flow between blocks K-1 and K.

3. I1, I2, J1, J2, K1, K2, VALPV

Omit this record if NUMPV = 0.

I1	Coordinate of first region block in I direction.
I2	Coordinate of last region block in I direction.
J1	Coordinate of first region block in J direction.
J2	Coordinate of last region block in J direction.
K1	Coordinate of first region block in K direction.
K2	Coordinate of last region block in K direction.
VALPV	Multiplier of pore volume for region.

NOTE: NUMPV records must be read.

4. I1, I2, J1, J2, K1, K2, VALTX

Omit this record if NUMTX = 0.

I1	Coordinate of first region block in I direction.
I2	Coordinate of last region block in I direction.
J1	Coordinate of first region block in J direction.
J2	Coordinate of last region block in J direction.
K1	Coordinate of first region block in K direction.
K2	Coordinate of last region block in K direction.
VALTX	Multiplier of x direction transmissibility for region.

NOTE: NUMTX records must be read.

5. I1, I2, J1, J2, K1, K2, VALTY

Omit this record if NUMTY = 0.

I1	Coordinate of first region block in I direction.
I2	Coordinate of last region block in I direction.
J1	Coordinate of first region block in J direction.
J2	Coordinate of last region block in J direction.
K1	Coordinate of first region block in K direction.
K2	Coordinate of last region block in K direction.
VALTY	Multiplier of y direction transmissibility for region.

NOTE: NUMTY records must be read.

6. **I1, I2, J1, J2, K1, K2, VALTZ**

Omit this record if NUMTZ = 0.

I1	Coordinate of first region block in I direction.
I2	Coordinate of last region block in I direction.
J1	Coordinate of first region block in J direction.
J2	Coordinate of last region block in J direction.
K1	Coordinate of first region block in K direction.
K2	Coordinate of last region block in K direction.
VALTZ	Multiplier of z direction transmissibility for region.

NOTE: NUMTZ records must be read.

B.4 Rock Regions

1. **Heading** Up to 80 characters.

2. **KR3P, NROCK**

KR3P Code specifying desired relative permeability option.

NROCK Number of distinct Rock regions. A separate set of saturation dependent tables must be entered for each Rock region.

Code	Value	Meaning
KR3P	0	Oil relative permeability calculated from the relative permeability data for the two-phase water-oil system.
	1	Oil relative permeability calculated from the relative permeability data for the two-phase gas-oil system.
	2	Three-phase oil relative permeability based on modified Stone equation

3. **Heading** Up to 80 characters.
Omit this record if NROCK = 1.
4. **NUMROK**
Omit this record if NROCK = 1.
NUMROK = 0 Enter Rock region value for each block.
NUMROK > 0 Number of regions where the Rock region default value of 1 is changed.
5. **IVAL**
Omit this record if NROCK = 1 or NUMROK > 0.
IVAL Array of Rock region values. Read II × JJ × KK values.
6. **I1, I2, J1, J2, K1, K2, IVAL**
Omit this record if NROCK = 1 or NUMROK = 0.
I1 Coordinate of first region block in I direction.
I2 Coordinate of last region block in I direction.
J1 Coordinate of first region block in J direction.
J2 Coordinate of last region block in J direction.
K1 Coordinate of first region block in K direction.
K2 Coordinate of last region block in K direction.
IVAL Number of the saturation dependent data set to be assigned to this Rock region and IVAL ≤ NROCK.

NOTE: NUMROK records must be read.

B.5 Relative Permeability and Capillary Pressure Tables

1. **Heading** Up to 80 characters.
2. **SAT1 KROW1 KRW1 PCOW1**
⋮
SATn KROWn KRWN PCOWn

SAT	Water phase saturation (fr). Set SATn = 1.0.
KROW	Oil relative permeability for oil-water system (fr).
KRW	Water relative permeability for oil-water system (fr).
PCOW	Oil-water capillary pressure (psi).

NOTE: There must be table entries for irreducible water saturation (S_{wr}) and residual oil saturation (S_{orw}). Capillary pressure is defined as PCOW = $P_o - P_w$ where P_o and P_w are the oil and water phase pressures respectively.

Repeat records 1 and 2 a total of NROCK times.

3. **Heading** Up to 80 characters.

4. **SAT1 KROG1 KRG1 PCGO1**

:

SATn KROGn KRGn PCGOn

SAT	Gas phase saturation (fr). Set SAT1 = 0.0 and SATn = 1.0.
KROG	Oil relative permeability for oil-water system (fr).
KRG	Gas relative permeability for gas-oil system (fr).
PCGO	Gas-oil capillary pressure (psi).

NOTE: The gas-oil table assumes that an irreducible water saturation (S_{wr}) is present. As a matter of consistency, KROG at SAT1 = 0 must equal KROW at S_{wr} . There must be table entries for residual gas saturation (S_{gr}) and residual oil saturation (S_{org}). Capillary pressure is defined as PCGO = $P_g - P_o$ where P_o and P_g are the oil and gas phase pressures respectively. If solvent is included in the model, gas-oil capillary pressure will only be used at gridblocks that have pressures below the miscibility pressure.

Repeat records 3 and 4 a total of NROCK times.

B.6 Fluid PVT Tables

1. **Heading** Up to 80 characters.

2. **PBO, VOSLP, BOSLP, BWSLP, PMAX**

PBO	Initial reservoir oil bubble point pressure (psia). If no oil or natural gas exist, set PBO = 14.7 psia.
VOSLP	Slope of the oil viscosity versus pressure curve for undersaturated oil, i.e. for pressures above PBO. The slope ($\Delta\mu_o/\Delta P_o$) should be in cp/psia.
BOSLP	Slope of the oil formation volume factor versus pressure curve for undersaturated oil. The slope ($\Delta B_o/\Delta P_o$) should be in RB/STB/psia and should be negative or zero.
BWSLP	Slope of the water formation volume factor versus pressure curve for undersaturated water, i.e. for pressures above PBO. The slope ($\Delta B_w/\Delta P_o$) should be in RB/STB/psia and should be negative or zero.
PMAX	Maximum pressure entry for all PVT tables (psia).

NOTE: VOSLP, BOSLP and BWSLP are used only for undersaturated oil and water. The slope ($\Delta R_{so}/\Delta P_o$) of the solution natural gas-oil ratio versus pressure curve for undersaturated oil is assumed to be zero.

5. **Heading** Up to 80 characters; oil table follows.

6. **P1** **MUO1** **BO1** **RSO1**
 :
PMAX **MUO(PMAX)** **BO(PMAX)** **RSO(PMAX)**
P Pressure (psia). Pressures must be in ascending order from P1 (normally 14.7 psia) to PMAX. The last table entry must be PMAX.
MUO Oil viscosity (cp).
BO Oil formation volume factor (RB/STB).

RSO Solution natural gas-oil ratio (SCF/STB).

NOTE: Oil properties must be entered as saturated data over the entire pressure range. Saturated oil data is required because of the bubble point pressure tracking algorithm.

7. **Heading** Up to 80 characters; water table follows.

8. **P1** **MUW1** **BW1** **RSW1**

:

PMAX **MUW(PMAX)** **BW(PMAX)** **RSW(PMAX)**

P Pressure (psia). Pressures must be in ascending order from P1 (normally 14.7 psia) to PMAX. The last table entry must be PMAX.

MUW Water viscosity (cp).

BW Water formation volume factor (RB/STB).

RSW Solution natural gas-water ratio (SCF/STB). Water properties must be entered as saturated data over the entire pressure range if RSW is nonzero.

NOTE: It is usually assumed in black oil simulations that the solubility of gas in water can be neglected. In this case, set RSW = 0.0 for all pressures. IFLO includes gas solubility in the water phase to account for CO₂ solubility in water, gas production from geopressured aquifers, or any other case where gas solubility in water can be significant.

9. **Heading** Up to 80 characters; gas table follows.

10. **P1** **MUG1** **BG1** **CR1**

:

PMAX **MUG(PMAX)** **BG(PMAX)** **CR(PMAX)**

P	Pressure (psia). Pressures must be in ascending order from P1 (normally 14.7 psia) to PMAX. The last table entry must be PMAX.
MUG	Natural gas viscosity (cp).
BG	Natural gas formation volume factor (RCF/SCF).
CR	Rock compressibility (1/psia).

11. **Heading** Up to 80 characters.
12. **RHOSCO, RHOSCW, RHOSCG**
RHOSCO Stock tank oil density (lbm/cu ft).
RHOSCW Stock tank water density (lbm/cu ft).
RHOSCG Gas density at standard conditions (lbm/cu ft). If no natural gas exists, set RHOSCG = 0.

NOTE: At stock tank conditions (14.7 psia and 60 degrees F for oilfield units) pure water has a density of 62.4 lbm/cu ft and air has a density of 0.0765 lbm/cu ft.

B.7 Miscible Solvent Data

1. **Heading** Up to 80 characters.
2. **NSLUGS, NSREAD**
NSLUGS Number of solvents.
NSREAD Number of solvent PVT tables to be read (up to 4). NSREAD must be equal to or greater than NSLUGS.

NOTE: NSREAD is provided as a convenience. PVT data for one to four solvents may be left in the input data set for an oil-water-natural gas run by setting NSREAD = 1 to 4 and NSLUGS = 0.

If NSREAD = 0, omit the data in the remainder of this section and proceed to Appendix B.8.

3. **Heading** Up to 80 characters.

4. **PBO1, VO1OPE, BO1OPE**

PBO1 Initial base solvent-oil bubble point pressure (psia).

VO1OPE Undersaturated slope of oil viscosity (cp/psi).

BO1OPE Undersaturated slope of oil formation volume factor (RB/STB/psi).

5. **Heading** Up to 80 characters.

6. **PBW1, VW1OPE, BW1OPE**

PBW1 Initial base solvent-water bubble point pressure (psia).

VW1OPE Undersaturated slope of water viscosity (cp/psi).

BW1OPE Undersaturated slope of water formation volume factor (RB/STB/psi).

7. **Heading** Up to 80 characters.

8. **PMISC, FPMISC, SOMIN, REDK, BETA, SORM, VSMISC**

PMISC Miscibility pressure (psia).

FPMISC Fraction of PMISC (fr) for calculating multi-contact miscibility pressure PMCM (psia). PMISC and PMCM are related by $PMCM = FPMISC \times PMISC$.

SOMIN Minimum oil saturation for solid precipitation (fr). SOMIN > 0 only if SORM = 0.

REDK Relative permeability reduction factor for solid precipitation (fr).

BETA Parameter for water blocking function.

SORM Miscible region residual oil saturation (fr). SORM > 0 only if SOMIN = 0.

VSMISC Total solvent volume fraction required to obtain full miscibility (fr).

Code	Value	Meaning
SOMIN	0	No solid precipitation.
	> 0	Allow solid precipitation.
BETA	< 0	No water blocking.
	≥ 0	Water blocking on.

NOTE: If the automatic time step control is on, saturation convergence requires that SOMIN < DSMAX (Appendix B.9).

9. **Heading** Up to 80 characters.

10. **OM1, OM2**

OM1 Mixing parameter ω_1 for natural gas-solvent miscibility.
OM2 Mixing parameter ω_2 for oil-gas-solvent miscibility.

NOTE: Only OM1 is used if the grid block pressure $P < PMCM$. Only OM2 is used if $P > PMISC$. Both OM1 and OM2 are used if P is in the multicontact miscibility pressure range $PMCM < P < PMISC$.

11. **Heading** Up to 80 characters.

12. **RHOSC1, RHOSC2, RHOSC3, RHOSC4**

RHOSC1 Stock tank density of base solvent (lbm/cu ft).
RHOSC2 Stock tank density of solvent 2 (lbm/cu ft).
RHOSC3 Stock tank density of solvent 3 (lbm/cu ft).
RHOSC4 Stock tank density of solvent 4 (lbm/cu ft).

13. **Heading** Up to 80 characters.

14. **Heading** Up to 80 characters.

15.

P1	MUS1	BS1	RSOS1	RSWS1	BO1	MUO1	BW1	MUW1
:	:	:	:	:	:	:	:	:
PMAX	MUS1 @ PMAX	BS1 @ PMAX	RSOS1 @ PMAX	RSWS1 @ PMAX	BO1 @ PMAX	MUO1 @ PMAX	BW1 @ PMAX	MUW1 @ PMAX

P Pressure (psia). Pressures must be in ascending order from P1 (normally 14.7 psia) to PMAX. The last table entry must be PMAX.

MUS1 Viscosity of base solvent (cp).
BS1 Formation volume factor of base solvent (RB/STB).
RSOS1 Solubility of base solvent in oil (SCF/STB).
RSWS1 Solubility of base solvent in water (SCF/STB).
BO1 Formation volume factor of oil with base solvent (RB/STB).
MUO1 Viscosity of oil with base solvent (cp).
BW1 Formation volume factor of water with base solvent (RB/STB).
MUW1 Viscosity of water with base solvent (cp).

NOTE: Base solvent PVT data is required if NSREAD > 0. Base solvent PVT data is used only if NSLUGS > 0. Oil and water properties must be entered as base solvent saturated data over the entire pressure range. Saturated oil and water data are required because of the bubble point pressure tracking algorithm. Oil-base solvent properties should be determined with a dead oil that is fully saturated with base solvent at each pressure.

16. **Heading** Up to 80 characters.

17. **Heading** Up to 80 characters.

240 Integrated Flow Modeling

- | | | | | |
|-----|--------------|--|------------------|--------------------|
| 18. | P1 | MUS2 | BS2 | RSOS2 |
| | : | | | |
| | PMAX | MUS2(PMAX) | BS2(PMAX) | RSOS2(PMAX) |
| | P | Pressure (psia). Pressures must be in ascending order from P1 (normally 14.7 psia) to PMAX. The last table entry must be PMAX. | | |
| | MUS2 | Viscosity of solvent 2 (cp). | | |
| | BS2 | Formation volume factor of solvent 2 (RB/STB). | | |
| | RSOS2 | Solubility of solvent 2 in oil (SCF/STB). | | |
- NOTE:** Solvent 2 PVT data is required if NSREAD > 1. Solvent 2 PVT data is used only if NSLUGS > 1.
19. **Heading** Up to 80 characters.
20. **Heading** Up to 80 characters.
- | | | | | |
|-----|--------------|--|------------------|--------------------|
| 21. | P1 | MUS3 | BS3 | RSOS3 |
| | : | | | |
| | PMAX | MUS3(PMAX) | BS3(PMAX) | RSOS3(PMAX) |
| | P | Pressure (psia). Pressures must be in ascending order from P1 (normally 14.7 psia) to PMAX. The last table entry must be PMAX. | | |
| | MUS3 | Viscosity of solvent 3 (cp). | | |
| | BS3 | Formation volume factor of solvent 3 (RB/STB). | | |
| | RSOS3 | Solubility of solvent 3 in oil (SCF/STB). | | |
- NOTE:** Solvent 3 PVT data is required if NSREAD > 2. Solvent 3 PVT data is used only if NSLUGS > 2.
22. **Heading** Up to 80 characters.
23. **Heading** Up to 80 characters.

24.	P1	MUS4	BS4	RSOS4
	:			
	PMAX	MUS4(PMAX)	BS4(PMAX)	RSOS4(PMAX)
	P	Pressure (psia). Pressures must be in ascending order from P1 (normally 14.7 psia) to PMAX. The last table entry must be PMAX.		
	MUS4	Viscosity of solvent 4 (cp).		
	BS4	Formation volume factor of solvent 4 (RB/STB).		
	RSOS4	Solubility of solvent 4 in oil (SCF/STB).		

NOTE: Solvent 4 PVT data is required if NSREAD > 3. Solvent 4 PVT data is used only if NSLUGS > 3.

25. **Heading** Up to 80 characters.

26. **NOMOB, MOBCTL, SCI**

NOMOB Number of entries in the mobility control table.

MOBCTL Mobility control switch.

SCI Surfactant concentration index. SCI multiplies the mobility reduction values FRCO2 defined below.

Code	Value	Meaning
MOBCTL	0	No mobility control.
	1	Apply mobility control.

27. **Heading** Up to 80 characters.

Omit this record if MOBCTL = 0.

28. **NSC, FRCO2**

Omit this record if MOBCTL = 0.

NSC Normalized surfactant concentration (fr).

FRCO2 Reduction of base solvent mobility (fr).

NOTE: NOMOB records must be read.

B.8 Pressure and Saturation Initialization

1. **Heading** Up to 80 characters.
2. **KPI, KSI**
 - KPI Pressure initialization code.
 - KSI Saturation initialization code.

Code Values		Meaning
KPI	KSI	
0	0	Equilibrium pressure and saturation initialization. Enter pressures and depths at the OWC and GOC. This option assumes no solvent present at initialization. Saturations are calculated from capillary pressures.
1		Specify pressure throughout grid. Read II × JJ × KK values of P.
	1	Specify constant initial oil, water and gas saturations; specify constant initial solvent volume fractions.
	2	Specify variable saturations throughout grid. Read II × JJ × KK values of SO, SW, and solvent volume fractions. IFLO sets SG = 1 – SO – SW internally.
0	3	Gravity segregated oil, water and gas saturations. This option assumes no solvent present at initialization.

NOTE: Option {KPI = 1, KSI = 2} may be used to prepare a restart data file.

3. **WOC, PWOC, GOC, PGOC**

Enter this record if KPI = 0.

WOC Depth to the water-oil contact (ft below datum).

PWOC	Pressure at the water-oil contact (psia).
GOC	Depth to the gas-oil contact (ft below datum).
PGOC	Pressure at the gas-oil contact (psia).

NOTE: Repeat this record a total of NROCK times – one record for each Rock region (Appendix B.4).

4. **PO**

Enter this record if KPI = 1.

PO Oil phase pressure (psia). Read II × JJ × KK values.

5. **SOI, SWI, SGI, VS1I, VS2I, VS3I, VS4I**

Enter this record if KSI = 1.

SOI Initial oil saturation (fr).

SWI Initial water saturation (fr).

SGI Initial gas saturation (fr).

Omit the following values if NSLUGS = 0.

VS1I Initial base solvent volume fraction in the gaseous phase (fr).
Enter this value if NSLUGS ≥ 1.

VS2I Initial solvent 2 volume fraction in the gaseous phase (fr).
Enter this value if NSLUGS ≥ 2.

VS3I Initial solvent 3 volume fraction in the gaseous phase (fr).
Enter this value if NSLUGS ≥ 3.

VS4I Initial solvent 4 volume fraction in the gaseous phase (fr).
Enter this value if NSLUGS ≥ 4.

NOTE: The sum of the saturations must satisfy $SOI + SWI + SGI = 1$ and the sum of the volume fractions must satisfy the constraint $VGG + VS1 + VS2 + VS3 + VS4 = 1.0$ where VGG is the fraction of natural gas in the gaseous phase.

6. SO, SW, VS1, VS2, VS3, VS4

Enter this record if KSI = 2.

SO Oil saturation (fr). Read $II \times JJ \times KK$ values.

SW Water saturation (fr). Read $II \times JJ \times KK$ values.

Omit the following arrays if NSLUGS = 0.

VS1 Base solvent volume fraction in the gaseous phase (fr). Read $II \times JJ \times KK$ values. Enter this array if $NSLUGS \geq 1$.

VS2 Solvent 2 volume fraction in the gaseous phase (fr). Read $II \times JJ \times KK$ values. Enter this array if $NSLUGS \geq 2$.

VS3 Solvent 3 volume fraction in the gaseous phase (fr). Read $II \times JJ \times KK$ values. Enter this array if $NSLUGS \geq 3$.

VS4 Solvent 4 volume fraction in the gaseous phase (fr). Read $II \times JJ \times KK$ values. Enter this array if $NSLUGS \geq 4$.

NOTE: If $NSLUGS > 0$, then the sum of the volume fractions must satisfy the constraint $VGG + VS1 + VS2 + VS3 + VS4 = 1.0$ where VGG is the fraction of natural gas in the gaseous phase.

7. SOI, SGI, SOR

Enter this record if KSI = 3.

SOI Initial oil saturation (fr) for the oil-water zone. Initial water saturation in the oil-water zone is $1 - SOI$.

SGI Initial gas saturation (fr) for the gas-water zone. Initial water saturation in the gas-water zone is $1 - SGI$.

SOR Irreducible oil saturation (fr). If $SOR > 0$, set $S_o = 0$ when $S_o < SOR$. Water and gas saturations are then renormalized.

NOTE: Repeat this record a total of NROCK times – one record for each Rock region (Appendix B.4).

B.9 Run Control Parameters

1. **Heading** Up to 80 characters.
2. **KSW1, KSW2, KSW3**

KSW1	Control code for printing material balance information to the material balance error file ITEMP.MBE.
KSW2	Control code for printing material balance information to the primary output file ITEMP.ROF.
KSW3	Control code for printing the number of iterations required for convergence of the iterative solution techniques (SSOR, LSOR, ORTHOMIN) to the primary output file ITEMP.ROF. If KSW1 = KSW3 =1, the same information is printed to the material balance error file ITEMP.MBE.

NOTE: Material balance information identifies the gridblock with the largest component material balance error, the magnitude of the error, and the elapsed time.

Code Value	Meaning
0	Do not print the information
1	Print the information

3. **Heading** Up to 80 characters.
4. **NMAX, FACT1, FACT2, TMAX, WORMAX, GORMAX, PAMIN, PAMAX**

NMAX	Maximum number of timesteps per simulation run.
FACT1	Factor for increasing timestep size using automatic timestep control. FACT1 = 1.0 for fixed timestep size. A common value for FACT1 is 1.25.

FACT2	Factor for decreasing timestep size using automatic timestep control. FACT2 = 1.0 for fixed timestep size. A common value for FACT2 is 0.5.
TMAX	Maximum elapsed time to be simulated (days); the run will be terminated when the time exceeds TMAX.
WORMAX	Maximum allowed water-oil ratio for a producing oil well (STB/STB).
GORMAX	Maximum allowed gas-oil ratio for a producing oil well (SCF/STB).
PAMIN	Minimum field average pressure (psia).
PAMAX	Maximum field average pressure (psia).

NOTE: The run will be terminated if producing WOR > WORMAX or producing GOR > GORMAX. GORMAX is the total natural gas plus solvent-oil ratio. PAMIN and PAMAX should be within the range of pressures covered by the fluid PVT tables discussed in Appendix B.6. The run will be terminated when the pore volume weighted average reservoir pressure $P_{avg} < PAMIN$ or $P_{avg} > PAMAX$.

5. **Heading** Up to 80 characters.
6. **KSOL, MITR, OMEGA, TOL, NCYCLE, DSMAX, DPMAX, ITMAX, RTOL, NERR**
 - KSOL Solution method code.
 - MITR For KSOL = 1 or 2: maximum number of SOR iterations for convergence with a typical value of 100. For KSOL = 4: maximum number of conjugate gradient iterations for convergence with a typical value of 50.
 - OMEGA For KSOL = 1 or 2: initial SOR acceleration parameter. Initial value of OMEGA should be between 1.0 and 2.0. A typical

	initial value is 1.2. The model will attempt to optimize OMEGA if NCYCLE ≠ 0.
TOL	For KSOL = 1 or 2: maximum acceptable SOR pressure convergence tolerance with a typical value of 0.001 psia. For KSOL = 4: pressure convergence tolerance with a typical value of 0.001 psia to 0.0001 psia.
NCYCLE	For KSOL = 1 or 2: number of SOR iteration cycles for determining when to change (optimize) OMEGA. A typical value is 12. If NCYCLE = 0, the initial value of OMEGA will be used for the entire run.
DSMAX	Maximum saturation change (fraction) allowed per timestep. The timestep size DT will be reduced by FACT2 if the saturation change of any phase or any component in any gridblock exceeds DSMAX and DT > DTMIN (the user-specified minimum timestep size defined in Appendix C.1). If the resulting step size is less than DTMIN, the timestep will be repeated with DT = DTMIN. A typical value of DSMAX is 0.05.
DPMAX	Maximum pressure change (psia) allowed per timestep. The timestep size will be reduced by FACT2 if the pressure change in any gridblock exceeds DPMAX and DT > DTMIN. If the resulting step size is less than DTMIN, the timestep will be repeated with DT = DTMIN. A typical value of DPMAX is 100 psia.
ITMAX	Maximum number of Newton-Raphson iterations per timestep for convergence. A typical value is 5.
RTOL	Maximum allowed residual for Newton-Raphson convergence. A typical value is 0.001. ITMAX overrides RTOL if RTOL is not reached.

NERR Code for controlling material balance error technique. NERR = 1 is recommended.

Code	Value	Meaning
KSOL	1	SSOR: iterative, slice (planar) successive over relaxation method for 2D and 3D models.
	2	LSOR: iterative, line successive over relaxation method for 2D and 3D models.
	3	D4: direct solution method for 2D and moderate sized 3D models.
	4	ORTHOMIN: iterative, preconditioned conjugate gradient algorithm for large 2D and 3D models.
NERR	0	Material balance error control technique is off.
	1	Material balance error control technique is on.

7. **Heading** Up to 80 characters.

8. **WEIGHT**

WEIGHT Fluid property weighting factor.

Code Value	Meaning
0.5	Average properties are used.
1.0	Upstream properties are used.

NOTE: The weighting factor applies to formation volume factor and viscosity of oil, water, natural gas and solvents; the solubility of natural gas and solvents in oil; and the solubility of natural gas and base solvent in water.

B.10 Analytic Aquifer Models

1. **Heading** Up to 80 characters.

2. **IAQOPT**

IAQOPT Analytic aquifer model code.

Code	Value	Meaning
	0	No analytic aquifer model
IAQOPT	1	Steady-state aquifer model (constant aquifer pressure)

NOTE: Different aquifer influx strengths may be specified for a given aquifer.

3. **NAQEN**

Omit this record if IAQOPT ≠ 1.

NAQEN Number of regions containing a steady-state aquifer.

4. **I1, I2, J1, J2, K1, K2, SSAQ**

Omit this record if IAQOPT ≠ 1.

I1 Coordinate of first region block in I direction.

I2 Coordinate of last region block in I direction.

J1 Coordinate of first region block in J direction.

J2 Coordinate of last region block in J direction.

K1 Coordinate of first region block in K direction.

K2 Coordinate of last region block in K direction.

SSAQ Steady-state aquifer strength (SCF/day/psia).

NOTE: NAQEN records must be read.

Appendix C

Recurrent Data

Recurrent data records are read periodically during the course of the simulation run. These data include the location and specification of wells in the model, changes in well completions and field operations over time, a schedule of well rate and/or pressure performance over time, timestep control information for advancing the simulation through time, and controls on the type and frequency of printout information provided by the simulator.

1. **Major Heading** Up to 80 characters.

NOTE: This record signifies the start of the recurrent data section.

C.1 Timestep and Output Control

1. **Heading** Up to 80 characters.
2. **IWREAD, IOMETH, IWLREP, ISUMRY**
IWREAD Controls input of well information.
IOMETH Controls scheduling of well input and array print controls.
IWLREP Controls output of well report.

ISUMRY Controls output of summary report.

Code	Value	Meaning
IWREAD	0	Do not read well information
	1	Read well information
IOMETH	≥ 1	Number of elapsed time values to be read on record 3. The program will print results to output files at these elapsed times and allow you to change well characteristics after the last elapsed time entered during this recurrent data period.
IWLREP	0	Do not print well report
	1	Print well report
ISUMRY	0	Do not print summary report
	1	Print summary report

3. **FTIO**

FTIO Array containing total elapsed times at which output will occur (days). Up to 50 monotonically increasing values may be entered. The first entry must be greater than 0 and each succeeding entry must be greater than any previous entry.

NOTE: When the elapsed time of a run equals an FTIO value, the well and basic summary reports will be printed. Maps will also be printed according to the instructions given below. When the elapsed time of a run equals the last FTIO value, the program will allow the user to enter a new set of recurrent data records (repeat Appendices C.1 and C.2).

4. **IPMAP, ISOMAP, ISWMAP, ISGMAP, IPBMAP, IRSMAP**

IPMAP Control code for printing pressure array.

ISOMAP Control code for printing oil saturation array.

ISWMAP Control code for printing water saturation array.

ISGMAP Control code for printing gas saturation array.

- IPBMAP Control code for printing bubble point pressure array.
IRSMAP Control code for printing natural gas solubility array.

Code Value	Meaning
0	Do not print the array
1	Print the array

5. IS1MAP, IS2MAP, IS3MAP, IS4MAP, IAQMAP

- ISIMAP Control code for printing base solvent volume fraction array.
IS2MAP Control code for printing solvent 2 volume fraction array.
IS3MAP Control code for printing solvent 3 volume fraction array.
IS4MAP Control code for printing solvent 4 volume fraction array.
IAQMAP Control code for printing aquifer influx array (not active).

Code Value	Meaning
0	Do not print the array
1	Print the array

6. IVPMAP, IZMAP, IRCMAP, IVSMAP, IVRMAP,

- IVPMAP Control code for printing seismic compressional velocity (V_p) array.
IZMAP Control code for printing seismic acoustic impedance array.
IRCMAP Control code for printing seismic reflection coefficient array.
IVSMAP Control code for printing seismic shear velocity (V_s) array.
IVRMAP Control code for printing seismic velocity ratio V_p/V_s array.

Code Value	Meaning
0	Do not print the array
1	Print the array

7. DT, DTMIN, DTMAX

DT Starting timestep size (days).

DTMIN Minimum timestep size (days). A typical value is 1 day.

DTMAX Maximum timestep size (days). A typical value is 30 days.

C.2 Well Information

Omit this section if IWREAD = 0.

1. **Heading** Up to 80 characters.

2. **NWELLN, NWELLO, KSIS**

NWELLN Number of new wells for which complete well information is entered.

NWELLO Number of previously defined wells for which new rates and/or rate controls are entered.

KSIS Control code for surfactant-water injection.

Code	Value	Meaning
NWELLN	0	Do not read new well information
	≥ 1	Read new well information
NWELLO	0	Do not change data for previously defined wells
	≥ 1	Change data for previously defined wells
KSIS	0	Do not inject surfactant
	2, -2, or -12	Inject surfactant in the water phase as a gas phase mobility control agent

3. **Heading** Up to 80 characters.

Omit this record if NWELLN = 0.

4. **WELLID**

Omit this record if NWELLN = 0.

WELLID Well name with up to five characters.

5. IDWELL, KONECT, KWCNTL

Omit this record if NWELLN = 0.

IDWELL Well identification number. Each well should have a unique IDWELL number. If two or more wells have the same IDWELL number, the characteristics of the last well entered will be used.

KONECT Total number of gridblocks connected to well IDWELL.

KWCNTL Control code for well limits applied to well IDWELL.

Code	Value	Meaning
KWCNTL	0	Do not read well rate constraints and workover
KWCNTL	1	Read well rate constraints and workover

6. I, J, K, PID, PWF

Omit this record if NWELLN = 0.

I x coordinate of gridblock containing well.

J y coordinate of gridblock containing well.

K z coordinate of gridblock containing well.

PID Layer flow index for gridblock.

PWF Flowing bottomhole pressure for block (psia).

NOTE: KONECT records must be read.

Deviated (slanted) and horizontal wells may be represented by calculating an appropriate PID and specifying gridblock locations that model the expected well trajectory. For example, a horizontal well that is aligned in the x direction will have constant J and K indices, and index I will vary if there is more than one connection.

To shut in a connection, set that connection PID to 0. To shut in a well, set all of its connection PID values to zero.

7. KIP, QO, QW, QG, QT, QS

Omit this record if NWELLN = 0.

KIP	Code for specifying well operating characteristics.
QO	Oil rate (STB/D).
QW	Water rate (STB/D).
QG	Natural gas rate (MSCF/D).
QT	Total fluid voidage rate (RB/D). QT includes oil, water, natural gas, and solvent.
QS	Solvent rate (MSCF/D).

NOTE: Sign conventions for rates: negative rates indicate fluid injection; and positive rates indicate fluid production. To impose a maximum target rate on an explicit pressure controlled well, set KWCNTL = 1 and set the primary phase rate (QO, QW, QG, or QT) to the maximum target rate.

8. **WQMAX, WQMIN, WWOR, WGOR**

Omit this record if NWELLN = 0 or KWCNTL = 0.

WQMAX	Maximum allowed rate for primary phase (QO, QW, QG, or QT).
WQMIN	Minimum allowed rate for primary phase (QO, QW, QG, or QT).
WWOR	Maximum allowed WOR (STB/STB); shut worst offending connection. Set WWOR = 0 to ignore.
WGOR	Maximum allowed GOR (SCF/STB); shut worst offending connection. Set WGOR = 0 to ignore.

NOTE: Rates are expressed in the same units as the rates in Record 7. WOR and GOR constraints apply to production wells only. If a maximum target rate is set in Record 7 for an explicit pressure controlled well, the value of WQMAX will take precedence.

Records 4 through 8 should be repeated NWELLN times.

9. **Heading** Up to 80 characters.

Omit this record if NWELLO = 0.

256 Integrated Flow Modeling

10. WELLID

Omit this record if NWELLO = 0.

WELLID Well name with up to five characters.

11. IDWELL, KONECT, KWCNTL

Omit this record if NWELLO = 0.

IDWELL Well identification number.

KONECT Total number of gridblocks connected to well IDWELL.

KWCNTL Control code for well limits applied to well IDWELL.

12. I, J, K, PID, PWF

Omit this record if NWELLO = 0.

I x coordinate of gridblock containing well.

J y coordinate of gridblock containing well.

K z coordinate of gridblock containing well.

PID Layer flow index for gridblock.

PWF Flowing bottomhole pressure for block (psia).

NOTE: KONECT records must be read.

13. KIP, QO, QW, QG, QT, QS

Omit this record if NWELLO = 0.

KIP Code for specifying well operating characteristics.

QO Oil rate (STB/D).

QW Water rate (STB/D).

QG Natural gas rate (MSCF/D).

QT Total fluid voidage rate (RB/D).

QS Solvent rate (MSCF/D).

NOTE: Sign conventions for rates: negative rates indicate fluid injection; and positive rates indicate fluid production. To impose a maximum target rate on an explicit pressure controlled well, set KWCNTL = 1 and set the primary phase rate (QO, QW, QG, or QT) to the maximum target rate.

14. WQMAX, WQMIN, WWOR, WGOR

Omit this record if NWELLO = 0 or KWCNTL = 0.

- WQMAX Maximum allowed rate for primary phase (QO, QW, QG, or QT).
WQMIN Minimum allowed rate for primary phase (QO, QW, QG, or QT).
WWOR Maximum allowed WOR (STB/STB); shut worst offending connection. Set WWOR = 0 to ignore.
WGOR Maximum allowed GOR (SCF/STB); shut worst offending connection. Set WGOR = 0 to ignore.

NOTE: Rates are expressed in the same units as the rates in Record 13. WOR and GOR constraints apply to production wells only. If a maximum target rate is set in Record 13 for an explicit pressure controlled well, the value of WQMAX will take precedence.

Records 9 through 14 should be repeated NWELLO times.

Table C-1. Options for Controlling Production Wells

Primary Phase	Well Control	KIP	Non-Zero Rates	Well Controls?
Oil	Rate	1	$Q_O > 0$	Yes
	Explicit P	-1	$Q_O > 0$	Yes
	Implicit P	-11		No
Gas	Rate	1	$Q_G > 0$	Yes
	Explicit P	-1	$Q_G > 0$	Yes
	Implicit P			No
Water	Rate	1	$Q_W > 0$	Yes
	Explicit P	-1	$Q_W > 0$	Yes
	Implicit P			No
Total OWG	Rate	1	$Q_T > 0$	Yes
	Explicit P	-1	$Q_T > 0$	Yes
	Implicit P			No

Table C-2. Options for Controlling Injection Wells

Primary Phase	Well Control	KIP	Non-Zero Rates	Well Controls?
Water	Rate	2	QW < 0	Yes
	Explicit P	-2	QW < 0	Yes
	Implicit P	-12		No
Gas	Rate	3	QG < 0	Yes
	Explicit P	-3	QG < 0	Yes
	Implicit P	-13		No
Base Solvent (Solvent 1)	Rate	100	QS < 0	No
	Explicit P	-4		No
	Implicit P	-14		No
Solvent 2	Rate	200	QS < 0	No
	Explicit P	-5		No
	Implicit P	-15		No
Solvent 3	Rate	300	QS < 0	No
	Explicit P	-6		No
	Implicit P	-16		No
Solvent 4	Rate	400	QS < 0	No
	Explicit P	-7		No
	Implicit P	-17		No

Appendix D

Program Supplement

Several supplementary topics are discussed in this Appendix. Topical details are specific to the program IFLO.

D.1 Initialization Options

Options for initializing pressure and saturation distributions in the model are described below.

Equilibrium Initialization

Consider a gridblock that may have a gas-oil contact and a water-oil contact as in Figure D-1.

The initial oil phase pressure assigned to the gridblock in Figure D-1 is determined by PWOC, PGOC and the depth of the node (midpoint) relative to the respective contact elevations. The equilibrium algorithm.

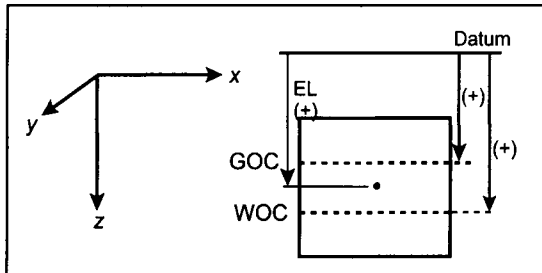


Figure D-1. Depths for initialization contact elevations.

initialization algorithm described in detail in Ammer, et al. [1991]. We follow their presentation here.

The pressure at the gas-oil contact GOC is PGOC. Similarly, PWOC is the pressure at the water-oil contact WOC. The oil density RO_{WOC} and water density RW_{WOC} at WOC are calculated using the pressure PWOC. The water-oil capillary pressure PCOW is calculated for the gridblock at the midpoint elevation EL using the densities at WOC, thus:

$$PCOW = \frac{1}{144} (RW_{WOC} - RO_{WOC}) \cdot (WOC - EL)$$

The initial water saturation SWI for the gridblock is calculated at the midpoint elevation using PCOW and the following algorithm:

- a. If PCOW ≥ PCOW at irreducible water saturation S_{wr}, set SWI = S_{wr}.
- b. If PCOW ≤ PCOW at water saturation S_w = 1, set SWI = 1.
- c. If PCOW at S_w = 1 < PCOW < PCOW at S_{wr}, then interpolate the value of SWI from the user-input water-oil capillary pressure curve.

A similar calculation is performed to determine initial oil phase pressure at the GOC using gas and oil densities. The gas density RG_{GOC} and oil density RO_{GOC} at GOC are calculated using the pressure PGOC. The gas-oil capillary pressure PCGO is calculated for the gridblock at the midpoint elevation EL using the densities at GOC, thus:

$$PCGO = \frac{1}{144} (RO_{GOC} - RG_{GOC}) \cdot (GOC - EL)$$

The initial gas and oil saturations SGI and SOI for the gridblock are calculated at the midpoint elevation using PCGO, the previous calculation of SWI, and the following algorithm:

- a. If PCGO ≤ PCGO at total liquid saturation S_L = 1, set SGI = 0.
- b. If PCGO ≥ PCGO at S_L = S_{wr}, set SGI = 1 - SWI.
- c. If PCGO at S_L = 1 < PCGO < PCGO at S_L = S_{wr}, then interpolate the value of SGI from the user-input water-oil capillary pressure curve.

262 Integrated Flow Modeling

Oil saturation is obtained from the constraint $S_o + S_w + S_g = 1$. The above algorithm should be reasonable for systems with initial transition zones that are small relative to the total thickness of the formation.

The initial oil phase pressure P is calculated using the saturations determined above to define the appropriate pressure gradient. The algorithm for calculating P is the following:

Case 1: If SWI = 1, then

$$P = PW_{WOC} + \frac{1}{144}(RW_{WOC}) \cdot (EL - WOC) + PC_{WOW}(S_w = 1)$$

Case 2: If SOI > 0, then

$$P = PW_{WOC} - \frac{1}{144}(RO_{WOC}) \cdot (WOC - EL)$$

Case 3: If SGI > 0 and SOI = 0, then

$$\begin{aligned} P = PW_{WOC} + \frac{1}{144}(RO_{WOC}) \cdot (EL - WOC) \\ + \frac{1}{144}(RO_{GOC}) \cdot (GOC - EL) \\ + \frac{1}{144}(RG_{GOC}) \cdot (EL - GOC) - PC_{GO}(S_g = 1) \end{aligned}$$

A natural gas-water system can be initialized by setting PWOC = PGOC and WOC = GOC + ϵ , where ϵ is a small incremental displacement (such as 1 ft).

The oil-water transition zone thickness is given by

$$H_{owTZ} = \frac{PCWO(SW = S_{wr}) - PCWO(SW = 1)}{|\gamma_w - \gamma_o|}$$

where γ_o and γ_w are the oil and water gradients in psia/ft. A similar calculation is performed to determine the gas-oil transition zone thickness.

Gravity Segregated Saturation Initialization

A simple model of a gravity segregated saturation distribution is calculated when KSI = 2. The algorithm assumes no solvent exists in the reservoir at the beginning of the run. For depths increasing downward, we calculate elevations and thicknesses using the geometry shown in Figure D-1 as follows:

$$\text{Block BOT} = \text{EL} + 0.5 * \text{DZ}$$

$$\text{Block THICK} = \text{DZ}$$

$$\text{Block TOP} = \text{BOT} - \text{THICK}$$

Water zone thickness:

$$\text{WTHICK} = \text{BOT} - \text{WOC}$$

Gas zone thickness:

$$\text{GTHICK} = \text{GOC} - \text{TOP}$$

The user must specify the initial oil saturation (SOI) for an oil-water system and the initial gas saturation (SGI) for a water-gas system. Given the initial saturations SOI and SGI, the algorithm in Table D-1 is applied [Fanchi, 1986]. Water saturation is calculated from the saturation constraint $S_w = 1 - S_o - S_g$ in all cases. Cases 2 through 4 require the user to enter residual oil saturation S_{or} .

Table D-1
Algorithm for Gravity Segregated Saturation Initialization

Case	GOC _____	$S_g = 0$	
1	TOP _____	$S_o = \text{SOI}$	
	BOT _____	$S_w = 1 - \text{SOI}$	
	WOC _____		

Table D-1
Algorithm for Gravity Segregated Saturation Initialization

Case 2	TOP _____ } f_g GOC _____ } WOC _____ } f_w BOT _____ }	$f_g = \frac{GTHICK}{THICK}$ $f_w = \frac{WTHICK}{THICK}$ $S_g = f_g * SGI$ $S_o = (1 - f_g - f_w) * SOI$ $S_w = 1 - S_o - S_g$	If $S_o < S_{or}$, then $S_o = 0$ $S_g = \frac{f_g * SGI}{(f_g + f_w)}$ $S_w = 1 - S_g$
Case 3	TOP _____ GOC _____ BOT _____ } f WOC _____	$f = 1 - \frac{GTHICK}{THICK}$ $S_o = 1 - SOI * f$ $S_g = (1 - f) * SGI$ $S_w = 1 - S_o - S_g$	If $S_o < S_{or}$, then $S_o = 0$ $S_w = 1 - SGI$ $S_g = SGI$
Case 4	GOC _____ TOP _____ } f WOC _____ BOT _____	$f = 1 - \frac{WTHICK}{THICK}$ $S_g = 0$ $S_w = 1 - SOI * f$ $S_o = SOI * f$	If $S_o < S_{or}$, then $S_o = 0$ $S_w = 1$
Case 5	TOP _____ BOT _____ GOC _____ WOC _____	$S_o = 0$ $S_w = 1 - SGI$ $S_g = SGI$	
Case 6	GOC _____ WOC _____ TOP _____ BOT _____	$S_o = S_g = 0$ $S_w = 1$	

Solvent Initialization

If the IFLO user plans to include solvent in the model, then NSLUGS > 0. In this case, the equilibrium initialization option and the gravity segregation option will assume that none of the solvents are initially present in the reservoir. The presence of solvents in the reservoir at the start of a run is handled in IFLO by the selection of a nonequilibrium initialization option.

Run control features are best learned by experience with the simulator, which has been an objective of the exercises presented throughout the text.

D.2 Run Control Features

This section describes some of the run control features in IFLO that allow the user to monitor and control the performance of the simulator during a run.

Material Balance Error

Material balance is one measure of the numerical stability and accuracy of a simulator. Two types of material balance errors may be considered: local and global. Local material balance error is the error in the material balance calculation for each gridblock over a timestep. The sum of all local material balance errors gives the global material balance error.

The global material balance in IFLO at time t is given by

$$\text{Global Material Balance} = \frac{\text{FIP}}{\text{OFIP} - \text{Prod} + \text{Inj}} \quad (\text{D.1})$$

where

FIP Fluid in place at time t

OFIP Original fluid in place

Prod Cumulative fluid produced at time t

Inj Cumulative fluid injected at time t

Global material balance error reported by IFLO is calculated using the formula

$$\% \text{ Error} = \left\{ \frac{\text{FIP}}{\text{OFIP} - \text{Prod} + \text{Inj}} - 1 \right\} \times 100\% \quad (\text{D.2})$$

Material balance can be a sensitive indicator of error. Material balance error is greatest in IFLO when a gridblock undergoes a phase transition, for example, when a gridblock passes from single phase oil to two-phase oil and gas during a timestep. Blocks undergoing a phase transition generally require more iterations to reduce the associated residual.

Material balance errors can be corrected by adding or subtracting enough fluid to reestablish an exact material balance [Nolen and Berry, 1973; Spillette, et al., 1986]. This material balance correction technique is equivalent to adding a source/sink term to the mass conservation equations for every gridblock. These terms are included in the IFLO formulation [Ammer, et al., 1991]. The magnitude of the error can be estimated by turning off the correction using the control code NERR (Section B.9) and rerunning the model.

A precise solution is achieved when both local and global material balance error equal zero. The solution may not be accurate, however, if the model is incorrect. Nevertheless, the simulation study should strive to minimize both local and global material balance errors.

Automatic Timestep Control

The IFLO user has the option of specifying a constant timestep, or an initial timestep which the simulator can then modify within bounds imposed by the user. The ability to automatically change the timestep size is referred to as automatic timestep control (ATSC). ATSC lets the model take large timesteps when changes occur slowly in the model, and small timesteps when changes occur rapidly.

ATSC is activated when the user-specified factors FACT1 and FACT2 in Section B.9 are not equal to 1, and the user-specified timestep controls DT, DTMIN and DTMAX in Section B.9 are not all equal. The program finds the maximum saturation (DSMC) and pressure (DPMC) changes which occurred in a gridblock over the timestep. When the changes DSMC and DPMC are less than user-specified maximum allowable changes in saturation (DSMAX) and

pressure (DPMAX), the timestep size DT will be multiplied by FACT1 to increase the timestep size for the next timestep. DT will not be allowed to exceed DTMAX.

By contrast, if either DSMC > DSMAX or DPMC > DPMAX, the timestep size DT will be multiplied by FACT2 to decrease the timestep size for the next timestep. DT will not be allowed to be less than DTMIN.

A timestep is repeated only if the following conditions apply:

- DSMAX or DPMAX is exceeded,
- DT > DTMIN, and
- FACT2 < 1.0.

Notice that timesteps are not repeated if DT = DTMIN or FACT2 = 1.

Matrix Solvers

The finite difference form of the pressure equation leads to a system of linear equations for the $I \cdot J \cdot K$ unknowns δP . The system of equations may be written as

$$\begin{aligned} a_{1,1}\delta P_1 + a_{1,2}\delta P_2 + \dots + a_{1,N}\delta P_N &= b_1 \\ a_{2,1}\delta P_1 + a_{2,2}\delta P_2 + \dots + a_{2,N}\delta P_N &= b_2 \\ &\vdots \\ a_{N,1}\delta P_1 + a_{N,2}\delta P_2 + \dots + a_{N,N}\delta P_N &= b_N \end{aligned} \quad (\text{D.3})$$

where the total number of equations N is equal to the total number of blocks, thus $N = I \cdot J \cdot K$, and the time level superscripts are suppressed. This set of equations may be expressed in a more compact form using matrix notation. The resulting matrix equation is

$$\underline{\underline{A}} \underline{\delta P} = \underline{B} \quad (\text{D.4})$$

where the coefficient matrix $\underline{\underline{A}}$ and the column vectors $\underline{\delta P}$, \underline{B} are

$$\underline{\underline{A}} = \begin{bmatrix} a_{1,1} & a_{1,2} & \cdots & a_{1,N} \\ a_{2,1} & a_{2,2} & \cdots & a_{2,N} \\ \vdots & & & \vdots \\ a_{N,1} & a_{N,2} & \cdots & a_{N,N} \end{bmatrix}, \underline{\delta P} = \begin{bmatrix} \delta P_1 \\ \delta P_2 \\ \vdots \\ \delta P_N \end{bmatrix}, \underline{B} = \begin{bmatrix} b_1 \\ b_2 \\ \vdots \\ b_N \end{bmatrix} \quad (\text{D.5})$$

It is standard practice to present the user with a choice of several different techniques for solving systems of equations, since the efficiency of any one technique is highly problem-dependent and *a priori* it is usually difficult to tell which technique will work best for any particular problem.

Several options are available for solving the matrix equations generated by the finite difference formulation in IFLO. These include iterative matrix solvers and direct matrix solvers. In general, direct matrix solvers like D4 [Price and Coats, 1973] provide a more reliable means of solving a matrix equation, but they require more computer storage and work. Computer work refers to the number of multiplications and divisions that must be performed.

Iterative solvers like LSOR [Young, 1971] and ORTHOMIN [Vinsome, 1976] require less computer storage and work, but are not as robust as direct matrix solvers. Iterative solvers are more likely to encounter a problem in which the solution to the matrix equation does not converge. On the other hand, iterative solvers may be the only techniques available for solving large model problems.

As a rule, direct matrix solvers are useful for relatively small problems, and iterative matrix solvers are more useful for large problems. It is easy to try different matrix solvers in IFLO, so the user may wish to experiment with the matrix solver. This is probably the best way to determine which solver will work best for a particular application.

D.3 Output Options

You are given the option at the start of an IFLO run to direct output to either the screen or to a set of files. It is often worthwhile to send output to the screen when first building and debugging a data set. IFLO will abort at the point in the data set where it encounters improperly entered data. For evaluating run results, it is preferable to send output to files. In this case, a one line timestep summary is sent to the screen each timestep so that you can monitor the progress of a run. All output files are in ASCII format.

A run may be aborted by typing <Ctrl> C. You may then choose to terminate the job.

Initialization Data

IFLO outputs the following initialization data in the text Run Output File called ITEMP.ROF:

- ◆ Gridblock sizes
- ◆ Node midpoint elevations
- ◆ Porosity distributions
- ◆ Permeability distributions
- ◆ Rock and PVT region distributions
- ◆ Relative permeability and capillary pressure tables
- ◆ PVT tables
- ◆ Slopes calculated from PVT data
- ◆ Timestep control parameters
- ◆ Analytic aquifer model selection
- ◆ Initial fluid volumes-in-place
- ◆ Initial pressure and saturation arrays
- ◆ Initial seismic velocities array
- ◆ Initial acoustic impedance array
- ◆ Initial well information

Other output can be obtained at your request. For example, if a modification option is invoked, you may print out the altered array. It is worthwhile to do this as a check on the input changes, but it will also increase the size of the run output file.

Recurrent Data

All output files are text files so that they may be read by a variety of commercially available spreadsheets. IFLO output may then be manipulated using spreadsheet options. This is especially useful for making plots or displaying array data. Different output files are defined so that simulator output file sizes are more manageable. The output files are designed to contain information that is logically connected, e.g. well data in one file, reservoir property distributions in another file. The different output files are described below.

Timestep Summary File – ITEMP.TSS

A one line timestep summary is automatically printed out as a record of the progress of the run. This summary provides you with necessary information for evaluating the stability of the solution as a function of time. Significant oscillations in GOR or WOR, or large material balance errors, are indicative of simulation problems and should be corrected. A smaller timestep through the period with computational difficulties is often sufficient to correct IMPES instabilities.

Run Summary And Plot File – ITEMP.PLT

The run summary file contains a concise summary of total field production and injection, and fieldwide aquifer influx. The WOR and GOR are ratios of total producing fluid rates. Consequently these ratios are comparable to observed fieldwide ratios.

The output quantities include: cumulative production of oil, water and gas; cumulative injection of water and gas; pore volume weighted average pressure; aquifer influx rate and cumulative aquifer influx; and fieldwide WOR and GOR values. These quantities are output as functions of time and timestep number.

Well Report File – ITEMP.WEL

Rates and cumulative production/injection data for each layer of each well are summarized in the well report at times you specify. Field totals are also included.

Distribution Arrays File – ITEMP.ROF

You may output the following arrays whenever desired: pressure, phase saturations, bubble point pressure, cumulative aquifer influx, compressional velocity, acoustic impedance and seismic reflection coefficient. Output arrays may be used as input pressure and saturation distributions for restarting a run.

It is usually unnecessary to print all of the arrays. To avoid excessive output and correspondingly large output files, you should be judicious in deciding which arrays are printed.

This Page Intentionally Left Blank

References

- Ammer, J.R., A.C. Brummert, and W.N. Sams (1991): "Miscible Applied Simulation Techniques for Energy Recovery – Version 2.0," Report DOE/BC-91/2/SP, U.S. Department of Energy, Morgantown Energy Technology Center, WV.
- Amyx, J.W., D.M. Bass, and R.L. Whiting (1960); **Petroleum Reservoir Engineering**, New York: McGraw-Hill.
- Anderson, R.N. (1995): "Method Described for Using 4D Seismic to Track Reservoir Fluid Movement," *Oil & Gas Journal*, pp. 70-74, April 3.
- Babu, D.K. and A.S. Odeh (1989): "Productivity of a Horizontal Well," *Society of Petroleum Engineers Journal*, pp. 417-421, Nov.
- Bear, J. (1972): **Dynamics of Fluids in Porous Media**, New York: Elsevier.
- Bernard, G. B., L.W. Holm, and C. F. Harvey (1980): "Use of Surfactant to Reduce CO₂ Mobility in Oil Displacement," *Society of Petroleum Engineers Journal*, pp. 281-292.
- Biot, M.A. (1956): "Theory of Propagation of Elastic Waves in a Fluid-Saturated Porous Solid, I. Low Frequency Range," *Journal of the Acoustical Society of America* **28**, pp. 168-179; and "II. Higher Frequency Range," *ibid.*, pp. 179 ff.

- Burger, J.M. (1948): "A Mathematical Model Illustrating the Theory of Turbulence," *Advances in Applied Mechanics* 1, pp. 171-199.
- Carter, R.D. and G.W. Tracy (1960) "An Improved Method for Calculating Water Influx," *Transactions of the AIME*, Volume 219, pp. 415-417.
- Castagna, J.P., M.L. Batzle and Eastwood (1985): "Relationships Between Compressional Wave and Shear Wave Velocities in Clastic Silicate Rocks," *Geophysics* 50, 571-581.
- Chase, C. A., Jr. and M. R. Todd (1984): "Numerical Simulation of CO₂ Flood Performance," *Society of Petroleum Engineers Journal*, pp. 597-604.
- Christie, M.A. and D.J. Bond (1987): "Detailed Simulation of Unstable Processes in Miscible Flooding," *SPE Reservoir Engineering Journal*, pp. 514-522.
- Collins, R.E. (1961): **Flow of Fluids Through Porous Materials**, Tulsa, OK: Petroleum Publishing-Reinhold.
- Collins, R.E. (1985): "Characterization of Heterogeneous Reservoirs," Research & Engineering Consultants, and private communication.
- Craig, F.F. (1971): **The Reservoir Engineering Aspects of Waterflooding**, SPE Monograph Series, Richardson, TX: Society of Petroleum Engineers.
- Crichlow, H. B. (1977): **Modern Reservoir Engineering – A Simulation Approach**, Englewood Cliffs, NJ: Prentice Hall.
- Dake, L.P. (1978): **Fundamentals of Reservoir Engineering**, Amsterdam: Elsevier.
- Dietrich, J. K. and P. L. Bondor (1976): "Three-Phase Oil Relative Permeability Models," SPE Paper 6044, *Proceedings of 51st Fall Technical Conference and Exhibition of Society of Petroleum Engineers and AIME*, New Orleans, LA, Oct. 3-6.
- van Everdingen, A.F. and W. Hurst (1949): "The Application of the Laplace Transformation to Flow Problems in Reservoirs," *Transactions of the AIME*, Volume 186, pp. 305-324.

- Fancher, G.H. and J.A. Lewis (1933): "Flow of Simple Fluids Through Porous Materials," *Ind. Eng. Chem.*, Vol. 25, pp. 1139-1147.
- Fanchi, J.R., K.J. Harpole, and S.W. Bujnowski (1982): "BOAST: A Three-Dimensional, Three-Phase Black Oil Applied Simulation Tool", 2 Volumes, U.S. Department of Energy, Bartlesville Energy Technology Center, OK.
- Fanchi, J.R. (1983): "Multidimensional Numerical Dispersion," *Society of Petroleum Engineering Journal*, pp. 143-151.
- Fanchi, J.R. (1986): "BOAST-DRC: Black Oil and Condensate Reservoir Simulation on an IBM-PC," Paper SPE 15297, *Proceedings from Symposium on Petroleum Industry Applications of Microcomputers of SPE*, Silver Creek, CO, June 18-20.
- Fanchi, J.R., J.E. Kennedy, and D.L. Dauben (1987): "BOAST II: A Three-Dimensional, Three-Phase Black Oil Applied Simulation Tool", U.S. Department of Energy, Bartlesville Energy Technology Center, OK.
- Fanchi, J.R. (1990): "Calculation of Parachors for Compositional Simulation: An Update," *SPE Reservoir Engineering*, pp. 433-436.
- Fanchi, J. R.(2000): **Math Refresher for Scientists and Engineers**, 2nd edition, New York: Wiley.
- Fanchi, J.R. (2000): **Principles of Applied Reservoir Simulation**, 2nd edition, Houston: Gulf Publishing.
- Fanchi, J.R. (1999): "Flow models time 4-D seismic surveys," *Oil & Gas Journal*, pp. 46-51 (15 March).
- Fanchi, J.R and M.L. Batzle (2000): "Petrophysical Data for Integrated Flow Modeling," *Journal of Petroleum Science and Engineering*, pp.1-8.
- Fanchi, J.R., T.A. Pagano, and T.L. Davis (1999): "State of the art of 4-D seismic monitoring," *Oil & Gas Journal*, pp. 38-43 (31 May).
- Fayers, J.F. (1988): "An Approximate Model with Physically Interpretable Parameters for Representing Miscible Viscous Fingers," *SPE Reservoir Engineering*, pp. 551-558.
- Fetkovitch (1971): *Journal of Petroleum Technology* (July), pp. 814-828

- Gassmann, F. (1951): "Elastic Waves Through a Packing of Spheres," *Geophysics*, Volume 16, 673-685.
- Geertsma, J. and D.C. Smit (1961): "Some Aspects of Elastic Wave Propagation in Fluid-Saturated Porous solids, *Geophysics*, Vol. 26, pp. 169-181.
- Govier, G.W. Editor (1978): **Theory and Practice of the Testing of Gas Wells**, Calgary: Energy Resources Conservation Board.
- Green, D.W. and G.P. Willhite (1998): **Enhanced Oil Recovery**, Richardson, TX: Society of Petroleum Engineers.
- Grigg, R.B. and D.S. Schechter (1998): "Improved Efficiency of Miscible CO₂ Floods and Enhanced Prospects for CO₂ Flooding Heterogeneous Reservoirs," Report PRRC 98-29, and Annual Report to the U.S. Department of Energy for the period June 1, 1997 through May 31, 1998: Tulsa, OK: National Petroleum Technology Office.
- Haldorsen, H.H. and L.W. Lake (1989): "A New Approach to Shale Management in Field-Scale Simulation Models," **Reservoir Characterization - 2**, SPE Reprint Series #27. Richardson, TX: Society of Petroleum Engineers.
- Han, D.L., A. Nur, and D. Morgan (1986): "Effects of Porosity and Clay Content on Wave Velocities in Sandstones," *Geophysics* 51, 2093-2107.
- He, W., R.N. Anderson, L. Xu, A. Boulanger, B. Meadow, and R. Neal (1996): "4D Seismic Monitoring Grows as Production Tool," *Oil & Gas Journal*, pp. 41-46, May 20.
- Honarpour, M., L.F. Koederitz, and A.H. Harvey (1982): "Empirical Equations for Estimating Two-Phase Relative Permeability in Consolidated Rock," *Journal of Petroleum Technology*, pp. 2905-2908.
- Jack, I. (1998): **Time-Lapse Seismic in Reservoir Management**, 1998 Distinguished Instructor Short Course, Tulsa, OK: Society of Exploration Geophysicists.
- Joshi, S.D. (1991): **Horizontal Well Technology**, Tulsa, OK: PennWell Publishing Company.

- Kelamis, P.G., R.C. Uden, and I. Dunderdale (1997): "4D Seismic Aspects of Reservoir Management," Paper OTC 8293, Richardson, TX: Society of Petroleum Engineers.
- Kenyon, D.E. and G.A. Behie (1987): "Third SPE Comparative Solution Project: Gas Cycling of Retrograde Condensate Reservoirs," *Journal of Petroleum Technology*, pp. 981-997.
- Killough, J.E. (1976): "Reservoir Simulation with History-Dependent Saturation Functions," *Society of Petroleum Engineers Journal*, pp. 37-48.
- Killough, J.E. and C.A. Kossack (1987): "Fifth Comparative Solution Project: Evaluation of Miscible Flood Simulators," SPE Paper 16000, Richardson, TX: Society of Petroleum Engineers.
- Koval, E.J. (1963): "A Method for Predicting the Performance of Unstable Miscible Displacement in Heterogeneous Media," *Society of Petroleum Engineers Journal*, pp. 145-154.
- Kreyszig, E. (1999): **Advanced Engineering Mathematics**, New York, NY: Wiley.
- Lake, L.W. (1989): **Enhanced Oil Recovery**, Englewood Cliffs, NJ: Prentice-Hall.
- Lake, L.W. (1988): "The Origins of Anisotropy," *Journal of Petroleum Technology*, pp. 395-396.
- Lake, L.W. and J.L. Jensen (1989): "A Review of Heterogeneity Measures Used in Reservoir Characterization," SPE Paper 20156, Richardson, TX: Society of Petroleum Engineers.
- Larsen, R.J. and M.L. Marx (1985): **An Introduction to Probability and Its Applications**, Englewood Cliffs, NJ: Prentice-Hall.
- Larson, R.E., R.P. Hostetler and B.H. Edwards (1990): **Calculus with Analytic Geometry**, 4th Edition, Lexington, Mass.: D.C. Heath
- Lumley, D. and R. Behrens (1997): "Practical Issues for 4D Reservoir Modeling," *Journal of Petroleum Technology*, pp. 998-999.
- McCain, W.D., Jr. (1990): **The Properties of Petroleum Fluids**, Second Edition, Tulsa, OK: Petroleum Publishing.

- McCain, W.D., Jr. (1991): "Reservoir-Fluid Property Correlations – State of the Art," *Society of Petroleum Engineers Reservoir Engineering*, pp. 266-272.
- McQuillin, R., M. Bacon, and W. Barclay (1984): **An Introduction to Seismic Interpretation**, Houston: Gulf Publishing
- Mian, M.A. (1992): **Petroleum Engineering**, Tulsa: Penn Well, pp. 486-489, Volume I.
- Moses, P.L. (July 1986): "Engineering Applications of Phase Behavior of Crude Oil and Condensate Systems," *Journal of Petroleum Technology*, pp. 715-723
- Murphy, W., A. Reisher, and K. Hsu (1993): "Modulus Decomposition of Compressional and Shear Velocities in Sand Bodies," *Geophysics*, Vol. 58, pp. 227-239.
- Nolen, J.S. and D.W. Berry (1973): "Test of the Stability and Time Step Sensitivity of Semi-Implicit Reservoir Simulation Techniques," **Numerical Simulation**, SPE Reprint Series #11, Richardson, TX: Society of Petroleum Engineers.
- Odeh, A.S. (1981): "Comparison of Solutions to a Three-Dimensional Black-Oil Reservoir Simulation Problem," *Journal of Petroleum Technology*, pp. 13-25.
- Peaceman, D. W. (1977): **Fundamentals of Numerical Reservoir Simulation**, New York: Elsevier.
- Peaceman, D.W. (June 1978): "Interpretation of Well-Block Pressures in Numerical Reservoir Simulation," *Society of Petroleum Engineering Journal*, pp. 183-194. See also Peaceman, D.W. (June 1983): "Interpretation of Well-Block Pressures in Numerical Reservoir Simulation With Nonsquare Grid Blocks and Anisotropic Permeability," *Society of Petroleum Engineering Journal*, pp. 531-543.
- Pedersen, K.S., A. Fredenslund, and P. Thomassen (1989): **Properties of Oil and Natural Gases**, Houston: Gulf Publishing.

- Price, H. S. and K. H. Coats (1973): "Direct Methods in Reservoir Simulation", SPE Paper 4278, Richardson, TX: Society of Petroleum Engineers.
- Schön, J.H. (1996): **Physical Properties of Rocks: Fundamentals and Principles of Petrophysics**, Volume 18, New York: Elsevier.
- Shelton, J.L. and L. Yarborough (Sept. 1977): "Multiple Phase Behavior in Porous Media During CO₂ or Rich-Gas Flooding," *Journal of Petroleum Technology*, pp. 1171-1178.
- Stone, H. L. (Oct.-Dec. 1973); "Estimation of Three-Phase Relative Permeability and Residual Oil Data," *Journal of Canadian Petroleum Technology*, pp. 53ff.
- Taber, J.J., F.D. Martin and R.S. Seright (1996): "EOR Screening Criteria Revisited," Paper SPE 35385, *Proceedings of the 1996 SPE Improved Oil Recovery Symposium*, Richardson, TX: Society of Petroleum Engineers.
- Thomas, L. K., W. B. Lumkin and G. M. Reheis (1976): "Reservoir Simulation of Variable Bubble Point Problems," *Society of Petroleum Engineers Journal*, pp. 10-16.
- Tiab, D. and E.C. Donaldson (1996): **Petrophysics**, Houston: Gulf Publishing.
- Tobias, S. (1998): "From G&G to S&S: Watershed Changes in Exploration-Development Work Flow," *Oil and Gas Journal*, pp. 38-47 (30 November).
- Todd, M. R. and W. J. Longstaff (1972): "The Development, Testing and Application of a Numerical Simulator for Predicting Miscible Flood Performance," *Journal of Petroleum Technology* **24**, pp. 874-882.
- Vernik, L. (1998): "Acoustic Velocity and Porosity Systematics in Siliciclastics," *Log Analyst* **39** (July-August), 27-35.
- Vinsome, P. K. W. (1976): "Orthomin, an Iterative Method for Solving Sparse Sets of Simultaneous Linear Equations", SPE Paper 5729 and **Numerical Simulation II**, SPE Reprint Series #20, Richardson, TX: Society of Petroleum Engineers.

- Watkins, R. W. (1982): "The Development and Testing of a Sequential, Semi-Implicit Four Component Reservoir Simulator," Paper SPE 10513, Richardson, Texas: Society of Petroleum Engineers.
- Weinstein, H.G., J.E. Chappelar, and J.S. Nolen (1986): "Second Comparative Solution Project: A Three-Phase Coning Style," *Journal of Petroleum Technology*, pp. 345-353.
- Young, D. M. (1971): **Iterative Solution of Large Linear Systems**, New York: Academic Press.

INDEX

A

absolute permeability 48, 85, 86, 119, 141, 145, 170
accumulation 88, 151-154, 157, 186, 187
acoustic 2, 3, 74-77, 83, 84, 195, 197, 198, 200, 202, 207, 208, 212, 252, 269, 270
algorithm 100, 116, 136, 191, 210, 235, 239, 248, 260-263
allocation 8, 172, 175, 210
analytic aquifer 3, 169, 178-180, 209, 249, 269
aquifer 3, 4, 100, 139, 169, 178-180, 193, 196, 197, 209, 212, 249, 252, 269, 270
aquifer model 3, 178, 179, 209, 249, 269
average 16, 17, 21, 33, 39, 40, 43, 52-55, 60, 66, 67, 69, 73, 82, 91-93, 99, 119, 120, 126, 129, 169, 246, 248, 270

B

barrier 117
base case 198
black oil model 130
black oil simulator 2, 4, 5, 7, 74, 124, 131, 156, 162, 166, 169, 181, 198, 208
block pressure 175
bottomhole pressure 254, 256
boundaries 17, 122, 148, 169, 195
boundary conditions 122, 152
bubble point 130, 132-134, 136, 138, 147, 189, 198, 200, 202,

212, 234, 235, 237, 239, 252, 270
Buckley-Leverett 25, 101, 155, 167, 211
bulk density 72, 75, 76
bulk modulus 72-76, 83, 221-224
bulk volume 20-22, 24, 25, 27, 29, 37, 122, 217
Burger's equation 151, 152

C

C-D equation 151, 152
capillary pressure 6, 89, 102, 105-114, 115, 118, 140, 141, 143-146, 164, 189, 232, 233, 261, 269
Carter-Tracy 179
Cartesian 24, 213
chemical 28, 104, 150
completion 176
compressibility 7, 46, 73, 127, 128, 131-133, 136, 191, 196, 236
compressional velocity 71, 72, 74, 76, 198-202, 212, 252, 270
computer
mapping 18
program 15
concentration 118, 125, 151-154, 157, 241
condensate 130, 150, 158, 166
configuration 8, 210
conservation of mass 156, 157
constraint 5, 29, 30, 36, 160, 166, 172, 175, 243, 244, 262, 263

contact angle 102, 104, 106, 109-113
continuity equation 158
contour 13, 14
convection 121, 151
core 18-20, 28, 31-34, 36, 38, 48, 59, 60, 62, 66, 69, 80, 89, 91, 105, 111-113, 152, 183
core analysis 28
correction 4, 209, 266
correlation 39, 47, 48, 62, 75, 77, 80, 81, 83, 99, 103, 111, 112, 198, 199
critical sample size 57, 58, 60, 64, 66, 69
cross-section 55, 100, 123, 179, 180, 191, 193, 196, 197, 203
cross-section model 55
cubic 127
cylindrical 69, 105

D

Darcy's law 41-46, 49, 119, 129, 169
datum 49, 219, 242, 243
density 5, 7, 43, 44, 72, 74-76, 78, 103, 106, 107, 112, 124, 127-130, 136, 144, 146, 158, 200, 221-223, 225, 236, 238, 261
density gradient 107
depletion 4, 25, 39, 138, 149, 150, 155, 209, 211, 212
depth 6, 49, 126, 155, 157, 176, 188, 220, 242, 243, 260
deterministic 19
dew point 130, 150
differential equations 181, 183
differential liberation 131, 132

dipping 49, 144, 149, 196
direct solution 248
directory 10
discretize 186
dispersion 35-37, 58, 64, 66, 151
distribution 12, 17-19, 21, 22, 27, 30-39, 47, 57, 58, 60-64, 66, 67, 69, 77, 78, 80-82, 102, 107, 111, 191, 198, 213, 263, 270
downstream 184
drive 8, 10, 149, 189, 210
dry gas 150, 166
dyadic 163
Dykstra-Parsons 66, 67, 70
dynamic viscosity 129, 130

E

elevation 108, 155, 261
endpoint 214
Enhanced Oil Recovery 147, 150
environment 8, 19, 87
equation of state 46, 125, 128
equilibration 49
equilibrium 105, 107, 125, 127, 191, 242, 260, 265
expectation value 35, 60, 82
explicit pressure 175, 177, 179, 255-257

F

fault 203
files 8-10, 40, 210, 212, 251, 268, 269, 271
finite difference 121, 122, 178, 181-183, 185, 186, 188, 267, 268
flash 131, 132
flow equations 1, 2, 5, 7, 8, 29, 51,

156, 158, 162, 164, 166, 169,
176, 179, 181, 185, 186, 188
fluid
movement 74, 108, 129
properties 8, 9, 76, 124, 130,
133, 134, 178, 195, 197, 211
fluidity 129
flux 151-154, 156-158
format 1, 9, 214, 268
formation volume factor 5, 45, 46,
90, 116, 119, 127, 128 130,
131, 135, 138, 147, 234-237,
239-241, 248
fractional flow 140, 142-146, 154
fracture 48
frontal advance 194
fully implicit 188

G

gas cap 10, 26, 149, 196
gas-oil 6, 92, 94-99, 103, 118,
130, 131, 133, 138, 141, 146,
164, 176, 212, 231, 233, 234,
243, 246, 260-262
gas-oil
contact 243, 260, 261
ratio 131, 133, 138, 212, 234,
246
gas-water 98, 173, 189, 262
geometry 215, 263
geostatistics 18, 22, 27
giga scale 20
gradient 49, 101, 107, 149, 152,
246, 248, 262
grain density 221-223, 225
gravity
drainage 149
segregated 242, 263

segregation 99, 191, 265
grid 11, 13, 13, 25, 29, 99, 100,
121, 122, 178, 179, 195, 198,
211, 215, 216, 218, 219, 242
grid size 215, 218, 219
gross thickness 13, 24-26, 29,
215, 216, 218, 219

H

hard drive 8, 10, 210
heterogeneity 18, 19, 52, 66-68
history matching 122, 194, 195
Honarpour 93, 95, 96
horizontal
permeability 52, 56, 172, 171,
197
well 171, 172, 254
hysteresis 88, 89, 107, 108

I

immiscible 73, 86, 102, 104, 105,
107, 109, 115, 116, 140, 145,
146, 150, 151, 154, 198-202
IMPES 2, 188, 190, 208, 270
implicit 2, 175, 176, 188, 208, 257-
259
Improved Oil Recovery 198
influx 4, 139, 178-180, 196, 209,
212, 249, 252, 270
initialization 9, 107, 191, 211, 214,
242, 260, 261, 263, 265, 269
integration 1, 2, 46, 186, 187, 207
interfacial tension 86, 102, 103,
109, 140, 151
interstitial velocity 42, 43
irreducible 87, 92, 93, 108, 109,
175, 196, 233, 244, 261
isothermal 1, 207

isotropic 52, 71, 73, 74, 171, 197
iterations 190-192, 245-247, 266
iterative 181, 188, 190, 193, 245,
248, 268

J

Jacobian 190
Joshi formula 171

K

K value 125
kinematic viscosity, 129, 130
Klinkenberg 48, 49

L

laboratory measurements 74, 87,
89, 93, 97, 105, 109
layer cake 220
linear 17, 18, 42, 52-54, 75, 89,
132, 144, 145, 152, 154, 190,
191, 195, 198, 200, 202, 267
logging 74
Lorenz coefficient 66-68, 70

M

Macleod-Sugden 103
macro scale 20
mapping 12, 13, 18
mass conservation 4, 157, 158,
160, 266
material
balance equation 188, 245, 248
balance error 4, 179, 186, 191-
193, 209, 210, 265, 266
matrix 19, 47, 48, 50, 72-76, 190,
192, 193, 195, 221, 267, 268
matrix material 19, 72, 221
mean 34-37, 39, 48, 60-63, 77,

121
mega scale 20
micro scale 20, 47
microbial 150
miscible 2, 7, 115-118, 136, 137,
147, 150-152, 166, 181, 198,
199, 201, 202, 208, 236, 237
miscibility 118, 151, 199-202, 233,
237, 238
mixing parameter 134, 137, 151,
154, 202, 238
mobility 85, 90, 91, 117-120, 140,
142, 150, 152, 159, 172, 173,
175, 241, 253
mobility ratio 142
mole fraction 103, 125, 128
molecular weight 103, 126, 128,
129
momentum 43

N

neutron 72
Newton-Raphson 4, 181, 188, 190,
192, 209, 247
nonlinear 44, 151, 152, 181
normal distribution 21, 34, 36, 60
numerical aquifer 178

O

objectives 22, 23
oil-water 6, 30, 87, 88, 91, 96, 98,
104, 108, 117, 118, 141, 164,
189, 233, 236, 244, 262, 263
oscillations 270
output 9, 10, 40, 83, 210, 212,
245, 250, 251, 268-271

P

parallelogram 13
parachor 103
partial differential equations 181, 183
performance predictions 1, 22, 23
permeability 6
petrophysical model 1, 2, 71, 196, 207
phase behavior 97
plot file 212, 270
Poisson's ratio 74
pore
 radius 106, 109, 114
 volume 3, 21, 25-27, 29, 37, 39, 147, 209, 217, 229, 230, 246, 270
porous 18-20, 27-29, 41-44, 48, 49, 62, 72-74, 87, 108, 129, 159, 221
pressure
 equation 6, 121, 191, 267
 initialization 242
 maintenance 150
primary recovery 149
probability 21, 30-32, 34, 36, 37, 58, 61, 62, 68, 77-80
PVT 6, 130-133, 234, 236, 239-241, 246, 269
PVT region 269

R

radial
 coordinates 45
 flow 44-46, 54
radius 17, 44-46, 54, 105, 106, 109, 114, 170-172, 179
rate constraint 172

realizations 22

recovery efficiency 140, 146-148, 150
recurrent data 9, 211, 250, 251, 269
reflection coefficient 3, 76, 208, 212, 252, 270
regression 17, 18, 103
reliability 18
representation 3, 12, 22, 47, 52, 96, 172, 175, 178, 183, 199, 208

reserves 197

reservoir
 characterization 1, 20, 22, 48, 197
 description 9, 211
 engineering 2, 3, 208
 management 1, 2, 22, 197, 207
 simulation 45, 88, 131
 structure 10, 12
residual 87, 89, 92-94, 96, 97, 108, 117, 147, 150, 188-190, 192, 202, 233, 237, 247, 263, 266
restart 242
Reynolds number 43
robustness 210
rock
 compressibility 73, 236
 quality 47
rock region 231, 232, 243, 244
rock-fluid interaction 199, 201
run summary 212, 270

S

saturated 6, 130, 132-134, 136, 189, 195, 211, 235, 239

saturation constraint 5, 29, 30, 166, 263
scale 19, 20, 22, 47, 83, 104, 126, 127
secondary recovery 150
seismic
 methods 15
 velocity 100, 220, 252
semi-variance 23, 24
sensitivity 100, 202
sensitivity study 100
separator 131
shear
 modulus 72, 74, 75, 221-224
 velocity 3, 71, 72, 74-76, 198-203, 208, 252
slanted well 179
slope 136, 138, 234, 237
solubilities 130, 158, 159
solution method 246, 248
source/sink 157, 169, 179, 190, 191, 266
spacing 81, 122
specific gravity 128, 129, 145, 146, 199, 201
stability 212, 265, 270
standard deviation 21, 22, 34, 35, 38, 57, 59, 60, 64, 65
steady-state aquifer 179, 180
superficial velocity 42, 43
sweep 147, 148
sweep efficiency 148
symmetry 12, 13

T

Taylor 181, 182, 184, 185
temperature 46, 109, 110, 124, 126-129, 149

tensor 6, 50-52, 121, 163
thermal 150
thickness 3, 13, 15, 24-26, 29, 44, 45, 53-55, 67, 68, 99, 148, 170-172, 209, 215-220, 262, 263
three-phase
 flow 100, 158
 relative permeability 97, 100
time-lapse (4-D) seismic 2, 71, 194, 197, 207
timestep 4, 9, 168, 183, 186, 188, 191, 192, 209-212, 238, 245-247, 250, 253, 265-270
timestep summary 9, 212, 268, 270
transient tests 52
transition zone 107, 108, 114, 262
transmissibility 3, 115, 119, 121-123, 185, 188, 191, 203, 209, 225, 229-231
transmission coefficient 77

U

uncertainty 23
undersaturated 4, 130, 133, 134, 138, 189, 195, 197, 209, 211, 234, 237
upstream 119, 120, 184, 248

V

validity 43
variance 19, 23, 24, 35, 58, 60, 63, 69
vector 23, 49, 50, 74, 83, 162, 187, 190
velocity 2, 3, 5, 6, 42, 43, 71, 72, 74-76, 83, 84, 100, 151, 152, 158, 195-203, 207, 208, 212,

- 220, 252, 270
vertical well 170, 179
viscosity 6, 42, 43, 45, 53, 90,
 129, 130, 135, 136, 139, 142,
 145, 146, 153, 154, 159, 167,
 170, 234-237, 239-241, 248
voidage 174, 255, 256
volume element 38, 119
volumetric 42, 45, 119, 134, 143,
 146-148
- W**
water drive 149
water-oil
 contact 242, 243, 260, 261
 ratio 212, 246
waterflood 88, 89, 100, 123, 142,
- 147, 155, 167, 180, 192, 195,
 198-202, 211
wave 74, 76
Weinaug-Katz 103
well
 log 22, 107
 productivity 173
 report 212, 250, 251, 270
wellbore 44, 46, 169-172, 179
wettability 87, 88, 91, 93, 94, 102,
 104, 105, 109, 110, 113, 114,
 117
workover 254
- Y**
yield 33, 75, 111, 130, 151, 194

This Page Intentionally Left Blank